

Optimization of the Performance of an Artificial Imine Reductase by Directed Evolution and Encapsulation

Inauguraldissertation

zur

Erlangung der Würde eines Doktors der Philosophie

vorgelrgrt der

Philosophisch-Naturwissenschaftlichen Fakultät

der Universität Basel

von

Martina Ribar Hesticová

aus Snina, Slowakei

Basel, 2020

Originaldokument gespeichert auf dem
Dokumentenserver der Universität Basel edoc.unibas.ch

Genehmigt von der Philosophisch-Naturwissenschaftlichen Fakultät
Auf Antrag von

Prof. Dr. Thomas R. Ward

Prof. Dr. Florian P. Seebeck

Basel, den 24.04.2018

Prof. Dr. Martin Spiess

Dekan

“There is no real ending. It’s just the place where you stop the story.”

— Frank Herbert

*To my grandfather Roman.
Dedkovi Romanovi.*

ACKNOWLEDGEMENTS

It was a warm September day I will always remember. I had just arrived to Switzerland after an exhausting 11-hour train ride from Vienna. First, I had to collect the keys from my first apartment and run to the Chemistry Department to start my first official day as a PhD. student. I was anxious, tired and overwhelmed after having to leave my family, friends and all connections behind. However, I was lucky enough to get the warmest welcome by the Ward group and I immediately knew that I would love working with them.

The 4.5 years I spent in the group have been a great lesson in multitasking and project management and allowed me to grow both as a scientist and as a person. For this, I am most grateful to **Prof. Thomas Ward**: thank you for accepting me as a PhD. candidate in your amazingly interdisciplinary group. I will always cherish your guidance, mentoring, valuable lessons and the occasional high-fives!

I would sincerely like to thank **Prof. Florian Seebeck** for agreeing to co-referee this dissertation and **Prof. Dennis Gillingham** for chairing my PhD *viva*.

Parts of the presented results have been conducted as collaborations with research groups from other universities. I am grateful for the support of **Prof. Patrick Shahgaldian** and **Rita M. Correro** from FHNW for allowing me to get insight into the “nano” world and teaching me how to prepare and characterize the nanoparticles. **Markus**, thank you for the ICP measurements and precious brainstorming sessions! Secondly, I am thankful for the collaboration with **Prof. Jean-Didier Marèchal** and his research group, which turned out to be a great life and research lesson.

My last project required me to perform some experiments in the Biozentrum. I am most grateful for **Tim Sharpe** and **Marc Creus** and his team. Thank you for your time, amazing patience, useful tips and for helping me with setting up the instruments and experiments.

My huge THANKS goes to the whole **DrEAM team**, including the past and present members I met only for a short while. I would especially like to mention **Michela**, your friendship, guidance and support have helped me to get through both the darkest and brightest moments of my PhD. studies, and I cannot imagine how I would have done it without you. Thank you for becoming a part of my life! **Vincent**, your humor, friendliness and listening to all my stories have brightened my days. I do not believe in love at first sight, but I do believe in friendship at first sight. You were a beautiful demonstration of that! **Christian**, you always knew what to say when I needed tips on new methods and ideas I was trying out. Thank you for supporting me, inside and outside of the lab! **Tillmann**, it is hard for me to describe how much I will miss you, your amazingly wide area of knowledge and our conversations. It felt like I could always talk to you, no matter the problem or the situation. Thank you for always being there for me! **Tommaso**, your friendship was a key element at the beginning of my PhD. studies. Thank you for becoming my partner in crime and an endless source of support, and fun! **Sascha**, thank you for all the fun we had together, I already miss you! **Jaicy**, you will always hold a special place in my heart. You were my very first student I have ever mentored in Basel and your feedback encouraged me to keep my fun and enthusiastic attitude towards all my other students. It was amazing to watch you develop into an amazing scientist and a great and independent woman; keep it up! **Juliane**, you were the “mom” of the DrEAm group, you always took care of us, supported us and taught the less biologically-skilled ones all the necessary techniques. Thank you for all the time we had together, both as scientists and as friends. **Yasu**, I am most grateful for your mentorship, support and all the help over my entire PhD! **Joan, Jo, Yoann** and **Fadri**, your sense of humor is something I missed since the first moment I left the lab. Shame that I cannot take you along with me. I enjoyed all the fun, memorable moments, jokes, and serious conversations I had with **Valentin, Fabian, Jingming, Anamitra, Maxime, Jonas, Ryan** and **Valerio**.

My big thanks also goes to **Isa** and **Esthi**, for all your kind words and help with organizational tasks and documentation! Also, the research would not be possible without the constant support of the **Werkstatt** team.

For the past three years, I have been active as a science journalist. It is only logical to express my gratitude for being able to contribute to The Daily N (**Denník N**) and to the **Sci Five** blog of the University of Basel. Writing for you was a beautiful way to relax and to get an insight into other fields than the development of artificial metalloenzymes. Moreover, I got to improve my writing style and effectiveness, which helped me tremendously during writing this thesis and later to publish in Chemistry World, Physics Today, Physics World and Education in Chemistry. Let's see what the future holds!

During my second year of PhD. I was given the chance to participate in **Antelope**, the Uni Basel career program for female researchers. Thank you, **Patricia** and **Andrea**, for selecting me and changing my life! In addition, my fellow "antelopes", thank you all for your support and all the fun we had together. This program has showed me my strengths and helped me discover what my true passion really is. Moreover, it gave me the possibility to visit **Prof. Gerard Roelfes** – thank you for becoming my mentor and hosting me for a little while in your group.

I would not be where I am without the support of my family. My greatest appreciation goes to my parents and grandparents, who were always there for me. Their endless support could be felt even from more than 1000 km away. My siblings Saška, Jurko and Romanka, with all their strength, joy, passion and endurance, were my greatest motivation. I love and adore you!

I like to think that friends are family we get to choose. I would like to name **Kalmi**, **Kaja**, **Miška**, **Alex**, **Angelo**, **Marcel**, **Sylvie**, **Lukino** (bratmmmm), **Bzdušekovci** and **Zmajkovičovci**, your friendship means the world to me. Not to forget, "**Ozvena zvláštností**" has always made me feel like I never left.

My greatest appreciation and thanks goes to my best friend, the love of my life and the biggest wall of support one can imagine. **Pet'o**, vďačím ti za všetko- kto som a kde som. Ďakujem láska!

PREFACE

The present PhD dissertation summarizes the research findings of the research group of prof. Dr. Thomas R. Ward from the period of September 2013 to December 2017.

The main goal of the Ward group is the development and optimization of artificial metalloenzymes for their use in asymmetric catalysis. These hybrid catalysts, resulting from an incorporation of a metal-containing cofactor within a protein or DNA scaffold, can be optimized by either chemical or genetic means.

The present work aims at the genetic optimization of the protein scaffold and exploration of the use of the resulting hybrid catalysts in nano-applications. Apart from a general introduction section, this dissertation is divided into two chapters. Each chapter represents research performed in context of several projects, which were published or will be submitted to peer-reviewed journals. These chapters contain a brief introduction into the topic, followed by the corresponding publications, and author contributions. The electronic supplementary information for each publication can be found in the Appendices chapter.

The first chapter describes our efforts in genetic optimization of artificial metalloenzymes, design of a screening library and directed evolution of the resulting mutants. The second chapter illustrates two possibilities of applying artificial metalloenzymes in nano-applications, specifically the immobilization on silica nanoparticles or encapsulation in a ferritin protein cage.

LIST OF PUBLICATIONS

Excerpts from this thesis have been published or will be submitted in the following journals:

- Mallin, H.; Hesticová, M.; Reuter, R.; Ward, T. R. “*Library design and screening protocol for artificial metalloenzymes based on the biotin-streptavidin technology*” *Nat. Protoc.* **2016**, *11* (5), 835–852.
- Hesticová, M.; Correro, M. R.; Lenz, M.; Corvini, P. F.-X.; Shahgaldian, P.; Ward, T. R. “*Immobilization of an artificial imine reductase within silica nanoparticles improves its performance*” *Chem. Commun.* **2016**, *52*, 9462–9465.
- Hesticová, M.; Heinisch, T.; Alonso-Cotchico, L.; Marèchal, J.-D.; Vidossich, P.; Ward, T. R. “*Directed evolution of an artificial imine reductase*” *Angew. Chem. Int. Ed.* **2018**, *130*, 1881–1886.
- Hesticová, M. “*Directed Evolution of Artificial Metalloenzymes: Genetic optimization of the catalytic activity*” *Chim. Int. J. Chem.* **2018**, *4*, 1–4.
- Hesticová, M.; Heinisch, T.; Sharpe, T.; Lenz, M.; Ward, T. R. “*Ferritin encapsulation of artificial metalloenzymes: engineering a tertiary coordination sphere for an artificial transfer hydrogenase*” *Dalton Trans.* **2018**, *47*, 10837-10841.

CONTENTS

Acknowledgements	I
Preface	IV
List of publications	V
Table of contents	VI
List of abbreviations	IX
Chapter I: Introduction	1
1.1 Asymmetric catalysis.....	1
1.2 Biocatalysis.....	2
1.3 Artificial metalloenzymes.....	4
1.3.1 Anchoring strategies.....	4
1.3.2 Sav-biot technology.....	6
1.4 Artificial imine reductase.....	8
1.5 Goals of the thesis.....	14
1.6 References.....	16
Chapter II: Genetic optimization of ArMs	20
2.1 Introduction.....	20
2.2 Directed evolution of ArMs.....	22
2.4 <u>Library design and screening protocol for artificial metalloenzymes based on the biotin-streptavidin technology</u>	26
2.4.1 Abstract.....	27
2.4.2 Introduction.....	28
2.4.3 Experimental design.....	30
2.4.3.1 Overview.....	30
2.4.3.2 Library design.....	31
2.4.3.3 Expression of Sav mutants in 24-deep well plates.....	33

2.4.3.4	Determination of Sav free binding sites in CFE	35
2.4.3.5	Artificial transfer hydrogenase for the reduction of cyclic imines	36
2.4.3.6	Catalysis with immobilized Sav mutants using iminobiotin sepharose beads	37
2.4.3.7	Limitations	37
2.4.4	Troubleshooting	38
2.4.5	Anticipated results.....	41
2.4.5.1	Artificial transfer hydrogenase (option A)	42
2.4.5.2	Ring-closing olefin metathesis (option B).....	43
2.4.6	Acknowledgement.....	44
2.4.7	Supporting information	44
2.4.8	Author contributions	44
2.5	<u>Directed evolution of an artificial imine reductase</u>	45
2.5.1	Abstract	46
2.5.2	Introduction	47
2.5.3	Results and discussion	48
2.5.4	Conclusion	58
2.5.5	Acknowledgement.....	58
2.5.6	Supporting information	59
2.5.7	Author contributions	59
2.6	<u>Directed Evolution of Artificial Metalloenzymes: Genetic optimization of the Catalytic Activity</u>	60
2.6.1	Abstract	61
2.6.2	Introduction	61
2.6.3	Discussion	64
2.6.4	Conclusion	67
2.6.5	Acknowledgement.....	67
2.7	References.....	68

Chapter III: Nanooptimization of ArMs.....	73
3.1 Introduction	73
3.2 Immobilization on nanoparticles	75
3.3 Enzyme entrapment in a protein cage.....	76
3.4 <u>Immobilization of an artificial imine reductase within silica nanoparticles improves its performance</u>	79
3.4.1 Abstract.....	80
3.4.2 Introduction.....	81
3.4.3 Results and discussion	82
3.4.4 Conclusion	89
3.4.5 Acknowledgement	89
3.4.6 Supporting information.....	89
3.4.7 Author contributions	89
3.5 <u>Ferritin encapsulation of artificial metalloenzymes: engineering a tertiary coordination sphere for an artificial transfer hydrogenase</u>	90
3.5.1 Abstract.....	91
3.5.2 Introduction.....	92
3.5.3 Results and discussion	93
3.5.4 Conclusion	98
3.5.5 Acknowledgement	99
3.5.6 Supporting information.....	99
3.5.7 Author contributions	99
3.6 References	100
Summary and outlook.....	103
Appendices	A1
Appendix A (suppl. information for 2.4).....	A1
A.1 Materials	A1
A.2 Reagent setup.....	A1

A.3 Box 1, primer design	A8
A.4 Box 2, competent cells	A9
A.5 Timing	A20
A.6 Supplementary method.....	A21
A.7 Sequences	A26
A.7.1 Sav K121A codon-optimized sequence (Construct cloned into pET-24A)	A26
A.7.2 Primer sequences used for mutagenesis.....	A27
Appendix B (suppl. information for 2.5)	B1
B.1 General information.....	B1
B.2 Stock solutions and buffers	B2
B.3 Experimental procedures	B3
B.3.1 Primer design	B3
B.3.2 Site-directed mutagenesis	B3
B.3.3 Transformation of plasmids into cloning expression strain.....	B4
B.3.4 Large-scale expression in 3l conical flasks.....	B4
B.3.5 Cell harvest and lysis	B5
B.3.6 Protein purification	B5
B.3.7 Determination of Sav free binding capacity on purified protein samples	B6
B.3.8 Typical catalysis procedure in buffer.....	B7
B.3.9 Typical catalysis procedure in cell free extracts	B8
B.3.10 Typical catalysis procedure in a biphasic system	B8
B.3.11 Work-up and analysis.....	B10
B.3.12 Kinetic measurements	B13
B.3.13 Preparative scale catalysis.....	B15
B.4 X-ray analysis.....	B18
B.5 Computational details.....	B24
B.6 References	B27

Appendix C (suppl. information for 3.4).....	C1
C.1 General information	C1
C.2 Stock solutions and buffers	C2
C.3 Synthesis of the biotinylated catalyst 22	C2
C.4 SNPs preparation and characterization	C9
C.5 Catalysis	C12
C.6 References	C16
Appendix D (suppl. information for 3.5).....	D1
D.1 General information	D1
D.2 Stock solutions and buffers	D2
D.3 Sav preincubation and lyophilization.....	D2
D.4 Apoferritin encapsulation.....	D2
D.5 Size-exclusion chromatography.....	D3
D.6 Dynamic light scattering	D4
D.7 Electrophoresis.....	D5
D.8 ICP-MS determination of the total Ir content	D7
D.9 Catalysis.....	D8
D.10 HPLC analysis	D9
D.11 References.....	D9

LIST OF ABBREVIATIONS

♻️	First recylation
♻️	Second recylation
δ	Chemical schift
@	Immobilized at / embedded in
[S]	Substrate concentration
ACN	Acetonitrile
APO	Apoferritin
APTES	3-aminopropyltriethoxysilane
ATH	Asymmetric transfer hydrogenation
ATHase	Artificial transfer hydrogenase
B4F	Biotin-4-fluorescein
CDMT	2-chloro-4,6-dimethoxy-1,3,5-triazine
CFE	Cell free extract
cfu	Colony forming unit
conc.	Concentration
conv.	Conversion
DCM	Dichloromethane
DEE	Diethylether
DLS	Dynamic light scattering
DME	1,2-dimethoxyethane
DMF	Dimethylformamide
DMSO	Dimethyl sulfoxide
DANN	Deoxyribonucleic acid
DpnI	<i>Diplococcus pneumoniae</i> restriction enzyme
E. coli	<i>Escherichia coli</i>
ee	Enantiomeric excess
eqPCR	Error-prone polymerase chain reaction
ESI-MS	Electron-spray ionization mass spectroscopy
EtOAc	Ethylacetate
EtOH	Ethanol
FBS	Free biotin binding sites

FESEM	Field Emission Scanning Electron Microscope
GABA	γ -Aminobutyric acid
GC	Gas chromatography
GSH	Glutathione
GSSG	Glutathione disulfide
h	Hours
HOV-I	<i>Hoveyda-Grubbs Catalyst</i> 2nd generation
HPLC	High performance liquid chromatography
HsAf	Horse spleen apoferritin
HTS	High throughput screening
ICP-MS	Inductively-coupled plasma mass spectroscopy
IPTG	Isopropyl β -D-1-thiogalactopyranoside
IRED	Imine reductase
LC	Liquid chromatography
M	mol \cdot dm ⁻¹
MAO	Monoamine oxidase
MD	Molecular dynamics
MeOH	Methanol
Metathesase	Artificial metathesase
min	Minutes
MOPS	3-(N-morpholino)propanesulfonic acid
NAD ⁺	Nicotinamide adenine dinucleotide
NADH	Nicotinamide adenine dinucleotide hydride (reduced form)
native PAGE	Native polyacrylamide gel electrophoresis
NMM	N-methylmorpholine
NMR	Nuclear magnetic resonance
OD	Optical density
PCR	Polymerase chain reaction
Pd/C	Palladium-saturated charcoal
PDB	Protein Data Bank
pH	Potential of hydrogen
ppm	Parts per million
prot-SNPs	Silica nanoparticles protected in an organosilane layer
rac.	Racemic mixture

rpm	Rotations per minute
RT	Room temperature
s.d.	Standard deviation
Sav	Streptavidin
Sav-biot	Streptavidin-biotin technology
SDS-PAGE	Sodium dodecylsulphate polyacrylamide gel electrophoresis
SEC	Size exclusion chromatography
SNPs	Silica nanoparticles
Sub.	Substrate
TEMED	Tetramethylethylenediamine
TEOS	Tetraethyl orthosilicate
TFA	Trifluoroacetic acid
TFAA	Trifluoroacetic anhydride
TMS	Tetramethylsilane
TOF	Turnover frequency
TON	Turnover number
Tris	Tris(hydroxymethyl)aminomethane
UPLC	Ultra-performance liquid chromatography
WT	Wild type
X-ray	X-ray crystallography
ZYP	ZYP-5052 medium for auto-induction

CHAPTER I:

INTRODUCTION

1.1 ASYMMETRIC CATALYSIS

In nature, biomolecules such as nucleotides, DNA, RNA, amino acids, proteins, or sugars are present in an enantiopure form. The homochirality of biological molecules represents a challenge for the development of novel drug substances, flavors and fragrances, as two enantiomers of a compound will display different biological effects (Table 1).¹ In addition, stereoselective synthesis is of great importance in polymer industry (offering a higher degree of crystallinity or non-linear behavior) and materials (such as liquid crystals),^{2,3} pesticides and herbicides.⁴

Table 1 Differences in the biological effects of enantiomers.

Compound	Enantiomer	Biological effect
Thalidomide	(<i>R</i>)-(+)-thalidomide	teratogenic ⁵ (eutomer)
	(<i>S</i>)-(-)-thalidomide	sedative
Ethambutol	(<i>S,S</i>)-ethambutol	tuberculostatic
	(<i>R,R</i>)-ethambutol	blindness ⁶ (eutomer)
Tetramisole	(<i>S</i>)-tetramisole (levamisole)	nematocide
	(<i>R</i>)-tetramisole	causing numerous side-effects ⁷ (eutomer)
Warfarin	(<i>S</i>)-warfarin	anticoagulant
	(<i>R</i>)-warfarin	5 -6 times less potent ⁸ (eutomer)
Propranolol	(<i>S</i>)-(-)-propranolol	β -blocker
	(<i>R</i>)-(+)-propranolol	100 times less potent ⁹ (eutomer)

Approximately 50 % of all pharmaceuticals currently in use are chiral.¹⁰ The proportion of single-enantiomer drugs introduced into the market has been growing over the years and currently represents approximately 70 % of new molecular entity drugs.¹¹ The demand for the synthesis of enantioenriched or enantiopure compounds is therefore immense and is likely to increase.

The production of enantiopure drugs can be performed by multiple ways, such as the chiral pool strategy,¹² or separation of racemates.¹³ Both of these strategies come with disadvantages, either due to the requirement of enantiomerically pure starting material, or by maximum 50 % yield of the desired enantiomer. Asymmetric catalysis,¹⁴ i.e. the selective formation of a single stereoisomer of a given compound, represents an alternative method to the chiral pool and racemate separation. This field has experienced a rapid growth over the last few years and nowadays represents a fundamental synthetic method in pharma industry and drug discovery.¹⁵ The efficiency of this process profits from the high turnover number (TON), meaning that even small amounts of a chiral catalyst produces large quantities of products.

Homogeneous asymmetric catalysis based on transition metal complexes represents a well-established method with advantages of high catalytic activity, high enantioselectivity for either of the enantiomers, good atom economy, and tolerance towards organic solvents and harsh reaction conditions (extreme temperature, high pressure). Moreover, transition metal complexes can easily tolerate high substrate concentrations and possess a large substrate scope. However, it was not until recently ago that enantiomeric excess of >99 % was achieved with a synthetic catalyst.¹⁶

1.2 BIOCATALYSIS

Enantiomerically pure compounds are produced in nature by means of transferring the chiral information from enzymes. Although their substrate scope and operational stability might be limited in some cases, enzymes can produce valuable products selectively and with high turnover numbers (TONs) and turnover frequencies (TOF).¹⁷ Their implementation in organic synthesis brings a benefit of mild reaction conditions, and biorthogonality with great advantages such as eco-friendliness, renewability and sustainability.¹⁸ In contrast to non-catalyzed processes, the reaction rate of an enzyme-catalyzed process can be enhanced by a

factor of 10^{10} - 10^{17} .¹⁹ A process, which would require 300 to 3 billion years in the absence of enzymes can be, upon utilization of enzymatic catalysis, performed in one second. Such control over the reaction rate makes enzymatic catalysis a very attractive alternative method to traditional homogeneous catalysis.

The high efficiency of enzymatic catalysis lies in the stabilization of the reaction's transition state within the active site.²⁰⁻²⁴ The catalytic elements within the active site, i.e. the amino acid residues, are precisely positioned and allow for formation of van der Waals and electrostatic interactions, hydrogen bonding, steric and differential solvation effects, leading to conformational changes.^{25,26} Upon substrate binding, the effective concentration is increased,²⁴ and the "tightness" of the reaction transition state changes, i.e. circumvents the loss of translational or rotational entropy in the transition state compared to catalysis in solution.^{27,28} This entropy advantage lowers the free energy barriers²⁹⁻³¹ of chemical reactions and gets compensated in formation of the enzyme-substrate complex (the Cice effect).³² The degree of contribution of the entropic effects is, however, still under discussion.^{33,34}

As a result of the recent advances³⁵ in bioinformatics, directed evolution,³⁵ protein engineering, and high throughput screening techniques, new properties can be now encoded into the protein scaffolds. Enzymes can be enhanced to accept non-natural substrates,³⁶ tolerate organic solvents,³⁷ or to increase their robustness under operating conditions.³⁸ On the other hand, enzymes have been evolving over millions of generations to perform under physiological conditions. Their window of activity has therefore its limitations,³⁹ such as low substrate concentrations, ambient temperature and pressure, requirement of aqueous media and mild pH and relatively narrow substrate scope. Another limitation of enzymatic catalysis is the level of expression, stability, refolding and solubility in the reaction medium, the time-consuming purification, requirement of expensive cofactors, or the specificity of used enzymes.

1.3 ARTIFICIAL METALLOENZYMES

Historically, homogeneous and enzymatic catalysis have been operating on independent grounds. However, these two systems are complementary in multiple aspects (Table 2).

Table 2. Features of homogeneous and enzymatic catalysis.⁴⁰

Feature	Homogeneous catalysis	Enzymatic catalysis
Reaction medium	Organic solvents	Aqueous medium
Reaction repertoire	Large	Small
Substrate scope	Large	Limited
Selectivity	Both enantiomers	Single enantiomer
TON	Small	Large
Optimization	Chemical	Genetic

In the past fifteen years, the field of biocatalysis has been enhanced by introduction of artificial metalloenzymes (ArMs), resulting from an incorporation of a catalytically active metal cofactor within a bioscaffold.⁴¹⁻⁴⁵ These combine the broad reaction scope of metal catalysts with high selectivity and turnovers of enzymatic catalysis, thus bridging the gap between the two.

The basic concept for ArMs was first established by Kaiser and Yamamura in 1976⁴⁶ and Wilson and Whitesides in 1978.⁴⁷ Since the new millennium, the field of ArMs has experienced rapid growth.⁴⁸ The metal (usually a transition metal) is surrounded by its first coordination sphere represented by an endogenous ligand. Upon embedding within the biomolecular scaffold, the resulting second coordination sphere around the metal interacts with the metal and its ligand, but also substrates, intermediates and products.

1.3.1 ANCHORING STRATEGIES

To avoid random localization and to stabilize the catalytic moiety within the biomolecular scaffold, various anchoring strategies have been developed (Figure 1):

- a) The covalent anchoring strategy relies on an irreversible reaction between a reactive amino acid side chain residue of the protein with a functional group of the cofactor. Typical examples include introduction of cysteine,⁴⁹⁻⁵⁵ lysine^{53,54} and serine modifications,⁵⁵ or the introduction of an unnatural amino acid residue.⁵⁶⁻⁶⁰
- (b) The supramolecular anchoring strategy (also known as non-covalent) relies on the formation of weak interactions between host bioscaffolds and small molecules resulting from the self-assembly of the resulting ArM.^{47,60-67} Since a strong interaction is necessary to avoid catalysis taking place outside of the biomolecular host, natural cofactors are often covalently modified and linked to the catalyst. One of the advantages of this approach is avoiding post-biosynthetic modification or purification.
- (c) Dative anchoring strategy uses the amino acid residue (cysteine, histidine, aspartate, serine, etc.) of the biomolecule as a ligand for a coordinately unsaturated metal center.^{46,63,64} This approach is often combined with covalent or supramolecular strategy.
- (d) Metal substitution uses the possibility to exchange a metal center in a natural metalloenzyme by a non-native metal.⁶⁵⁻⁷⁰ This strategy allows for introducing new-to-nature reactivity.

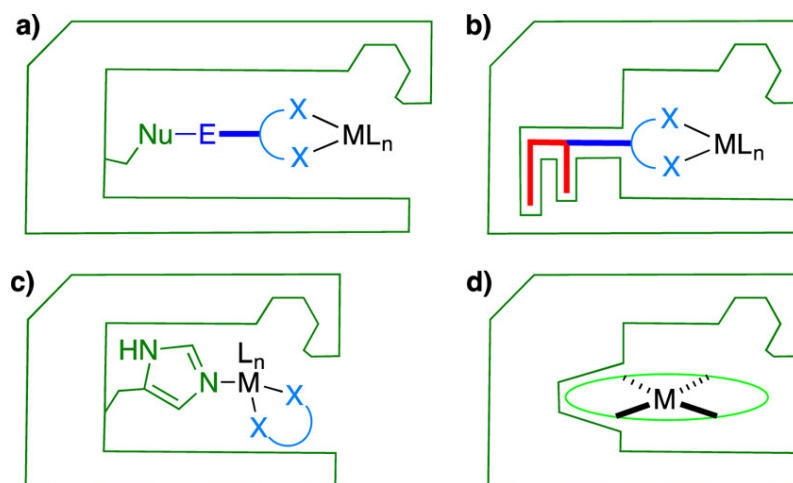


Figure 1. Anchoring strategies for localizing metal cofactors within a biomolecule.⁴¹

All of these strategies lead to new enzymatic activities, providing that they are implemented using purified proteins. Operating in complex cellular media or *in vivo* is not likely with all of the methods⁷¹ (Table 3), especially if we take into account the possibility of off-target binding and high amount of cofactor required for successful loading.

Table 3. Characteristics of anchoring strategies⁷²

Anchoring	Coupling mechanism	Coupling efficiency	Off-target binding	Bond stability	<i>In vivo</i> coupling
Covalent	Reactive	Low	Likely	High	Challenging
Supramolecular	Spontaneous	High	Unlikely	Variable	Straightforward
Dative	Spontaneous	High	Moderate	Intermediate	Possible
Metal substitution	Spontaneous	High	Unlikely	Variable	Possible

1.3.2 SAV-BIOT TECHNOLOGY

In the context of overcoming the anchoring challenges for ArMs creation, the supramolecular approach of streptavidin-biotin (Sav-biot) technology has been proven particularly versatile.^{72,73} Streptavidin (Sav) is a homotetrameric protein representing a bacterial equivalent to avidin. Its high affinity towards biotin ($K_D < 10^{-13}$ M) and its analogs represents one of the strongest non-covalent interactions known to nature.⁷⁴⁻⁷⁹ Additionally, the biotin dissociation rate can be further decreased by introducing mutations S52G and R53D.⁸⁰ This technology therefore allows for quantitative and specific loading of biotinylated probes even at sub-nanomolar concentration of both Sav and biot.

Because of the versatility of this anchoring strategy, the Sav-biot technology has found numerous applications across a wide range of technologies and methods.⁸¹ These include: cell biology, proteomics, immobilization, protein purification, detection, labelling, drug delivery, and diagnostic applications etc.⁸²⁻⁸⁴

The tight biotin anchoring relies on a hydrogen bonding network arising from the S27, Y43 and N23 interactions with the carboxyl oxygen of biotin, interactions of D128 and

S45 and the ureido nitrogens, T90 and the sulfur of the thiolane moiety, and N49 and S88 interactions with the carboxyl group of the valeric acid moiety. Moreover, the three tryptophan residues W79, W92 and W108 (and W120 from the adjacent Sav monomer) create additional hydrophobic interactions (Figure 2).⁸⁸⁻⁸⁸

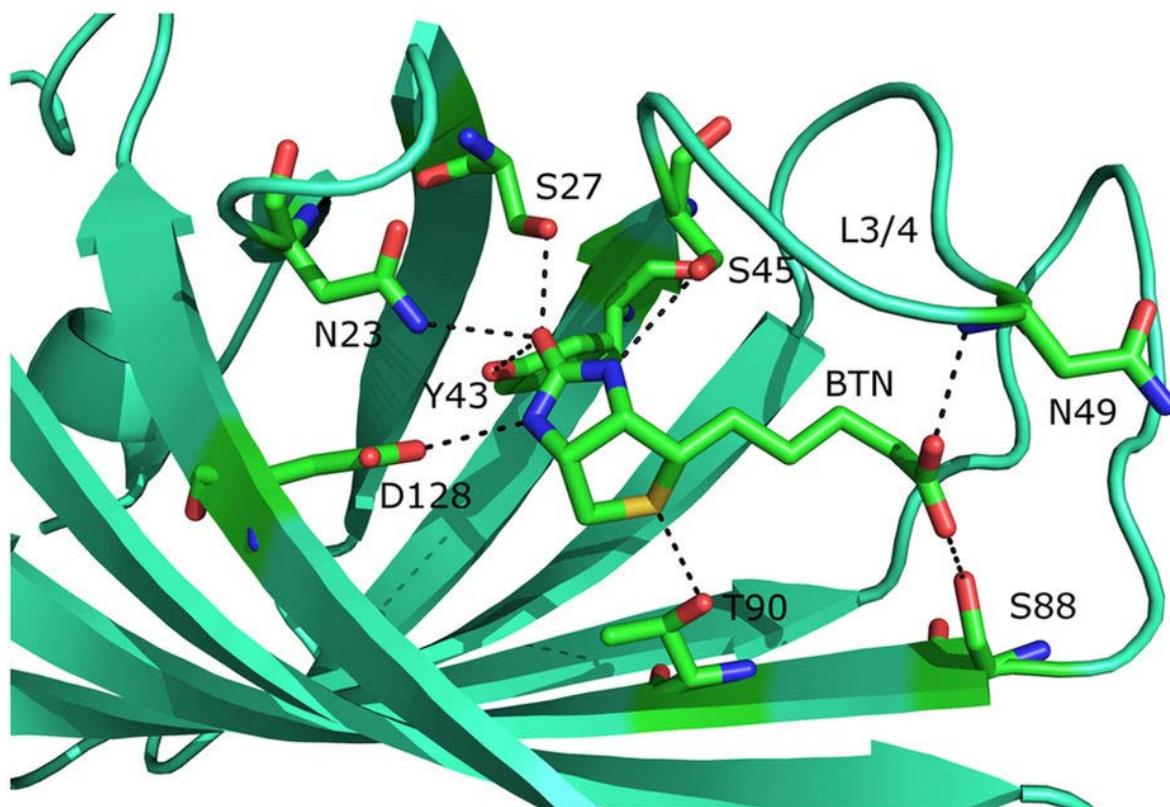
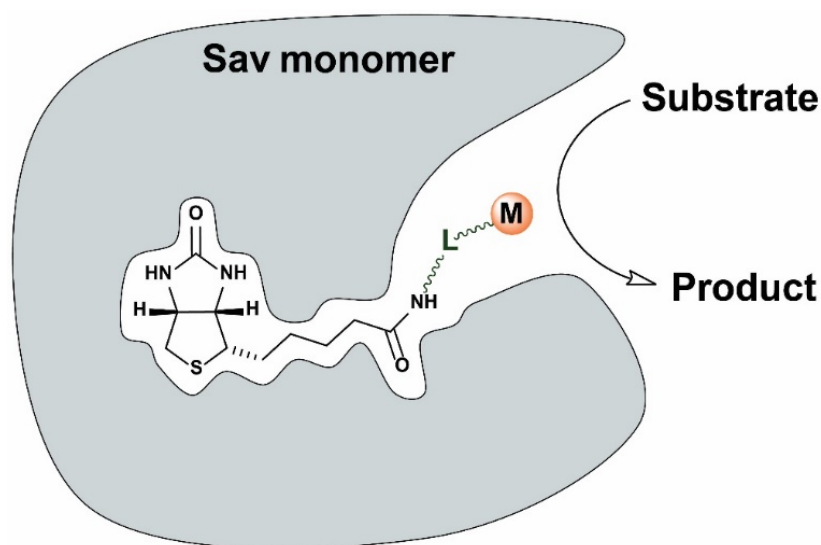


Figure 2. Interactions between the biotin moiety and the amino acid residues present in streptavidin's biotin binding pocket.⁸⁸

Streptavidin represents a remarkably robust protein capable of withstanding very harsh conditions such as elevated temperature, extreme pH, presence of organic solvents and denaturing agents, or sonication,⁸⁹⁻⁹¹ which makes it an ideal selection for the creation of ArMs. Relying on a non-covalent incorporation of a biotinylated metal catalyst, the resulting hybrid catalyst takes advantage of the secondary coordination sphere formed by the Sav amino acid residues and catalyzes the formation of chiral products from prochiral substrates (Scheme 1).

Following the initial report of an ArM derived from the biotin-avidin technology,⁴⁷ numerous catalytic systems implementing the Sav-biot technology have been reported. These include hydrogenation^{47,92,93} and transfer hydrogenation,⁹⁴⁻¹⁰³ C-H activation,¹⁰⁴ dihydroxylation,¹⁰⁵ alcohol oxidation,¹⁰⁶ sulfoxidation,^{107,108} allylic activation,¹⁰⁹ Suzuki cross-coupling¹¹⁰ and metathesis.^{111,112} Some of these transformation do not take place in natural biological systems, which highlight the ability of ArMs to catalyze new-to-nature reactions that are absent from the (natural) biocatalysis repertoire.¹¹³⁻¹¹⁷



Scheme 1. Creation of an ArM based on the Sav-biot technology. If catalyzing a prochiral substrate, the resulting hybrid catalysts can use the interactions of the second coordination sphere as a source for enantioselectivity.

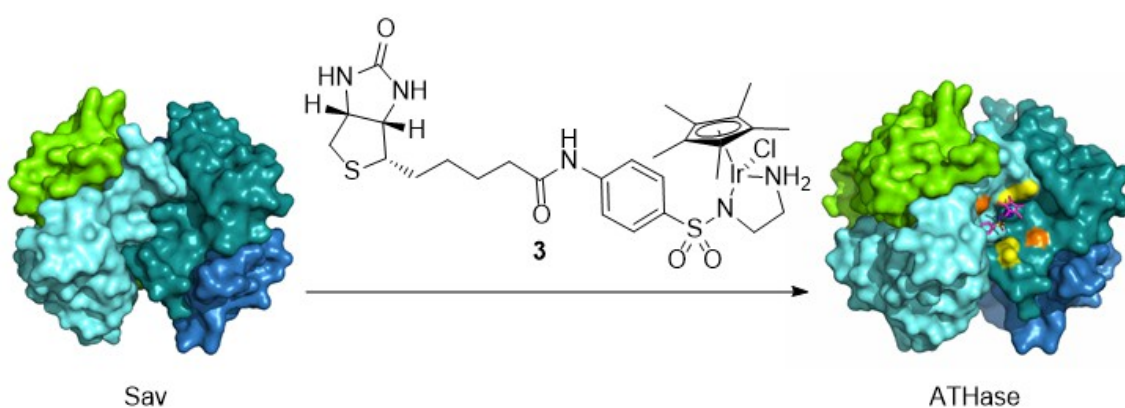
1.4 ARTIFICIAL IMINE REDUCTASE

Enantiopure amines represent important intermediates for the synthesis of biologically active compounds, flavors and fragrances and agrochemicals. Their relevance is underlined by the fact that approximately 40 % of all pharmaceuticals contain at least one enantiopure amine moiety.¹¹⁸ There are multiple strategies for their production such as organic synthesis and homogeneous catalysis,¹¹⁹⁻¹²¹ biocatalysis,¹²²⁻¹²⁹ and resolution of racemates.¹³⁰ Enzymatic synthesis of chiral amines has been achieved with amine

dehydrogenases,¹³¹⁻¹³³ transaminases,¹³⁴⁻¹³⁸ phenylalanine ammonia lyases¹³⁹⁻¹⁴¹ and imine reductases,¹⁴²⁻¹⁴⁷ or by dynamic kinetic resolution of amines by relying on monoamine oxidases¹⁴⁷⁻¹⁵² or lipases.¹⁵³⁻¹⁵⁶

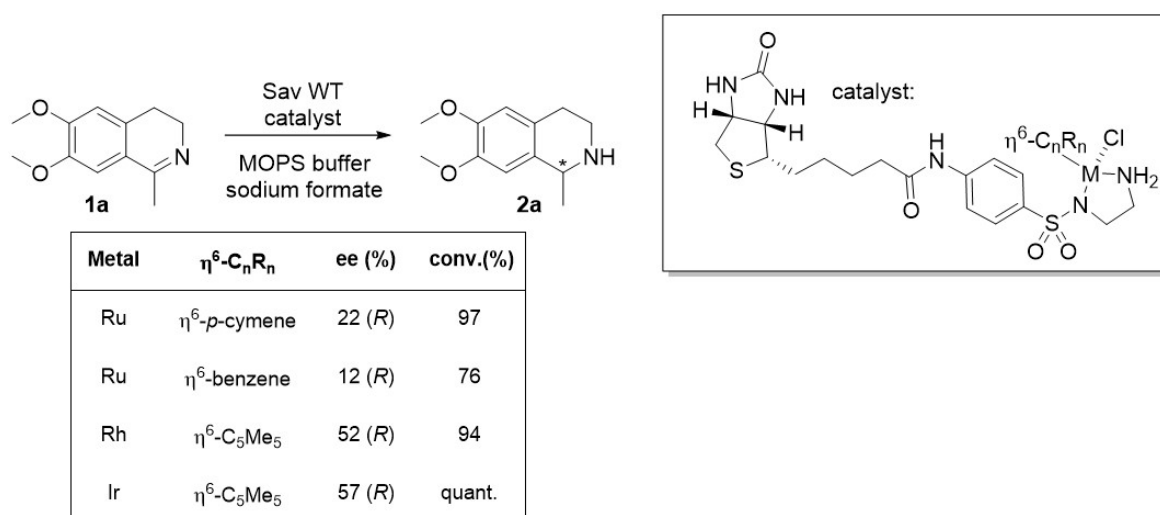
Since their first report in 2010,¹⁴² imine reductases have gained importance in biocatalysis and synthesis. However, their industrial usage remains limited for the following reasons: i) their non-competitive price, ii) restricted number of available enzymes iii) limited substrate scope and iv) instability of their substrates in water. These limitations call for the development of an alternative approach.

One of the options for biocatalytic reduction of imines is to use an artificial transfer hydrogenase (ATHase). The path of their development started in 1996, when Noyori showed that the $[(\eta^6\text{-arene})\text{Ru}((S,S)\text{-TsDPEN}))\text{Cl}]$ catalyst reduces imines in various aprotic polar organic solvents using azeotropic mixtures with trimethylamine and formic acid, achieving 97 % ee in the reduction of various isoquinolines¹⁵⁷. The possibility to perform this type of reaction in aqueous solutions^{95, 158-161} opened exciting new opportunities, which ultimately led to the development of an ATHase of ketones and imines, i.e. an artificial imine reductase (IRED) (Scheme 2).



Scheme 2. An artificial IRED is created by a combination of a biotinylated three-legged piannostool iridium catalyst **3** with Sav. Its activity has been utilized in ketone and imine reduction.

In the initial screening, the iridium-containing complex $[\text{Cp}^*\text{Ir}(\text{biot-}p\text{-L})\text{Cl}]$ outperformed⁹⁵ ruthenium and rhodium containing complexes $[\text{Cp}^*\text{Rh}(\text{biot-}p\text{-L})\text{Cl}]$ and $[(p\text{-cymene})\text{Ru}(\text{biot-}p\text{-L})\text{Cl}]$, when incorporated in Sav WT, representing contrasting results to ATH of ketones.⁹⁴ Screening with a library S112X, K121X and double mutants thereof revealed several mutants with improved activity. Catalyst $[\text{Cp}^*\text{Ir}(\text{biot-}p\text{-L})\text{Cl}] \cdot \text{S112A Sav}$ reduced 6,7-dimethoxy-1-methyl-3,4-dihydroisoquinoline **1a** to salsolidine **2a** in full conversion and 91 % ee (*R*), whereas $[\text{Cp}^*\text{Ir}(\text{biot-}p\text{-L})\text{Cl}] \cdot \text{S112K Sav}$ displayed opposite enantioselectivity and produced salsolidine in 78 % ee (*S*). A subsequent study identified that a double mutant $[\text{Cp}^*\text{Ir}(\text{biot-}p\text{-L})\text{Cl}] \cdot \text{S112A-K121A Sav}$ display improved catalytic efficiency for the reduction of 1-methyl-3,4-dihydroisoquinoline **1b**.¹⁶²



Scheme 3. Initial screening with various ruthenium, rhodium and iridium pianeostool complexes for the transfer hydrogenation of salsolidine precursor **1a**.⁹⁵

X-Ray structure analysis of crystals of S112A Sav soaked with an excess of the iridium cofactor suggested that the configuration at Ir is (*S*)- $[\text{Cp}^*\text{Ir}(\text{Biot-}p\text{-L})\text{Cl}]$, which corresponds to (*R*)- $[\text{Cp}^*\text{Ir}(\text{Biot-}p\text{-L})\text{H}]$ for the catalytically active hydride form.¹⁶² Regarding the mechanism, a non-concerted transition state allowing $\text{CH}\cdots\pi$ interaction between the Cp^* moiety and the aromatic moiety of the substrate has been suggested.^{94,163}

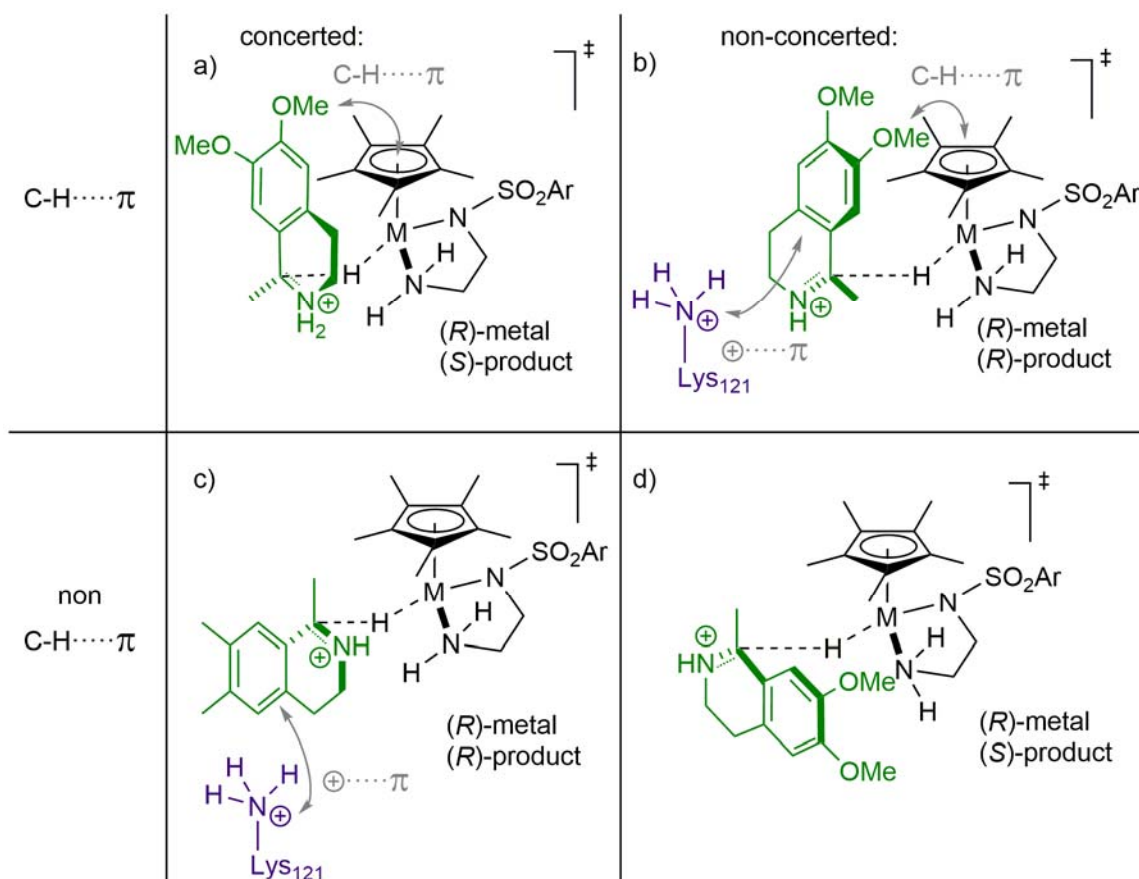
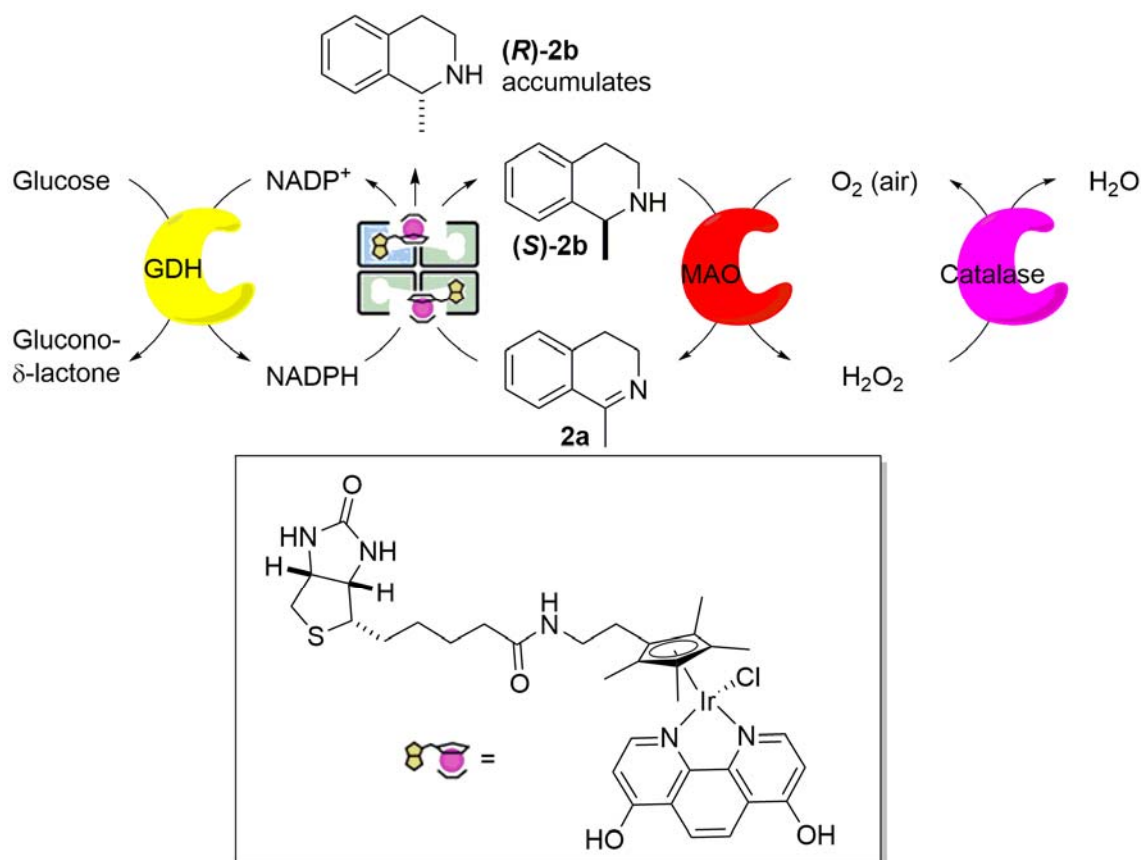


Figure 3. Postulated transition states for the d^6 pianostool-catalyzed asymmetric transfer hydrogenation of **1a** showcasing the $\text{CH}\cdots\pi$ interaction along with the cation $\cdots\pi$ interaction with K121 (b).⁹⁵

Furthermore, the ratio between the Sav tetramer and $[\text{Cp}^*\text{Ir}(\text{Biot-}p\text{-L})\text{Cl}]$ has a strong influence on the performance of the resulting artificial IREDS.¹⁶⁴ In the case of $[\text{Cp}^*\text{Ir}(\text{biot-}p\text{-L})\text{Cl}] \cdot \text{S112A Sav}$, increasing the Ir:Sav ratio from 1:1 (i.e. on average one biotin binding site occupied per tetramer) to 1:4 (all biotin binding sites occupied) decreased the enantioselectivity in the reduction of **1a** from 69 to 45 % along with the catalytic efficiency from $k_{\text{cat}}/K_{\text{M}} = 0.22 \text{ min}^{-1}\text{mM}^{-1}$ to $0.011 \text{ min}^{-1}\text{mM}^{-1}$. In contrast to S112A mutant, the enantioselectivity of $[\text{Cp}^*\text{Ir}(\text{biot-}p\text{-L})\text{Cl}] \cdot \text{S112K}$ remained almost constant across all tested ratios, while the activity decreases only by 1.5 fold. This observation suggested that the catalyst moieties within Sav operate independently. This hypothesis was confirmed by the

X-ray analysis of the obtained crystal; the four cofactors are able to occupy the binding sites without any steric clashes between them.

The development of artificial IREDs was recently further advanced by implementation of a dual anchoring strategy. This approach relies on using a biotinylated iridium cofactor with three available coordination sites, which can be used for coordination with amino acids present in the binding site.⁶⁴ Introducing histidines (either K121H or S112H) in close proximity of the rhodium metal center affected the enantioselectivity for the reduction of salsolidine precursor compared to the use of WT Sav. A similar approach utilizing the free coordination sites around the metal was used for screening a bidentate library of 34 diamines, amino acids and amino amides for the reduction of 1-phenyl-3,4-dihydroisoquinoline **1c**.¹⁶⁵ Promising ligands were identified, [Ir(biot-en- η^5 -Cp*)(L-ThrNH₂)Cl] · WT Sav produced the (*S*)-product in 63 % ee and 190 TON.



Scheme 4. An artificial IRED was integrated in a four-enzyme cascade to produce enantioenriched **2b**.¹⁰²

1.5 GOALS OF THE THESIS

An ATHase results from a non-covalent incorporation of a biotinylated piano-stool metal complex into Sav. In this context, the Ward group has developed an Ar-IREC during the last seven years. In this respect, the aims and goals of the presented thesis are:

- (i) To develop a high-throughput genetic screening protocol for ArMs by streamlining a glutathione-scavenger approach.
- (ii) To genetically optimize the artificial IREC by means of directed evolution.
- (iii) To optimize the operational stability and reaction rates of ArMs by immobilization on nanoparticles and encapsulation within a protective organosilane layer.
- (iv) To further expand the potential of influencing the catalysis by implementing a third coordination sphere around the metal catalyst.

1.6 REFERENCES

- [1] A. K. Scott, *Drug Saf.* **1993**, *8*, 149–159.
- [2] S. Itsuno, An Overview of Polymer-Immobilized Chiral Catalysts and Synthetic Chiral Polymers. In *Polymeric Chiral Catalyst Design and Chiral Polymer Synthesis*; Wiley-VCH, **2011**; 1–15.
- [3] S. Furumi, *Chem. Rec.* **2010**, *10*, 394–408.
- [4] A. Williams, *Pestic. Sci.* **1996**, *46*, 3–9.
- [5] T. Eriksson, S. Björkman, B. Roth, P. Höglund, *J. Pharm. Pharmacol.* **2000**, *52*, 807–817.
- [6] S. A. Lim, *Ann. Acad. Med. Singapore* **2006**, *35*, 274–278.
- [7] L. A. Nguyen, H. He, C. Pham-Huy, *Int. J. Biomed. Sci.* **2006**, *2*, 85–100.
- [8] A. Breckenridge, M. Orme, H. Wesseling, R. J. Lewis, R. Gibbons, *Clin. Pharmacol. Ther.* **1974**, *15*, 424–430.
- [9] W. Lindner, M. Rath, K. Stoschitzky, H. J. Semmelrock, *Chirality* **1989**, *1*, 10–13.
- [10] K. M. Rentsch, *J. Biochem. Biophys. Methods* **2002**, *54*, 1–9.
- [11] A. Calcaterra, I. D’Acquarica, *J. Pharm. Biomed. Anal.* **2018**, *147*, 323–340.
- [12] H. U. Blaser, *Chem. Rev.* **1992**, *92*, 935–952.
- [13] M. Nunez, M. Garcia-Rubino, A. Conejo-Garcia, O. Cruz-Lopez, M. Kimatrai, M. Gallo, A. Espinosa, J. Campos, *Curr. Med. Chem.* **2009**, *16*, 2064–2074.
- [14] V. Farina, J. T. Reeves, C. H. Senanayake, J. J. Song, *Chem. Rev.* **2006**, *106*, 2734–2793.
- [15] G. Lelais, D. W. C. Macmillan, in *New Frontiers in Asymmetric Catalysis*, Wiley-VCH, **2006**, 313–358.
- [16] O. I. Kolodiaznyi, Asymmetric Catalysis with Metal Complexes. In *Asymmetric Synthesis in Organophosphorus Chemistry*; Wiley-VCH, 2016; 187–252.
- [17] A.S. Bommarius, B.R. Riebel, *Biocatalysis. Fundamentals and Applications*. Wiley-VCH, **2004**.
- [18] R. A. Sheldon, J. M. Woodley, *Chem. Rev.* **2018**, *118*, 801–838.
- [19] A. Radzicka, R. Wolfenden, *Science* **1995**, *267*, 90–93.
- [20] L.C. Pauling, *Nature* **1948**, *161*, 707–709.
- [21] E. Lolis, G. A. Petsko, *Annu. Rev. Biochem.* **1990**, *59*, 597–630.
- [22] V. L. Schramm, *Annu. Rev. Biochem.* **1998**, *67*, 693–720.
- [23] T. C. Bruice, *Acc. Chem. Res.* **2002**, *35*, 139–148.
- [24] S. J. Benkovic, S. Hammes-schiffer, *Science* **2003**, *301*, 1196–1202.
- [25] G. J. Bartlett, C. T. Porter, N. Borkakoti, J. M. Thornton, *J. Mol. Biol.* **2002**, *324*, 105–121.
- [26] A. Warshel, P. K. Sharma, M. Kato, Y. Xiang, H. Liu, M. H. M. Olsson, *Chem. Rev.* **2006**, *106*, 3210–3235.
- [27] M. J. Snider, D. Lazarevic, R. Wolfenden, *Biochemistry* **2002**, *41*, 3925–3930.
- [28] A. R. Fersht, *Structure and Mechanism in Protein Science: A Guide to Enzyme Catalysis and Protein Folding*. Freeman, New York, **2017**.
- [29] G. G. Hammes, S. J. Benkovic, S. Hammes-Schiffer, *Biochemistry* **2011**, *50*, 10422–10430.
- [30] D. Herschlag, A. Natarajan, *Biochemistry* **2013**, *52*, 2050–2067.
- [31] J. Åqvist, M. Kazemi, G. V. Isaksen, B. O. Brandsdal, *Acc. Chem. Res.* **2017**, *50*, 199–207.
- [32] W. P. Jencks, in *Advances in Enzymology and Related Areas of Molecular Biology*, Wiley-VCH, **1975**, 219–410.
- [33] M. Kazemi, F. Himo, J. Åqvist, *Proc. Natl. Acad. Sci.* **2016**, *113*, 2406–2411.
- [34] J. Villá, M. Štrajbl, T. M. Glennon, Y. Y. Sham, Z. T. Chu, A. Warshel, *Proc. Natl. Acad. Sci.* **2000**, *97*, 11899–11904.

- [35] U. T. Bornscheuer, G. W. Huisman, R. J. Kazlauskas, S. Lutz, J. C. Moore, K. Robins, *Nature* **2012**, *485*, 185–194.
- [36] J. Liang, J. Lalonde, B. Borup, V. Mitchell, E. Mundorff, N. Trinh, D. A. Kochrekar, R. Nair Cherat, G. G. Pai, *Org. Process Res. Dev.* **2010**, *14*, 193–198.
- [37] M. T. Reetz, P. Soni, L. Fernández, Y. Gumulya, J. D. Carballeira, *Chem. Commun.* **2010**, *46*, 8657.
- [38] M. T. Reetz, Directed evolution of enzyme robustness in *Directed evolution of selective enzymes: Catalysts for organic chemistry and biotechnology*, Wiley-VCH, **2016**, 205–235.
- [39] M.R. Kula, Introduction. In *Enzyme Catalysis in Organic Synthesis*; Wiley-VCH, **2002**; 1–39.
- [40] C. M. Thomas, T. R. Ward, *Chem. Soc. Rev.* **2005**, *34*, 337.
- [41] F. Schwizer, Y. Okamoto, T. Heinisch, Y. Gu, M. M. Pellizzoni, V. Lebrun, R. Reuter, V. Köhler, J. C. Lewis, T. R. Ward, *Chem. Rev.* **2018**, *118*, 142–231.
- [42] J. Bos, G. Roelfes, *Curr. Opin. Chem. Biol.* **2014**, *19*, 135–143.
- [43] J. C. Lewis, *ACS Catal.* **2013**, *3*, 2954–2975.
- [44] P. J. Deuss, R. den Heeten, W. Laan, P. C. J. Kamer, *Chem. Eur. J.* **2011**, *17*, 4680–4698.
- [45] T. Heinisch, T. R. Ward, *Curr. Opin. Chem. Biol.* **2010**, *14*, 184–199.
- [46] K. Yamamura, E. T. Kaiser, *J. Chem. Soc., Chem. Commun.* **1976**, 830–831.
- [47] M. E. Wilson, G. M. Whitesides, *J. Am. Chem. Soc.* **1978**, *100*, 306–307.
- [48] O. Pàmies, M. Diéguez, J.-E. Bäckvall, *Adv. Synth. Catal.* **2015**, *357*, 1567–1586.
- [49] B. Talbi, P. Haquette, A. Martel, F. de Montigny, C. Fosse, S. Cordier, T. Roisnel, G. Jaouen, M. Salmain, *Dalt. Trans.* **2010**, *39*, 5605–5607.
- [50] H. Yang, P. Srivastava, C. Zhang, J. C. Lewis, *ChemBioChem* **2014**, *15*, 223–227.
- [51] J. Bos, A. Garcia-Herraiz, G. Roelfes, *Chem. Sci.* **2013**, *4*, 3578–3582.
- [52] C. Mayer, D. G. Gillingham, T. R. Ward, D. Hilvert, *Chem. Commun.* **2011**, *47*, 12068–12070
- [53] C. H. Chen, D. S. Sigman, *Science* **1987**, *237*, 1197–1201.
- [54] K. M. Nicholas, P. Wentworth, C. W. Harwig, A. D. Wentworth, A. Shafton, K. D. Janda, *Proc. Natl. Acad. Sci. U.S.A.* **2002**, *99*, 2648–2653.
- [55] Z. P. Wu, D. Hilvert, *J. Am. Chem. Soc.* **1989**, *111*, 4513–4514.
- [56] J. C. Lewis, *Curr. Opin. Chem. Biol.* **2015**, *25*, 27–35.
- [57] I. Drienovská, A. Rioz-Martinez, A. Draksharapu, G. Roelfes, *Chem. Sci.* **2015**, *6*, 770–776.
- [58] I. Drienovská, L. Alonso-Cotchico, P. Vidossich, A. Lledós, J.-D. Maréchal, G. Roelfes, *Chem. Sci.* **2017**, *8*, 7228–7235.
- [59] Y. Yu, C. Hu, L. Xia, J. Wang, *ACS Catal.* **2018**, 1851–1863.
- [60] Keinan E, Sinha S C, Sinha-Bagchi A, Benory E, Ghazi M C, Eshhar Z, Green B S, *Pure Appl. Chem.* **1990**, *62*, 2013.
- [61] S. Nimri, E. Keinan, *J. Am. Chem. Soc.* **1999**, *121*, 8978–8982.
- [62] H. Yamaguchi, T. Hirano, H. Kiminami, D. Taura, A. Harada, *Org. Biomol. Chem.* **2006**, *4*, 3571–3573.
- [63] Q. Jing, R. J. Kazlauskas, *ChemCatChem* **2010**, *2*, 953–957.
- [64] J. M. Zimbron, T. Heinisch, M. Schmid, D. Hamels, E. S. Nogueira, T. Schirmer, T. R. Ward, *J. Am. Chem. Soc.* **2013**, *135*, 5384–5388.
- [65] Q. Jing, K. Okrasa, R. J. Kazlauskas, in *Top. Organomet. Chem.*, **2008**, 11533–11542.
- [66] P. S. Coelho, E. M. Brustad, A. Kannan, F. H. Arnold, *Science* **2013**, *339*, 307–310.
- [67] H. Renata, Z. J. Wang, F. H. Arnold, *Angew. Chem. Int. Ed.* **2015**, *54*, 3351–3367.
- [68] M. Bordeaux, V. Tyagi, R. Fasan, *Angew. Chem. Int. Ed.* **2015**, *54*, 1744–1748.
- [69] H. M. Key, P. Dydio, D. S. Clark, J. F. Hartwig, *Nature* **2016**, *534*, 534–537.
- [70] G. Sreenilayam, E. J. Moore, V. Steck, R. Fasan, *Adv. Synth. Catal.* **2017**, *359*, 2076–2089.

- [71] M. Jeschek, S. Panke, T.R. Ward, Periplasmic Screening for Artificial Metalloenzymes. In *Methods in Enzymology*, Academic Press, **2016**, 539–556.
- [72] T. R. Ward, *Acc. Chem. Res.* **2011**, *44*, 47–57.
- [73] T. Heinisch, T. R. Ward, *Acc. Chem. Res.* **2016**, *49*, 1711–1721.
- [74] N.M. Green, *Adv. Protein Chem.* **1975**, *29*, 85–133.
- [75] N. M. Green, *Biochem. J.* **1963**, *89*, 599–609.
- [76] N. M. Green, Avidin and streptavidin. In *Methods in Enzymology*, Academic Press, **1990**; *184*, 51–67.
- [77] M. Wilchek, E. A. Bayer, *Biomol. Eng.* **1999**, *16*, 1–4.
- [78] S. Miyamoto, P. A. Kollman, *Proteins Struct. Funct. Bioinforma.* **1993**, *16*, 226–245
- [79] P. C. Weber, D. H. Ohlendorf, J. J. Wendoloski, F. R. Salemme, *Science* **1989**, *243*, 85–88.
- [80] C. E. Chivers, E. Crozat, C. Chu, V. T. Moy, D. J. Sherratt, M. Howarth, *Nat. Methods* **2010**, *7*, 391–393.
- [81] C. M. Dundas, D. Demonte, S. Park, *Appl. Microbiol. Biotechnol.* **2013**, *97*, 9343–9353.
- [82] M. Wilchek, E.A. Bayer, *Methods Enzymol.* **1990**, *184*, 5–13.
- [83] O. H. Laitinen, V. P. Hytönen, H. R. Nordlund, M. S. Kulomaa, *Cell. Mol. Life Sci. C.* **2006**, *63*, 2992–3017.
- [84] T. G. M. Schmidt, A. Skerra, *Analysis* **2007**, *2*, 1528.
- [85] P. Weber, D. Ohlendorf, J. Wendoloski, F. Salemme, *Science* **1989**, *243*, 85–88.
- [86] W. A. Hendrickson, A. Pähler, J. L. Smith, Y. Satow, E. A. Merritt, R. P. Phizackerley, *Proc. Natl. Acad. Sci. U.S.A.* **1989**, *86*, 2190–2194.
- [87] J. DeChancie, K. N. Houk, *J. Am. Chem. Soc.* **2007**, *129*, 5419–5429.
- [88] F. Liu, J. Z. H. Zhang, Y. Mei, *Sci. Rep.* **2016**, *6*, 27190.
- [89] Y. Hiller, E. a Bayer, M. Wilchek, *Biochem. J.* **1991**, *278*, 573–85
- [90] M. González, C. E. Argaraña, G. D. Fidelio, *Biomol. Eng.* **1999**, *16*, 67–72.
- [91] J. A. E. Määttä, Y. Eisenberg-Domovich, H. R. Nordlund, R. Hayouka, M. S. Kulomaa, O. Livnah, V. P. Hytönen, *Biotechnol. Bioeng.* **2011**, *108*, 481–490.
- [92] J. Steinreiber, T. R. Ward, *Top. Organomet. Chem.* **2009**, *25*, 93–112.
- [93] M. T. Reetz, *Top. Organomet. Chem.* **2009**, *25*, 63–92.
- [94] C. Letondor, A. Pordea, N. Humbert, A. Ivanova, S. Mazurek, M. Novic, T. R. Ward, *J. Am. Chem. Soc.* **2006**, *128*, 8320–8328.
- [95] M. Dürrenberger, T. Heinisch, Y. M. Wilson, T. Rossel, E. Nogueira, L. Knörr, A. Mutschler, K. Kersten, M. J. Zimbron, J. Pierron, T. R. Ward., *Angew. Chem., Int. Ed.* **2011**, *50*, 3026–3029.
- [96] C. Letondor, N. Humbert, T. R. Ward, *Proc. Natl. Acad. Sci. U.S.A.* **2005**, *102*, 4683–4687.
- [97] V. Köhler, Y. M. Wilson, M. Dürrenberger, D. Ghislieri, E. Churakova, T. Quinto, L. Knörr, D. Häussinger, F. Hollmann, N. J. Turner, T. R. Ward, *Nat. Chem.* **2013**, *5*, 93–99.
- [98] T. Heinisch, K. Langowska, P. Tanner, J. L. Reymond, W. Meier, C. Palivan, T. R. Ward, *ChemCatChem* **2013**, *5*, 720–723.
- [99] T. Quinto, D. Häussinger, V. Köhler, T. R. Ward, *Org. Biomol. Chem.* **2015**, *13*, 357–360.
- [100] Y. Okamoto, V. Köhler, C. E. Paul, F. Hollmann, T. R. Ward, *ACS Catal.* **2016**, *6*, 3553–3557.
- [101] M. Hesticová, M. R. Correro, M. Lenz, P. F.-X. Corvini, P. Shahgaldian, T. R. Ward, *Chem. Commun.* **2016**, *52*, 9462–9465.
- [102] Y. Okamoto, V. Köhler, T. R. Ward, *J. Am. Chem. Soc.* **2016**, *138*, 5781–5784.
- [103] M. Hesticová, T. Heinisch, L. Alonso-Cotchico, J.-D. Maréchal, P. Vidossich, T. R. Ward, *Angew. Chem. Int. Ed.* **2018**, *57*, 1863–1868.
- [104] T. K. Hyster, L. Knorr, T. R. Ward, T. Rovis, *Science* **2012**, *338*, 500–503.

- [105] V. Köhler, J. Mao, T. Heinisch, A. Pordea, A. Sardo, Y. M. Wilson, L. Knörr, M. Creus, J.-C. Prost, T. Schirmer, T. R. Ward, *Angew. Chem. Int. Ed.* **2011**, *50*, 10863–10866.
- [106] C. M. Thomas, C. Letondor, N. Humbert, T. R. Ward, *J. Organomet. Chem.* **2005**, *690*, 4488–4491.
- [107] A. Pordea, M. Creus, J. Panek, C. Duboc, D. Mathis, M. Novic, T. R. Ward, *J. Am. Chem. Soc.* **2008**, *130*, 8085–8088.
- [108] A. Pordea, D. Mathis, T. R. Ward, *J. Organomet. Chem.* **2009**, *694*, 930–936.
- [109] J. Pierron, C. Malan, M. Creus, J. Gradinaru, I. Hafner, A. Ivanova, A. Sardo, T. R. Ward, *Angew. Chem. Int. Ed.* **2008**, *47*, 701–705.
- [110] A. Chatterjee, H. Mallin, J. Klehr, J. Vallapurackal, A. D. Finke, L. Vera, M. Marsh, T. R. Ward, *Chem. Sci.* **2016**, *7*, 673–677.
- [111] C. Lo, M. R. Ringenberg, D. Gndt, Y. Wilson, T. R. Ward, *Chem. Commun.* **2011**, *47*, 12065–12067.
- [112] M. Jeschek, R. Reuter, T. Heinisch, C. Trindler, J. Klehr, S. Panke, T. R. Ward, *Nature* **2016**, *537*, 661–665.
- [113] F. H. Arnold, *Angew. Chem. Int. Ed.* 2017, doi: 10.1002/anie.201708408.
- [114] T. K. Hyster, T. R. Ward, *Angew. Chem. Int. Ed.* **2016**, 2–16.
- [115] S. C. Hammer, A. M. Knight, F. H. Arnold, *Curr. Opin. Green Sustain. Chem.* **2017**, *7*, 23–30.
- [116] M. Jeschek, S. Panke, T. R. Ward, *Trends Biotechnol.* **2018**, *36*, 60–72.
- [117] J. G. Rebelein, T. R. Ward, *Curr. Opin. Biotechnol.* **2018**, *53*, 106–114.
- [118] Jarvis, L. M., *Chem. Eng. News* **2014**, *94*, 12–17.
- [119] T. C. Nugent, *Chiral Amine Synthesis: Methods, Developments and Applications*, Wiley-VCH, Weinheim, Germany, **2010**.
- [120] M. Chrzanowska, A. Grajewska, M. D. Rozwadowska, *Chem. Rev.* **2016**, *116*, 12369–12465
- [121] T. C. Nugent, M. El-Shazly, *Adv. Synth. Catal.* **2010**, *352*, 753–819.
- [122] G. Grogan, *Curr. Opin. Chem. Biol.* **2018**, *43*, 15–22.
- [123] E. O'Reilly, N. J. Turner, *Perspect. Sci.* **2015**, *4*, 55–61
- [124] M. Nestl, S. C. Hammer, B. A. Nebel, B. Hauer, *Angew. Chem. Int. Ed.* **2014**, *53*, 3070–3095.
- [125] H. Kohls, F. Steffen-Munsberg, M. Höhne, *Curr. Opin. Chem. Biol.* **2014**, *19*, 180–192.
- [126] D. Ghislieri, N. J. Turner, *Top. Catal.* **2014**, *57*, 284–300.
- [127] F. Hollmann, I. W. C. E. Arends, D. Holtmann, *Green Chem.* **2011**, *13*, 2285.
- [128] M. Hall, A. S. Bommarius, *Chem. Rev.* **2011**, *111*, 4088–4110.
- [129] M. Höhne, U. T. Bornscheuer, *ChemCatChem* **2009**, *1*, 42–51.
- [130] M. Breuer, K. Ditrich, T. Habicher, B. Hauer, M. Keßeler, R. Stürmer, T. Zelinski, *Angew. Chem. Int. Ed.* **2004**, *43*, 788–824.
- [131] T. Knaus, W. Böhmer, F. G. Mutti, *Green Chem.* **2017**, *19*, 453–463.
- [132] M. J. Abrahamson, E. Vázquez-Figueroa, N. B. Woodall, J. C. Moore, A. S. Bommarius, *Angew. Chem. Int. Ed.* **2012**, *51*, 3969–3972.
- [133] F. G. Mutti, T. Knaus, N. S. Scrutton, M. Breuer, N. J. Turner, *Science* **2015**, *349*, 1525–1529.
- [134] H. Brundiek, M. Höhne, *Appl. Biocatal. From Fundam. Sci. to Ind. Appl.* **2016**, 199–218.
- [135] R. C. Simon, N. Richter, E. Busto, W. Kroutil, *ACS Catal.* **2014**, *4*, 129–143.
- [136] C. E. Paul, M. Rodríguez-Mata, E. Busto, I. Lavandera, V. Gotor-Fernández, V. Gotor, S. García-Cerrada, J. Mendiola, Ó. De Frutos, I. Collado, *Org. Process Res. Dev.* **2014**, *18*, 788–792.
- [137] S. Mathew, H. Yun, *ACS Catal.* **2012**, *2*, 993–1001.
- [138] C. K. Saville, J. M. Janey, W. R. Jarvis, J. C. Colbeck, A. Krebber, F. J. Fleitz, J. Brands, *Science* **2010**, *329*, 305–310.

- [139] M. M. Heberling, B. Wu, S. Bartsch, D. B. Janssen, *Curr. Opin. Chem. Biol.* **2013**, *17*, 250–260.
- [140] B. DeLange, D. J. Hyett, P. J. D. Maas, D. Mink, F. B. J. van Assema, N. Sereinig, A. H. M. de Vries, J. G. de Vries, *ChemCatChem* **2011**, *3*, 289–292.
- [141] D. Koszelewski, K. Tauber, K. Faber, W. Kroutil, *Trends Biotechnol.* **2010**, *28*, 324–332.
- [142] K. Mitsukura, M. Suzuki, K. Tada, T. Yoshida, T. Nagasawa, *Org. Biomol. Chem.* **2010**, *8*, 4533.
- [143] K. Mitsukura, M. Suzuki, S. Shinoda, T. Kuramoto, T. Yoshida, T. Nagasawa, *Biosci. Biotechnol. Biochem.* **2011**, *75*, 1778–1782.
- [144] M. Lenz, N. Borlinghaus, L. Weinmann, B. M. Nestl, *World J. Microbiol. Biotechnol.* **2017**, *33*, 199.
- [145] J. Mangas-Sanchez, S. P. France, S. L. Montgomery, G. A. Aleku, H. Man, M. Sharma, J. I. Ramsden, G. Grogan, N. J. Turner, *Curr. Opin. Chem. Biol.* **2017**, *37*, 19–25.
- [146] Z. Maugeri, D. Rother, *J. Biotechnol.* **2017**, *258*, 167–170.
- [147] M. Gand, H. Müller, R. Wardenga, M. Höhne, *J. Mol. Catal. B Enzym.* **2014**, *110*, 126–132.
- [148] S. Herter, F. Medina, S. Wagschal, C. Benhaïm, F. Leipold, N. J. Turner, *Bioorganic Med. Chem.* **2017**, DOI 10.1016/j.bmc.2017.07.023.
- [149] P. Zajkoska, M. Cárdenas-Fernández, G. J. Lye, M. Rosenberg, N. J. Turner, M. Rebroš, *J. Chem. Technol. Biotechnol.* **2017**, *92*, 1558–1565.
- [150] N. Scalacci, G. W. Black, G. Mattedi, N. L. Brown, N. J. Turner, D. Castagnolo, *ACS Catal.* **2017**, *7*, 1295–1300.
- [151] R. S. Heath, M. Pontini, S. Hussain, N. J. Turner, *ChemCatChem* **2016**, *8*, 117–120.
- [152] D. Ghislieri, A. P. Green, M. Pontini, S. C. Willies, I. Rowles, A. Frank, G. Grogan, N. J. Turner, *J. Am. Chem. Soc.* **2013**, *135*, 10863–10869.
- [153] Z. S. Seddigi, M. S. Malik, S. A. Ahmed, A. O. Babalghith, A. Kamal, *Coord. Chem. Rev.* **2017**, *348*, 54–70.
- [154] U. T. Bornscheuer, R. J. Kazlauskas, *Hydrolases in Organic Synthesis, 2nd ed.*, Wiley-VCH, Weinheim, **2006**.
- [155] J. Paetzold, J. E. Bäckvall, *J. Am. Chem. Soc.* **2005**, *127*, 17620–17621.
- [156] F. Balkenhohl, K. Ditrich, B. Hauer, W. Ladner, *J. für Prakt. Chem.* **1997**, *339*, 381–384.
- [157] N. Uematsu, A. Fujii, S. Hashiguchi, T. Ikariya, R. Noyori, *J. Am. Chem. Soc.* **1996**, *118*, 4916–4917.
- [158] C. Wang, X. Wu, J. Xiao, *Chem. Asian J.* **2008**, *3*, 1750–1770.
- [159] C. Wang, C. Li, X. Wu, A. Pettman, J. Xiao, *Angew. Chem. Int. Ed.* **2009**, *48*, 6524–6528.
- [160] X. Zhou, X. Wu, B. Yang, J. Xiao, *J. Mol. Catal. A Chem.* **2012**, *357*, 133–140.
- [161] X. Wu, J. Xiao, Hydrogenation and Transfer Hydrogenation in Water. In *Metal-Catalyzed Reactions in Water*, 1st ed.; Wiley-VCH, Weinheim, Germany, **2013**, 173–242
- [162] F. Schwizer, V. Köhler, M. Dürrenberger, L. Knörr, T. R. Ward, *ACS Catal.* **2013**, *3*, 1752–1755.
- [163] V. Muñoz Robles, P. Vidossich, A. Lledós, T. R. Ward, J.-D. Maréchal, *ACS Catal.* **2014**, *4*, 833–842.
- [164] V. M. Robles, M. Dürrenberger, T. Heinisch, A. Lledós, T. Schirmer, T. R. Ward, J.-D. Maréchal, *J. Am. Chem. Soc.* **2014**, *136*, 15676–15683.
- [165] T. Quinto, F. Schwizer, J. M. Zimbron, A. Morina, V. Köhler, T. R. Ward, *ChemCatChem* **2014**, *6*, 1010–1014.
- [166] Z. Liu, V. Lebrun, T. Kitanosono, H. Mallin, V. Köhler, D. Häussinger, D. Hilvert, S. Kobayashi, T. R. Ward, *Angew. Chem. Int. Ed.* **2016**, *128*, 11759–11762.
- [167] V. Lebrun, *Chim. Int. J. Chem.* **2017**, *71*, 199–201.

CHAPTER II:

GENETIC OPTIMIZATION OF ARMS

2.1 INTRODUCTION

The immense diversity of natural biocatalysts originates from the activity of ancestral enzymes, whose performance has been optimized by natural evolution over the course of millions of years.¹⁶⁸ Consisting of recursive cycles of mutagenesis and selection followed by amplification of the “fittest”, evolution represents the driving force of nature and ensures that organisms can adapt over generations to the ever-changing conditions of their environment.

To mimic natural evolution on a much shorter time scale and in a laboratory set-up, a step-wise procedure of directed evolution¹⁶⁹⁻¹⁷⁷ can be implemented for accelerated enzyme discovery. This Darwinian method relies on repeated cycles of mutagenesis combined with high throughput screening (HTS) techniques for activity and selectivity evaluation.

As a starting point, a protein with a pre-existing activity is often used, although the activity can be also implemented into an existing active site or by *de novo* design.^{178,179} As an alternative to install a non-natural reactivity, utilization of a low promiscuous activity of a given enzyme is also possible.¹⁸⁰

The gene encoding the starting protein is subjected to mutagenesis and the resulting DNA library is translated into corresponding mutant variants. After the first round of mutagenesis, the genetically modified gene of the best mutant, i.e. displaying the best attributes that were screened for, is subjected to another round of mutation and screening (Figure 4). This process is repeated until the desired degree of stability (thermal¹⁸¹, oxidative^{182,183} or general robustness³⁸), solubility,^{184,185} organic solvent¹⁷⁰ and alkaline

tolerance,¹⁸⁶ activity or selectivity is achieved and allows for either altering already existing features, or for engineering new functions.¹⁸⁷⁻¹⁹¹

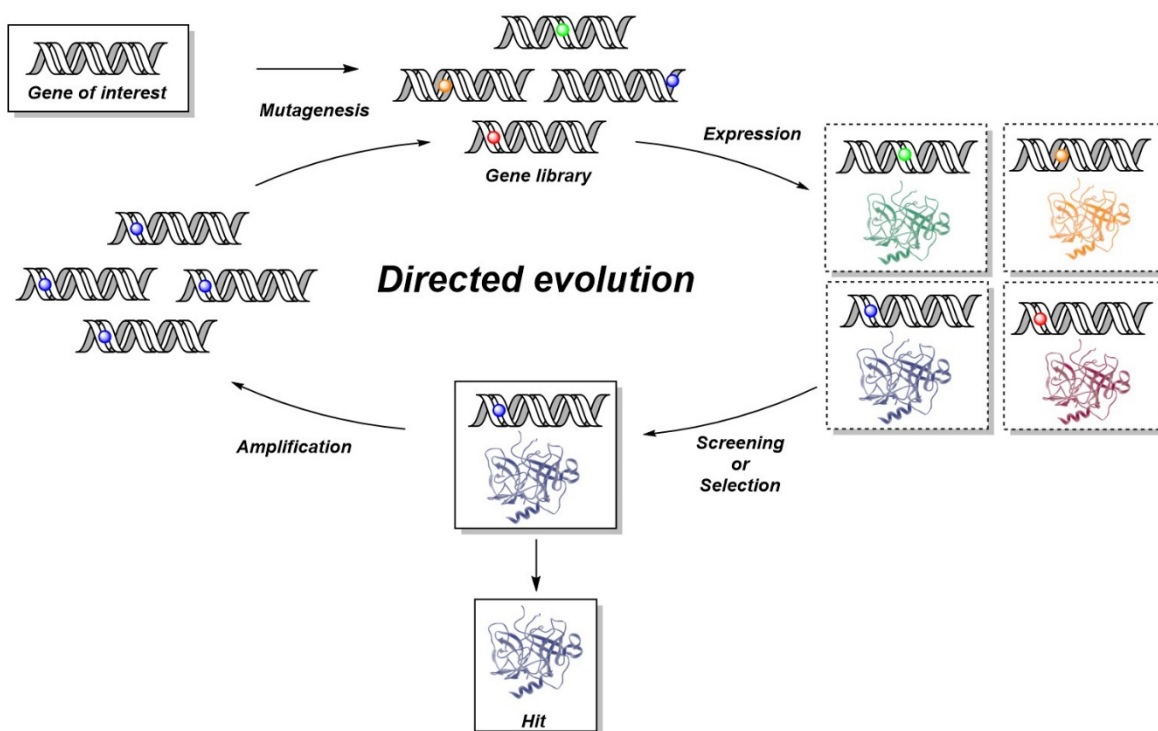


Figure 4. Strategy for directed evolution of enzymes.

In principle, no structural information of the protein is required for directed evolution. Alternatively, relying on rational design creates informed libraries of mutant protein variants, which contain targeted mutations emerging from the X-ray structure of the starting protein, phylogenetics, reaction mechanism, or computational modelling. This structure-guided^{192,193} approach to directed evolution, i.e. designed evolution,¹⁹⁴ helps to overcome the searchable-size library limitation.

The genetic diversity can be generated by various methods (Figure 5):¹⁷⁶

- (i) Focused libraries target specific enzyme sites that are expected to have an impact on the catalytic activity, protein folding, or stabilization.^{195,196} This method widens the possibility that the produced mutant library will contain improved variants. Since simultaneous saturation of multiple positions requires excessive screening, a defined selection of amino acid residues to be introduced as mutations can be

implemented.¹⁹⁷ Another popular semi-rational design is consensus protein design, which introduces consensus mutations identified from phylogenetic analyses.¹⁹⁸

- (ii) Random mutagenesis¹⁹⁹⁻²⁰³ targets the entire gene, allowing for introducing mutations distant from the active site. These changes in the protein structure might influence the protein dynamics, allosteric binding or the catalytic activity. The first error prone polymerase chains reaction (epPCR) was first described in 1989.²⁰² The technique relies on the low fidelity of DNA polymerases. Under certain conditions, single-point mutations can be introduced into the gene of interest. Moreover, increasing the manganese concentration reduces the base-pair fidelity and allows for mutation rate acceleration to 10^{-4} - 10^{-3} per replicated base.²⁰³
- (iii) DNA shuffling, originally described in 1994,²⁰⁴ utilizes diversification by homologous recombination of DNA fragments. This promising method creates large libraries of variants with swapped genetic information and is performed by means of PCR without primers.^{205, 206}

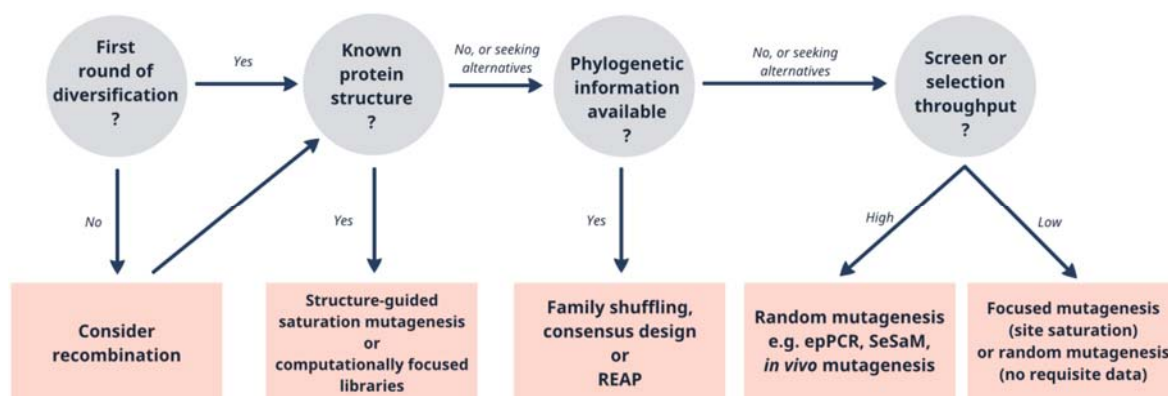


Figure 5. Decision-tree for selecting the diversification strategy.¹⁷⁶

2.2 DIRECTED EVOLUTION OF ARMS

Since ArMs comprise of an organometallic catalyst and a biomolecule, they bear the potential to be optimized by genetic means, either by using random mutagenesis²⁰⁷⁻²¹¹ or rational design.^{67,194, 210-212} Structure-guided directed evolution is based on the structure of the apo-bioscaffold. Introducing mutations within the secondary coordination sphere has

been shown to have a striking impact on the activity, selectivity, and robustness of the resulting hybrid catalysts. Moreover, the mutated variants have the potential to achieve efficiencies close to those of naturally evolved enzymes.^{213, 214}

One of the limitations of directed evolution of enzymes is that with an increasing library size, the screening step becomes excessive. Multiple high-throughput assays exist,²¹⁵ but their applicability remains limited. In an ideal case, the expressed library of mutant enzyme variants could be screened directly *in vivo* in a high-throughput fashion, i.e. bypassing the time-consuming protein-purification step. In the case of an enantioselective ArM, the product of the reaction could ideally be analyzed by means of GC or LC with a chiral stationary phase.

2.3 CELLULAR MATRIX LIMITATION

The introduction of a synthetic cofactor containing a transition metal complicates the directed evolution of the resulting hybrid catalysts by multiple ways. First, the activity arising from the presence of the free cofactor should be minimized. This can be achieved either by a time-consuming protein purification, or by measuring the concentration of the free cofactor binding sites. In the case of ArMs based on the biot-Sav technology, a simple spectrophotometric assay using the large decrease in extinction coefficient of biotin-4-fluorescein (B4F) after binding to Sav.²¹⁶

Secondly, the activity of the corresponding metal cofactor has to be retained even in the context of synthetic biology. For the directed evolution of a transition metal containing ArM, this represents a major bottleneck, as the activity of the metal cofactor is hindered by the cellular constitution of the expression model (Table 4).²¹⁷

Table 4. Selection of intracellular metabolite concentrations in exponentially growing *E. coli* fed with glucose.²¹⁷

Metabolite	Concentration [mM]	Metabolite	Concentration [mM]
Glutamate	96	UTP	8.3
Glutathione	17	GTP	4.9
Fructose-1.6-bisphosphate	15	dTTP	4.6
ATP	9.6	Aspartate	4.2
UDP-N-acetylglucosamine	9.2	NAD ⁺	2.6
Hexose	8.8	Glutathione disulfide	2.4

Glutathione (GSH) is a tripeptide consisting of glutamic acid, cysteine, and glycine (γ -glutamyl-cysteinyl-glycine). This most abundant cytosolic thiol²¹⁷ acts as a single electron donor capable of scavenging a wide variety of free radicals, thereby playing a role in cell signaling and non-enzymatic antioxidant protection (i.e. redox buffer).²¹⁸ In the context of performing catalysis with soft transition metals, GSH represents a detrimental agent, as it easily coordinates to both soft metal ions.^{218,219}

Catalysis in a cellular matrix can be achieved by using purified proteins, by mechanically shielding the catalyst in a protective layer,¹⁰¹ by performing catalysis in the periplasm of *E. coli*,²¹¹ or by utilizing various GSH neutralizing agents.²²⁰ As the presence of GHS, but not glutathione disulfide (GSSG) inhibits the activity of the [Cp*Ir(biot-*p*-L)Cl] and the resulting ATHases, a pre-incubation step with a GSH-oxidizing agent or a Micheal acceptor is necessary, should the catalysis be performed in the presence of cellular debris. As can be appreciated from the data summarized in Figure 6, pre-incubation of *E. coli* cell free extracts (CFE) or cell lysates with 1,1'-azobis(N, N-dimethylformamide) (diamide) proved to be most efficient both in terms of activity and selectivity.²²⁰ Treatment with Cu^{II} also proved to be efficient.²²¹

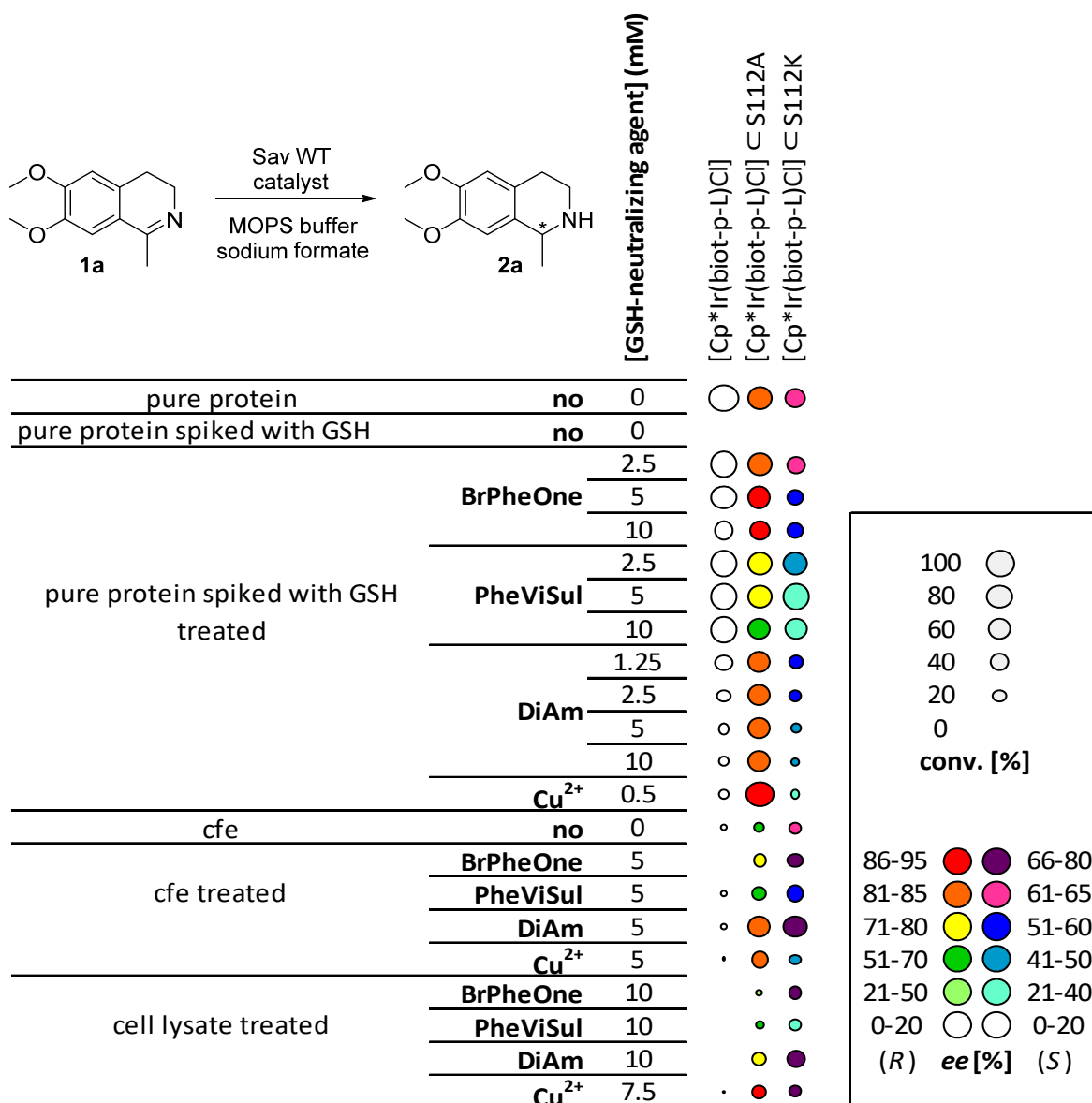


Figure 6. Bubble-chart representation of the activity of ATHase in the presence of various GSH neutralizing agents.²²⁰

Given the fact that expression of Sav in *Escherichia coli* (*E. coli*) can be performed in small quantities of medium²²² without the need of manual induction of Sav expression,²²³ the ease of parallelization enabled the use of diamide for the implementation of a directed evolution strategy of ATHases.

2.4 LIBRARY DESIGN AND SCREENING PROTOCOL FOR ARTIFICIAL METALLOENZYMES BASED ON THE BIOTIN-STREPTAVIDIN TECHNOLOGY

*The following section has been published in
Nat. Protoc. 2016, 11, 835–852,
doi: 10.1038/nprot.2016.019*

Library design and screening protocol for artificial metalloenzymes based on the biotin-streptavidin technology

Hendrik Mallin, Martina Hesticová, Raphael Reuter and Thomas R. Ward*

Department of Chemistry, University of Basel, Spitalstrasse 51, CH-4056 Basel, Switzerland. E-mail: thomas.ward@unibas.ch

KEYWORDS: biotin-streptavidin technology, artificial metalloenzymes, chemogenetic optimization, hybrid catalyst, protein engineering

2.4.1 ABSTRACT

ArMs based on the incorporation of a biotinylated metal cofactor within Sav combine attractive features of both homogeneous and enzymatic catalysts. To speed up their optimization, we present a streamlined protocol for the design, expression, partial purification and screening of Sav libraries. Twenty-eight positions have been subjected to mutagenesis to yield 335 Sav isoforms, which can be expressed in 24-deep-well plates using autoinduction medium. The resulting CFEs typically contain >1 mg of soluble Sav. Two straightforward alternatives are presented, which allow the screening of ArMs using CFEs containing Sav. To produce an artificial transfer hydrogenase, Sav is coupled to a biotinylated three-legged iridium piano stool complex Cp*Ir(Biot-*p*-L)Cl (the cofactor). To screen Sav variants for this application, you would determine the number of free binding sites, treat them with diamide, incubate them with the cofactor and then perform the reaction with your test compound (the example used in this protocol is 1-phenyl-3,4-dihydroisoquinoline). This process takes 20 d. If you want to perform metathesis reactions, Sav is coupled to a biotinylated second-generation Grubbs-Hoveyda catalyst. In this application, it is best to first immobilize Sav on Sepharose-*iminobiotin* beads and then perform washing steps. Elution from the beads is achieved in an acidic reaction buffer before incubation with the cofactor. Catalysis using your test compound (in this protocol, 2-(4-(*N,N*-diallylsulfamoyl)phenyl)-*N,N,N*-trimethylethan-1-aminium iodide) is performed using the formed metalloenzyme. Screening using this approach takes 19 d.

2.4.2 INTRODUCTION

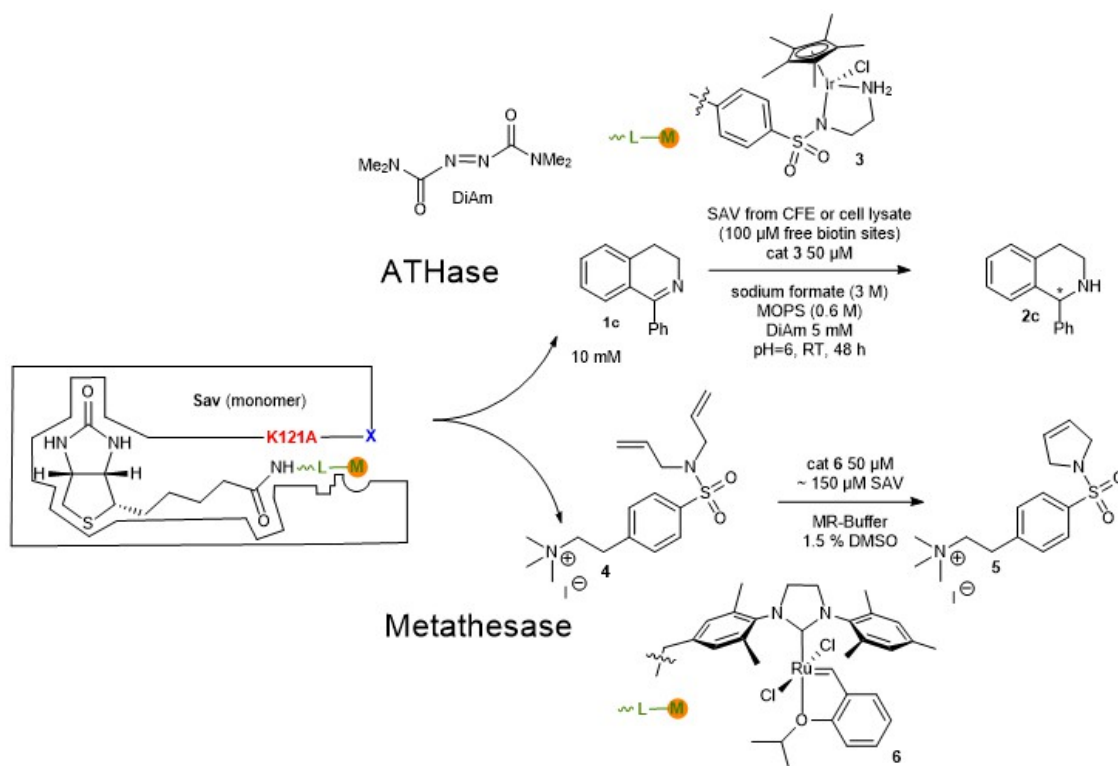
In recent years, artificial metalloenzymes have attracted increasing attention as an alternative to homogenous catalysts (such as Rh-based hydrogenation- or Os-based dihydroxylation catalysts) and naturally occurring enzymes (including variants produced by standard mutations).^{226, 48} Such hybrid catalysts result from the incorporation of an artificial cofactor within a host protein and combine attractive features of both systems. Several anchoring strategies have been pursued to ensure localization of the metal moiety within a well-defined protein environment: dative, covalent and supramolecular.⁴³

In this context, the biot-Sav system has proven particularly versatile for the creation of ArMs.⁷² Indeed, the hemispheric biotin-binding vestibule, which consists of loops between sheets $\beta_{3,4}$, $\beta_{4,5}$, $\beta_{5,6}$ and $\beta_{7,8}$, is ideally sized to harbor a biotinylated cofactor and its substrate. Inspired by a visionary publication by Wilson and Whitesides,⁴⁷ eight catalytic transformations have been implemented relying on ArMs derived from the biotin-(strept)avidin technology which include hydrogenation,^{47, 227, 93, 228} transfer-hydrogenation (of ketones, imines and enones),⁹⁶ allylic alkylation,¹⁰⁹ C–H activation,¹⁰⁴ metathesis,¹¹¹ sulfoxidation,^{107, 108} dihydroxylation¹⁰⁵ and alcohol oxidation.¹⁰⁶ Although initial studies have relied on avidin as a host protein,^{47,227} Sav is preferred in most cases thanks to its straightforward expression in *E. coli*. To minimize laborious steps, mature Sav is preferred over core Sav as the latter is expressed as inclusion bodies.^{229, 230} The biotin-streptavidin technology has proven to be a versatile tool for the implementation of ArMs, offering the possibility to implement abiotic reactions within a biological environment. In this context, olefin metathesis (Metathesase) is particularly attractive as it is a bio-orthogonal reaction²³¹ which has no equivalent in nature. Recently, it was shown that an ATHase based on the biotin-streptavidin technology could be combined with enzymes in cascades by preventing mutual inactivation.⁹⁷ Compared to other abiotic cofactor anchoring strategies,⁴³

supramolecular anchoring allows faster screening as the ArMs are generated quantitatively and thus require no additional reagents, coupling steps or purification.

Sav is a highly versatile protein often referred to as “molecular velcro”. In the past 40 years, it has found numerous applications in a variety of fields including protein purification, immobilization, interaction studies and diagnostic applications.^{37, 82-84} The protocol described herein may be applicable to any application of the biotin-streptavidin technology requiring fine-tuning of Sav properties.

A chemogenetic optimization strategy opens up the possibility to rapidly improve the catalytic performance of ArMs based on the biotin-streptavidin technology (Scheme 6).



Scheme 6. Model reactions and structures of the ATHase cofactor [Cp*Ir(biot-*p*-L)Cl] **3** and the metathesase cofactor **6** (for a synthesis overview see Appendix A Schemes A2 and A3). Upon incorporation of the biotinylated cofactor within Sav, an artificial transfer hydrogenase (see Step 28A) and an artificial metathesase (see Step 28B) are formed. The reaction conditions for the hydrogenation of **1c** and for the ring-closing metathesis reaction of 2-(4-(*N,N*-diallylsulfamoyl)phenyl)-*N,N,N*-trimethylethan-1-aminium iodide **4** are displayed. MR buffer, metathesase reaction buffer; cat., catalyst.

Systematic variation of the biotinylated spacer–ligand moiety can be combined with genetic modification of Sav to afford ArMs with improved characteristics (kinetics, stability, TON and selectivity). In view of the requirement of purified Sav samples to ensure activity of the abiotic metal cofactor, optimization efforts thus far have been limited to large scale expression and purified Sav mutant libraries.^{37, 95} Thus far, mostly close lying amino acid residues have been subjected to saturation mutagenesis. An attractive feature of this strategy is the possibility to exploit the same Sav libraries for a variety of ArMs.

To fully capitalize on the potential of ArMs based on the biotin-streptavidin technology, a streamlined screening protocol relying on CFE or partially purified Sav is highly desirable (Figure 7). Indeed, thus far, screening has been performed on purified Sav samples, thus seriously limiting the number of mutants accessible. The protocol described herein allows to screen hundreds of Sav mutants within a reasonable time frame using CFE. With this goal in mind, we selected a twenty-four well-plate based screening assay to streamline the entire screening process, thus significantly increasing the throughput.

2.4.3 EXPERIMENTAL DESIGN

2.4.3.1 OVERVIEW

Herein, we detail a protocol for the creation of Sav isoforms, their functional overexpression, the generation of ArMs and two complementary screening methods (Figure 7). The protocol is broken down in the following sections: (i) Basic primer design for QuikChange mutagenesis and generation of the Sav library (mutagenesis section); (ii) recombinant protein expression in 24 deep well plate format from the glycerol stock culture to the final CFE containing the overexpressed soluble Sav (library expression section); (iii) the determination of the free biotin binding sites present in the CFE using B4F (Fig. 7, Step 28A); and (iv) the optimization of the performance of ArMs for an artificial ATHase (Step 28A) and a metathesase (Step 28B) using CFE relying on two partial Sav purification

schemes. For the ATHase, a diamide treatment is used to neutralize the deleterious GSH,²²² and for the metathesase a reversible immobilization on a Sepharose-iminobiotin resin is performed (Fig. 7, Step 28B).^{111, 232}

2.4.3.2 LIBRARY DESIGN

Precise primers are designed for each mutation. In the present context, this strategy offers several advantages: (i) the introduced amino acid can be chosen freely (i.e., not dictated by the choice of degenerate primers),²³³ (ii) the screening effort is reduced as no oversampling is required, and (iii) as each well contains a defined Sav mutant, structure-activity relationships can be obtained for each experiment. For this purpose, a protocol for using site-directed mutagenesis²³⁴ in 96 well format is implemented. Based on previous screening efforts with a variety of artificial metalloenzymes, mature Sav²²⁹ bearing an alanine mutation at position 121 as starting isoform for the library generation is selected. The sequence of pET-24a SavK121A is codon optimized to reduce the G/C content from 68 %²²⁹ to 52 %. This significantly improves mutagenesis success rate without influencing Sav expression levels.

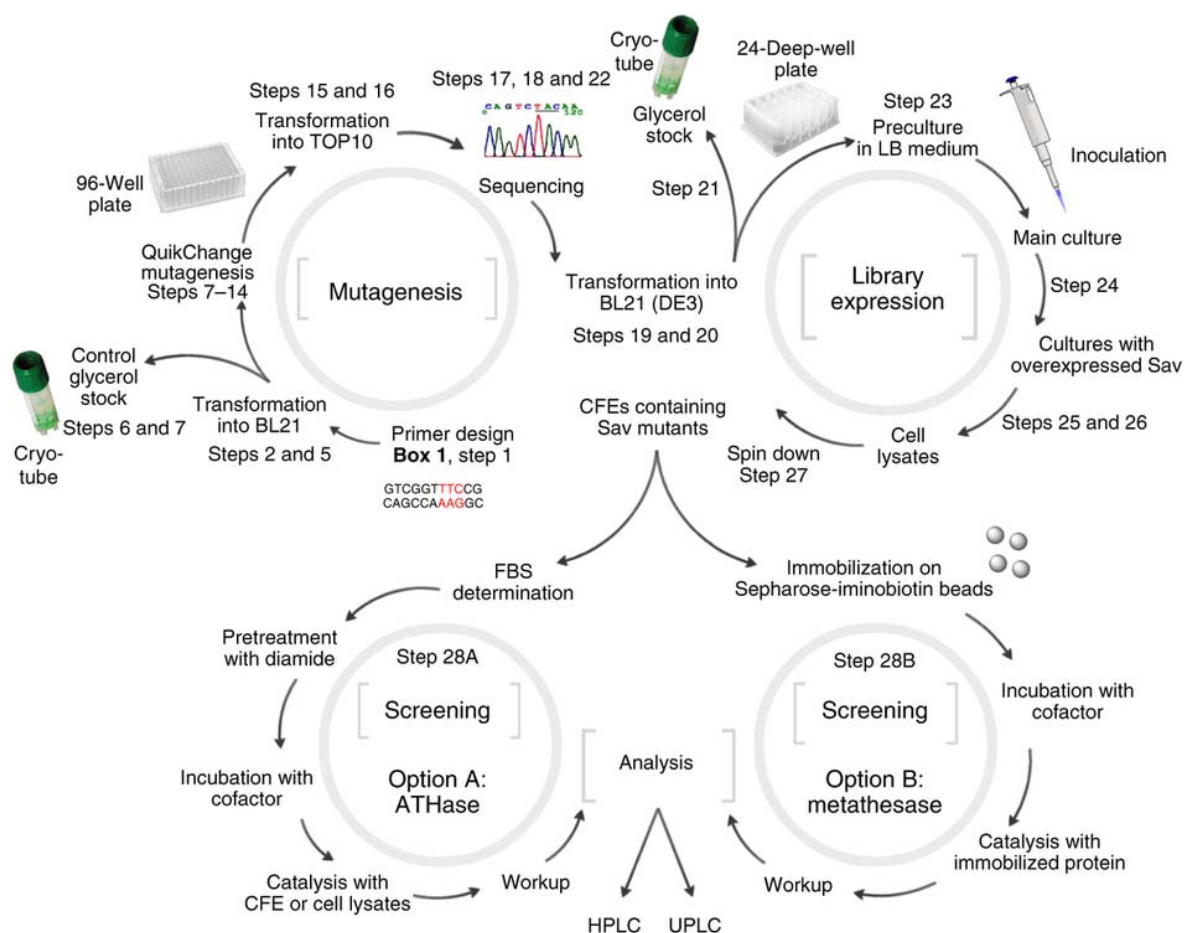


Figure 7. Workflow used in this protocol. Mutagenesis, expression and screening for the identification of genetically engineered ArMs variants based on the biotin-Sav technology. Step numbers are listed according to the PROCEDURE.

The positions for mutagenesis are selected by identifying residues that lie within a 15 Å radius around the averaged position of the biotinylated metal moiety bound to Sav (Protein Data Bank (PDB) codes: 2QCB, 2WPU, 3PK2, 4GJS, 4GJV).^{95, 232, 235, 64} This led to the identification of 21 amino acid positions, namely G48, A50, A65, D67, S69, R84, N85, A86, H87, L110, T111, S112, G113, T114, T115, A117, N118, A119, S122, T123, L124. By examination of the X-ray structures, four further amino acid positions (R53, P64, G68, E116) lying close to mutated areas, one (G98) within the backbone of loops between sheets $\beta_{5,6}$ and $\beta_{7,8}$ and two (K144, N150) within the non-resolved, flexible C-termini from mature Sav are selected. In total, 28 positions are subjected to mutagenesis (Figure 8).

Unique primers are designed for each Sav mutant according to the guidelines summarized in Box 1.²³⁶ The following amino acids are substituted at the above positions in the template Sav K121A sequence (Figure 9): A, V, L, D, E, Q, K, H, M, Y, S, P (or N if one of the targeted mutation is present at this position). It should be noted that the primer library used for the first round of mutagenesis may be used for the second round. However, this requires that the position to be mutated is distant enough from the mutation position from the previous round (typically six amino acids). If this is not the case, new primers need to be designed for use in the second round of mutagenesis. For the library production and the Sav expression, the *E. coli* strains TOP10 and BL21 (DE3) are used respectively. The TOP10 strain is versatile for the site-directed mutagenesis steps, whereas the BL21 (DE3) strain is very efficient for the production of soluble Sav.²²⁹

2.4.3.3 EXPRESSION OF SAV MUTANTS IN 24 WELL DEEP PLATES

To maximize the amounts of soluble Sav in small scale expression (i.e., > 1 mg Sav, corresponding to 61 nmol free binding sites (Sav FBS) or 15 nmol tetrameric Sav in 6 ml medium), a simple and robust protocol based on the Lac-operon induction system is applied. For this purpose, the ZYP-5052 medium is used. It contains defined amounts of glucose and lactose in the culture medium.²²³ Upon using this medium, the recombinant protein's expression is induced by lactose in the exponential growth phase once glucose is consumed, thus requiring no manual induction by IPTG. The protein production is automatically turned on in each well at nearly the same optical density (OD). Relying on this simple and reproducible procedure, good yields of soluble and functional Sav are obtained within 24 h. Typically, final ODs of 6 – 7 are reached for each culture. A slight modification of the ZYP-5052 media is required for a 24 h expression: compared to the original recipe, the amount of carbohydrates (lactose and glucose) and the MgSO₄ concentration are doubled. To improve aeration within the wells, a pipette tip (0.1 to 10 µl) is added. This leads to an increase in OD and Sav yields. Following this procedure, Sav yields > 1 mg (61 nmol Sav FBS) per

well are consistently obtained. This is sufficient to perform one to two ArM screening experiments. Slightly higher Sav yields can be achieved if the expression time is increased to 48 h using the same culture volume. In this case, the original ZYP-5052 media and no pipette tip are required.

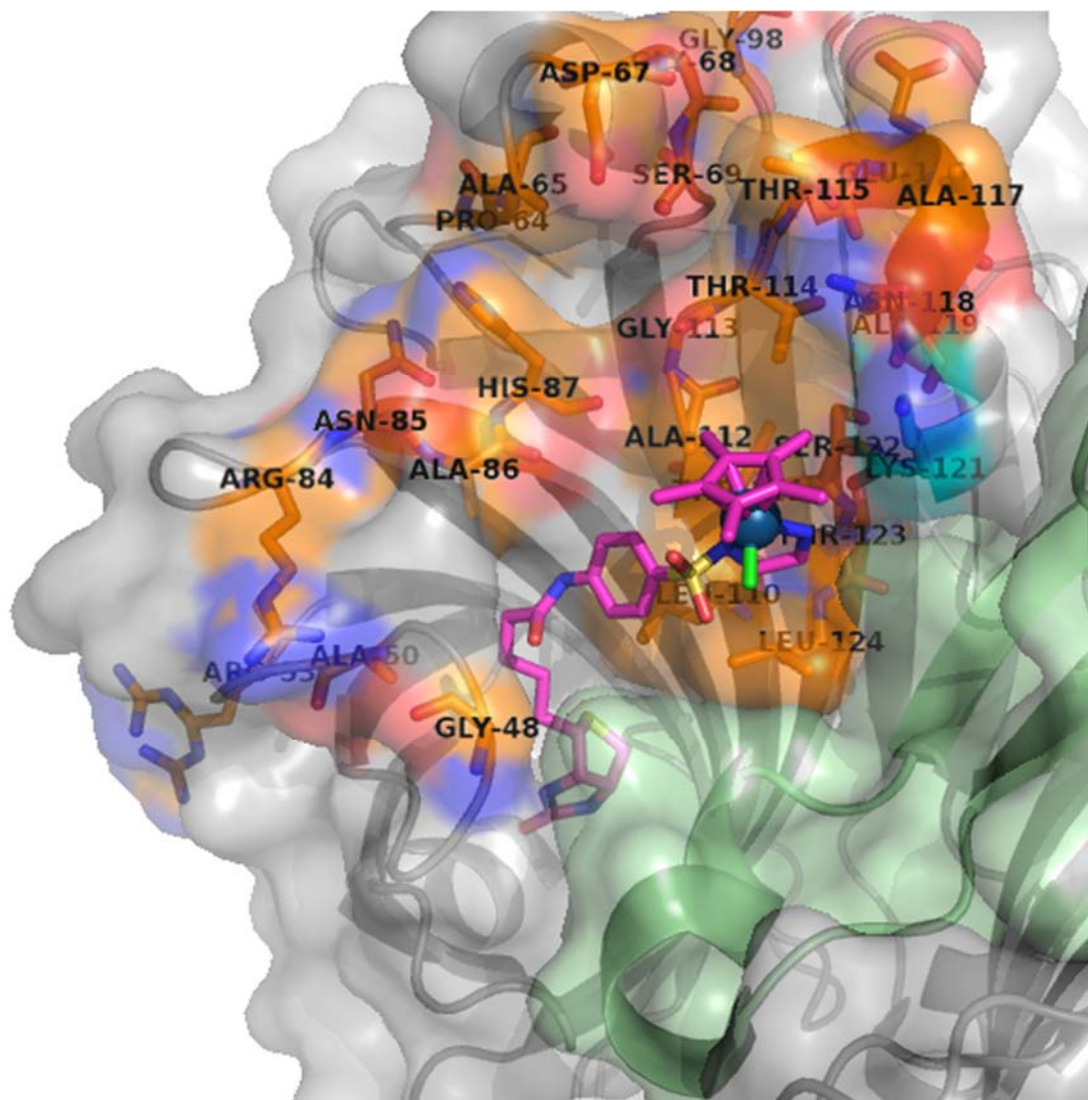


Figure 8. Close-up view of the X-ray structure of an artificial transfer hydrogenase based on the biotin-Sav technology. For clarity, only one cofactor [Cp*Ir(Biot-p-L)Cl] (compound **3**) is displayed (as stick), and Sav (mutant S112A, displayed as surface/cartoon representation). The positions selected for mutagenesis are highlighted in orange and residue K121 is highlighted in cyan (PDB code: 3PK2).

A technical issue concerns the necessary laboratory equipment. Although the protocol described herein may be adapted to culture tubes, we strongly favor a 24-well plate format. For this purpose, we recommend shaking-flask incubators that are equipped with sticky pads. In our experience, the 24-well plates can be conveniently fixed and are held securely up to at least 250-rpm shaking speed. This enables the cultivation of many plates in parallel in a single incubator. To save time, a plate centrifuge is recommended to harvest and to clarify the supernatants. In our experience, adapting this protocol to culture tubes is less efficient and unpractical. Indeed, we routinely observe lower cell densities, leading to higher deviations in catalysis. Additionally, the handling of tubes versus 24-well plates is more time consuming.



Gratifyingly, upon cultivating ninety replicates in four 24-well expression plates, an 11% (Step 28A) and a 9% (Step 28B) s.d. in conversion for the ArM-catalyzed reaction is obtained, highlighting the excellent reproducibility of the protein expression protocol using this format.

2.4.3.4 DETERMINATION OF SAV FREE BINDING SITES IN CFE

Previous experience suggests that the concentration of the biotinylated cofactor (50 μM) should not exceed half of the Sav FBS (100 μM). Although each ArM behaves differently, it has been found that saturating all the biotin-binding sites with a metal cofactor may lead to significant erosion of an ATHase's performance.¹⁶⁴ To determine the Sav FBS concentration within the CFE, a modified assay using B4F is implemented.^{237, 216} Gruber and colleagues²³⁷ and Mascotti and Waner²¹⁶ demonstrated that B4F can be used for the Sav FBS determination in CFE using either fluorescence (excitation 485 nm; emission 520 nm) or absorbance at 493 nm. We adapted this assay to a 96-well-plate format measuring simultaneously the drop in absorption and in fluorescence of B4F in the presence of the Sav CFE. With this assay, multiple samples can be handled in parallel. The biotinylated fluorophore B4F (40 μM) is added to each Sav-containing well and the resulting decrease in

absorbance and fluorescence are determined. Depending on the expression levels, 30 – 60 μ l CFE is required to determine the Sav FBS concentration in triplicate. The single point determination yields a 10 – 20 % error margin. However, when evaluating Sav FBS < 10 μ M the error increases substantially. Importantly, the pET-24a empty vector CFE background must be subtracted from both the absorbance and fluorescence determinations.

(b)	(a)	A	V	L	D	E	Q	K	H	M	Y	S	N	P	G	R	T	C	W	I	F	# Mutants
48																						13
50																						12
53																						12
64																						12
65																						12
67																						11
68																						12
69																						12
84																						12
85																						12
86																						12
87																						12
98																						12
110																						12
111																						12
112																						12
113																						12
114																						12
115																						12
116																						12
117																						11
118																						12
119																						12
122																						12
123																						12
124																						12
144																						12
150																						12
																						Σ 335

 Not targeted
 Wild-type position



 Mutant obtained
 Mutagenesis failed

Figure 9. Summary of designed mutants. Matrix of Sav isoforms designed and produced for screening purposes. As template for mutagenesis, the mutant Sav K121A is used. (a) amino acids (b) position in Sav template.

2.4.3.5 ARTIFICIAL TRANSFER HYDROGENASE FOR THE REDUCTION OF CYCLIC IMINES

Prochiral cyclic imines are versatile substrates for the production of enantioenriched amines. We have previously demonstrated that artificial transfer hydrogenases resulting

from the incorporation of a biotinylated pnanostool complex within Sav are promising hybrid catalysts for this transformation (Scheme 6, Route A). The biotinylated three-legged iridium pnanostool complex **3** was synthesized according to a published procedure²³⁸ and added to Sav isoforms to afford an ATHase. Unfortunately, the recombinant Sav isoforms overexpressed in *E. coli* need to be purified by affinity chromatography as traces of glutathione, present in cellular debris,²¹⁷ irreversibly poison the precious metal cofactor. To circumvent this severe bottleneck, we recently identified that diamide neutralizes the dendrimental effect of GSH on Compound **3** by oxidizing it to GSSG.²²² This finding allows us to screen samples of Sav contained in *E. coli* CFEs and cell lysates.

2.4.3.6 CATALYSIS WITH IMMOBILIZED SAV-MUTANTS USING IMINOBIO TIN-SEPHAROSE BEADS

As a model reaction with Sav using iminobiotin-sepharose beads as a rapid purification tool,²³² the ring closing metathesis of olefins was selected (Scheme 6, Route B). An artificial metathesase based on the biotin-streptavidin technology was previously reported by us.¹¹¹ As the ring-closing reaction using diallylsulfonamides works best at pH 4, an acetate buffer is selected as reaction medium. At this low pH, iminobiotin is protonated and the immobilized Sav is released from the iminobiotin-sepharose beads. As the metathesis cofactor **6**²³⁹ bears a biotin anchor, it binds tightly to Sav at this pH and catalyzes the ring-closing metathesis of substrate **4** to form product **5**.

2.4.3.7 LIMITATIONS

The main limitation of this protocol is the marked decrease in activity and reproducibility of ArMS when the Sav FBS concentration is low. For both reactions presented herein, cell cultures, with Sav FBS > 100 μ M should be targeted. Indeed, past experience with ATHase of cyclic imines reveals that highly reproducible results require 3 M sodium formate in 0.6 M MOPS at pH 6 and > 50 μ M Sav FBS. The limited solubility of both formate and MOPS does not allow preparation of more than 2x concentrated stock buffer solutions. In contrast, the metathesase performs well down to 10 μ M FBS Sav on

purified Sav samples. However, the immobilization protocol requires $> 100 \mu\text{M}$ Sav FBS. Indeed, Sav FBS in the CFE must be present in excess compared to the loading capacity of the iminobiotin-sepharose beads.

As illustrated by the ATHase and metathesase, each ArM behaves differently and exploratory screens should be performed to identify the most suitable screening strategy. For example, diamide treatment is not suitable for the metathesase as the ruthenium cofactor is inactivated by this reagent. Instead, iminobiotin sepharose beads are highly versatile for the metathesase as the Sav is released from the beads at pH 4 allowing to perform catalysis in solution. In our experience, the iminobiotin beads immobilization (Route B) is more versatile than diamide treatment (Route A). However, for reactions requiring neutral or basic conditions, an additional buffer-exchange step is necessary. For this purpose, the eluted fraction containing Sav at pH 4 can be back-titrated to the desired pH by the addition of concentrated base or a high molarity reaction buffer.

Concerning evolution strategies, a combination of synergistic mutations may be envisaged.²³³ In order to be able to re-use the initial design primer library, it is important to ensure that the fixed mutation (first mutation) does not overlap with the primer pair used for the mutation to be introduced (second mutation). For this purpose, the second mutation should be more than six amino acids away from first mutation. If this is not the case, a new set of primers for the second mutation needs to be designed and used.

2.4.4 TROUBLESHOOTING

Troubleshooting advice can be found in Table 5. For mutagenesis, Sav expression and Sav FBS, the following guidance applies:

After preparation of a fresh stock of the template plasmid it is recommended to validate it for the right Sav sequence by sequencing prior to mutagenesis. Prepare a positive control of the PCR by using a primer pair (Appendix A Table 1) which will give you a

specific amplification. If, after site directed mutagenesis, no amplified vector is visible on the gel, reduce the annealing temperature. If several amplified fragments are visible and no mutant is obtained, increase the annealing temperature. The transformation efficiency of competent cells can decrease during storage due to their low viability. It is thus suggested to always use a positive-control transformation using the pUC19 vector. Due to the lower transformation efficiency of the BL21 (DE3), the transformation into this strain is less effective in 24 deep well plates. If no colonies are obtained, a transformation in 1.5 ml tubes can lead to fewer colony-forming units (cfu).

This Sav expression protocol is highly robust, but reduced Sav yields can exceptionally be obtained with no apparent reason. When this is the case, it is recommended to perform a new transformation into BL21 (DE3) and to prepare a new glycerol stock resulting from an overnight culture inoculated by a single colony. During expression of the Sav library, it is recommended to include controls on each 24 deep well plate to validate the screening for hits and background. For this purpose, wild-type Sav, SavK121A and pET-24a empty vector should be included in each 24 deep well plate.

The B4F-absorption-fluorescence assay has a limited precision window ranging from 10 to 40 μM Sav FBS. It is thus recommend to re-determine data for samples with Sav FBS < 10 μM or Sav FBS > 35 μM after having adapted the concentration. It is important to subtract the background spectrum for the pET-24a empty vector (both for the absorbance and fluorescence determination). As residual biotin and biotinylated *E. coli* proteins may be present in cell lysates, the B4F assay may underestimate the [Sav]: it is, however highly reliable for the Sav FBS determination, which is the relevant concentration for catalysis with ArMs.

Table 5. Troubleshooting table.

Step	Problem	Possible reason	Possible solution
5	No colonies	Transformation failed	<p>Positive control with no colonies: prepare new competent cells (Box 2)</p> <p>Positive control with colonies: band on gel: repeat transformation of mutant, plate all, perform transformation in +1.5-ml tubes (especially for <i>E. coli</i> BL21 (DE3) because of the naturally lower transformation efficiency of the strain compared with <i>E. coli</i> TOP10)</p>
14	No band present on agarose gel	Composition of PCR mixture is wrong	Include a positive control using a gene-specific primer (Supplementary table 1)
		Primers are annealing during PCR	Test a lower annealing temperature (>50 °C)
	There are multiple nonspecific bands on agarose gel	Primer binds nonspecifically	<p>Vary the DMSO content</p> <p>Re-design primers (Box 1)</p> <p>Proceed with transformation; often colonies carry the right mutation if one of the fragments has the right vector size</p> <p>Perform PCR at higher annealing temperatures (up to 65 °C)</p> <p>Re-design primers (Box 1)</p>
17	Plasmid preparation has low yield	Low OD in overnight culture; pH of LB is not adjusted (important for kanamycin resistance)	<p>Check the pH of LB medium (>7.25) and increase the culture time</p> <p>Elute in 2 x 15 µl of elution buffer</p> <p>Prepare 6 ml of overnight culture in a 2-deep-well plate</p>
18	Wild-type background	DpnI digestion failed/inefficient	<p>Use fresh DpnI and increase the digestion by 1 h</p> <p>Reduce the template amount in PCR to 0.1 ng µl⁻¹</p>
27	Reduced Sav yield	Viability of glycerol stock reduced	<p>New transformation into <i>E.coli</i> BL21 (DE3) and new glycerol stock</p> <p>Avoid thawing the glycerol stock solution; keep it on dry ice</p>

28A (xiv)	Possible formation of gel-like emulsion during work-up Protein layer during phase separation	Protein denaturation due to organic solvent, high protein content Sav precipitates due to organic solvent	Spin down the emulsion in a small centrifuge before separating the phases Spin down the emulsion in a small centrifuge before separating the phases (Route A: Step xiv.)
28B (i)	Beads cannot be taken up by Eppendorf pipette	Suspension is too thick	Make sure that the total volume of the bead suspension is 2x the volume of settled beads. Thoroughly shake suspension before adding the beads Use pipette tips with wider opening
28B (iv)	Catalyst stock solution turns brown	Catalyst slowly decomposes in pure DMSO	Directly use the catalyst after dissolving the aliquot in DMSO

2.4.5 ANTICIPATED RESULTS

Upon sequencing a single colony for each mutagenesis reaction, a coverage of 80-90% of the targeted Sav mutants was achieved following PCR and transformation in *E. coli* TOP10. This value is achieved by sequencing one colony for each mutant. If amplification is visible on the analytical agarose gel, sequencing an additional one or two colonies from the transformation plate leads to nearly complete coverage of all targeted Sav mutants. Following this protocol, 335 Sav mutants from the targeted 336 Sav mutants are obtained.

Comparable ODs and Sav yields are obtained for each well when using the ZYP-media expression protocol in 24 deep well plates. Routinely, ≥ 1 mg Sav (corresponding to 15 nmol tetrameric Sav or 240 μ M Sav FBS in 250 μ l) is obtained per well after 24 h using the modified ZYP and adding a pipette tip. Following this procedure, 250 μ l CFE can be obtained. This is sufficient to determine the Sav FBS and to perform two catalytic runs either for the ATHase or the metathesase reaction (100 μ M Sav FBS required). Upon increasing the expression time to 48 h, the Sav FBS typically increases by 40 %. For this purpose, no pipette tip should be added to the well and the standard ZYP media is recommended.

Both the absorption and the fluorescence Sav FBS single point determinations afford 10 to 20 % errors. This is perfectly acceptable for the screening procedure as catalysis is performed using twice the Sav FBS concentration vs. the biotinylated catalyst, thus ensuring quantitative binding of the latter to Sav. The standard curves either for absorbance or fluorescence display high linearity with a $R^2 = 0.95 - 0.99$ (Appendix A, Figure A7). Using this dilution, the CFE samples typically yield Sav FBS = 20 – 30 μM . For CFE of the empty pET-vector, the background absorption or fluorescence corresponds to 1 – 5 μM Sav FBS.

Because of the high affinity of biotinylated probes for Sav, the ATHase or Metathesase are immediately formed upon addition of the biotinylated catalyst to Sav isoforms. The success rate for catalysis depends on factors including activity, stability and expression level of the specific mutants. The excellent reproducibility of the protocol may allow to evaluate NNK libraries, as hits of different screening plates can be compared. The success rate for catalysis is improved thanks to the normalization of the FBS present in each sample prior to catalysis: Route A is normalized by the FBS determination and Route B by the specific binding capacity of the applied beads if Sav is present in excess in the CFE.

2.4.5.1 ARTIFICIAL TRANSFER HYDROGENASE (OPTION A)

The protocol allows highly reproducible preparation of cell lysates and corresponding CFEs containing the overexpressed Sav isoforms. Sav is produced in high concentrations, which allows to set up two catalysis experiments (200 μl final volume) from a 6 ml cell culture (corresponds to approx. 0.25 ml of cell lysate).

Preincubation of either cell lysates or CFEs for 2 h with 5 mM diamide, before addition of the transition metal catalyst, leads to the partial restoration of the activity of artificial metalloenzymes performed in the presence of purified Sav samples. Screening results from ATHase in the $[\text{Cp}^*\text{Ir}(\text{biot-}p\text{-L})\text{Cl}] \mathbf{3} \subset \text{K121A Sav}$ are summarized in Table 6. As can be appreciated, upon addition of diamide, the catalytic activity is partially restored for samples containing either cell lysates or CFEs.

Table 6. Expected results for the transfer hydrogenase (Step 28A).

Sav source	ATHase		
	ee [% (R)]	conv. [%]	TON
No protein	rac.	58	116
K121A purified protein	71	91	183
K121A CFE untreated	0	0	0
K121A CFE + DiAm	59	21	42
K121A cell lysate ^a untreated	0	0	0
K121A cell lysate ^a + DiAm	42	19	39
Empty vector CFE untreated	0	0	0
Empty vector CFE + DiAm	rac.	3	6
Empty vector cell lysate ^a untreated	0	0	0
Empty vector cell lysate ^a +DiAm	0	2	4

^a The use of cell lysates alleviates an additional clarification step. Nevertheless, CFE (clarified supernatants) are preferred because the number of background contaminants is significantly reduced.

2.4.5.2 RING-CLOSING OLEFIN METATHESIS (OPTION B)

CFEs and cell lysates contain unidentified catalyst poisons that inhibit ring closing metathesis on substrate **4**. Upon immobilization of Sav from CFEs on the iminobiotin-sepharose beads, impurities from the CFEs can be washed away, thus partially restoring metathesase activity. Duplicate measurements performed without protein, with Sav K121A mutant and pET-24a empty vector CFE typically yield the following results (Table 7).

Table 7. Expected results for the metathesis (Step 28B).

Sav source	Metathesase^a	
	conv. [%]	TON
No protein	19 ± 0.5	38 ± 0
K121A purified protein	33 ± 0.5	66 ± 1
Empty vector CFE untreated	0 ± 0	0 ± 0
Empty vector CFE bead-treated	5 ± 0.5	10 ± 1
SavK121A CFE untreated	0 ± 0	0 ± 0
SavK121A CFE bead-treated	9 ± 0.5	18 ± 1

^a average of duplicate measurements

2.4.6 ACKNOWLEDGEMENT

TRW thanks the Swiss National Science Foundation (grants 200020_162348 and the NCCR (National Centres of Competence in Research) Molecular Systems Engineering) and the Seventh Framework Programme Project METACODE (KBBE (Knowledge-Based BioEconomy), ‘Code-engineered new-to nature microbial cell factories for novel and safety enhanced bioproduction’) and the US National Institutes of Health (NIH; Grant GM050781) for generous support. MH thanks the SNI (Swiss nanoscience Institute) for a PhD scholarship. The authors provide the library free of charge upon request to academic institutions.

2.4.7 SUPPORTING INFORMATION

The full supporting information can be found in Appendix A.

2.4.8 AUTHOR CONTRIBUTIONS

General idea: Prof. Dr. Thomas R. Ward

Design of the mutant library, establishment of the expression protocol and the absorbance and the fluorescence plate assay: Dr. Hendrik Mallin

Library expression, screening of the streptavidin mutants and biotinylated metal complexes for transfer hydrogenation: Martina Hesticová

Screening of the streptavidin mutants and biotinylated metal complexes for ring closing metathesis: Dr. Raphael Reuter

Manuscript writing: All authors

2.5 DIRECTED EVOLUTION OF AN ARTIFICIAL IMINE REDUCTASE

*The following section has been published in
Angew. Chem. Int. Ed.. 2018, 130, 1881–1886,
doi: 10.1002/ange.201711016*

Directed Evolution of an Artificial Imine Reductase

Martina Hesticová^a, Tillman Heinisch^a, Lur Alonso-Cotchico^b, J.-D. Maréchal^{*b}, Pietro Vidossich^b, and Thomas R. Ward^{*a}

^aDepartment of Chemistry, University of Basel, Mattenstrasse 24a, BPR 1096, Basel, 4002, Switzerland. E-mail: thom-as.ward@unibas.ch

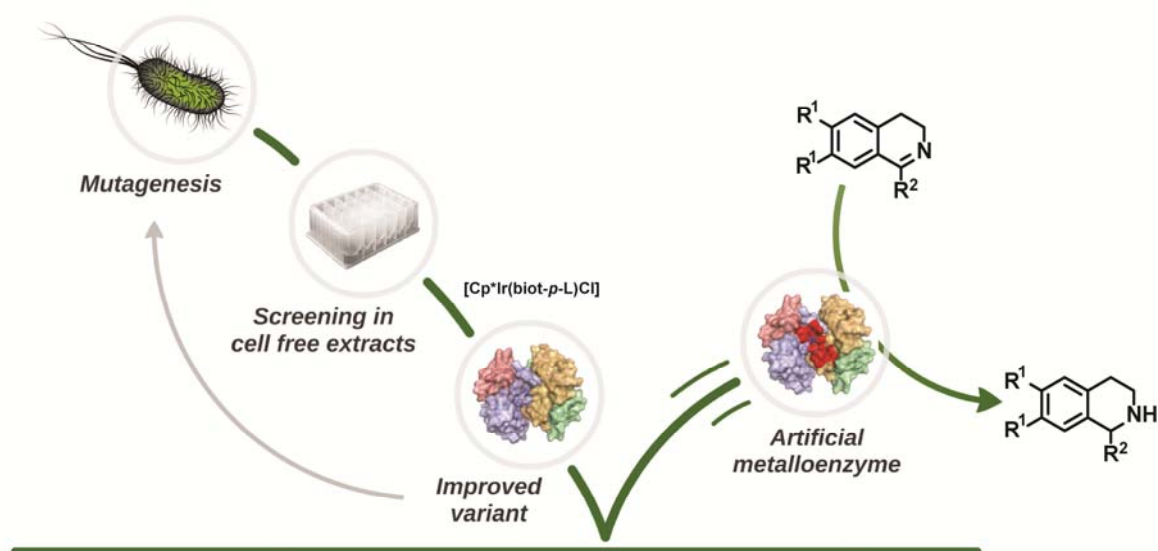
^bDepartment de Química, Universitat de Autònoma de Barcelona, Edifici C.n., 08193 Cerdonyola del Vallès, Barcelona, Spain

KEYWORDS: artificial metalloenzymes, directed evolution, enzyme catalysis, transfer hydrogenation, cyclic imines

2.5.1 ABSTRACT

Artificial metalloenzymes, resulting from incorporation of a metal cofactor within a host protein, have received increasing attention in the last decade. Herein, we report on the directed evolution of an ATHase based on the biotin-streptavidin technology using a straightforward optimized protocol allowing screening in cell free extracts. Our efforts yielded two streptavidin isoforms with improved catalytic activity and selectivity for the reduction of cyclic imines. Gratifyingly, the evolved ATHases proved stable under biphasic catalytic conditions. The X-ray structure analysis reveals that introducing bulky residues within the active site results in flexibility changes of the cofactor, thus increasing exposure of the metal to the protein surface and leading to a reversal of enantioselectivity. This hypothesis was confirmed by a multiscale approach based mostly on molecular dynamics and protein-ligand dockings.

TOC:



2.5.2 INTRODUCTION

Biocatalysis offers an attractive means to produce high-added value products.^{35,190,247} Its limitations in reaction repertoire, substrate scope and operational stability can be overcome using directed evolution or encapsulation techniques.²⁴⁸⁻²⁵⁰

Enantiopure amines, representing important intermediates for synthesis of biologically active compounds, agrochemicals, and flavors, are gaining increasing importance in both academic and industrial sectors. Indeed, approximately 40 % of all pharmaceuticals contain at least one enantiopure amine moiety.¹¹⁸ There is thus a high demand for versatile tools to produce these. Current strategies include: homogeneous catalysis and organic synthesis,¹¹⁹⁻¹²¹ resolution of racemates¹³⁰ or biocatalysis.^{122,125,126,129, 251} Amine dehydrogenases,¹³¹⁻¹³³ phenylalanine ammonia lyases,¹³⁹⁻¹⁴¹ transaminases¹³⁴⁻¹³⁷ and imine reductases¹⁴²⁻¹⁴⁶ have been reported for the synthesis of enantiopure amines. The dynamic kinetic resolution of amines can be achieved using monoamine oxidases^{148, 150, 151} or lipases¹⁵³⁻¹⁵⁶. Following the first reports by Mitsukura in 2010,¹⁴² imine reductases have gained significant interest from the synthetic community. The limited number of available imine reductases calls for alternative biocatalytic approaches.¹⁴⁶

In the past fifteen years, biocatalysis has been complemented with ArMs. These combine attractive features of enzymatic catalysis with the vast reaction repertoire of organometallic catalysis.^{41,42,47,104,227,252-254} In this context, the biotin-streptavidin technology^{73,96,255} has proven versatile, allowing the development of numerous ArMs that have been optimized to catalyze new-to-nature transformations.^{67,114,116}

In order to fine-tune the performance of enzymes, directed evolution has proven extremely powerful.^{173,176,258,259} Consisting of iterative cycles of (random) mutagenesis, protein overexpression and screening, this versatile technique allows to incrementally improve a targeted feature of an enzyme: activity, selectivity, stability etc. As ArMs consist

of an abiotic cofactor and a genetically-encoded host protein, directed evolution can also be applied to the optimization of such hybrid catalysts.^{69,112,189,208,260,261}

To speed-up the directed evolution of ArMs, we set out to perform catalysis using *E. coli* CFE rather than purified protein samples. Previously, we identified GSH as a main contaminant,^{217,222} leading to the irreversible poisoning of the precious metal cofactor when catalysis is performed in CFE. Addition of diamide to CFE containing Sav prior to the addition of the cofactor significantly restores the catalytic performance of ArMs.²²² To test the usefulness of this screening protocol, we set out to optimize the performance of an artificial imine reductase based on the biot-Sav technology by directed evolution.

In this work, we present the implementation of a streamlined optimization protocol,²²² which allows us to screen protein variants using CFE pre-incubated with DiAm. Upon screening 300 variants contained in CFE, which corresponds to four weeks of mutagenesis and expression, four weeks of protein purification, and 200 hours of analytical measurements, two mutants with an increased catalytic activity and opposite enantioselectivity for the reduction of cyclic imines were identified.

2.5.3 RESULTS AND DISCUSSION

To improve the catalytic performance of the ATHase, we selected a volume of 10 Å around the iridium center anchored within Sav and subjected the corresponding amino acids to iterative saturation mutagenesis (Figure 10). As starting point for the screen, we selected Sav K121A. For the first generation of the directed evolution, a reduced library of amino acids was included. At positions T111, S112, G113, T114, A116, N118, S122, T123 and L124, the following residues were introduced relying on precise primers: A, V, L, D, E, Q, K, H, M, Y, S, P (or N if one of the targeted mutation is present at this position). For the following generations, all canonical amino acids were individually introduced.

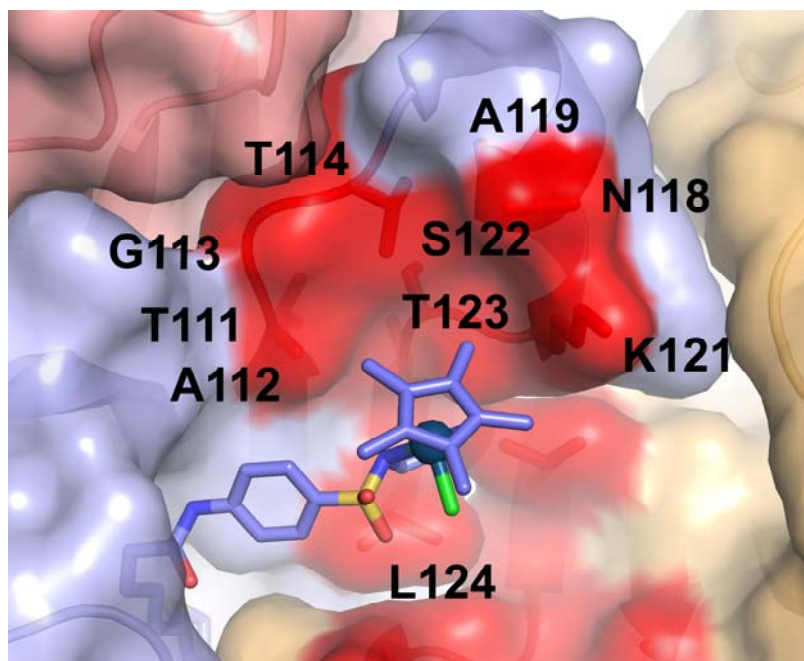
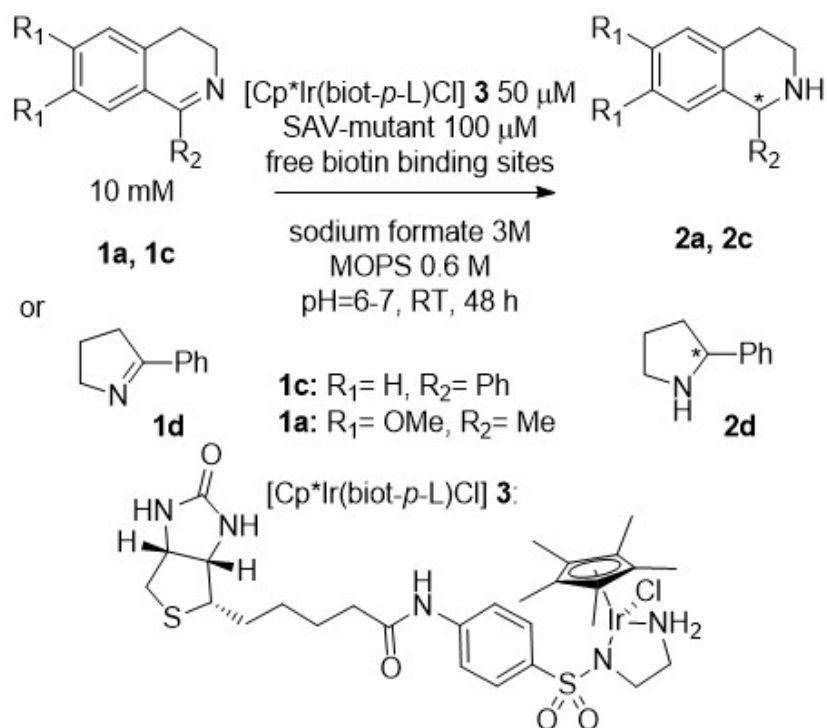


Figure 10. Close-up view of the active site of an artificial imine reductase. The protein is displayed as solvent accessible surface and the biotinylated cofactor as color-coded stick. Positions selected for mutagenesis are highlighted (PDB 3PK2).

Mutants were overexpressed in *E. coli* in 96 deep-well plates, and the cells were lysed, incubated with DiAm for 15 minutes, supplemented with [Cp*Ir(biot-*p*-L)Cl] and screened for the transfer hydrogenation of cyclic imines **1a**, **1c** and **1d** (Scheme 7, See Appendix B for details). After identification of improved variants using CFE, the corresponding mutants were overexpressed in 1 L autoinduction medium,²²³ purified by iminobiotin-sepharose affinity chromatography and lyophilized. The pure Sav mutants were then tested for their ATHase activity.

In the first generation, positions S112 and N118 were screened, yielding (*S*)- and (*R*)-selective mutants K121A-S112R and K121A-N118P (Table 8, entry 4 and 5; Figure 11). Next, K121A-N118P was subjected to focused saturation mutagenesis at position S112. Mutant K121A-N118P-S112A yielded (*R*)-**2c** with 86 % ee (entry 6). Position S122 was mutated next. Substituting the polar serine to a methionine further improved the enantioselectivity for the reduction of **1c**, yielding (*R*)-**2c** in 92 % ee and full conversion (conv., entry 7).



Scheme 7. Reduction of cyclic imines **1a**, **1c** and **1d** using ATHase based on the biot-Sav technology. We hypothesized that mutating alanine to bulky arginine at position 112 would afford the opposite enantiomer of **2c**. To our delight, the resulting Sav variant produced (*S*)-**2c** in 63 % ee and with improved conv. (entry 9). The (*S*)-selectivity was further improved by introducing tyrosine instead of lysine at position 124, which yielded (*S*)-**2c** with 78 % ee and full conv. (entry 10). Because of the low solubility of **1c** in water, we performed experiments under a biphasic set-up²⁶² with 100 mM **1c** dissolved in ethyl acetate. To our delight, improved enantioselectivity was observed for both (*R*)- and (*S*)-selective ATHases (entry 8 and 12). In stark contrast, [Cp*Ir(biot-*p*-L)Cl] · K121A proved less active under biphasic conditions (entry 3). Preparative-scale experiments (>120 mg of **1c**) resulted in >99 % HPLC yield (70 % isolated yield) and 91 % ee (*R*) for S112A-N118P-K121A-S122M and >75 % HPLC yield (55 % isolated yield) and 71 % ee (*S*) for S112R-N118P-K121A-S122M-L124Y (Table 8, entry 9 and 13).

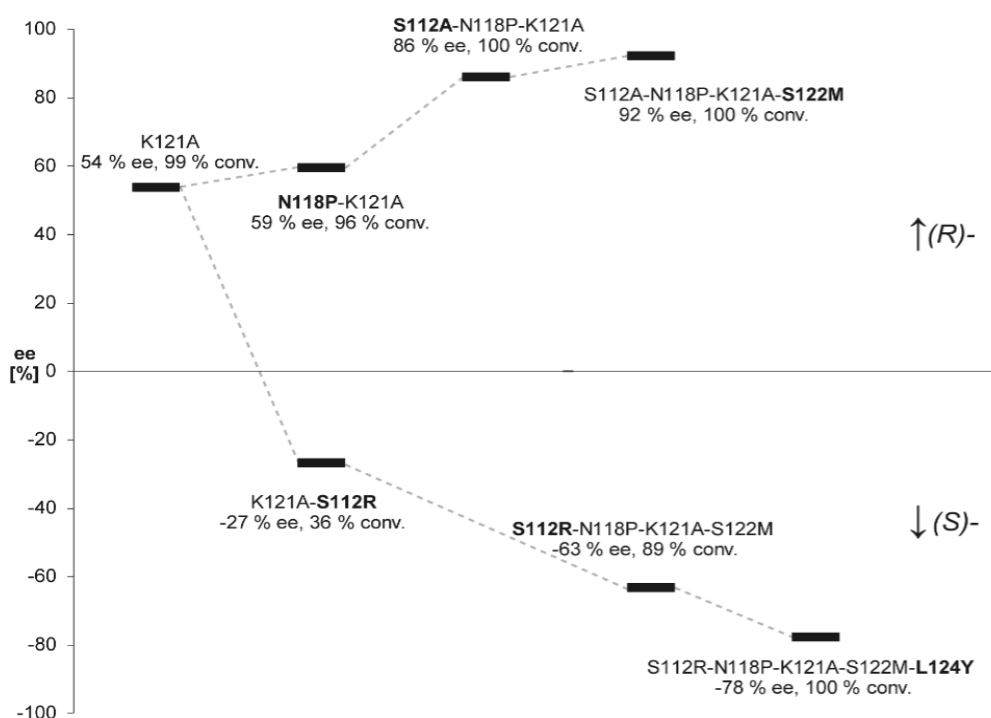


Figure 11. Summary of the directed evolution path to afford both an (*R*)- and an (*S*)-selective ATHase for the reduction of **1c**.

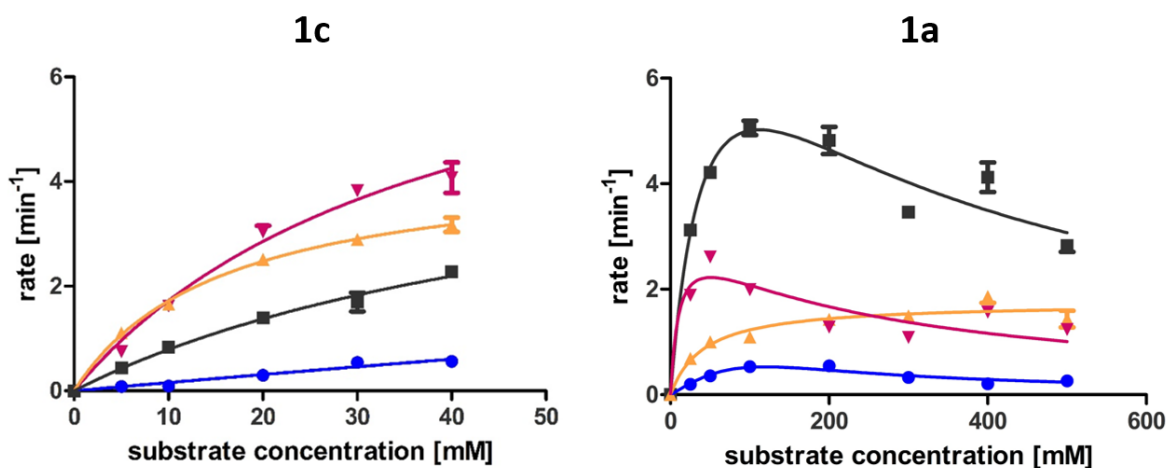
Table 8. Selected results for the reduction of cyclic imine **1c** using purified proteins.^[a]

Entry	Sav	ee (%) ^[d]	conv. (%) ^[d]	TON
1	[Cp*Ir(biot- <i>p</i> -L)Cl]	0	17	35
2	K121A	54	99	198
3	K121A ^[b]	31	5	100
4	N118P-K121A	59	96	193
5	S112R-K121A	-27	36	72
6	S112A-N118P-K121A	86	100	200
7	S112A-N118P-K121A-S122M	92	100	200
8	S112A-N118P-K121A-S122M ^[b]	95	19	380
9	S112R-N118P-K121A-S122M ^[c]	91	99 (70 ^e)	198
10	S112R-N118P-K121A-S122M	-63	90	179
11	S112R-N118P-K121A-S122M-L124Y	-78	99	198
12	S112R-N118P-K121A-S122M-L124Y ^[b]	-85	11	220
13	S112R-N118P-K121A-S122M-L124Y ^[c]	-72	75 (55 ^e)	150

^[a] The reactions were performed with 10 mM substrate at 37°C for 48 h (see SI). ^[b] Reactions were performed in a biphasic system with 100 mM substrate at RT for 4 days. ^[c] Preparative-scale reaction, 124 mg of **1c** were added to the reaction mixture (60 ml). ^[d] Enantiomeric excess and conv. were determined by HPLC. Positive ee values correspond to (*R*)-product and negative ee values correspond to (*S*)-product. ^[e] Isolated yield.

The resulting Sav library was tested for the reduction of the bulky isoquinoline **1a** as well as cyclic imine **1d** (Table S3). For the reduction of **1a**, an (*S*)-selective ATHase was identified; S112T-N118K-K121A-S122K affords (*S*)-**2a** in 50% ee and 75 % conv. (Appendix B, Table B3, entry 8). The highest (*S*)-selectivity for the reduction of **1d** was obtained with S112R-N118P-K121A-S122M-L124Y, yielding (*S*)-**2d** in 55 % ee and 86 % conv. (Table B3, entry 22).

Next, the saturation kinetic behavior of the bare cofactor and the best performing ATHases was determined (Scheme 8; Table B4). Variant K121A displays an 8-fold increased k_{cat} value for the reduction of **1a** compared to the bare cofactor. Moreover, both mutants S112A-N118P-K121A-S122M and S112R-N118P-K121A-S122M-L124Y display improved reaction rates for the reduction of **1a** compared to the bare cofactor. Introducing a bulky tyrosine residue at position 124 has a dramatic effect on K_M , increasing its value to 50 mM from 7.4 mM for the bare cofactor. Both tested ATHases display very similar K_M values, while their k_{cat} differ significantly. This suggests that introducing a second bulky substituent contributes to stabilization of the reaction transition state, thus improving the reaction rate for the (*S*)-selective ATHase. Substrate inhibition is encountered for mutants K121A and S112R-N118P-K121A-S122M-L124Y, whereas the free cofactor and mutant S112A-N118P-K121A-S122M display classical Michaelis–Menten kinetics. Unlike the results obtained with **1a**, the reduction of **1c** by ATHases revealed that none of the mutants could reach substrate inhibition due to limited solubility of **1c**. Compared to the bare cofactor, all mutants display slightly higher k_{cat} coupled with lower K_M values.



Substrate						
Sample		k_{cat} (min ⁻¹)	K_M (mM)	k_{cat} (min ⁻¹)	K_M (mM)	K_i (mM)
●	[Cp*Ir(biot- <i>p</i> -L)Cl]	3.2	182.5	0.4	7.4	-
▼	K121A	8.3	38.5	3.1	11	243.5
▲	S112A-N118P-K121A-S122M	4.4	15.8	1.7	42.2	-
■	S112R-N118P-K121A-S122M-L124Y	5.4	58.3	9.5	50.5	249.3

Scheme 8. Saturation kinetic data for selected ATHases based on incorporation of [Cp*Ir(biot-*p*-L)Cl] **3** (2 eq.) in various Sav isoforms (1 eq.) for the reduction of imine **1a** or **1c**. Error bars represent \pm standard deviation.

To gain structural insight into the best performing ATHases, crystals of the most evolved variants were soaked with an excess of [Cp*Ir(biot-*p*-L)Cl] **3**. Inspection of the X-ray structure of [Cp*Ir(biot-*p*-L)Cl] · S112A-N118P-K121A-S122M (Figure 12a) highlights the structural similarities to the structure of [Cp*Ir(biot-*p*-L)Cl] · S112A.^{95,164} The overall ATHase structure and the position and absolute configuration of the piano stool moiety are virtually identical (RMSD of all C α = 0.693). Due to potential steric clashes between two symmetry-related cofactors, the chloride ligand was not modeled. However, the crystal structure suggests the preferred formation of an (*S*)-configuration at the metal for [Cp*Ir(biot-*p*-L)Cl] (i.e. (*R*)-configuration for the catalytically active hydride [Cp*Ir(biot-*p*-L)H]) (Figure B6a). The piano stool localization is stabilized by an H-bond between the A121 backbone carbonyl oxygen and the piano stool amine nitrogen. As the cationic lysine at position 121 is substituted by an apolar alanine, it prevents a possible interaction with the

imine nitrogen of the substrate. The non-concerted transition state allowing CH $\cdots\pi$ interaction between the Cp* moiety and the phenyl of **1c** allows for the formation of (*R*)-**2c**. The X-ray structure of [Cp*Ir(biot-*p*-L)Cl] · S112R-N118P-K121A-S122M-L124Y (Figure 3b) reveals that introducing bulky residues S112R and L124Y within the Sav monomer-monomer interface results in a nearly 180° rotation of the piano stool moiety around the C_{benzene}-S_{sulfonamide} bond. The position of the pianostool is stabilized by an H-bond between the Y124 hydroxyl and the cofactor amino group (Figure B7b,c). Unfortunately, no electron density was present to model the {Cp*IrCl} moiety. We speculate that is may be due to increased flexibility of the surface-exposed complex or partial dissociation of the {Cp*IrCl}. Increased cofactor exposure presumably leads to increased solvent exposure of the substrate (Figure S7b), reminiscent to the structure of [Cp*Ir(biot-*p*-L)Cl] · S112K (PDB 4OKA).^{95,164} Importantly, both crystal structures of the evolved ATHases reveal increased atomic B-factors within the loop-7,8 and the surface-exposed terminus of the cofactor when compared to published ATHases S112A and S112K (PDB 3PK2 and 4OKA) (Figure B10, Table B5).^{217,222} In the latter structures, the loop-7,8 is conformationally rigidified by an H-bonding network including i) the N118 side chain amide, ii) a water molecule and iii) the T115 backbone amide. Mutation N118P results in elimination of this H-bonding network (Figure B11a). Additional flexibility is produced in loop 7,8 through mutation S122M that induces breaking of H-bonds in a Sav monomer-monomer interface (Figure B11b). These observations are reminiscent of the elevated atomic B-factors found in the crystal structure of a Sav-based metathase.¹¹²

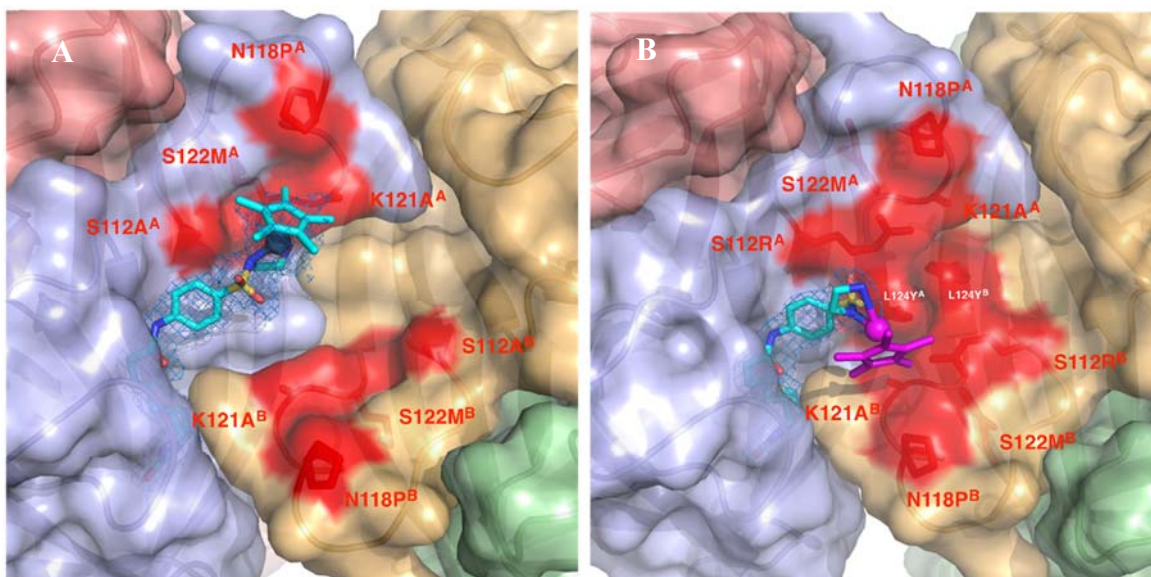


Figure 12. Close-up view of the crystal structure of $[(\text{Cp}^*)\text{Ir}(\text{Biot-}p\text{-L})\text{Cl}] \cdot \text{S112A-N118P-K121A-S122M}$ (PDB 6ESS) (A) and $[(\text{Cp}^*)\text{Ir}(\text{Biot-}p\text{-L})\text{Cl}] \cdot \text{S112R-N118P-K121A-S122M-L124Y}$ (PDB 6ESU) (B). The protein is displayed as transparent surface and cartoon model with mutations highlighted in red. For clarity, one cofactor per Sav tetramer is displayed. The cofactor is contoured with electron density from a 2FoFc map in marine (1.0σ) and an anomalous dispersion density map in red (4.0σ). Magenta atoms are not resolved in the electron density.

Crystal structures were determined assuming saturation of Sav monomers by the cofactor. However, catalysis was performed under a 1:2 ratio of cofactor per Sav monomer. To structurally characterize the assemblies under catalytic conditions, Molecular Dynamics (MD) simulations were performed using an implicit solvent approach and applying metadynamics to initially boost the exploration of conformational space (see Appendix B). The achiral planar $[\text{Ir}(\text{III})]$ $16e^-$ two-legged pianostool was considered. Conformations from the MD trajectories were grouped (clustered) based on the cofactor position in the vestibule. The number of configurations in each group (cluster) is displayed in Figure B13a,b together with an estimate of the interaction energy between the $[\text{Ir}]$ complex excluding the biotin fragment and the protein (Figure B13c,d). Variant S112R-N118P-K121A-S122M-L124Y was computed to bind the cofactor more tightly than variant S112A-N118P-K121A-S122M. This observation may be explained based on the polarity of the residues in the vestibule,

which is more hydrophobic for S112A-N118P-K121A-S122M. Accordingly, the MD trajectory of S112R-N118P-K121A-S122M-L124Y shows reduced mobility of the cofactor compared to S112A-N118P-K121A-S122M. The conformation of the cofactor in the most populated cluster in the trajectory of S112A-N118P-K121A-S122M is very similar to the X-ray determination (Figure B14a). However, further conformations are accessible to the cofactor via rotation around the S–N bond (Figure B14b). Similarly, the cofactor conformation in the most populated cluster in the trajectory of S112R-N118P-K121A-S122M-L124Y is consistent with the X-ray structure (Figure B12c).

Next, we used this structural insight to rationalize the opposite enantioselectivity resulting from the most evolved ATHases towards substrate **1c**. For this purpose, we docked the protonated form of **1c** to the representative structures of selected clusters. The resulting structures were energy-minimized, and the substrate binding energy estimated. We did not attempt to estimate reaction energies (i.e. with QM/MM methods). In the most populated cluster from the MD trajectory of S112R-N118P-K121A-S122M-L124Y, [Cp*Ir(biot-*p*-L)H] leads to the formation of (*R*)-**2c**. The best docking solutions for the pro-*R* and pro-*S* faces of **1c** project the phenyl substituent in a pocket formed by residues R112 and Y124 from both monomers and P118 of the adjacent monomer. The difference between the two binding poses consists in the orientation of the imine plane: the NH group points towards the hydroxyl of tyrosine Y124 in the pro-*S* structure (Figure 13a), whereas it is rotated by 180 degrees and does not display interactions in the pro-*R* structure (Figure 13b). From a docking point of view, the pro-*R* binding mode is slightly favored over the pro-*S* one. However, MD simulations starting from these structures reveal that the pro-*R* binding mode is not stable, whereas the pro-*S* displays a longer lifetime (i.e. about 200 ps). During this time, the NH group reorients to form an H-bond to the backbone carbonyl of A121. Therefore, we conclude that [Cp*Ir(biot-*p*-L)H] · S112R-N118P-K121A-S122M-L124Y

should preferentially reduce the pro-*S* face of **1c**, an observation in agreement with the experiments.

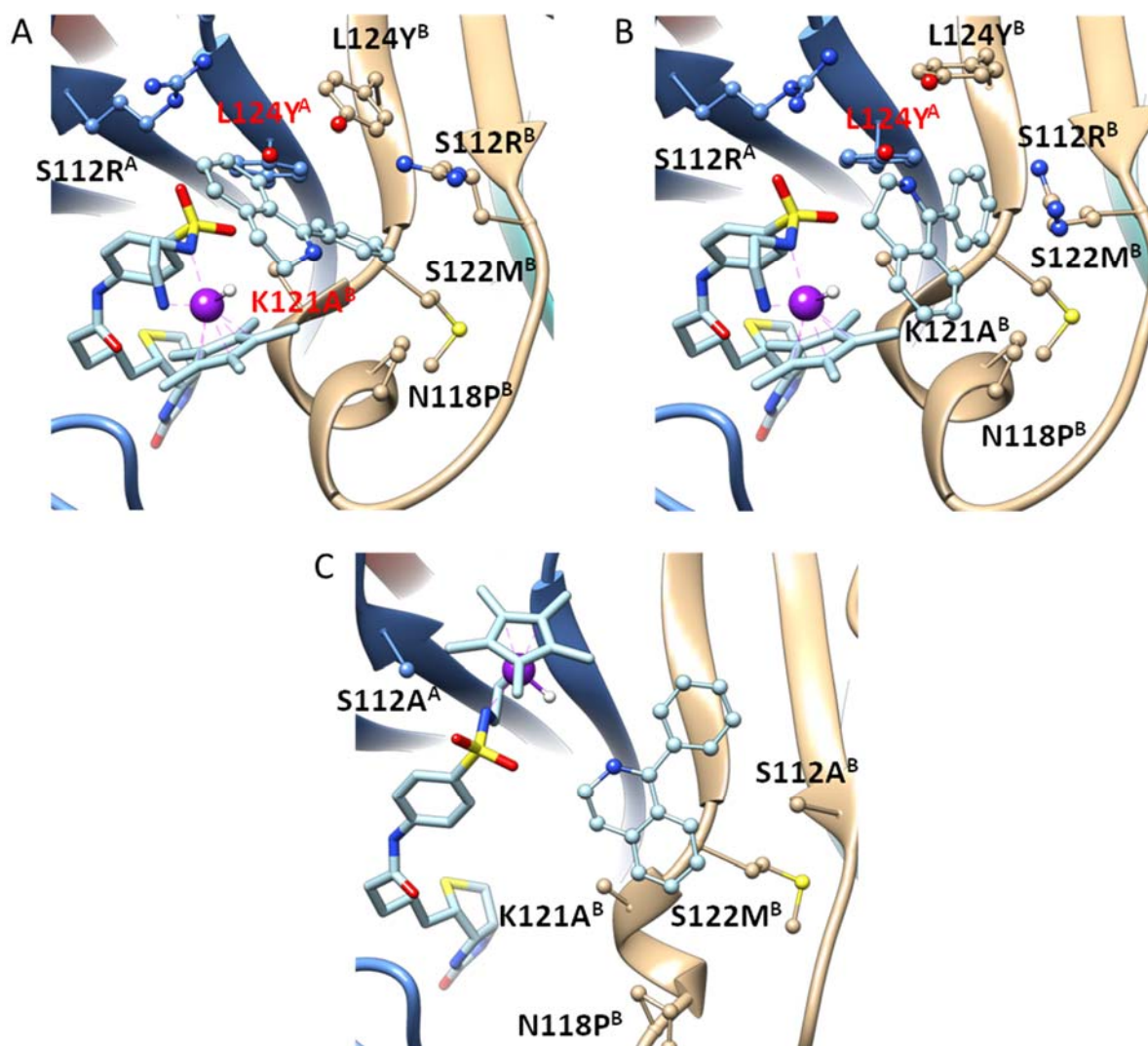


Figure 13. Substrate **1c** docked to the most populated cluster from MD simulations of variants S112R-N118P-K121A-S122M-L124Y (panel a and b) and S112A-N118P-K121A-S122M (c). The cofactor is shown in blue stick, with the Cp* group in cyan and the Ir-H atoms as balls; the substrate is shown as sticks; the protein surface is shown in gray, with the residues within 4 Å colored by type: white for hydrophobic residues, green for polar, blue for positively charged.

Concerning mutant S112A-N118P-K121A-S122M, docking of **1c** to the representative structure of the most populated cluster (which would form the (*R*)-configuration of the metal-hydride) results in a binding mode with no clear preference for the reduction of either the

pro-*R* or the pro-*S* faces of the substrate **1c**. In this binding mode, **1c** sits on the hydrophobic surface formed by residues L110, A112, T114, P118, A121, L124 (Figure 13c). We also considered binding of **1c** to representative structures of other clusters. In all cases, binding was weaker than for the most populated. The MD simulations started from these bound structures did not reveal any alternative long-lived binding mode. It seems then that the ee observed experimentally for this mutant cannot be easily rationalized from a pure binding process and further aspects including the calculation of reaction barriers may be required.

2.5.4 CONCLUSION

In summary, introduction of [Cp*Ir(Biot-*p*-L)Cl] **3** within Sav isoforms affords ATHases. These can be optimized by directed evolution protocols using unpurified CFE, thus dramatically improving the throughput of the effort. Two mutants with increased reaction rates and enantioselectivities were identified for the reduction of cyclic imine **1c**, allowing for the formation of both (*R*)-**2c** (95 % ee) and (*S*)-**2c** (86 % ee). The possibility of performing catalysis in a biphasic medium paves the way for greater scope of applications of such hybrid catalysts.

2.5.5 ACKNOWLEDGEMENT

This research was supported by the Swiss Nanoscience Institute, and advanced ERC grant (DrEAM) and the SNF (grant 200020 162348). TRW thanks Umicore for a generous loan of [Cp*IrCl₂]₂. JDM, PV and LAC are thankful for the support given by the Spanish grant CTQ2014-54071-P, Generalitat de Catalunya grant 2014SGR989 and the COST Action CM1306.

2.5.6 SUPPORTING INFORMATION

The full supporting information can be found in Appendix B.

2.5.7 AUTHOR CONTRIBUTIONS

General idea: Prof. Dr. Thomas R. Ward

Design and expression of the mutant library, protein purification and characterization, kinetic experiments, screening of the streptavidin mutants and biotinylated iridium complex:

Martina Hesticová

Protein crystallization and crystal structure analysis: Dr. Tillmann Heinisch

Molecular Dynamics (MD) simulations: Lur Alonso-Cotchico, Dr. Pietro Vidossich, Prof.

Dr. Jean-Didier Maréchal

Manuscript writing: All authors

2.6 DIRECTED EVOLUTION OF ARTIFICIAL METALLOENZYMES: GENETIC OPTIMIZATION OF THE CATALYTIC ACTIVITY

*The following section has been published in
Chimia* **2018**, 72, 189-192
doi: 10.2533/chimia.2018.189

Directed Evolution of Artificial Metalloenzymes: Genetic optimization of the Catalytic Activity

Martina Hesticová

Group of Prof. Dr. T. R. Ward, Department of Chemistry, University of Basel, Mattenstrasse
24a, BPR 1096, 4002 Basel, Switzerland, e-mail: martina.hesticova@unibas.ch

KEYWORDS: artificial metalloenzymes, directed evolution, enzyme catalysis, transfer
hydrogenation, cyclic imines

2.6.1 ABSTRACT

ArMs based on the incorporation of a biotinylated metal cofactor within Sav combine attractive features of both enzymatic and homogeneous catalysis. To speed up their optimization, we present a directed evolution of an ATHase based on a streamlined and optimized protocol for the design, overexpression and screening of Sav isoforms. Ten positions have been subjected to mutagenesis to yield two variants with improved catalytic activity and selectivity for the reduction of cyclic imines, along with higher stability in a biphasic medium.

2.6.2 INTRODUCTION

Catalysis represents an essential technique in synthetic organic chemistry. Thanks to its extraordinary value, various synthetic systems, including organocatalysts, heterogeneous solids, enzymes and metal complexes, have been developed.²⁶³ Biocatalytic use of enzymes, either in the whole cell format, contained in cell lysates or as purified proteins, has proved useful in multiple industries, such as fine and bulk chemicals, cosmetics, textile, pulp and paper, food and pharmaceuticals.^{190,247,264-267}

Chiral amines serve as important intermediates in synthesis of fragrances and flavors, agrochemicals and biologically active compounds. Since approximately 40 % of all pharmaceuticals contain at least one chiral amine building block,¹¹⁸ the demand for their enantioselective synthesis is immense and multiple methods are available. Current strategies to produce enantiopure amines include resolution of racemates,¹³⁰ organic synthesis^{119,121} or biocatalysis.^{122,126,251} Biocatalytic production of chiral amines can be achieved by direct enzymatic synthesis using phenylalanine ammonia lyases,^{139,268,269} transaminases,^{134,135,270,271} imine reductases,^{142-145,272} and amine dehydrogenases,^{131,133} or by dynamic kinetic resolution by implementing lipases,^{153,155,156} or monoamine oxidases.^{148-150,152} Industrial use of imine reductases represents a challenge, which is predominantly

caused by the restricted amount of available enzyme types, their price, finite substrate scope and low stability of their substrates in water or buffer. Development of novel imine reductases and optimization of their catalytic performance is therefore highly desirable.

ArMs are created by incorporating a synthetic metal cofactor within a protein or a DNA scaffold.^{41,42,47,227,525-254} Multiple anchoring strategies are available:^{43,44,65,272-274} covalent, non-covalent, dative, and metal substitution. Since ArMs comprise of a biological and synthetic part, the performance of both components can be optimized independently. The selection of the macromolecular protein or DNA scaffold determines the anchoring strategy and the methods for its genetic optimization, whereas the rationally designed synthetic cofactor determines which type of reaction could be performed.^{104,224,225,273,274} The (strept)avidin-biotin (Sav-biot) technology^[16] has been established as a very versatile anchoring strategy for the preparation of ArMs. Following the initial reports of ArMs by Wilson and Whitesides in 1978,⁴⁷ multiple catalytic systems have been realized. These include allylic alkylation,¹⁰⁹ C-H activation,¹⁰⁴ metathesis,^{111,112} dihydroxylation,¹⁰⁵ alcohol oxidation,¹⁰⁶ sulfoxidation,^{107,108} hydrogenation,^{93,227,228} and transfer hydrogenation.^{95-103,221} Noteworthy, some of these reactions do not exist in biological systems, ArMs have therefore brought new-to-nature chemical transformations into enzymatic catalysis.^{114,116,117,191,210} ATHase has received an increased amount of attention, which resulted in their application in reduction of enones and ketones, and, more recently, of imines, NAD(P)⁺ and its analogs.

To mimic the natural process of enzyme evolution, directed evolution^{67,113,169,176,189,204,210,259} was established by Arnold, Chen¹⁶⁹ and Stemmer²⁰⁴ almost two decades ago. Since then, this powerful method has been used to fine-tune the selective formation of enantiomers, broaden the substrate acceptance of enzymes or to improve their stability in a targeted manner. This versatile methodology, comprising iterative cycles of mutagenesis followed by protein expression and their screening, can also be applied in the evolution of hybrid catalysts, allowing for their Darwinistic progression (Figure 14).¹⁷⁶

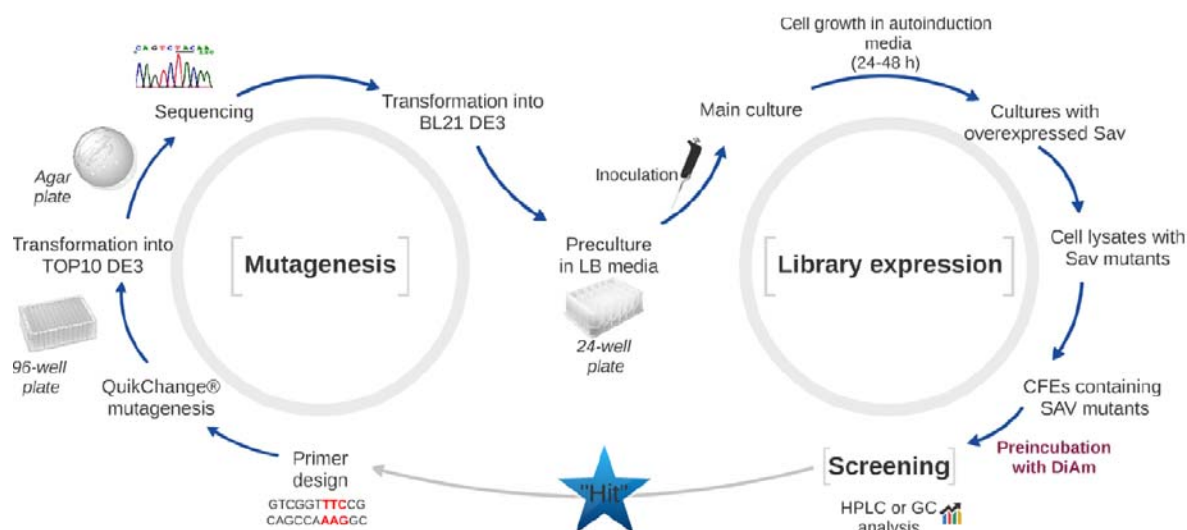


Figure 14. Workflow for directed evolution of ArMs. Mutagenesis based on precise primers is followed by expression in *E. coli*. The lysed cells are treated with DiAm prior to the addition of a biotinylated cofactor, which leads to the constitution of an active artificial metalloenzyme with an ATHase activity. After screening and identification of a “hit”, the mutation of interest is used as a template for another round of mutagenesis.

The development of high-throughput screening methods for evolution of ArMs has a bottleneck; the *E. coli* cellular environment contains millimolar concentrations of GSH and other metabolites capable of poisoning the soft metal containing catalyst.^{216,220} Screening utilizing protein purification is therefore often necessary. Since the workload increases exponentially with the increasing library size, a system circumventing the protein purification stage is highly desirable. Our group has recently described a streamlined optimization protocol²²² that allows parallel *in vivo* expression of Sav in *E. coli* in a 24-deep well plate format. The cells are grown in an autoinduction medium based on low amount of glucose and high amounts of lactose. Upon consuming glucose, the expression of the recombinant protein is induced by lactose during the exponential growth phase, which allows for automated protein production without the need of manual induction. After cell harvest and lysis, the resulting CFE are treated with diamide. This GSH scavenger capable of oxidizing GSH to GSSG notably recovers the catalytic performance²²² when applied to CFE

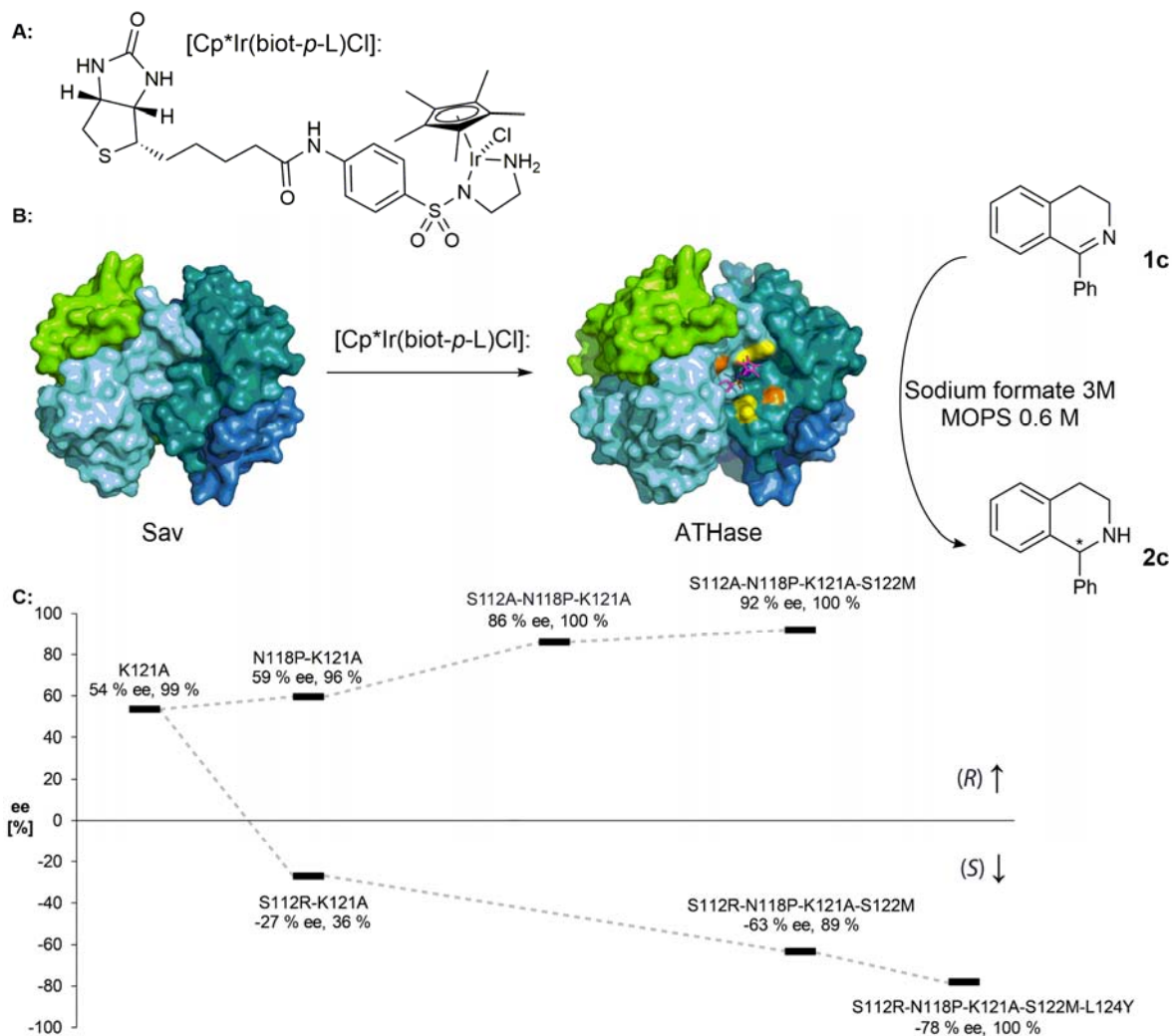
prior to the addition of the metal cofactor. Building upon this technique, we selected an area of 10 Å around the iridium center of the biotinylated cofactor anchored within the Sav active site and subjected the corresponding amino acids to targeted mutation. Our efforts in directed evolution of the ATHase resulted in four generations of mutant variants, which showed improved activity in transfer hydrogenation of various cyclic imine substrates.¹⁰³

2.6.3 DISCUSSION

Based on our previous screening results, mature Sav with alanine at position 121 was selected for the library generation. In the first round of directed evolution, a reduced library of amino acids constituting of A, V, L, D, E, Q, K, H, M, Y, S, P, and N was introduced at positions T111, S112, G113, T114, A116, N118, S122, T123 and L124. In the following generations, all canonical amino acids were individually introduced relying on precise primers. The resulting mutants were overexpressed in *E. coli* using an autoinduction medium in 24-deep well plates. The harvested cells were lysed and the concentration of the biotin free binding sites in the resulting CFE was determined by means of a biotin-4-fluorescein absorption-fluorescence assay.^{222,237} The extracts were consequently treated with DiAm followed by the addition of [Cp*Ir(biot-*p*-L)Cl] **3** and screened for their ATHase activity a cyclic imine substrate (Scheme 9). After identification of a successful “hit”, the results were reproduced, the corresponding mutant overexpressed in 1L shaking flasks, purified using an iminobiotin affinity chromatography column and confirmed by screening in MOPS buffer using sodium formate as the hydride source. In these experiments, the ratio between Sav and [Cp*Ir(biot-*p*-L)Cl] was fixed to 2:1 to ensure optimal reaction rate and the selectivity.¹⁶⁴

The first generation screening revealed two mutants with an improved activity. In the reduction of **1c**, an (*S*)-selective mutant S112R-K121A (Table 9, entry 5) was identified along with and an (*R*)-selective mutant N118P-K121A (entry 4), which was subjected to saturation mutagenesis at position S112. In the resulting second generation, mutant S112A-

N118P-K121A yielded (*R*)-**2c** in 86 % ee and full conversion (entry 6). Introducing an additional substitution of serine to methionine at position 122 in the third generation further improved the selectivity and yielded (*R*)-**2c** in 92 % ee (entry 7).



Scheme 9. Directed evolution of ATHase. (A) Structure of the biotinylated pianostool Cp*Ir cofactor **3**. (B) ATHase is created upon incorporation of the biotinylated cofactor within Sav. (C) Directed evolution tree of ATHase of a model cyclic imine **1c**.

The (*S*)-selective route was evolved starting from the arginine-containing mutant S112R-K121A. Upon introducing proline at position 118 and methionine at position 122, the selectivity for (*S*)-**2c** was increased to 63 % ee (entry 10).

Table 9. Reduction of substrate **1c** catalyzed by various ATHases using purified proteins.[a]

Entry	ATHase	conv. (%)	TON	ee (%)
1	[Cp*Ir(biot- <i>p</i> -L)Cl]	17	35	-
2	K121A	99	198	54 (<i>R</i>)
3	K121A [c]	5	100	31 (<i>R</i>)
4	N118P-K121A	96	193	59 (<i>R</i>)
5	S112R-K121A	36	72	-27 (<i>S</i>)
6	S112A-N118P-K121A	100	200	86 (<i>R</i>)
7	S112A-N118P-K121A-S122M	100	200	92 (<i>R</i>)
8	S112A-N118P-K121A-S122M ^[b]	100 (70 ^[d])	200	91 (<i>R</i>)
9	S112A-N118P-K121A-S122M ^[c]	19	380	95 (<i>R</i>)
10	S112R-N118P-K121A-S122M	90	179	-63 (<i>S</i>)
11	S112R-N118P-K121A-S122M-L124Y	100	200	-78 (<i>S</i>)
12	S112R-N118P-K121A-S122M-L124Y ^[b]	75 (55 ^[d])	150	-72 (<i>S</i>)
13	S112R-N118P-K121A-S122M-L124Y ^[c]	11	220	-85 (<i>S</i>)

^[a] Reactions were carried out with 10 mM substrate, 100 μ M biotin binding sites and 50 μ M [Cp*Ir(biot-*p*-L)Cl] at 37 $^{\circ}$ C for 48 h in 0.6 M MOPS and 3 M sodium formate at pH 6. ^[b] Reactions were carried out on a preparative scale (>120 mg of **1c**) in 60 ml. ^[c] Reactions were carried out using a biphasic set-up with 100 mM substrate at RT for 4 days. ^[d] Isolated yield.

In the last generation, the introduction of tyrosine at position 124 as a second bulky residue within the Sav active site further improved the (*S*)-selectivity and the mutant S112R-N118P-K121A-S122M-L124Y yielded (*S*)-**2c** in 78 % ee and full conversion (entry 11).

Preparative scale experiments, performed in degassed buffer and with >120 mg of substrate, resulted in full conversion (GC; 70 % after purification) and 91 % ee (*R*) for S112A-N118P-K121A-S122M Sav (entry 8) and 75 % conversion (GC; 55 % after purification) and 72 % ee (*S*) for S112R-N118P-K121A-S122M-L124Y Sav (entry 12). Due to the low water solubility of the cyclic imine selected for screening, experiments in a biphasic set up using 100 mM of substrate were performed. Both most evolved Sav variants performed better in the terms of enantioselectivity and TON (entries 9 and 13) compared to mutant K121A, representing the starting point of our directed evolution (entry 3).

Analysis of the obtained X-ray structure of [Cp*Ir(biot-*p*-L)Cl] · S112A-N118P-K121A-S122M suggests formation of the catalytically active hydride form of Cp*Ir cofactor in (*R*)-configuration. The non-concerted transition state grants a formation of a CH... π interaction between the substrate and the Cp* moiety of the catalyst, thus predominantly producing the (*R*)-enantiomer of **2c**. The crystal structure of [Cp*Ir(biot-*p*-L)Cl] · S112R-N118P-K121A-S122M-L124Y revealed that the introduction of two bulky amino acid residues at positions 112 and 124 within the Sav active site resulted in an approximately 180° rotation of the pianostool moiety around the C_{benzene}-S_{sulfonamide} bond. The cofactor becomes more surface-exposed, which may lead to increased solvent exposure of the substrate.¹⁰³

2.6.4 CONCLUSION

In conclusion, introduction of a biotinylated pianostool Cp*Ir catalyst within Sav variants produces ATHases. Directed evolution of such hybrid catalysts using the streamlined optimization protocol for Sav production allows for screening hundreds of Sav variants contained in CFE, hence notably improving the throughput of the process. After only four rounds of directed evolution, two mutants with an improved activity and selectivity on the model cyclic imine substrate were identified. These mutants perform well on a preparative scale and under biphasic reaction conditions, thus implying a wide range of application possibilities.

2.6.5 ACKNOWLEDGEMENT

The author is grateful to Metrohm and the Swiss Chemical Society for being awarded with the best oral presentation award. The author would like to thank Professor Thomas R. Ward for his supervision and the SNI (Swiss Nanoscience Institute) and SNF (Swiss National Science Foundation) for financial support.

2.7 REFERENCES

- [168] R. A. Jensen, *Annu. Rev. Microbiol.* **1976**, *30*, 409–425.
- [169] K. Chen, F. H. Arnold, *Proc. Natl. Acad. Sci. U. S. A.* **1993**, *90*, 5618–5622.
- [170] L. You, F. H. Arnold, *Protein Eng. Des. Sel.* **1995**, *9*, 77–83.
- [171] J. C. Moore, F. H. Arnold, *Nat. Biotechnol.* **1996**, *14*, 458–467.
- [172] F. H. Arnold, A. A. Volkov, *Curr. Opin. Chem. Biol.* **1999**, *3*, 54–59.
- [173] E. T. Farinas, T. Bulter, F. H. Arnold, *Curr. Opin. Biotechnol.* **2001**, *12*, 545–551
- [174] N. J. Turner, *Trends Biotechnol.* **2003**, *21*, 474–478.
- [175] M. T. Reetz, *Angew. Chem. Int. Ed.* **2001**, *40*, 284–310
- [176] M. S. Packer, D. R. Liu, *Nat. Rev. Genet.* **2015**, *16*, 379.
- [177] C. Zeymer, D. Hilvert, *Annu. Rev. Biochem.* **2018**, *87*, annurev-biochem-062917-012034.
- [178] O. Khersonsky, G. Kiss, D. Rothlisberger, O. Dym, S. Albeck, K. N. Houk, D. Baker, D. S. Tawfik, *Proc. Natl. Acad. Sci.* **2012**, *109*, 10358–10363.
- [179] D. N. Woolfson, G. J. Bartlett, A. J. Burton, J. W. Heal, A. Niitsu, A. R. Thomson, C. W. Wood, *Curr. Opin. Struct. Biol.* **2015**, *33*, 16–26.
- [180] A. Aharoni, L. Gaidukov, O. Khersonsky, S. M. Q. Gould, C. Roodveldt, D. S. Tawfik, *Nat Genet* **2004**, *37*, 73–76.
- [181] L. Giver, A. Gershenson, P.-O. Freskgard, F. H. Arnold, *Proc. Natl. Acad. Sci.* **1998**, *95*, 12809–12813.
- [182] V. Saez-Jimenez, S. Acebes, A. T. Martinez, F. J. Ruiz-Dueñas, S. Acebes, V. Guallar, A. T. Martínez, *PLoS One* **2015**, *10*, e0124750.
- [183] B. Valderrama, H. García-Arellano, S. Giansanti, M. C. Baratto, R. Pogni, R. Vazquez-Duhalt, *FASEB J.* **2006**, *20*, 1233–1235.
- [184] S. van den Berg, P.-Å. Löfdahl, T. Härd, H. Berglund, *J. Biotechnol.* **2006**, *121*, 291–298.
- [185] J. W. Liu, K. S. Hadler, G. Schenk, D. Ollis, *FEBS J.* **2007**, *274*, 4742–4751.
- [186] S. Gülich, M. Linhult, S. Ståhl, S. Hober, *Protein Eng. Des. Sel.* **2002**, *15*, 835–842.
- [187] Z. Shao, F. H. Arnold, *Curr. Opin. Struct. Biol.* **1996**, *6*, 513–518.
- [188] C. Jäckel, P. Kast, D. Hilvert, *Annu. Rev. Biophys* **2008**, *37*, 153–73.
- [189] E. M. Brustad, F. H. Arnold, *Curr. Opin. Chem. Biol.* **2011**, *15*, 201–210.
- [190] M. T. Reetz, *J. Am. Chem. Soc.* **2013**, *135*, 12480–12496.
- [191] S. C. Hammer, A. M. Knight, F. H. Arnold, *Curr. Opin. Green Sustain. Chem.* **2017**, *7*, 23–30.
- [192] J. Wang, G. Li, M. T. Reetz, *Chem. Commun.* **2017**, *53*, 3916–3928.
- [193] G. Li, J. Wang, M. T. Reetz, *Bioorg. Med. Chem.* **2017**, DOI: 10.1016/j.bmc.2017.05.021

- [194] M. Creus, T. R. Ward, *Org. Biomol. Chem.* **2007**, *5*, 1835–1844.
- [195] R. Das, D. Baker, *Annu. Rev. Biochem.* **2008**, *77*, 363–382.
- [196] H. J. Wijma, R. J. Floor, P. A. Jekel, D. Baker, S. J. Marrink, D. B. Janssen, *Protein Eng. Des. Sel.* **2014**, *27*, 49–58.
- [197] M. Lehmann, L. Pasamontes, S. F. Lassen, M. Wyss, *Biochim. Biophys. Acta, Protein Struct. Mol. Enzymol.* **2000**, *1543*, 408–415.
- [198] B. T. Porebski, A. M. Buckle, *Protein Eng. Des. Sel.* **2016**, *29*, 245–251.
- [199] T. S. Wong, *Nucleic Acids Res.* **2004**, *32*, e26.
- [200] M. Forloni, A. Y. Liu, N. Wajapeyee, *Cold Spring Harb. Protoc.* **2018**, *2018*, pdb.prot097741.
- [201] N. E. Labrou, *Curr. Protein Pept. Sci.* **2010**, *11*, 91–100.
- [202] D. W. Leung, E. Chen, D. V. Goeddel, *Technique* **1989**, *1*, 11–15.
- [203] Eckert, K. A. & Kunkel, T. A. *Nucleic Acids Res.* **1990**, *18*, 3739–3744.
- [204] W. P. C. Stemmer, *Nature* **1994**, *370*, 389–391.
- [205] W. M. Coco, W. E. Levinson, M. J. Crist, H. J. Hektor, A. Darzins, P. T. Pienkos, C. H. Squires, D. J. Monticello, *Nat. Biotechnol.* **2001**, *19*, 354–359.
- [206] J. B. Y. H. Behrendorff, W. A. Johnston, E. M. J. Gillam, in (Eds.: E.M.J. Gillam, J.N. Copp, D. Ackerley), Springer New York, New York, NY, **2014**, 175–187.
- [207] H. Yang, A. M. Swartz, H. J. Park, P. Srivastava, K. Ellis-Guardiola, D. M. Upp, G. Lee, K. Belsare, Y. Gu, C. Zhang, R. E. Moellering, J. C. Lewis, *Nat. Chem* **2018**, *10*, 318–324.
- [208] A. Ilie, M. T. Reetz, *Isr. J. Chem.* **2015**, *55*, 51–60.
- [209] R. K. Zhang, D. K. Romney, S. B. J. Kan, F. H. Arnold, *Directed evolution of artificial metalloenzymes: bridging synthetic chemistry and biology*. In *Artificial Metalloenzymes and MetalloDNAzymes in Catalysis. From Design to Applications*, Wiley-VCH **2018**.
- [210] M. T. Reetz, *Recent Advances in Directed Evolution of Stereoselective Enzymes*. In 'Directed Enzyme Evolution: Advances and Applications', Springer, Cham, **2017**.
- [211] M. Jeschek, R. Reuter, T. Heinisch, C. Trindler, J. Klehr, S. Panke, T. R. Ward, *Nature* **2016**, *537*, 661–665.
- [212] R. Blomberg, H. Kries, D. M. Pinkas, P. R. E. Mittl, M. G. Grütter, H. K. Privett, S. L. Mayo, D. Hilvert, *Nature* **2013**, *503*, 418–421.
- [213] O. Khersonsky, G. Kiss, D. Rothlisberger, O. Dym, S. Albeck, K. N. Houk, D. Baker, D. S. Tawfik, *Proc. Natl. Acad. Sci.* **2012**, *109*, 10358–10363.
- [214] T. W. Johannes, R. D. Woodyer, H. Zhao, in *Enzyme Assays*, Wiley-VCH, **2005**.
- [215] M. J. Waner, D. P. Mascotti, *J. Biochem. Biophys. Methods* **2008**, *70*, 873–877.
- [216] B. D. Bennett, E. H. Kimball, M. Gao, R. Osterhout, S. J. Van Dien, J. D. Rabinowitz, *Nat Chem Biol* **2009**, *5*, 593–599.

- [217] A. Galano, J. R. Alvarez-Idaboy, *RSC Adv.* **2011**, *1*, 1763–1771.
- [218] A. Kręzel, W. Bal, *Acta Biochim. Pol.* **1999**, *46*, 567–580.
- [219] T. L. Ho, H. C. Ho, L. D. Hamilton, *Chem. Biol. Interact.* **1978**, *23*, 65–84.
- [220] Y. M. Wilson, M. Dürrenberger, E. S. Nogueira, T. R. Ward, *J. Am. Chem. Soc.* **2014**, *136*, 8928–8932.
- [221] S. A. S. Pope, R. Milton, S. J. R. Heales, *Neurochem. Res.* **2008**, *33*, 1410–1418.
- [222] H. Mallin, M. Hesticová, R. Reuter, T. R. Ward, *Nat. Protoc.* **2016**, *11*, 835–852.
- [223] F. W. Studier, *Protein Expr. Purif.* **2005**, *41*, 207–234.
- [224] C. Esmieu, M. V. Cherrier, P. Amara, E. Girgenti, C. Marchi-Delapierre, F. Oddon, M. Iannello, A. Jorge-Robin, C. Cavazza, S. Ménage, *Angew. Chem. Int. Ed.* **2013**, *52*, 3922–3925.
- [225] S. D. Khare, Y. Kipnis, P. Greisen, R. Takeuchi, Y. Ashani, M. Goldsmith, Y. Song, J. L. Gallaher, I. Silman, H. Leader, et al., *Nat. Chem. Biol.* **2012**, *8*, 294–300.
- [226] F. Yu, V. M. Cangelosi, M. L. Zastrow, M. Tegoni, J. S. Plegaria, A. G. Tebo, C. S. Mocny, L. Ruckthong, H. Qayyum, V. L. Pecoraro, *Chem. Rev.* **2014**, *114*, 3495–3578.
- [227] C.-C. Lin, C.-W. Lin, A. S. C. Chan, *Tetrahedron: Asymmetry* **1999**, *10*, 1887–1893.
- [228] J. Collot, J. Gradinaru, N. Humbert, M. Skander, A. Zocchi, T. R. Ward, *J. Am. Chem. Soc.* **2003**, *125*, 9030–9031.
- [229] T. Sano, C. R. Cantor, *Proc. Natl. Acad. Sci. U.S.A.* **1990**, *87*, 142–146.
- [230] A. Chilkoti, P. H. Tan, P. S. Stayton, *Proc. Natl. Acad. Sci. U. S. A.* **1995**, *92*, 1754–1758.
- [231] E. M. Sletten, C. R. Bertozzi, *Angew. Chem. Int. Ed.* **2009**, *48*, 6974–6998.
- [232] M. Creus, A. Pordea, T. Rossel, A. Sardo, C. Letondor, A. Ivanova, I. LeTrong, R. E. Stenkamp, T. R. Ward, *Angew. Chem. Int. Ed.* **2008**, *47*, 1400–1404.
- [233] M. T. Reetz, J. D. Carballeira, A. Vogel, *Angew. Chem. Int. Ed.* **2006**, *45*, 7745–7751.
- [234] C. Papworth, J. C. Bauer, J. Braman, D. A. Wright, *Strategies*, **1996**, *9*, 3–4.
- [235] J. M. Zimbron, A. Sardo, T. Heinisch, T. Wohlschlager, J. Gradinaru, C. Massa, T. Schirmer, M. Creus, T. R. Ward, *Chem. - A Eur. J.* **2010**, *16*, 12883–12889.
- [236] L. Zheng, U. Baumann, J. L. Reymond, *Nucleic Acids Res.* **2004**, *32*, e115.
- [237] G. Kada, K. Kaiser, H. Falk, H. J. Gruber, *Biochim. Biophys. Acta* **1999**, *1427*, 44–48.
- [238] Y. M. Wilson, M. Dürrenberger, T. R. Ward, *Organometallic chemistry in protein scaffolds*. in Protein Engineering Handbook Vol. 3, Wiley-VCH, Weinheim, **2012**, 215–238.
- [239] A. Kajetanowicz, A. Chatterjee, R. Reuter, T. R. Ward, *Catal. Letters* **2014**, *144*, 373–379.
- [240] I. Lantos, D. Bhattacharjee, D. S. Eggleston, *J. Org. Chem.* **1986**, *51*, 4147–4150.
- [241] G. Bertani, *J. Bacteriol.* **1951**, *62*, 293–300.
- [242] D. Hanahan, *J. Mol. Biol.* **1983**, *166*, 557–580.

- [243] D. Hanahan, J. Jessee, F. R. Bloom, *Techniques for transformation of E. coli*. in DNA Cloning. Oxford University Press, **1995**.
- [244] T. Muto, *Preparation of 1,4-diazepane-3,5-dione derivatives as chymase inhibitors and pharmaceutical use thereof*. Japanese patent no. WO 2010053182A1 **2010**.
- [245] G. O. Becker, *et al. Organikum* 19th edn., Barth Verlagsgesellschaft, **1993**.
- [246] E. Angov, *Biotechnol. J.* **2011**, *6*, 650–659.
- [247] N. J. Turner, M. D. Truppo, *Curr. Opin. Chem. Biol.* **2013**, *17*, 212–214.
- [248] K. M. Polizzi, A. S. Bommarius, J. M. Broering, J. F. Chaparro-Riggers, *Curr. Opin. Chem. Biol.* **2007**, *11*, 220–225.
- [249] U. Hanefeld, L. Gardossi, E. Magner, *Chem. Soc. Rev.* **2009**, *38*, 453–468.
- [250] U. T. Bornscheuer, *Angew. Chem., Int. Ed.* **2003**, *42*, 3336–3337.
- [251] W. Kroutil, E. M. Fischereider, C. S. Fuchs, H. Lechner, F. G. Mutti, D. Pressnitz, A. Rajagopalan, J. H. Sattler, R. C. Simon, E. Siirola, *Org. Process Res. Dev.* **2013**, *17*, 751–759.
- [252] J. Bos, F. Fusetti, A. J. M. Driessen, G. Roelfes, *Angew. Chem. Int. Ed.* **2012**, *51*, 7472–7475.
- [253] M. Pellizzoni, G. Facchetti, R. Gandolfi, M. Fusè, A. Contini, I. Rimoldi, *ChemCatChem* **2016**, *8*, 1665–1670.,
- [254] J. Podtetenieff, A. Taglieber, E. Bill, E. J. Reijerse, M. T. Reetz, *Angew. Chem. Int. Ed.* **2010**, *49*, 5151–5155.
- [255] M. T. Reetz, J. J.-P. Peyralans, A. Maichele, Y. Fu, M. Maywald, *Chem. Commun.* **2006**, 4318.
- [256] M. T. Reetz, A. Zonta, K. Schimossek, K.-E. Jaeger, K. Liebeton, K.-E. Jaeger, *Angew. Chem. Int. Ed.* **1997**, *36*, 2830–2832.
- [257] M. T. Reetz, K.-E. Jaeger, *Top. Curr. Chem.* **1999**, *200*, 31.
- [258] O. May, P. T. Nguyen, F. H. Arnold, *Nat. Biotechnol.* **2000**, *18*, 317–320.
- [259] C. A. Denard, H. Ren, H. Zhao, *Curr. Opin. Chem. Biol.* **2015**, *25*, 55–64.
- [260] M. T. Reetz, *Tetrahedron* **2002**, *58*, 6595–6602.
- [261] P. Dydio, H. M. Key, A. Nazarenko, J. Y.-E. Rha, V. Seyedkazemi, D. S. Clark, J. F. Hartwig, *Science* **2016**, *354*, 102–106.
- [262] U. E. Rusbandi, C. Lo, M. Skander, A. Ivanova, M. Creus, N. Humbert, T. R. Ward, *Adv. Synth. Catal.* **2007**, *349*, 1923–1930.
- [263] H. Krässig, J. Schurz, R. G. Steadman, K. Schliefer, W. Albrecht, M. Mohring, H. Schlosser, 'Ullmann's encyclopedia of industrial chemistry', Wiley-VCH, Weinheim, 2002.
- [264] F. Rudroff, M. D. Mihovilovic, H. Gröger, R. Snajdrova, H. Iding, U. T. Bornscheuer, *Nat. Catal.* **2018**, *1*, 12–22.

- [265] M. D. Truppo, *ACS Med. Chem. Lett.* **2017**, *8*, 476–480.
- [266] M. Hönig, P. Sondermann, N. J. Turner, E. M. Carreira, *Angew. Chem. Int. Ed.* **2017**, *56*, 8942–8973.
- [267] J. M. Choi, S. S. Han, H. S. Kim, *Biotechnol. Adv.* **2015**, *33*, 1443–1454.
- [268] N. J. Weise, F. Parmeggiani, S. T. Ahmed, N. J. Turner, *J. Am. Chem. Soc.* **2015**, *137*, 12977–12983.
- [269] F. Parmeggiani, S. L. Lovelock, N. J. Weise, S. T. Ahmed, N. J. Turner, *Angew. Chem., Int. Ed.* **2015**, *54*, 4608–4611.
- [270] A. Gomm, E. O'Reilly, *Curr. Opin. Chem. Biol.* **2018**, *43*, 106–112.
- [271] E. E. Ferrandi, D. Monti, *World J. Microbiol. Biotechnol.* **2018**, *34*, 13–23.
- [272] K. Mitsukura, T. Yoshida, *Chapter 5 - Imine Reductases for Chiral Amine Synthesis* In 'Future Directions in Biocatalysis', Elsevier, Amsterdam, **2017**, 97–117.
- [273] M. Allard, C. Dupont, V. Muñoz Robles, N. Doucet, A. Lledós, J. D. Maréchal, A. Urvoas, J. P. Mahy, R. Ricoux, *ChemBioChem* **2012**, *13*, 240–251.
- [274] T. Ueno, T. Koshiyama, S. Abe, N. Yokoi, M. Ohashi, H. Nakajima, Y. Watanabe, *J. Organomet. Chem.* **2007**, *692*, 142–147.

CHAPTER III:

ENCAPSULATION OF ARMS

3.1 INTRODUCTION

The design of ArMs represents an essential and far-reaching area of chemical biology and bioinorganic chemistry. Over the years, the main area of interest has shifted from understanding fundamental principles and mechanisms to providing potential utilization in nanoscience and biotechnology with possible industrial relevance.

However, the potential of enzyme utilization is hindered by aging, fragility, operational instability under non-physiological conditions and susceptibility to protease digestion. To allow the implementation of biocatalysis in biotechnology and material science, the reusability and stability issues must be thoroughly scrutinized and addressed.

Besides directed evolution and protein engineering, enzyme stability and performance can be improved by means of immobilization.²⁷⁵⁻²⁷⁹ This approach brings several advantages: i) possibility to modulate the catalytic properties, ii) increase in the catalytic turnover,¹⁰¹ iii) repeated or continuous use of catalyst, iv) easy separation from the reaction mixture, v) prevention from product contamination by the protein or catalyst, vi) enhanced protein stability,^{280, 281} and vii) possibility to develop efficient multi-enzyme cascades.²⁸²⁻²⁸⁶

In spite of limitations²⁷⁹ such as limited mass transfer due to the diffusion effects and physical hindrance of the enzyme, rarely quantitative protein binding, high cost of the carrier, low weight of the protein compared to the carrier, significantly reduced catalytic activity / weight ratio of the final material, enzyme immobilization represents a successful method with applications ranging from diagnostics, food and chemicals to pharmaceutical industry.²⁸⁶⁻²⁸⁹

The most widespread strategies²⁹⁰⁻²⁹⁵ for enzyme immobilization include: i) physical adsorption on solid support,^{296, 297} ii) covalent attachment on solid support, iii) protein entrapment or iv) encapsulation in inorganic or organic polymer matrices and cages,^{298, 299} or v) cross-linking (Figure 15).^{300, 301}

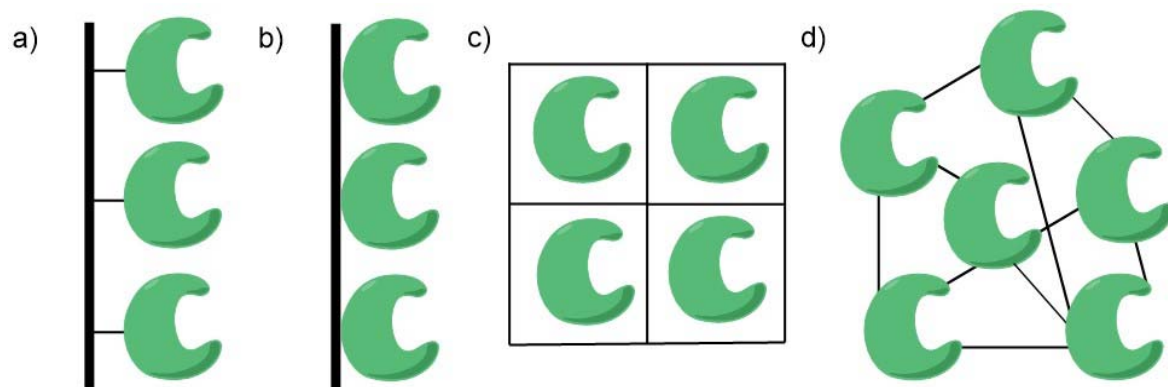


Figure 15. Techniques for the enzyme immobilization: a) covalent attachment to solid support b) physical adsorption c) entrapment and encapsulation d) cross-linking.

The first three methods rely on the implementation of solid support, which either acts as a solid carrier or provides a mechanical compartment. The last option involves linking of the enzymes without the need of an additional support matrix. Each of the methods presented includes various advantages and disadvantages originating in the selection of the support and the physical or chemical process of attachment, which impact the protein stability, tertiary and quaternary structure and microenvironment (Table 10).²⁹²

Table 10. Advantages and disadvantages of immobilization strategies.

Method	Advantage	Disadvantage
Covalent	Wide selection of supports	
	Wide selection of linkers	Chemical modification of the protein
	Tight binding	Low activity / carrier weight
	Control of enzyme loading	Limited mass transfer
	Compatible with harsh conditions (organic solvent, elevated temperature)	
Adsorption	Reversible	Weak binding
	Inexpensive	Leaching
	No chemical modification of the protein	Low protein stabilization
		Non-specific binding
Entrapment and encapsulation		Limited mass transfer
	No chemical modification of the protein	Low protein stabilization
	Possible for whole cells	Leaching
Cross-linking		Limited mass transfer
	High activity / carrier weight	Chemical modification of the protein
	Compatible with harsh conditions (organic solvent, elevated temperature)	Limited mass transfer
	Tight binding	Low size control
	Possible for whole cells	Often required crystallization
	No carrier, lower price	

3.2 IMMOBILIZATION ON NANOPARTICLES

Immobilizing enzymes by covalent attachment to a solid support requires formation of a covalent bond between a reactive group present on the support and an amino acid side chain residue of the protein, such as thiol (cysteine), hydroxyl (serine, tyrosine, threonine), amine (histidine, lysine, guanidine group of arginine, *N*-terminus), or carboxylate (*C*-terminus, glutamic and aspartic acid). Activation of carboxylic side chains relies on carbodiimide ($\text{RN}=\text{C}=\text{NR}$) activation, whereas amine-containing side chains can be cross-linked to the surface using glutaraldehyde.³⁰²

The selection of the solid support for enzyme immobilization is of crucial importance, as the characteristics of the matrix will have an impact on the performance of the enzyme. Ideal support characteristics include ease of derivatization, biocompatibility, resistance towards protease digestion, physical resistance to friction and compression, chemical resistance and low price. The options for support selection are wide, including: i) multiple natural polymers (starch, chitosan, sepharose, pectin, alginate, collagen, cellulose), ii) synthetic polymers and iii) inorganic materials (zeolites, silica, alumina, glass etc.).²⁹¹

Silica-based carriers represent one of the most suitable supports for both industrial and research applications.^{303, 304} Nanoparticles^{305, 306} are an efficient carrier material, mainly due to their effective enzyme loading, the ease of catalyst separation, large and specific surface area, tunable size and the ability to minimize diffusional limitations. It has been demonstrated that immobilizing enzymes on nanoparticles reduces their denaturation and positively influences their stability and catalytic activity.³⁰⁷ Further embedment in a protective layer acts as a shield, which in turn affects the turnover rate of the immobilized enzyme.^{101, 308}

3.3 ENZYME ENTRAPMENT IN A PROTEIN CAGE

Implementation of a tertiary coordination sphere around the catalyst,³⁰⁹ for instance by encapsulating the artificial metalloenzyme within a cage, could allow protection of the hybrid catalyst and further influence the catalytic activity. Moreover, the physical compartmentalization of molecular species allows for control of matter distribution.³¹⁰⁻³¹³ Encapsulation in protein cages^{311, 314-316} offers an elegant implementation of molecular containers as reaction vessels, delivery vehicles or templates for controlled synthesis of nanomaterials and nanodevices.³¹⁷⁻³²⁰

Ferritins are natural nanocages serving as iron-storing containers almost ubiquitously distributed³²¹ among all life forms. Their spherical protein shell consists of 24 subunits of different ratios between the light (L-) and heavy (H-) ferritin subunits; horse spleen ferritin, often implemented for research purposes due to its low cost, contains approx. 90 % of L-subunits.^{322, 323} The inner cavity of ferritin with outer and inner diameters of 12-13 and 7-8 nm respectively, can accommodate up to 4500 Fe-atoms. Removal of the iron cluster produces apoferritin,³²⁴ a remarkably stable protein cage capable of withstanding extreme conditions, such as elevated temperature (up to 70°C), a wide pH range (2.0 – 10.0) and the presence of chemical denaturants (Figure 16a).^{325, 326}

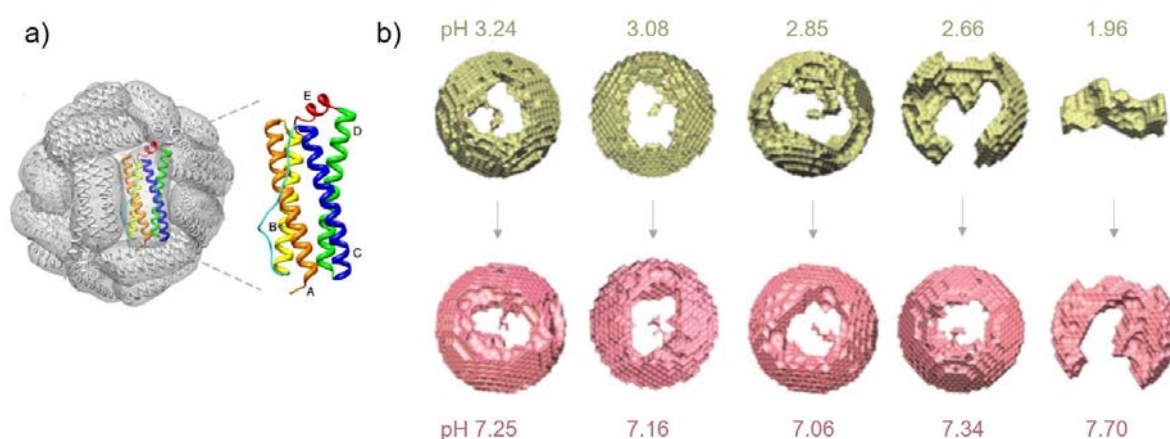


Figure 16. a) Structure of an octahedral ferritin (PDB 1BFR).³⁴¹ The helices in the bundle are colored orange (A helix), yellow (B helix), blue (C helix), green (D helix), red (E helix) and cyan (BC loop).³⁴² b) pH-dependent structures of apoferritin. The intact spherical apoferritin is stable within the pH range 10.1 – 3.40. Below this range, apoferritin undergoes a step-wise disassociation that was found to be only pseudo-reversible.³⁴³

Its spherical inner cavity, representing a convenient biotemplate in nanotechnology, has attracted widespread attention, as it allows encapsulation and delivery of drugs, nutrients, quantum dots, and imaging agents.³²⁷⁻³³⁹ Moreover, the apoferritin hollow can be utilized for nanoparticle synthesis and as a reaction vessel, allowing cellular uptake of its cargo.³⁴⁰ In the case of implementing *Archaeoglobus fulgidus* apoferritin, which contains large pores, proteins can be incorporated using electrostatic interactions with its negatively charged

cavity.³³² Encapsulation of neutral proteins within the cavity of apoferritin should be possible, providing that the selected protein would retain its structure and activity under harsh reassociation conditions. Given its remarkable robustness,^{90, 91} Sav represents an ideal selection.

A disassociation and reassociation route relying on the pH change can reversibly assemble the three-dimensional structure of apoferritin.³⁴⁴ This process has been shown to be pseudo-reversible, e.g. the reassembled apoferritin cage contains hole defects, which can be attributed to disassembly of several monomeric subunits (Figure 16b).³⁴³ However, these additional holes could theoretically be utilized for improving the transport of material during catalysis.

By virtue of its unique properties and robustness, ferritin and apoferritin found numerous applications in various research fields such as biomedical applications, materials, electronic devices, biosensors and catalysis.³³³ So far, the apoferritin shell was utilized for encapsulation of ions,³⁴⁵⁻³⁴⁷ small molecules³⁴⁸⁻³⁵⁴ and catalysts^{338, 339, 355, 356} and size-controlled synthesis of nanoparticles.³⁵⁷⁻³³⁶⁰ Encapsulating enzymes within confined environments of protein cages such as apoferritin might pose interesting means to develop new biohybrid materials with potential *in vivo* delivery.

3.4 IMMOBILIZATION OF AN ARTIFICIAL IMINE REDUCTASE WITHIN SILICA NANOPARTICLES IMPROVES ITS PERFORMANCE

*The following section has been published in
Chem. Commun. 2016, 52, 9462–9465,
doi: 10.1039/C6CC04604E*

Immobilization of an artificial imine reductase within silica nanoparticles improves its performance

Martina Hesticová^a, M. Rita Correro^b, Markus Lenz^c, Philippe F.-X. Corvini^c, Patrick Shahgaldian^{*b} and Thomas R. Ward^{*a}

^aDepartment of Chemistry, University of Basel, Spitalstrasse 51, CH-4056 Basel, Switzerland. E-mail: thomas.ward@unibas.ch

^bInstitute of Chemistry and Bioanalytics, School of Life Sciences, University of Applied Sciences and Arts Northwestern Switzerland, Gründenstrasse 40, CH-4132 Muttenz, Switzerland

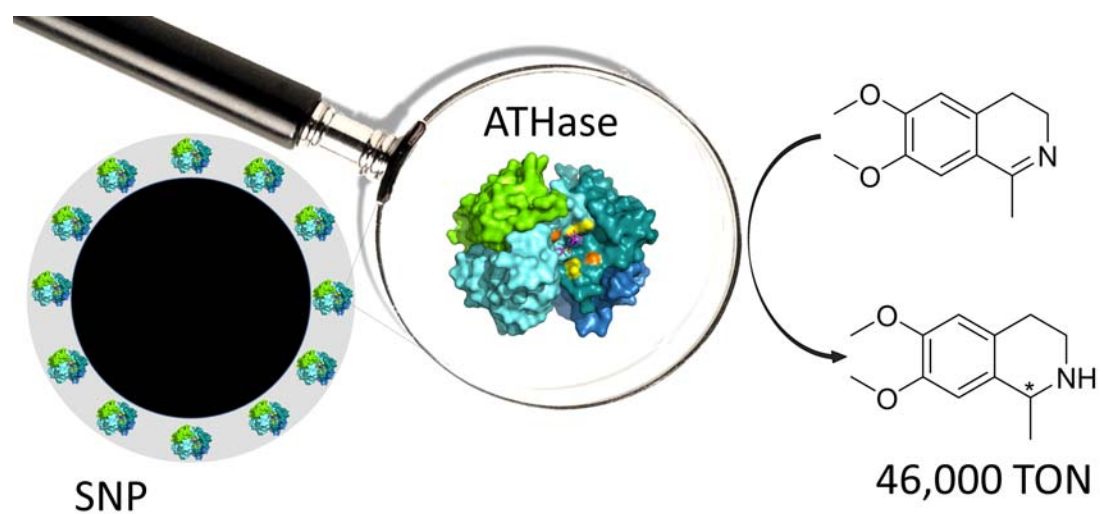
^cInstitute for Ecopreneurship, School of Life Sciences, University of Applied Sciences and Arts Northwestern Switzerland, Gründenstrasse 40, 4132 Muttenz, Switzerland

KEYWORDS: artificial metalloenzymes, directed evolution, enzyme catalysis, transfer hydrogenation, cyclic imines

3.4.1 ABSTRACT

Silica nanoparticles equipped with an artificial imine reductase display remarkable activity towards cyclic imine- and NAD^+ reduction. The method, based on immobilization and protection of streptavidin on silica nanoparticles, shields the biotinylated metal cofactor against deactivation yielding over 46 000 turnovers in pure samples and 4000 turnovers in crude cellular extracts

TOC



3.4.2 INTRODUCTION

Catalysis plays a crucial role in a variety of scientific fields including synthetic organic chemistry. Given this importance, a wide range of synthetic systems, including heterogeneous solids, organocatalysts, metal complexes and enzymes, have been developed in the past century.²⁶³ Transition metal catalysts and enzymes possess complementary properties, which can be exploited in the synthesis of various enantiopure compounds.³⁶¹

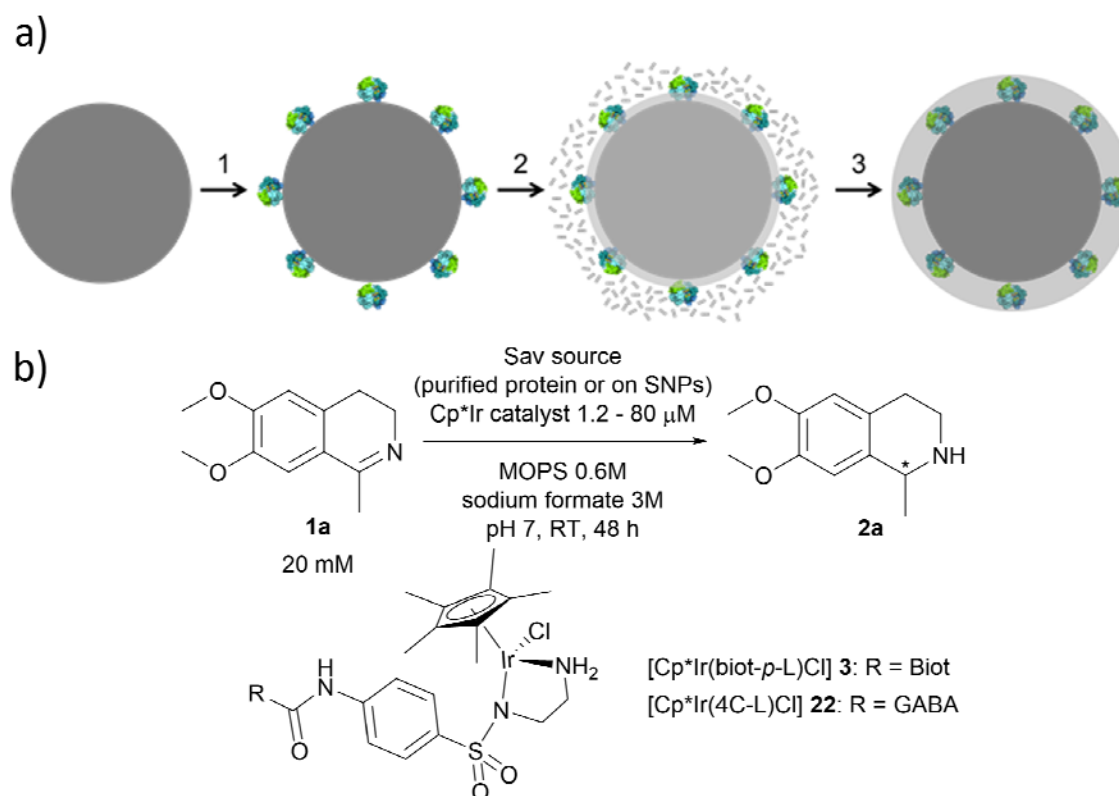
The industrial use of enzymes is partially limited by their operational instability and, in some cases, high price.²⁴⁸ Therefore, significant efforts have been invested in developing immobilization strategies that may contribute to stabilize enzymes, while allowing their recycling.²⁶²

An ArM results from the incorporation of a synthetic metal complex cofactor within a host protein.⁹⁶ The biotin–streptavidin technology has been widely exploited to ensure the localization of a biotinylated cofactor within the host protein.⁷² As ArMs often bear a soft metal, cellular metabolites, including organosulfur compounds present in the *E. coli* cellular debris, frequently deactivate the metal.²²⁰ Such hybrid catalysts can be viewed as complementary to both homogeneous catalysts and enzymes.^{43,47,114,226,361,363-365}

d⁶-piano stool complexes have shown great potential for *in vivo* catalysis as they display promising stability in biological environments.³⁶⁶ With the aim of improving its catalytic performance, we set out to shield an ATHase in a protective organosilica layer on silica nanoparticles (SNPs) and evaluate its catalytic performance towards the reduction of imines and the regeneration of NAD⁺.⁹⁵ Working on the development of nanomaterials endowed with virus recognition properties,^{367,368} we have designed a chemical strategy that allows embedding enzymes in a biomimetic and soft organosilica layer.^{369,370}

3.4.3 RESULTS AND DISCUSSION

In the present work, we have expanded this shielding strategy to artificial metalloenzymes and tested the resulting nanocatalysts for the reduction of cyclic imine **1a** in the presence of various cellular extracts. As shown previously with soluble ArMs, embedding the biotinylated pianostool iridium complex $[\text{Cp}^*\text{Ir}(\text{biot-}p\text{-L})\text{Cl}]$ **3** within various Sav mutants allows to access either (*R*)- and (*S*)-salsolidine **2a** (Scheme 10), depending on the Sav mutant (Table 11). This observation ensures that the biotinylated cofactor $[\text{Cp}^*\text{Ir}(\text{biot-}p\text{-L})\text{Cl}]$ is indeed incorporated within Sav, as the bare cofactor yields (*rac*)-**2a**.



Scheme 10. (a) Immobilization and protection of ATHase in a protective organosilica layer yielding active and protected nanoparticles. The ATHase is covalently anchored (1) on the surface of SNPs (dark grey), followed by self-assembly and polycondensation of silanes (2), which eventually build a protective layer (3). (b) ATHase of cyclic imine and structure of the iridium cofactors **3** and **22**.

Table 11. Reactions performed using purified proteins.

entry	Sav mutant	ee ^{a,b} (%)	Conv. ^a (%)	TON
1	Cp*Ir(biot- <i>p</i> -L)Cl]·Sav WT	38	70	140
2	Cp*Ir(biot- <i>p</i> -L)Cl]·S112A	87	89	178
3	Cp*Ir(biot- <i>p</i> -L)Cl]·S112K	-70	86	173
4	Cp*Ir(biot- <i>p</i> -L)Cl]·K121A	-35	99	198
5	Cp*Ir(biot- <i>p</i> -L)Cl]·S112A-K121A	79	98	196
6	Cp*Ir(biot- <i>p</i> -L)Cl]·R84A-S112A-K121A	68	99	198

Reactions were performed in 200 μ l of reaction mixture. ^[a] Enantiomeric excess and conversion were determined by HPLC analysis on a Chiracel-IC column. ^[b] Positive ee values correspond to (R)-**2a** and negative ee values correspond to (S)-**2a**.

Single mutants [Cp*Ir(biot-*p*-L)Cl]·S112A Sav and [Cp*Ir(biot-*p*-L)Cl]·S112K Sav were selected for immobilization and protection. These ArMs afford opposite enantiomers of amine **2**. Additionally, the double mutant [Cp*Ir(biot-*p*-L)Cl]·S112A-K121A Sav was selected for immobilization in view of its remarkable activity as purified ArM.¹⁶¹

Native SNPs (240 nm in diameter) were prepared by the Stöber method.³⁷¹ Next, in order to covalently anchor Sav on the surface of the nanoparticles, the SNPs were amino-modified by incubation with (3-aminopropyl)-triethoxysilane (APTES) and further reacted with glutaraldehyde. Sav isoforms preincubated with the iridium cofactor, [Cp*Ir(biot-*p*-L)Cl]·S112A Sav, [Cp*Ir(biot-*p*-L)Cl]·S112K Sav and [Cp*Ir(biot-*p*-L)Cl]·S112A-K121A Sav, were immobilized at the surface of SNPs by reacting with the free aldehyde functions present at the surface of the SNPs. The synthesis of a protective organosilica layer was achieved by incubating the SNPs with tetraethyl orthosilicate and APTES for one- and four hours respectively, yielding protected SNPs (prot-SNPs, Figure 17).

SNPs were imaged using a field emission scanning electron microscope (FESEM). The micrographs revealed monodisperse and well-defined nanoparticles with an average diameter of 260 nm. As illustrated in Figure 2, the SNPs equipped with the additional

protective silica layer (prot-SNPs) display a homogeneous size distribution with a diameter increase of approx. 10 nm upon protection.

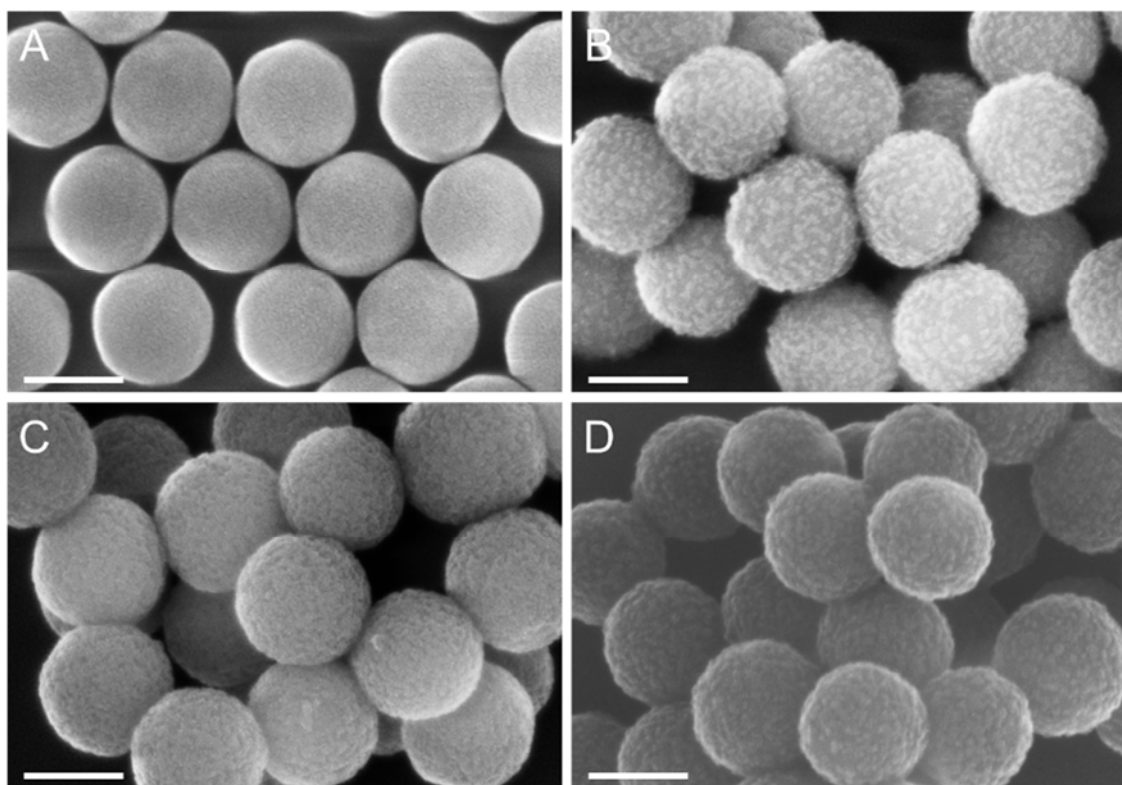


Figure 17. Scanning electron micrographs of the SNPs; A: native amino-modified SNPs, B: $[\text{Cp}^*\text{Ir}(\text{biot-}p\text{-L})\text{Cl}]\cdot\text{S112A@prot-SNP}$, C: $[\text{Cp}^*\text{Ir}(\text{biot-}p\text{-L})\text{Cl}]\cdot\text{S112K@prot-SNP}$ and D: $[\text{Cp}^*\text{Ir}(\text{biot-}p\text{-L})\text{Cl}]\cdot\text{S112A-K121A@prot-SNP}$. The scale bar corresponds to 200 nm.

Gratifyingly, immobilization and additional protection of the ATHase on the SNPs to yield $[\text{Cp}^*\text{Ir}(\text{biot-}p\text{-L})\text{Cl}]\cdot\text{Sav@SNP}$ and $[\text{Cp}^*\text{Ir}(\text{biot-}p\text{-L})\text{Cl}]\cdot\text{Sav@prot-SNP}$ respectively only led to a modest variation of the enantioselectivity of the hybrid catalyst towards the reduction of imine **1a** (Table 11, entries 6 and 10). The activity (i.e. TON) of the SNPs was established based on the iridium concentration. This latter was determined by inductively coupled plasma mass spectrometry (ICP-MS) for each SNP batch. Dried SNPs contain approximately 0.04 ng Ir per mg SNPs. Salsolidine reduction using $[\text{Cp}^*\text{Ir}(\text{biot-}p\text{-L})\text{Cl}]\cdot\text{S112A Sav SNPs}$ yielded total TON of 4294 after 2 days (Table 12, entry 1).

Table 12. Asymmetric imine reduction yielding **2a** using silica nanoparticles equipped with an artificial transfer hydrogenase.

Entry	Sav source ^a	Ir conc. ^b	ee ^{c,d}	Conv. ^c	TON
		μM	(%)	(%)	
1	[Cp*Ir(biot- <i>p</i> -L)Cl]·S112A@prot-SNP	2.6	90	56	4294
2	[Cp*Ir(biot- <i>p</i> -L)Cl]·S112A@prot-SNP $\hat{\text{c}}$	2.6	83	28	2172
3	[Cp*Ir(biot- <i>p</i> -L)Cl]·S112A@prot-SNP $\hat{\text{c}}$	2.6	80	24	1863
4	[Cp*Ir(biot- <i>p</i> -L)Cl]·S112A@prot-SNP ^e	2.6	88	22	16990
5	[Cp*Ir(biot- <i>p</i> -L)Cl]·S112A Sav Purified protein ^f	2.6	79	15	1154
6	[Cp*Ir(biot- <i>p</i> -L)Cl]·S112K@prot-SNP	1.2	-56	22	3775
7	[Cp*Ir(biot- <i>p</i> -L)Cl]·S112K@prot-SNP $\hat{\text{c}}$	1.2	-53	12	2000
8	[Cp*Ir(biot- <i>p</i> -L)Cl]·S112K@prot-SNP $\hat{\text{c}}$	1.2	-58	9	1580
9	[Cp*Ir(biot- <i>p</i> -L)Cl]·S112K@prot-SNP ^e	1.2	-48	10	16667
10	[Cp*Ir(biot- <i>p</i> -L)Cl]·S112K Sav Purified protein ^f	1.2	-66	5	833
11	[Cp*Ir(biot- <i>p</i> -L)Cl]·S112A-K121A@prot-SNP	1.5	70	97	12885
12	[Cp*Ir(biot- <i>p</i> -L)Cl]·S112A-K121A@prot-SNP $\hat{\text{c}}$	1.5	68	56	7294
13	[Cp*Ir(biot- <i>p</i> -L)Cl]·S112A-K121A@prot-SNP $\hat{\text{c}}$	1.5	67	50	6570
14	[Cp*Ir(biot- <i>p</i> -L)Cl]·S112A-K121A@prot-SNP ^e	1.5	76	36	46747
15	[Cp*Ir(biot- <i>p</i> -L)Cl]·S112A-K121A Sav Purified protein ^f	1.5	89	19	2513
16	native SNPs	0	0	0	0
17	empty prot-SNPs	0	0	0	0
18	[Cp*Ir(biot- <i>p</i> -L)Cl] free ^g	2.6	0	8	444
19	[Cp*Ir(4C-L)Cl] free ^g	80	0	42	104
20	[Cp*Ir(4C-L)Cl]@prot-SNPs	80	0	26	66

^[a]Reactions performed in a reaction buffer using 1 mg of SNPs in 100 μl reaction mixture with 20 mM substrate concentration for 48 hours, ^[b] Determined by means of ICP-MS, ^[c] The enantiomeric excess and conversion were determined by HPLC (see Appendix C). ^[d] Positive ee values correspond to (*R*)-**2a** and negative ee values correspond to (*S*)-**2a**, ^[e] Reactions performed with 200 mM substrate. ^[f] Reactions were performed with free purified enzymes with the same iridium concentration as use with SNPs, ^[g] Reactions performed without the presence of Sav using the iridium ligand **22** [Cp*Ir(4C-L)Cl] in reaction buffer.

In line with the performance of the soluble ArM, the immobilized [Cp*Ir(biot-*p*-L)Cl]·S112A-K121A Sav@prot-SNP yielded the best results, with TON of 12'885 and almost full conversion (entry 11). Upon increasing the substrate concentration (200 mM), a TON of 46'747 was obtained using SNPs with [Cp*Ir(biot-*p*-L)Cl]·S112A-K121A Sav@prot-SNP (entry 14). Compared to the homogeneous ArMs (entries 5, 10 and 15 respectively), the TONs are significantly increased, at the cost of slight erosion in selectivity.

We hypothesize that the increased TON rates result from the protective effect of organosilane layer and, partly, by the hydrophobicity around the enzyme within the layer. The preferential formation of enantioenriched salsolidine **1a**, depending on the Sav mutant, unambiguously demonstrates that the SNPs indeed contain the intact ArMs with preserved quaternary structure. Importantly, the SNPs can be recycled at least twice ($\hat{\mathcal{A}}$ and $\hat{\mathcal{B}}$), at the cost of an erosion in conversion (entries 2, 3, 7, 8, 12 and 13), yet with virtually the same enantiomeric excess.

Control experiments with native SNPs or SNPs without the presence of Sav (e.g. empty SNPs) did not show any activity towards NAD⁺ or imine reduction (entries 16 and 17). To address the synergistic effect of the silica layer and the streptavidin host on the catalytic performance of the iridium cofactor, a non-biotinylated [Cp*Ir(4C-L)Cl] analog **22** was synthesized, immobilized and protected within SNPs ([Cp*Ir(4C-L)Cl]@prot-SNP). In contrast to the ArM, upon immobilization, the activity of ([Cp*Ir(4C-L)Cl]@prot-SNP) decreases upon mineralization within SNPs, (Table 12, entries 19-20).

We have also demonstrated the stability of enantioselectivity over time (see Appendix C). The time-point assay showed only a slight erosion of enantioselectivity over the course of 7 days (decrease of 11 %), which could be explained by disruption of the protective layer and leakage of the catalyst caused by friction in solution.³⁷⁰ However, the ICP-MS measurements of the reaction medium after the reaction showed only traces of

leaked iridium. We thus argue that the decrease of activity is predominantly caused by loss of material during centrifugation and wash cycles.

With biomedical applications³⁷² in mind, we evaluated the regeneration of NAD⁺ by [Cp*Ir(biot-*p*-L)Cl]·S112A Sav@prot-SNP. For this purpose, the formation of NADH was monitored by absorbance spectroscopy at 340 nm (Appendix C). The results confirm that the immobilization does not significantly affect the catalytic properties of the hybrid catalysts towards the NAD⁺ reduction. The protected catalyst [Cp*Ir(biot-*p*-L)Cl]·Sav@prot-SNP has an initial lower reaction rate, but overall slightly improved TONs compared to [Cp*Ir(biot-*p*-L)Cl]·Sav.

In order to test the compatibility of SNPs with complex cellular media, we performed experiments in the presence of *E. coli* cell lysates. In stark contrast to the homogenous ArMs, which lose most of their activity in the presence of cellular debris solution, the SNPs partially maintained their catalytic activity. Up to 80 TONs were achieved with [Cp*Ir(biot-*p*-L)Cl]·S112A Sav@prot-SNPs and 171 TONs with [Cp*Ir(biot-*p*-L)Cl]·S112K Sav@prot-SNPs (for detailed data see Supporting Information). Other complex media were evaluated with [Cp*Ir(biot-*p*-L)Cl]·S112A-K121A Sav @prot-SNPs (Table 13).

Up to 4'500 TONs were obtained upon performing the imine reduction in urine. SNPs maintain their catalytic activity also in the presence of methanol (4'000 TONs, accompanied by an erosion in ee), which results in protein denaturation without the presence of protective organosilane layer and a complete loss of activity (Table 13, entries 9 and 10).

Table 13. Asymmetric imine reduction yielding **2a** using [Cp*Ir(biot-*p*-L)Cl]·S112A-K121A Sav@prot-SNP.

Entry	SNP	Cellular debris ^a	ee (%) ^{b,c}	Conv. (%) ^b	TON
1		milk	41	24	2569
2		yeast extract	37	1	158
3		urine pH 6	25	11	4554
4		blood pH 7	35	1	392
5	[Cp*Ir(biot- <i>p</i> -L)Cl]·S112A-K121A	blood serum	27	6	862
6	Sav@prot-SNP	empty vector CFE	89	3	1873
7		empty vector CL	33	1	132
8		GSH 5 mM	30	0.15	20
9		MeOH 50 %	14	30	4024
10	[Cp*Ir(biot- <i>p</i> -L)Cl]·S112A-K121A Sav Purified protein ^d	MeOH 50 %	0	0	0

Reactions were performed in a reaction buffer using 1 mg of SNPs in 100 μ l reaction mixture with 20 mM substrate concentration at RT for 48 h; ^[a] Reaction mixture contained 48 μ l of crude cellular extract, organic solvent or stock solution of glutathione, ^[b] Enantiomeric excess and conversion were determined by HPLC analysis on a Chiracel-IC column. ^[c] Positive ee values correspond to (*R*)-**2a** and negative ee values correspond to (*S*)-**2a**, ^[d] Reaction performed with purified protein without any protection against the organic solvent.

The catalytic experiments reported herein reveal several noteworthy features:

- (i) Immobilization of Sav isoforms on silica nanoparticles and their protection with organosilane layer yields catalysts with higher turnover number rates compared to the use of purified proteins.
- (ii) Such nanoparticles can be recycled up to three times with only a slight erosion in selectivity. Protected catalysts can withstand the presence of cellular debris without the need of diamide pretreatment²²⁰.
- (iii) The protective layer also prevents the protein denaturation in the presence of chaotropic agents.

3.4.4. CONCLUSION

In summary, we have successfully developed an artificial biocatalyst consisting of a pianostool iridium cofactor within Sav immobilized in SNPs. These nanoparticles display remarkable catalytic activity with TON > 46'000 using aqueous solutions and TON > 4'000 in the presence of cellular debris. Presented SNPs offer interesting perspectives towards green chemistry as they operate under nearly physiological conditions and can be recycled with only a slight erosion of reactivity. Immobilization and protection of artificial metalloenzymes on silica nanoparticles represents a promising technique for activity enhancement of such hybrid catalysts. The next steps will include cellular uptake and engineering enzyme cascades incorporating natural and artificial metalloenzymes within SNPs.

3.4.5 ACKNOWLEDGEMENTS

This research was supported by the Swiss Nanoscience Institute (Project NanoZyme, DPA2238) and the NCCR Molecular Systems Engineering.

3.4.6 SUPPORTING INFORMATION

The full supporting information can be found in Appendix C.

3.4.7 AUTHOR CONTRIBUTIONS

General idea: Prof. Dr. Thomas R. Ward and Prof. Dr. Patrick Shahgaldian

Protein immobilization and protection, screening of the resulting nanoparticles in transfer hydrogenation, synthesis of the iridium cofactors: Martina Hesticová

Scanning electron microscopy: Dr. Rita Maria Corroero

ICP-MS measurements: Dr. Markus Lenz

Manuscript writing: All authors

3.5 FERRITIN ENCAPSULATION OF ARTIFICIAL METALLOENZYMES: ENGINEERING A TERTIARY COORDINATION SPHERE FOR AN ARTIFICIAL TRANSFER HYDROGENASE

*The following section has been published in
Dalton Transactions, 2018, 47, 10837-10841
doi: 10.1039/C8DT02224K*

Ferritin encapsulation of artificial metalloenzymes: engineering a tertiary coordination sphere for an artificial transfer hydrogenase

Martina Hesticová,^a Tillmann Heinisch,^a Markus Lenz,^b and Thomas R. Ward^{*,a}

^a Department Chemistry, University of Basel, Mattenstrasse 24a, BPR 1096, Basel, 4002
(Switzerland) e-mail: thomas.ward@unibas.ch

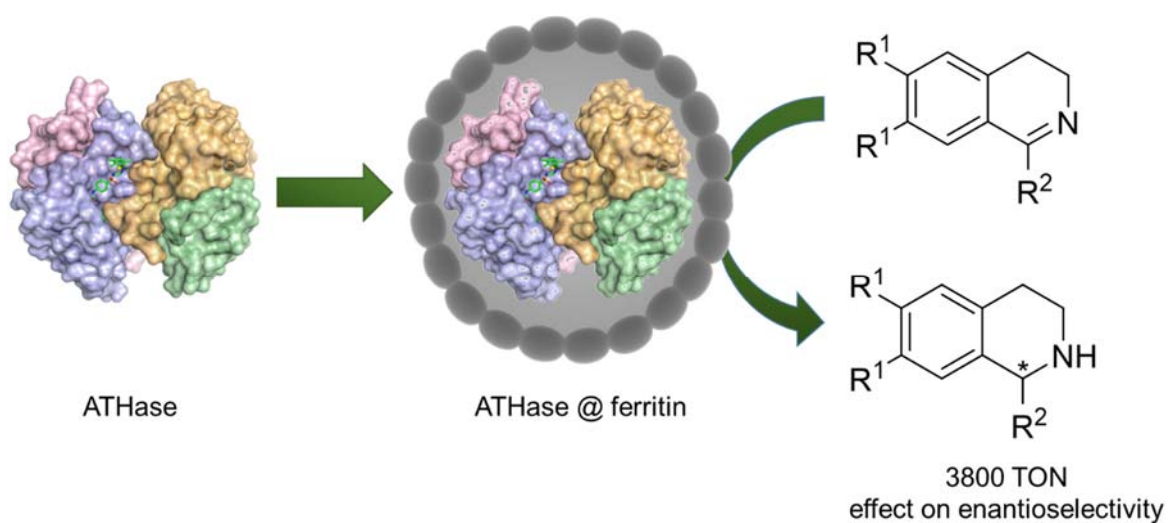
^b Institute for Ecopreneurship, School of Life Sciences, University of Applied Sciences and
Arts Northwestern Switzerland, Gründenstrasse 40, Muttenz, 4132 (Switzerland)

KEYWORDS: artificial metalloenzymes • protein encapsulation • nanocages • ferritin •
biocatalysis

3.5.1 ABSTRACT

Ferritin, a naturally occurring iron-storage protein, plays an important role in nanoengineering and biomedical applications. Upon iron removal, apoferritin was shown to allow the encapsulation of an artificial transfer hydrogenase (ATHase) based on the streptavidin-biotin technology. The third coordination sphere, provided by ferritin, significantly influences the catalytic activity of an ATHase for the reduction of cyclic imines.

TOC



3.5.2 INTRODUCTION

Biocatalysis is an attractive means to prepare high-added value products under environmentally benign conditions. Over the past few decades, the use of biocatalysis has expanded significantly and is now widely applied for the synthesis of chemicals, pharmaceuticals, fragrances etc.^{35, 247, 364-366, 373} To expand the rather limited biocatalytic repertoire, ArMs have attracted increasing attention.^{114, 361}

ArMs, that result from the incorporation of an organometallic moiety within a protein or DNA scaffold, combine attractive features of both enzymatic and homogeneous transition metal catalysis.^{41, 42, 47, 103, 116, 207, 227, 253, 254} To ensure the localization of the cofactor within the scaffold, the biot-Sav technology has found widespread use.^{73, 81, 96, 255} The protein scaffold provides a well-defined second coordination sphere around the metal moiety, and interacts with the cofactor, the substrates and intermediates. Accordingly, it significantly affects the selectivity and reaction rate of the ArM.^{207, 43, 374-378}

Inspection of the X-ray structures of various ArM based on the biot-Sav technology reveal that the biotinylated cofactor is partially solvent-exposed.^{103, 95, 164, 211} Efforts to genetically engineer the biotin-binding vestibule by introduction of various extended loops has shown promise.³⁷⁹ Building on our experience with mineralizing ArMs within silica nanoparticles,¹⁰¹ we reasoned that one could fully encapsulate an ATHase within a hollow protein shell. This additional protein environment, which provides the tertiary coordination sphere to the ArM³⁰⁹ was anticipated to influence the catalytic activity, both in terms of activity and selectivity.

Inspection of the size of homotetrameric Sav (4.5 nm · 5.5 nm · 5.1 nm) led us to hypothesize that ferritin (from horse spleen, inner diameter 7-8 nm) may offer an ideal capsule to host an ArM (Figure 18). Herein, we report on our efforts to compartmentalize an ATHase based on the biotin-streptavidin technology within apoferritin.

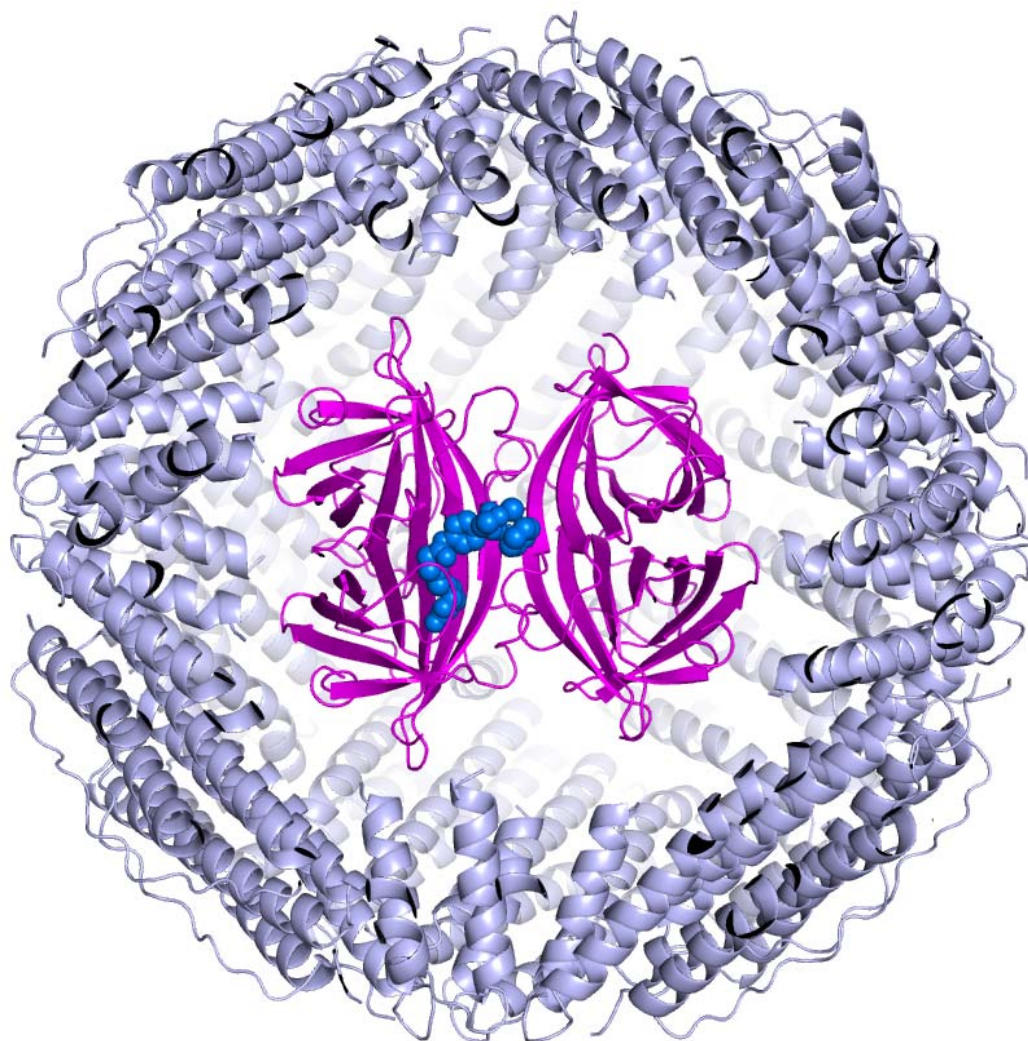


Figure 18. Apoferritin (indigo cartoon display, PDB code: 5c6f) offers a commensurate hollow to encapsulate an artificial metalloenzyme based on the biotin-streptavidin technology (Sav, magenta cartoon display, the $[\text{Cp}^*\text{Ir}(\text{biot-}p\text{-L})\text{Cl}]$ cofactor, blue, is displayed as space-filling; PDB code: 3pk2). The model was generated by manually docking the ATHase within apoferritin.

3.5.3 RESULTS AND DISCUSSION

Building on our experience with ATHase relying on the $[\text{Cp}^*\text{Ir}(\text{biot-}p\text{-L})\text{Cl}]$ cofactor, we set out to encapsulate the preassembled ArM $[\text{Cp}^*\text{Ir}(\text{biot-}p\text{-L})\text{Cl}] \cdot \text{Sav}$ within the cavity of horse spleen apoferritin. The following Sav mutants pre-assembled with the biotinylated iridium catalyst were selected for encapsulation: $[\text{Cp}^*\text{Ir}(\text{biot-}p\text{-L})\text{Cl}] \cdot \text{S112A Sav}$ (an (*R*)-selective imine reductase), $[\text{Cp}^*\text{Ir}(\text{biot-}p\text{-L})\text{Cl}] \cdot \text{S112K Sav}$ (an (*S*)-selective imine reductase) and $[\text{Cp}^*\text{Ir}(\text{biot-}p\text{-L})\text{Cl}] \cdot \text{K121A-S112A Sav}$ (the most active imine reductase based on the biot-

Sav complex).^{101,162} The ATHase was encapsulated within ferritin (ATHase@ferritin) by disassembling apoferritin upon decreasing the pH < 2. Upon increasing the pH to 8, the quaternary structure of ferritin is restored, thus allowing to encapsulate cargoes that are commensurate with the interior diameter of apoferritin. This strategy has been used to encapsulate various small molecules, nanoparticles, nanocrystals etc.³²⁸⁻³³⁶ To the best of our knowledge however, this approach has not been used to encapsulate proteins within apoferritin.

To highlight the encapsulation of Sav upon reassembly of the ferritin cage, we selected Sav equipped with one equivalent of a fluorescent biotinylated probe per four free biotin binding sites (fbs) of Sav. Accordingly, Sav S112A (tetramer, containing four fbs) was preincubated with one equivalent of biotin-4-fluorescein (B4F hereafter) and added to apoferritin at pH = 2 (i.e. disassembled apoferritin). Upon increasing the pH to 8, B4F·Sav S112A is encapsulated within ferritin (B4F·Sav S112A@ferritin hereafter). To remove the unspecifically adsorbed B4F·Sav S112A from the outer-surface of apoferritin, the solution was treated at pH = 8 with iminobiotin-sepharose beads and washed extensively. The iminobiotin moiety binds to free biotin-binding sites present in B4F·Sav S112A, thus allowing to remove B4F·Sav S112A that is not encapsulated within apoferritin by means of centrifugation and filtration. The solution that contains B4F·Sav S112A@ferritin was then subjected to preparative size-exclusion chromatography (SEC).

Fluorescence analysis of the ferritin band unambiguously revealed the presence of B4F. As no fluorescence was detected upon adding B4F (instead of B4F·Sav) by means of size-exclusion chromatography (See Appendix D, Figure D1), we hypothesize that B4F·Sav S112A@ferritin is formed (Figure 19).

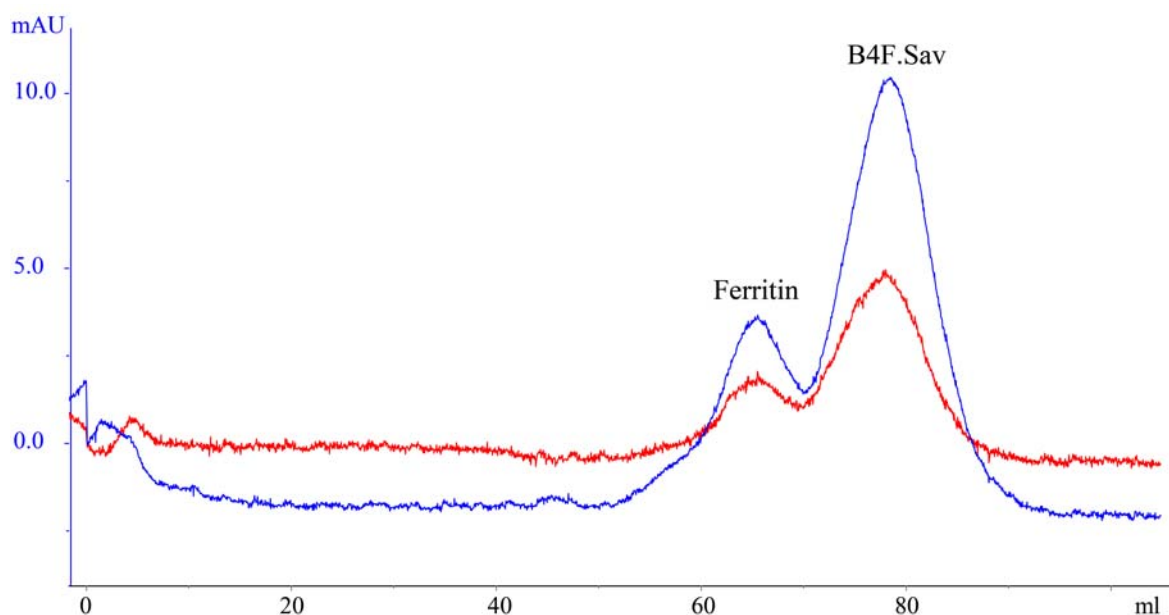


Figure 19. Preparative size-exclusion chromatogram of B4F·S112A-K121A Sav@ferritin. The blue line indicates absorbance at 280 nm. The absorbance at 495 nm (red trace) shows that B4F co-elutes with the apoferritin cage at 65 mL (run in 50 mM Tris-HCl, 100 mM NaCl, pH 8.0).

Having highlighted the formation of B4F·Sav S112A@ferritin by fluorescence, we proceeded to encapsulate various ATHases in apoferritin following the same protocol. The resulting ATHases [Cp*Ir(biot-*p*-L)Cl]·S112A@ferritin, [Cp*Ir(biot-*p*-L)Cl]·S112K@ferritin and [Cp*Ir(biot-*p*-L)Cl]·S112A-K121A@ferritin were purified by preparative SEC (Figure D2).

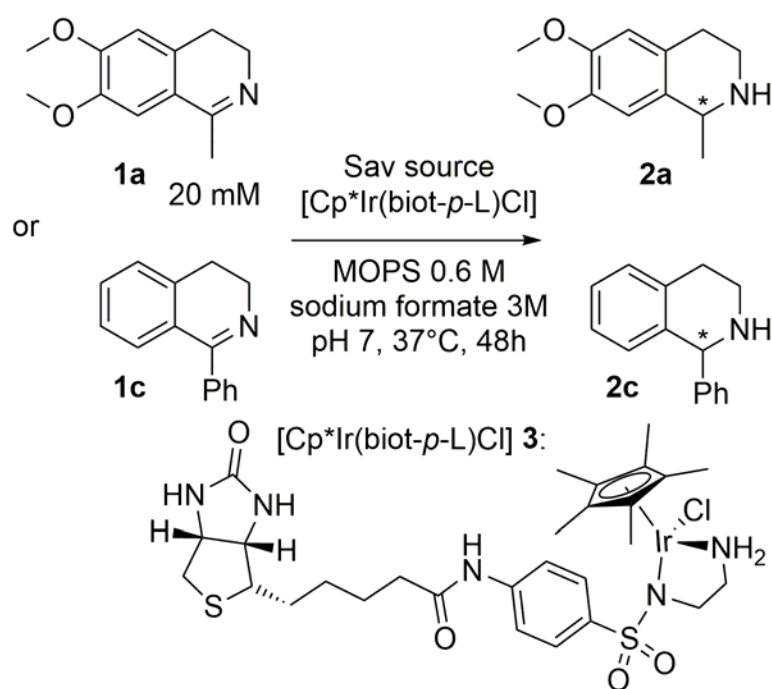
The presence of iridium in the purified Sav@ferritin samples was confirmed by means of ICP-MS. Upon sample digestion, the samples were diluted and directly analyzed.

Dynamic light scattering (DLS) measurements of the combined fractions containing the assembled ferritin shells revealed an increase in particle diameter of approx. 20% (Table D1). This observation suggests that the ATHase is indeed located within ferritin.

The presence of the ATHase within the ferritin cage [Cp*Ir(biot-*p*-L)Cl]·Sav@ferritin was further confirmed by comparison of the SDS- and native PAGE analysis. Under native conditions, the samples containing [Cp*Ir(biot-*p*-L)Cl]·Sav@ferritin revealed no band attributable to Sav (Figure D3). In contrast, under denaturing conditions, the Sav was released from the denatured ferritin cage and could be visualized by B4F on the

SDS PAGE, as it contained two available fbs sites. Due to the remarkable stability of homotetrameric Sav, Sav maintained its tetrameric structure and biotin-binding activity, even under denaturing SDS PAGE conditions (Figure D4). In stark contrast, native PAGE analysis of a 1:1 mixture of $[\text{Cp}^*\text{Ir}(\text{biot-}p\text{-L})\text{Cl}]\cdot\text{Sav}$ and apoferritin revealed two bands (Figure D4, lane 5). This demonstrates that $[\text{Cp}^*\text{Ir}(\text{biot-}p\text{-L})\text{Cl}]\cdot\text{Sav}$ is encapsulated within ferritin, rather than unspecifically adsorbed on the outer-surface of ferritin, thus confirming the DLS observations.

Next, the encapsulated ATHases were tested for the reduction of cyclic imines **1a** and **1c** (Scheme 11). To determine the turnover number of the encapsulated ATHases (TON), ICP-MS analysis of samples containing Ir as $[\text{Cp}^*\text{Ir}(\text{biot-}p\text{-L})\text{Cl}]\cdot\text{Sav}@ferritin$ was carried out. The catalytic performance of the ATHases $[\text{Cp}^*\text{Ir}(\text{biot-}p\text{-L})\text{Cl}]\cdot\text{Sav}@ferritin$ was compared to the corresponding "free" ATHases: $[\text{Cp}^*\text{Ir}(\text{biot-}p\text{-L})\text{Cl}]\cdot\text{Sav}$.



Scheme 11. Reduction of cyclic imines **1a** and **1c** using the ATHase.

Since the isoquinoline substrates are protonated under the reaction conditions,⁹⁵ they can penetrate through the ferritin 3-fold channels. In line with this assumption, we observed catalysis with all encapsulated ATHases.

All tested [Cp*Ir(biot-*p*-L)Cl]·Sav@ferritin, afforded preferentially (*S*)-**2a**. This contrasts with [Cp*Ir(biot-*p*-L)Cl]·Sav, which affords either (*R*)-**2a** or (*S*)-**2a**, depending on the Sav mutant: i) [Cp*Ir(biot-*p*-L)Cl]·Sav S112A affords **2a** in 75 % ee (*R*) and 35 % conversion (Table 14, entry 3) and [Cp*Ir(biot-*p*-L)Cl]·Sav S112K affords **2a** in 41 % ee (*S*) and 20 % conversion (Table 14, entry 5). Reduction of imine **1a** in the presence of the encapsulated [Cp*Ir(biot-*p*-L)Cl]·S112A Sav@ferritin affords (*S*)- **2a** in 46 % ee (*S*) (Table 14, entry 11).

Similarly, catalysis with [Cp*Ir(biot-*p*-L)Cl]·S112A-K121A Sav yields **2a** in 60 % ee (*R*) and 90 % conversion (Table 14, entry 7), while the encapsulated [Cp*Ir(biot-*p*-L)Cl]·S112A-K121A Sav@ferritin affords (*S*)-**2a** in 44 % ee (Table 14, entry 15). Control experiments with [Cp*Ir(biot-*p*-L)Cl]·S112A-K121A Sav at 1 μM catalyst loading afforded 56 % ee (*R*)-**2a** and 72 TON.

Table 14. Results obtained from the reduction of cyclic imine **1a** or **1c**. The reactions were performed using 20 mM substrate concentration at 37°C for 48 h (See Appendix D for experimental details).

Entry	Catalyst	[Ir] (μM) ^a	Sub.	ee (%) ^b , c	conv. (%) ^b	TON ^d
1	[Cp*Ir(biot- <i>p</i> -L)Cl]	50	1a	<i>rac.</i>	16	65
2	[Cp*Ir(biot- <i>p</i> -L)Cl]	50	1c	<i>rac.</i>	18	71
3	[Cp*Ir(biot- <i>p</i> -L)Cl]·S112A	50	1a	75	35	142
4	[Cp*Ir(biot- <i>p</i> -L)Cl]·S112A	50	1c	43	39	154
5	[Cp*Ir(biot- <i>p</i> -L)Cl]·S112K	50	1a	-41	25	20
6	[Cp*Ir(biot- <i>p</i> -L)Cl]·S112K	50	1c	57	6	24
7	[Cp*Ir(biot- <i>p</i> -L)Cl]·S112A-K121A	50	1a	59	90	358
8	[Cp*Ir(biot- <i>p</i> -L)Cl]·S112A-K121A	50	1c	69	72	289
9	[Cp*Ir(biot- <i>p</i> -L)Cl]@ferritin	1.24 ^d	1a	0	0.08	13
10	[Cp*Ir(biot- <i>p</i> -L)Cl]@ferritin	1.24 ^d	1b	0	5	853
11	[Cp*Ir(biot- <i>p</i> -L)Cl]·S112A@ferritin	0.42 ^d	1a	-46	0.16	74
12	[Cp*Ir(biot- <i>p</i> -L)Cl]·S112A@ferritin	0.42 ^d	1c	24	5.58	2880
13	[Cp*Ir(biot- <i>p</i> -L)Cl]·S112K@ferritin	0.40 ^d	1a	-47	0.09	46
14	[Cp*Ir(biot- <i>p</i> -L)Cl]·S112K@ferritin	0.40 ^d	1c	24	5.57	2731
15	[Cp*Ir(biot- <i>p</i> -L)Cl]·S112A-K121A@ferritin	0.28 ^d	1a	-44	0.17	117
16	[Cp*Ir(biot- <i>p</i> -L)Cl]·S112A-K121A@ferritin	0.28 ^d	1c	20	5.55	3874
17	S112A-K121A@ferritin	0	1a	0	0	0
18	S112A-K121A@ferritin	0	1c	0	0	0
19	Apo-ferritin	0	1a	0	0	0
20	Apo-ferritin	0	1c	0	0	0
21	Apo-ferritin + [Cp*Ir(biot- <i>p</i> -L)Cl]·S112A-K121A	50	1a	55	85	340
22	Apo-ferritin + [Cp*Ir(biot- <i>p</i> -L)Cl]·S112A-K121A	50	1c	64	69	276
23	[Cp*Ir(biot- <i>p</i> -L)Cl]·S112A-K121A	1	1a	56	0.36	72
24	[Cp*Ir(biot- <i>p</i> -L)Cl]·S112A-K121A	1	1c	35	6	1108

^a Enantiomeric excess and conversion were determined by HPLC analysis. ^b Positive ee values correspond to (*R*)-product and negative ee values correspond to (*S*)-product. ^c Values were calculated based on the ICP-MS measurement of each batch (see Appendix D for details).

In the reduction of the less bulky **1c**, no inversion of enantioselectivity was observed in any of the tested encapsulated ATHases. However, the TONs have tripled with [Cp*Ir(biot-*p*-L)Cl]·S112A-K121A Sav@ferritin (entry 16) compared to the use of the free ATHase in buffer under similar conditions (entry 24). Similar TONs were also obtained for [Cp*Ir(biot-*p*-L)Cl]·S112A@ferritin, which afforded (*R*)-**2c** in 24 % ee and 2880 TON. The [Cp*Ir(biot-*p*-L)Cl]·S112K@ferritin afforded (*R*)-**2c** in 24 % ee and 2731 TON.

The effect on enantioselectivity and catalytic efficiency of the encapsulated ATHases depends on both the substrate and the used Sav mutant. Further studies in regards to the effect of point-mutations on the kinetic behavior of the hybrid catalysts are currently undergoing in our research group.

3.5.4. CONCLUSION

Overall, these findings highlight the influence of the third coordination sphere on the catalytic performance of the ferritin-encapsulated ATHases.

Taking advantage of the reversible dissociation and reassembly of apoferritin, we have compartmentalized an artificial metalloenzyme within a protein cage. The resulting ATHases maintained their catalytic activity, displaying up to > 3800 TON for the reduction of cyclic imines. The marked variation in enantioselectivity, observed upon ATHase encapsulation, highlights the combined effect of both the second- and third coordination sphere provided by Sav and ferritin respectively.

These results highlight the possibility to encapsulate an ArM within ferritin following a reassembly route. The significant improvement in TON compared to the free ArM suggests that this strategy may offer an attractive means to protect a precious metal in a cellular environment and possibly to deliver it *in vivo*, without eliciting an immune response.^{380, 381}

3.5.5 ACKNOWLEDGEMENTS

This research was supported by the Swiss Nanoscience Institute (Project NanoZyme, DPA2238), the ERC (DrEAM) and the NCCR Molecular Systems Engineering. MRH would like to thank the Biophysics Facility of the University of Basel for the use of the DLS instrument.

3.5.6 SUPPORTING INFORMATION

The full supporting information can be found in Appendix D.

3.5.7 AUTHOR CONTRIBUTIONS

General idea: Prof. Dr. Thomas R. Ward

Protein encapsulation, purification, and characterization, screening of the resulting hybrid catalysts in transfer hydrogenation of cyclic imines, protein crystallization: Martina Hesticová

Docking: Dr. Tillmann Heinisch

ICP-MS measurements: Dr. Markus Lenz

Manuscript writing: All authors

3.6 REFERENCES

- [275] R. A. Sheldon, *Adv. Synth. Catal.* **2007**, *349*, 1289–1307.
- [276] James, L.; Alexey, M. *Immobilization of Enzymes*. In *Enzyme Catalysis in Organic Synthesis*, Wiley-VCH **2018**.
- [277] S. Roger A., *Adv. Synth. Catal.* **2007**, *349*, 1289–1307.
- [278] D.N. Tran, K.J. Balkus, *ACS Catal.* **2011**, *1*, 956–968.
- [279] R. A. Sheldon, S. van Pelt, *Chem. Soc. Rev.* **2013**, *42*, 6223–6235.
- [280] J. M. S. Cabral, J. F. Kennedy, in: *Thermostability of Enzymes*, Springer Verlag, Berlin **1993**, 163–179.
- [281] J. C. Y. Wu, C. H. Hutchings, M. J. Lindsay, C. J. Werner, B. C. Bundy, *J. Biotechnol.* **2015**, *193*, 83–90.
- [282] J. Feng, N. Balaji, M. Surya, *Biotechnol. Bioeng.* **2013**, *111*, 209–222.
- [283] R. K. S., M. Joachim, S. Marc, N. C. M., *Angew. Chem. Int. Ed.* **2017**, *56*, 13574–13589.
- [284] L. Betancor, H. R. Luckarift, *Biotechnol. Genet. Eng. Rev.* **2010**, *27*, 95–114.
- [285] F. Kazenwadel, M. Franzreb, B. E. Rapp, *Anal. Methods* **2015**, *7*, 4030–4037.
- [286] S. Satagopan, Y. Sun, J. R. Parquette, F. R. Tabita, *Biotechnol. Biofuels* **2017**, *10*, 175.
- [287] R. DiCosimo, J. McAuliffe, A. J. Poulouse, G. Bohlmann, *Chem. Soc. Rev.* **2013**, *42*, 6437–6474.
- [288] A. Homaei, *Enzyme Immobilization and Its Application in the Food Industry*, **2015**.
- [289] A. Liese, L. Hilterhaus, *Chem. Soc. Rev.* **2013**, *42*, 6236–6249.
- [290] Weetall, H. H., *Applications of immobilized enzymes*. In *Immobilized Enzymes for Industrial Reactors*; Academic Press, **1975**, 201–226.
- [291] S. Datta, L. R. Christena, Y. R. S. Rajaram, *3 Biotech* **2013**, *3*, 1–9.
- [292] G. Cristina, B. Ángel, F. Roberto, R. R. C., *Adv. Synth. Catal.* **2011**, *353*, 2885–2904.
- [293] S. A. Roger, *Adv. Synth. Catal.* **2007**, *349*, 1289–1307.
- [294] M. J. Moehlenbrock, S. D. Minteer, *Introduction to the Field of Enzyme Immobilization and Stabilization*. In *Enzyme Stabilization and Immobilization: Methods and Protocols*, Springer New York, New York, NY, **2017**, 1–7.
- [295] J. Mehta, N. Bhardwaj, S. K. Bhardwaj, K.-H. Kim, A. Deep, *Coord. Chem. Rev.* **2016**, *322*, 30–40.
- [296] T. Jesionowski, J. Zdarta, B. Krajewska, *Adsorption* **2014**, *20*, 801–821.
- [297] S. Sakai, Y. Liu, T. Yamaguchi, R. Watanabe, M. Kawabe, K. Kawakami, *Biotechnol. Lett.* **2010**, *32*, 1059–1062.
- [298] I. Gill, A. Ballesteros, *Trends Biotechnol.* **2000**, *18*, 469–479.
- [299] Reetz M. T., Z. Albin, S. Jörg, *Biotechnol. Bioeng.* **2010**, *49*, 527–534.
- [300] R. A. Sheldon, *Org. Process Res. Dev.*, **2011**, *15*, 213–223.
- [301] H. Mallin, T. R. Ward, *ChemCatChem* **2018**, DOI 10.1002/cctc.201800162.
- [302] I. Migneault, C. Dartiguenave, M. J. Bertrand, K. C. Waldron, *Biotechniques* **2004**, *37*, 790–802.
- [303] M. Hartmann, X. Kostrov, *Chem. Soc. Rev.* **2013**, *42*, 6277–6289.
- [304] L.-F. Ho, S.-Y. Li, S.-C. Lin, W.-H. Hsu, *Process Biochem.* **2004**, *39*, 1573–1581.
- [305] R. A. Meryam Sardar, *Biochem. Anal. Biochem.* **2015**, *4*, 1–8.
- [306] L. Cheng-Kang, A. Ai-Nhan, *Emerg. Areas Bioeng.* **2018**, DOI doi:10.1002/9783527803293.ch4.
- [307] M. N. Gupta, M. Kaloti, M. Kapoor, K. Solanki, *Artif. Cells Blood Substit. Biotechnol.* **2011**, *39*, 98–109.
- [308] M. R. Correro, N. Moridi, H. Schätzingler, S. Sykora, E. M. Ammann, E. H. Peters, Y. Dudal, P. F. X. Corvini, P. Shahgaldian, *Angew. Chemie - Int. Ed.* **2016**, *55*, 6285–6289
- [309] J.-N. Rebilly, B. Colasson, O. Bistri, D. Over, O. Reinaud, *Chem. Soc. Rev.* **2015**, *44*, 467–489.
- [310] L. Klermund, S. T. Poschenrieder, K. Castiglione, *ACS Catal.* **2017**, *7*, 3900–3904.
- [311] S. Abe, B. Maity, T. Ueno, *Chem. Commun.* **2016**, *52*, 6496–6512.
- [312] A. H. Chen, P. A. Silver, *Trends Cell Biol.* **2012**, *22*, 662–670.
- [313] B. Wörsdörfer, K. J. Woycechowsky, D. Hilvert, *Science* **2011**, *331*, 589–592.
- [314] S. B. P. E. Timmermans, J. C. M. van Hest, *Curr. Opin. Colloid Interface Sci.* **2018**, *35*, 26–35.
- [315] J. G. Heddle, S. Chakraborti, K. Iwasaki, *Curr. Opin. Struct. Biol.* **2017**, *43*, 148–155.
- [316] A. Sciore, E. N. G. Marsh, *Symmetry-directed design of protein cages and protein lattices and their applications* in *Sub-Cellular Biochemistry*, Springer International Publishing, Cham, **2017**, 195–224.
- [317] J. G. Heddle, S. Chakraborti, K. Iwasaki, *Curr. Opin. Struct. Biol.* **2017**, *43*, 148–155.

- [318] S. Bhaskar, S. Lim, *NPG Asia Mater.* **2017**, *9*, e371.
- [319] Y. Zhang, M. S. Ardejani, B. P. Orner, *Chem. Asian J.* **2016**, *11*, 2814–2828.
- [320] T. Ueno, S. Abe, *Catalytic Reactions Promoted in Protein Assembly Cages*. In *Coordination Chemistry in Protein Cages: Principles, Design, and Applications*, Wiley-VCH, **2013**, 175–202.
- [321] E. C. Theil, *The Ferritin Family of Iron Storage Proteins* In *Advances in Enzymology and Related Areas of Molecular Biology*, Wiley-VCH, **2006**, 421–449.
- [322] J. K. Grady, J. Zang, T. M. Laue, P. Arosio, N. D. Chasteen, *Anal. Biochem.* **2002**, *302*, 263–268.
- [323] B. Gallois, B. L. D’Estaintot, M. A. Michaux, A. Dautant, T. Granier, G. Precigoux, J. A. Soruco, F. Roland, O. Chavas-Alba, A. Herbas, R. R. Crichton, *J. Biol. Inorg. Chem.* **1997**, *2*, 360–367.
- [324] L. Michaelis, *Adv. Protein Chem.* **1947**, *3*, 53–66.
- [325] R. R. Crichton, C. F. Bryce, *Biochem. J.* **1973**, *133*, 289–299.
- [326] S. Stefanini, S. Cavallo, C. Q. Wang, P. Tataseo, P. Vecchini, A. Giartosio, E. Chiancone, *Arch. Biochem. Biophys.* **1996**, *325*, 58–64.
- [327] Ş. N. K. Elmas, R. Güzel, M. G. Say, A. Ersoz, R. Say, *Biosens. Bioelectron.* **2018**, *103*, 19–25.
- [328] Belletti, F. Pederzoli, F. Forni, M. A. Vandelli, G. Tosi, B. Ruozi, *Expert Opin. Drug Deliv.* **2017**, *14*, 825–840.
- [329] Q. Wang, C. Zhang, L. Liu, Z. Li, F. Guo, X. Li, J. Luo, D. Zhao, Y. Liu, Z. Su, *J. Biotechnol.* **2017**, *254*, 34–42.
- [330] J. Zang, H. Chen, G. Zhao, F. Wang, F. Ren, *Crit. Rev. Food Sci. Nutr.* **2017**, *57*, 3673–3683.
- [331] J. Chen, G. C. Zhao, *Talanta* **2017**, *168*, 62–66.
- [332] S. Tetter, D. Hilvert, *Angew. Chem. Int. Ed.* **2017**, *56*, 14933–14936.
- [333] G. Jutz, P. Van Rijn, B. Santos Miranda, A. Böker, *Chem. Rev.* **2015**, *115*, 1653–1701.
- [334] K. W. Pulsipher, I. J. Dmochowski, *Ferritin encapsulation and templated synthesis of inorganic nanoparticles* In *Protein Cages: Methods and Protocols*, Springer New York, New York, NY, **2014**, 27–37.
- [335] I. Yamashita, K. Iwahori, S. Kumagai, *Biochim. Biophys. Acta Gen. Subj.* **2010**, *1800*, 846–857.
- [336] L. Turyanska, T. D. Bradshaw, J. Sharpe, M. Li, S. Mann, N. R. Thomas, A. Patané, *Small* **2009**, *5*, 1738–1741.
- [337] M. Suzuki, M. Abe, T. Ueno, S. Abe, T. Goto, Y. Toda, T. Akita, Y. Yamada, Y. Watanabe, *Chem. Commun.* **2009**, 487–4873.
- [338] S. Abe, J. Niemeyer, M. Abe, Y. Takezawa, T. Ueno, T. Hikage, G. Erker, Y. Watanabe, *J. Am. Chem. Soc.* **2008**, *130*, 10512–10514.
- [339] J. Niemeyer, S. Abe, T. Hikage, T. Ueno, G. Erker, Y. Watanabe, *Chem. Commun.* **2008**, 6519–6521.
- [340] L. Zhang, L. Laug, W. Münchgesang, E. Pippel, U. Gösele, M. Brandsch, M. Knez, *Nano Lett.* **2010**, *10*, 219–223.
- [341] A. Dautant, J.-B. Meyer, J. Yariv, G. Precigoux, R. M. Sweet, A. J. Kalb (Gilboa), F. Frolow, *Acta Crystallogr. Sect. D* **1998**, *54*, 16–24.
- [342] Y. Zhang, B. P. Orner, *Int. J. Mol. Sci.* **2011**, *12*, 5406–5421.
- [343] M. Kim, Y. Rho, K. S. Jin, B. Ahn, S. Jung, H. Kim, M. Ree, *Biomacromolecules* **2011**, *12*, 1629–1640.
- [344] M. Gerl, R. Jaenicke, *Eur. Biophys. J.* **1987**, *15*, 103–109.
- [345] T. Tosha, H.-L. Ng, O. Bhattasali, T. Alber, E. C. Theil, *J. Am. Chem. Soc.* **2010**, *132*, 14562–14569.
- [346] S. Pead, E. Durrant, B. Webb, C. Larsen, D. Heaton, J. Johnson, G. D. Watt, *J. Inorg. Biochem.* **1995**, *59*, 15–27.
- [347] J. Anu, H. Reija-Riitta, L. Urpo, K. Teemu, P. Lauri J., S. Tero, V. Marko, *Small* **2007**, *3*, 1362–1367.
- [348] B. Webb, J. Frame, Z. Zhao, M. L. Lee, G. D. Watt, *Arch. Biochem. Biophys.* **1994**, *309*, 178–183.
- [349] M. L. Flenniken, L. O. Liepold, B. E. Crowley, D. A. Willits, M. J. Young, T. Douglas, *Chem. Commun.* **2005**, 447–449.
- [350] N. Galvez, P. Sanchez, J. M. Dominguez-Vera, *Dalt. Trans.* **2005**, 2492–2494.
- [351] Y. Fei, Z. Yan, K. K. S., Y. Hsiang-Kuo, V. Tuan, *Photochem. Photobiol.* **2010**, *86*, 662–666.
- [352] A. Silvio, F. Luca, G. C. Simonetta, *Angew. Chemie Int. Ed.* **2002**, *41*, 1017–1019.
- [353] Z. Yang, X. Wang, H. Diao, J. Zhang, H. Li, H. Sun, Z. Guo, *Chem. Commun.* **2007**, 3453–3455.
- [354] G. Liu, J. Wang, H. Wu, Y. Lin, *Anal. Chem.* **2006**, *78*, 7417–7423.
- [355] Y. Takezawa, P. Bockmann, N. Sugi, Z. Wang, S. Abe, T. Murakami, T. Hikage, G. Erker, Y. Watanabe, S. Kitagawa, et al., *Dalt. Trans.* **2011**, *40*, 2190–2195.

- [356] Z. Wang, Y. Takezawa, H. Aoyagi, S. Abe, T. Hikage, Y. Watanabe, S. Kitagawa, T. Ueno, *Chem. Commun.* **2011**, 47, 170–172.
- [357] R. Ghirlando, R. Mutsikova, C. Schwartz, *Nanotechnology* **2015**, 27, 45102.
- [358] L. Qiu, R. McCaffrey, W. Zhang, *Chem. Asian J.* **2018**, 13, 362–372.
- [359] R. Fan, S. W. Chew, V. V. Cheong, B. P. Orner, *Small* **2010**, 6, 1483–1487.
- [360] F. C. Meldrum, V. J. Wade, D. L. Nimmo, B. R. Heywood, S. Mann, *Nature* **1991**, 349, 684–687.
- [361] O. Pàmies and J. E. Bäckvall, *Chem. Rev.* **2003**, 103, 3247–3261.
- [362] M. D. Truppo, H. Strotman, G. Hughes, *ChemCatChem* **2012**, 4, 1071–1074.
- [363] F. Rosati, G. Roelfes, *ChemCatChem* **2010**, 2, 916–927.
- [364] P. J. Deuss, R. Denheeten, W. Laan, P. C. J. Kamer, *Chem. Eur. J.* **2011**, 17, 4680–4698.
- [365] T. Ueno, S. Abe, N. Yokoi, Y. Watanabe, *Coord. Chem. Rev.* **2007**, 251, 2717–2731.
- [366] P. K. Sasmal, C. N. Streu, E. Meggers, *Chem. Commun.*, **2013**, 49, 1581–1587.
- [367] A. Cumbo, B. Lorber, P. F.-X. Corvini, W. Meier, P. Shahgaldian, *Nat. Commun.* **2013**, 4, 1503–1507.
- [368] S. Sykora, A. Cumbo, G. Belliot, P. Pothier, C. Arnal, Y. Dudal, P. F.-X. Corvini, P. Shahgaldian, *Chem. Commun.* **2015**, 51, 2256–2258.
- [369] P. Shahgaldian, R. Correro-Shahgaldian, A. Cumbo, P. F.-X. Corvini, WO/2015/014888, **2015**.
- [370] M. R. Correro, N. Moridi, H. Schützinger, S. Sykora, E. M. Amman, E. H. Peters, Y. Dudal, P. F.-X. Corvini, P. Shahgaldian, *Angew. Chem. Int. Ed.* **2016**, 55, 6285–6289.
- [371] W. Stöber, A. Fink, E. Bohn, *J. Colloid Interface Sci.* **1968**, 26, 62–69.
- [372] S. Betanzos-Lara, Z. Liu, A. Habtemariam, A. M. Pizarro, B. Qamar, P. J. Sadler, *Angew. Chem., Int. Ed.* **2012**, 51, 3897–3900.
- [373] M. Martínez-Calvo, J. L. Mascareñas, *Coord. Chem. Rev.* **2018**, 359, 57–79.
- [374] S. A. Vedha, G. Velmurugan, P. Venuvanalingam, *RSC Adv.* **2016**, 6, 81636–81646.
- [375] D. J. Sommer, M. D. Vaughn, G. Ghirlanda, *Chem. Commun.* **2014**, 50, 15852–15855.
- [376] S. Sahu, L. R. Widger, M. G. Quesne, S. P. de Visser, H. Matsumura, P. Moënné-Loccoz, M. A. Siegler, D. P. Goldberg, *J. Am. Chem. Soc.* **2013**, 135, 10590–10593.
- [378] R. L. Shook, A. S. Borovik, *Inorg. Chem.* **2010**, 49, 3646–3660.
- [379] J.-L. Zhang, D. K. Garner, L. Liang, D. A. Barrios, Y. Lu, *Chem. Eur. J.* **2009**, 15, 7481–7489.
- [380] M. M. Pellizzoni, F. Schwizer, C. W. Wood, V. Sabatino, Y. Cotelle, S. Matile, D. N. Woolfson, T. R. Ward, *ACS Catal.* **2018**, 8, 1476–1484.
- [381] Z. Heger, S. Skalickova, O. Zitka, V. Adam, R. Kizek, *Nanomedicine* **2014**, 9, 2233–2245.
- [382] X. Li, L. Qiu, P. Zhu, X. Tao, T. Imanaka, J. Zhao, Y. Huang, Y. Tu, X. Cao, *Small* **2012**, 8, 2505–2514.

SUMMARY AND OUTLOOK

Artificial metalloenzymes have emerged as a promising and valuable approach to combine the attractive features of homogeneous catalysis, enzymatic catalysis and the vast reaction repertoire of metal-catalyzed chemical transformations. This doctoral thesis represents our optimization efforts of the activity of an artificial imine reductase based on the streptavidin-biotin technology by either genetic or nanotechnological means.

First, the limitation of cellular matrix and the throughput of our screening efforts was addressed. Chapter II describes a design of a library of potentially active streptavidin mutants for the creation of artificial metalloenzymes and their following application in high throughput screening. Upon mutating 28 positions within the streptavidin active site lying in close proximity of the metal center of the catalyst, a library consisting of 335 mutants was prepared. Their implementation in two different reaction types was proven effective even without the need of protein purification and resulted in only 10 % deviations in conversion (results from 90 replicates of the same mutant). Following the optimized protocol, we continued with our efforts in directed evolution of an artificial imine reductase. After only four rounds of mutagenesis, expression and screening, two improved streptavidin variants with higher selectivity and activity toward the reduction of three cyclic imine substrates were identified. Moreover, these two variants were found to be active even in the presence of organic solvents, thus demonstrating the potential for future industrial utilization.

The second chapter describes optimization of an artificial imine reductase for nano applications by immobilization on silica nanoparticles or by encapsulation within a ferritin nanocage. Our efforts in immobilization of three artificial imine reductases on silica nanoparticles followed by their protection in a soft organosilane layer yielded immobilized catalysts with remarkably higher activity compared to free hybrid catalysts. The soft

organosilane layer, resulting from polycondensation of two types of organosilanes, allows for substrate diffusion, and simultaneously shields the metal cofactor from various chaotropic agents such as methanol, glutathione and complex cellular media such as blood, urine, cell lysates and milk. The protected catalysts yielded over 46 000 turnovers in pure samples and 4000 turnovers in crude cellular extracts. Encapsulation of the artificial imine reductase within a ferritin nanocage brought an additional advantage; the complex microenvironment created by the protein cage serves as a tertiary coordination sphere for the metal catalyst within streptavidin. Upon encapsulation, the hybrid catalyst yielded over 3800 turnovers in the reduction of cyclic imines and demonstrated different enantioselectivity when compared to the performance of the free artificial imine reductase.

In the future, the nano-optimized versions of artificial metalloenzymes could be further optimized by introducing mutations within the apoferritin scaffold. The immobilized hybrid catalysts protected in organosilane layer represent an intriguing possibility of preparing a flow-reactor for the production of enantioenriched or enantiopure cyclic imines.

APPENDICES

APPENDIX A

Supporting information and selected sections for *Nat. Protoc.* **2016**, *11*, 835–852

A.1 MATERIALS

All commercially available chemicals were purchased from commercial suppliers (Sigma-Aldrich, ABCR, Acros Organics, Alfa Aesar, AppliChem, Baker, BD, NEB, AnaSpec, Fisher Scientific, Fluka, Merck, or WWR) and used without further purification. *E. coli* bacterial strains (BL21 and TOP10) were purchased from NEB or Invitrogen, respectively. Empty vector plasmid pET-24a empty vector was purchased from Novagen.

PCR reactions were performed with an Eppendorf Mastercycler Gradient. ¹H and ¹³C spectra were recorded on a Bruker 400 MHz. The chemical shifts (δ) are reported in parts per million (ppm) relative to tetramethylsilane or a residual solvent peak. Analyses of the catalytic runs were performed on an Agilent 1100 normal phase HPLC with an analytical Chiralpak IC column (250 · 4.6 mm, 5 μ m), GC using Agilent CAM column (30 m x 0.25 μ m) and CP-Chirasil-DEX CB (25m x 0.25 μ m) using He as carrier gas, or by Aquity UPLC H-Class Bio from Waters using BEH C18 column 1.7 μ m, 2.1 x 50 mm for UPLC

. The absorbance spectra were measured on a microplate reader Tecan, model Infinite M200.

E. coli strains used:

- TOP10 (Invitrogen, cat. no. C4040): F⁻ *mcrA* Δ (*mrr-hsdRMS-mcrBC*) Φ 80*lacZ* Δ M15 Δ *lac*^{x74} *recA1* *araD139* Δ (*araleu*)7697 *galU galK rpsL* (Str^R) *endA1 nupG*
- BL21 (DE3; NEB, cat. no. C2527): *E. coli* B F⁻ *dcm ompT hsdS*(_{RB⁻ MB⁻}) *gal* λ (DE3)

A.2. REAGENT SETUP

20xZYP-salts: Dissolve 1 M KH₂PO₄ (54.4 g), 1 M Na₂HPO₄ (56.8 g) and 0.5 M (NH₄)₂SO₄ (26.4 g) in MQ water (final volume of 400 ml)³³. Autoclave (121°C for 20 min). The sterile solution can be stored at room temperature (RT corresponds to 25°C) for years.

20xZYP-sugar: Dissolve 10 % (v/v) anhydrous glycerol (40 ml), 55.5 mM glucose-monohydrate (4.4 g) and 4 % (w/v) Lactose XM (16 g) in MQ water (final volume of 400 ml)³³. Sterile filter with a cutoff of 0.22 μ m. The sterile solution can be stored at 4°C for up to one year.

100xMgSO₄: Dissolve 200 mM MgSO₄ (2.46 g) in MQ water (50 ml). Autoclave (121°C for 20 min). The sterile solution can be stored at 4°C for years.

Normal ZYP-5052 Medium: Dissolve tryptone (8 g) and yeast extract (4 g) in 712 ml MQ water and autoclave (121°C for 20 min)³³. Add 20xZYP-salts (40 ml), 20xZYP-sugar (40 ml) and MgSO₄ (8 ml) to the media. The sterile solution (without antibiotic) can be stored at 4°C for up to one year.

Modified ZYP-5052 Medium: Dissolve tryptone (8 g) and yeast extract (4 g) in 664 ml MQ water and autoclave (121°C for 20 min). Add 20xZYP-salts (40 ml), 20xZYP sugar (80 ml) and MgSO₄ (16 ml) to the media. The sterile solution (without antibiotic) can be stored at 4°C for up to one year.

Lysogeny Broth (LB): Dissolve 1 % tryptone (10 g), 0.5 % yeast extract and 1 % NaCl in MQ water (final volume of 1 l). Adjust pH to 7 using NaOH⁴¹. For LB-agar plates, use the same recipe but add 1.5 % agar (15 g, bacteriology grade). Autoclave (121°C for 20 min). For agar plates, cool to 55°C, add antibiotic and pour plates. The sterile solution (without antibiotic) can be stored at 4°C for up to one year. The plates can be stored at 4°C for up to 3 months (for kanamycin).

LB_{Soc}: Dissolve 2 % tryptone (2 g), 0.5 % yeast extract (0.5 g), 10 mM NaCl (0.05 g) and 2.5 mM KCl (0.019 g) in MQ water (final volume of 100 ml). Adjust pH to 7 using NaOH.⁴² Autoclave (121°C for 20 min) and add filter sterilized solutions (0.22 µm cutoff) of 1 M MgCl₂ (1 ml), 1 M MgSO₄ (1 ml) and 1 M glucose (2 ml). The sterile solution (without antibiotic) can be stored at 4°C for up to one year.

LB_{SOB}: Same composition as LB_{Soc} but without glucose⁴². The sterile solution (without antibiotic) can be stored at 4°C for up to one year.

RF 1-buffer: Weigh RbCl (100 mM, 2.42 g), MnCl₂ x 4 H₂O (50 mM, 1.98 g); KOAc (30 mM, 0.59 g) and CaCl₂ x 2 H₂O (10 mM, 0.29 g) and fill up with 15 % (v/v) Glycerol (200 ml final volume). Set the pH to 5.8 using 0.2 M CH₃COOH and filter sterilize solution⁴³. Solution can be prepared in advance and stored at 2-8°C for up to 6 months.

RF 2-buffer: Weigh in RbCl (10 mM); CaCl₂ x 2 H₂O (75 mM) and MOPS (10 mM) and fill up with 15 % (v/v) glycerol in MQ water (50 ml final volume). Set the pH to 7 using NaOH and filter-sterilize the solution⁴³. Solution can be prepared in advance and stored at 2-8°C for up to 6 months.

Reaction buffer for ATHase: Dissolve MOPS (12.556 g) and sodium formate (20.403 g) in MQ water (final volume 50 ml) to obtain final concentrations of 1.2 M MOPS and 6 M formate. Adjust the pH to 6 using NaOH. Solution can be prepared in advance and stored up to 6 months at 2-8°C.

ATHase substrate stock solution: Dissolve 1-phenyl-3,4-dihydroisoquinoline **1c** (165.8 mg, final concentration 400 mM) in DMSO (2 ml). Solution can be prepared in advance and stored up to 6 months at 2-8°C.

ATHase stock solution of the iridium catalyst: Dissolve [Cp*Ir(biot-*p*-L)Cl] ((1.6 mg, final concentration of 2 mM) in DMSO (1 ml). This solution can be stored at 4° for 30 days.

Diamide stock solution: Dissolve 1,1'-Azobis(*N,N*-dimethylformamide) [72.5 mg, final concentration 200 mM] in DMSO (2 ml). This solution needs to be prepared freshly before each catalysis campaign.

Lysis buffer for ATHase or methathesis: Dissolve MOPS (ATHase, 522.9 mg, final concentration 50 mM) in MQ water (50 ml) or use PBS (metathesase, 12 mM phosphate, pH 7.5). Adjust the pH to 7.4 with NaOH. Dissolve lysozyme (20 mg) and DNaseI (20 μ g) in this buffer (20 ml final volume). This solution needs to be prepared freshly before each catalysis campaign.

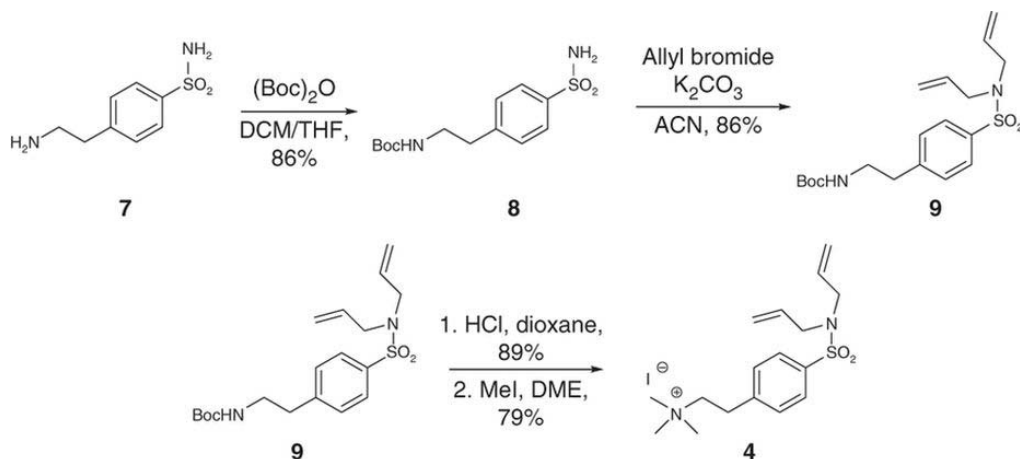
FBS Assay buffer: Dissolve MOPS (ATHase, 2092 mg, final concentration 100 mM) in MQ water (100 ml). Adjust the pH to 7.5 with NaOH. The solution can be stored at RT for up to one year.

Sav-stock solution for FBS determination: Prepare a pure 1 mM Sav FBS stock solution (Use the molecular weight of the monomer 16368 Da) in MQ water in a final volume of 1 ml. Dilute this in AB to a final concentration of 100 μ M Sav FBS. The solution can be stored at -20°C for 3 months if multiple freeze and thaw cycles are avoided.

B4F solution for FBS determination: First, prepare a B4F stock solution (10 mM) in DMSO. Then, dilute this stock solution to 0.4 mM using FBS assay buffer. The solutions can be stored at -20°C for 1 year if multiple freeze and thaw cycles are avoided. As B4F is light-sensitive, protect the solutions with aluminum foil.

Iminobiotin binding buffer: Adjust the pH of a NaHCO₃ buffer solution containing (1 l, 50 mM) and NaCl (0.5 M) to pH 9.8 by dropwise addition of NaOH (5 M stock solution). The buffer can be stored at RT for up to one year but the pH should be controlled before use.

Metathesase reaction buffer: For this buffer, add MgCl₂(H₂O)₆ (101.5 g) to an acetic acid stock solution (847 ml of a 100 mM solution) and a sodium acetate stock solution (153 ml of a 100 mM solution). Adjust the pH to 4 by dropwise addition of NaOH (5 M stock solution). The buffer can be stored at RT for up to one year but the pH should be controlled before use.



Scheme A1. Overview of the synthesis of the diolefinic substrate **4**.

tert-butyl (4-sulfamoylphenethyl)carbamate (abbreviated as compound **8 in Scheme A1):** To a flask containing 4-(2-aminoethyl)benzenesulfonamide (abbreviated as compound **7** in Scheme A1) (5.01 g, 24.5 mmol, 1.00 eq.) add DCM (20 ml) and THF (40 ml). Then, add Boc-anhydride (5.61 g, 25.7 mmol, 1.05 eq.) to the mixture and stir for 2 h. Dilute with 200 ml of EtOAc and wash with 1 M aq. HCl (2 x 100 ml) and brine (100 ml). Dry the organic phase

over MgSO_4 and remove the solvent under vacuum. Wash the white solid with hexane twice and dry under high vacuum to obtain the desired product **8** as a white solid (6.20 g, 86 %). MP: 181.5 °C – 182.5 °C. $^1\text{H NMR}$ (400 MHz, DMSO) δ = 7.74 (d, $^3J_{\text{HH}}$ = 8.3 Hz, 2H), 7.38 (d, $^3J_{\text{HH}}$ = 8.3 Hz, 2H), 7.29 (s, 2H), 6.93 (s, 1H), 3.20 – 3.11 (m, 2H), 2.81 – 2.73 (m, 2H), 1.38 (s, 9H).

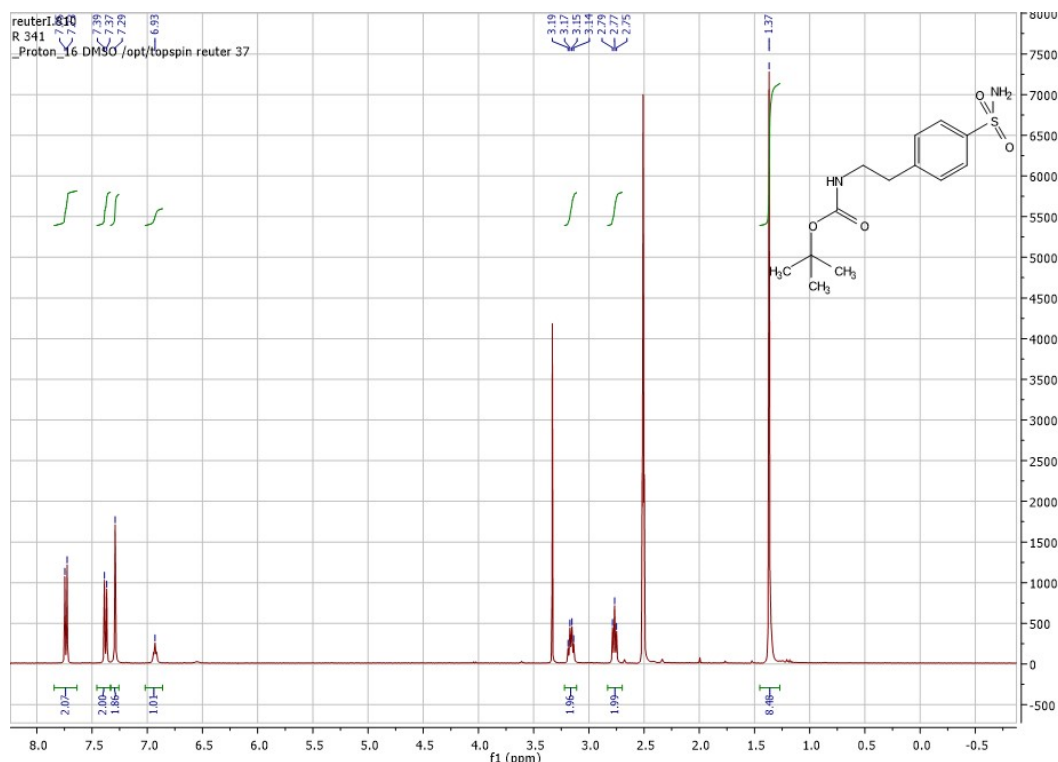


Figure A1. $^1\text{H NMR}$ spectra of compound **8**.

***tert*-butyl (4-(*N,N*-diallylsulfamoyl)phenethyl)carbamate (abbreviated as compound **9** in Scheme A1):** To a solution of *tert*-butyl (4-sulfamoylphenethyl)carbamate (**8**) (6.19 g, 20.6 mmol, 1.00 eq.) in ACN (100 ml), add allyl bromide (6.29 g, 4.53 ml, 51.5 mmol, 2.50 eq.) and K_2CO_3 (7.12 g, 51.5 mmol, 2.50 eq.). Stir the mixture at 85 °C overnight and allow it to cool to RT. Then, filter and remove the solvent from the filtrate under reduced pressure. Purify the residue by flash column chromatography (silica gel, Cyclohexane/EtOAc 2:1) to obtain **9** as a pale yellow oil (6.70 g, 86 %). $^1\text{H NMR}$ (400 MHz, CDCl_3) δ = 7.75 (d, $^3J_{\text{HH}}$ = 8.4 Hz, 2H), 7.33 (d, $^3J_{\text{HH}}$ = 8.3 Hz, 2H), 5.67 – 5.56 (m, 2H), 5.19 – 5.10 (m, 4H), 4.62 (bs, 1H), 3.81 (d, $^3J_{\text{HH}}$ = 6.3 Hz, 4H), 3.44 – 3.35 (m, 2H), 2.88 (t, $^3J_{\text{HH}}$ = 7.0 Hz, 2H), 1.43 (s, 9H). $^{13}\text{C NMR}$ (100 MHz, DMSO) δ = 155.8, 144.3, 138.5, 132.6, 129.5, 127.4, 119.1, 79.5, 49.4, 41.3, 36.1, 28.4. HRMS [ESI(+)]TOF: calculated for $\text{C}_{19}\text{H}_{28}\text{N}_2\text{NaO}_4\text{S}$ $[\text{M}]^+$ 403.1662; found 403.1665.

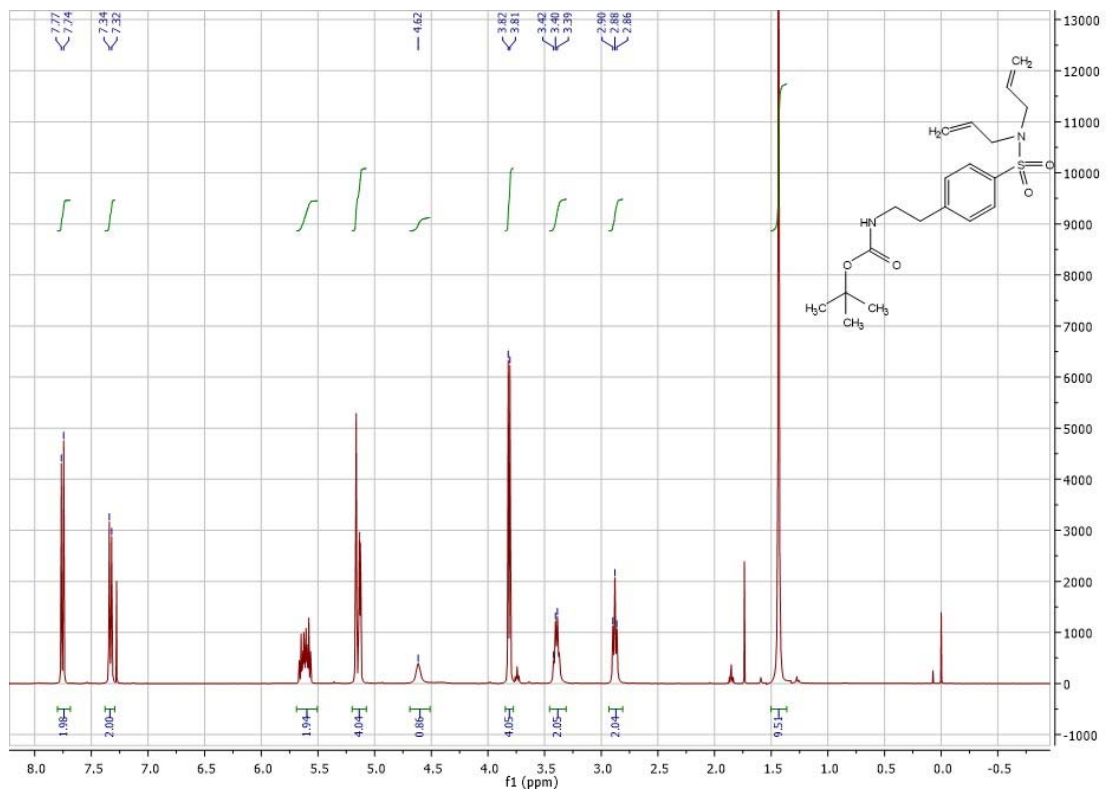


Figure A2. ^1H NMR spectra of compound 9.

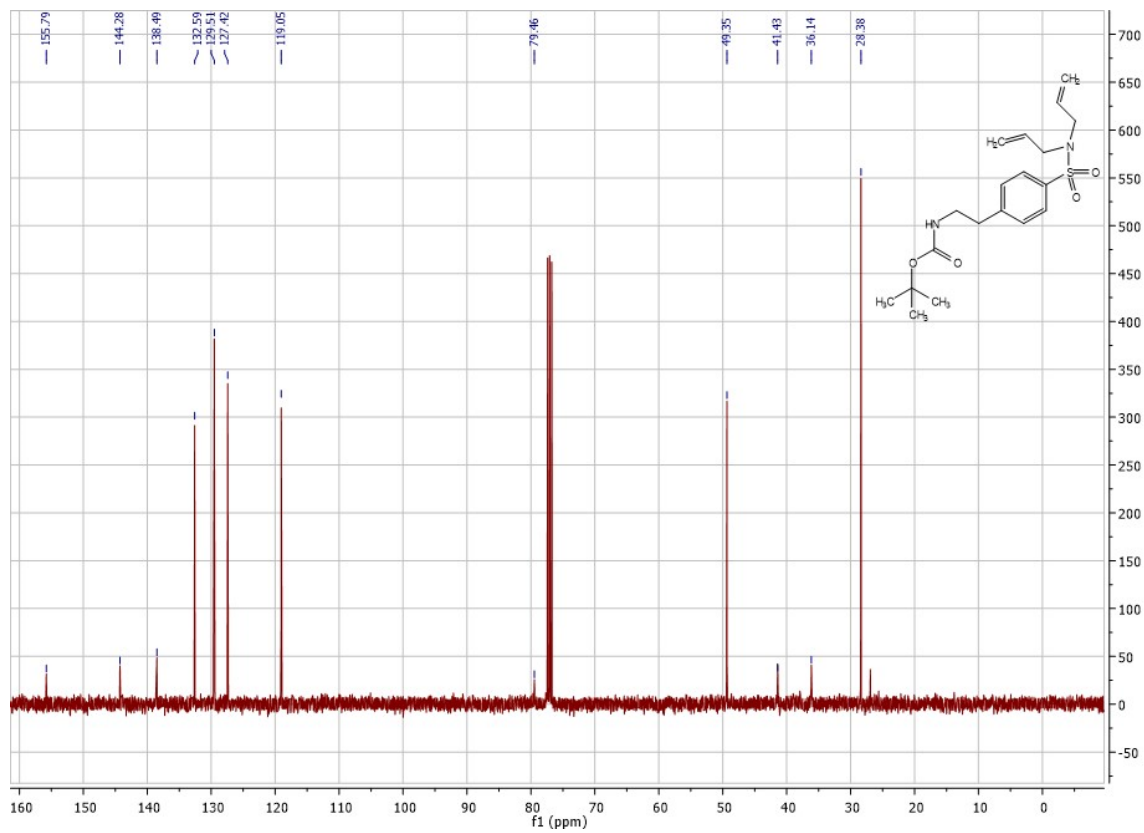


Figure A3. ^{13}C NMR spectra of compound 9.

Substrate for metathesase (abbreviated as compound 4 in in Scheme 6 and Scheme A1):

Dissolve *tert*-butyl (4-(*N,N*-diallylsulfamoyl)phenethyl)carbamate (**9**) (3.91 g, 10.3 mmol, 1.00 eq.) in dioxane (15 ml) and add a solution of HCl in dioxane (15 ml, 4 M solution) and stir at RT for 4 h till TLC indicates complete conversion. Precipitate the hydrochloride salt by pouring the mixture into cold DEE (300 ml), collect it by filtration and dry it under high vacuum to obtain a colorless solid (2.91 g, 89 %). Then, redissolve it in DCM (150 ml), add saturated aqueous NaHCO₃ (200 ml) and vigorously stir for 2 h. Collect the organic phase, extract the aqueous layer with DCM and dry the combined organic phases over MgSO₄. Remove the solvent under vacuum to yield the amine as a pale yellow oil. Take up a fraction of the amine (1.00 g, 3.16 mmol, 1.00 eq.) in DME (20 ml). Add iodomethane (4.49 g, 1.97 ml, 31.6 mmol, 10.0 eq.) and K₂CO₃ (2.62 g, 19.0 mmol, 6.00 eq.) and stir the mixture for 3 h at RT. Add DCM (80 ml) to redissolve the precipitated ammonium salt and remove the carbonate by filtration. Concentrate the filtrate under vacuum, decant with DEE and dry under high vacuum to obtain the pure substrate (**4**) as a colorless solid (1.13 g, 79 %). Use the standard Schlenk technique to prepare the catalyst⁴⁶. Degas solvents by flushing these with a nitrogen stream for 30 min. Use oven-dried glassware (110 °C, overnight). Remove traces of air using three vacuum- followed by nitrogen refills. Keep a small nitrogen overpressure throughout the entire reaction to prevent air from contaminating the flask. If you stir a reaction under reflux, place the tap connected to the Schlenk line at the top of the condenser, to prevent excessive evaporation. Use a rubber septum to add liquid via a syringe. Apply a gentle nitrogen overpressure before removing the septum to add a solid. When performing the ligand exchange or the biotinylation, remove the solvent using the Schlenk line equipped with a secondary cooling trap (not on a rotary evaporator). The catalyst should be stable in its solid form. However, it should always be kept in a freezer at -20 °C and under argon. Prepared aliquots of the catalyst should be used within 3 months. MP: 184 °C – 186 °C. ¹H NMR (400 MHz, DMSO) δ = 7.84 (d, ³J_{HH} = 8.4 Hz, 2H), 7.58 (d, ³J_{HH} = 8.4 Hz, 2H), 5.60 (ddt, ³J_{HH} = 16.3 Hz, ³J_{HH} = 10.1 Hz, ³J_{HH} = 6.2 Hz, 2H), 5.16 (d, ³J_{HH} = 17.1 Hz, 2H), 5.14 (d, ³J_{HH} = 11.0 Hz, 2H), 3.75 (d, ³J_{HH} = 6.2 Hz, 4H), 3.65 – 3.55 (m, 2H), 3.22 – 3.12 (m, 11H). ¹³C NMR (100 MHz, DMSO) δ = 141.7, 138.3, 132.8, 130.0, 127.3, 118.8, 65.0, 52.4, 49.3, 28.2. HRMS [ESI(+)]TOF: calculated for C₁₇H₂₇N₂O₂S [M]⁺ 323.1788; found 323.1791.

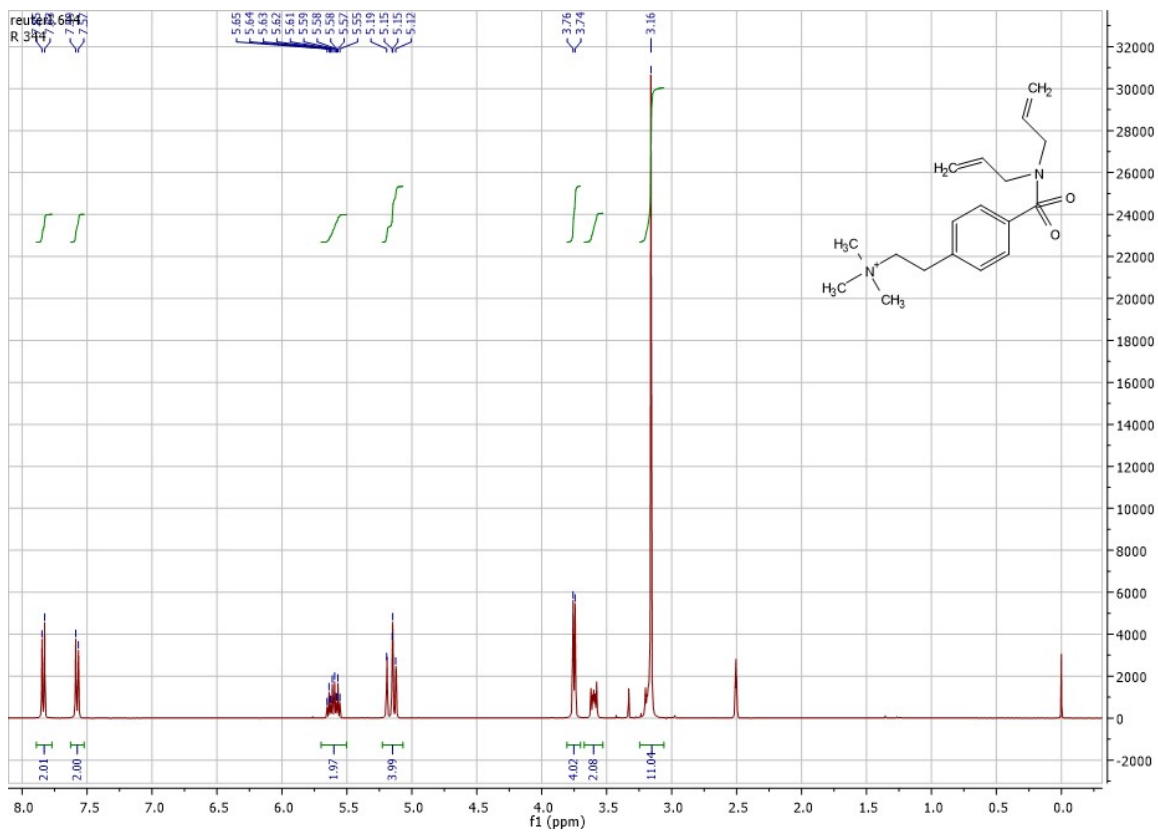


Figure A4. ¹H NMR spectra of compound 4.

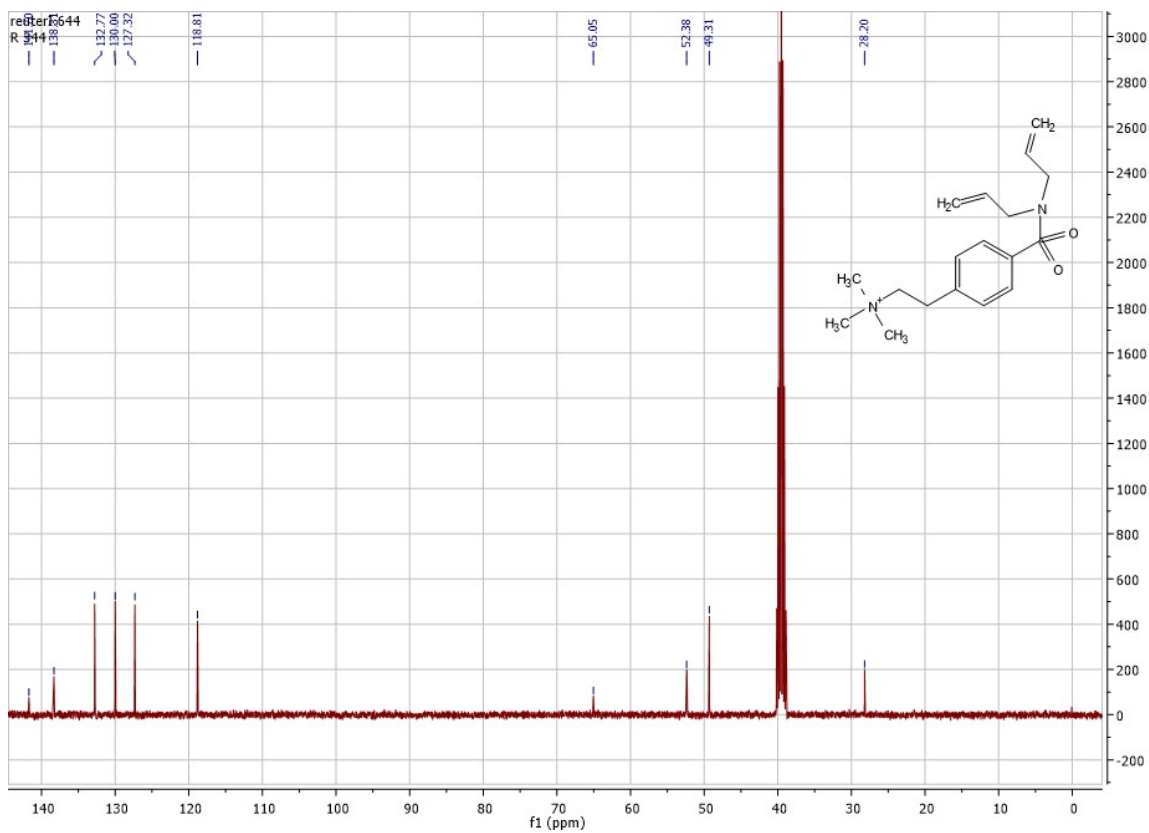


Figure A5. ¹³C NMR spectra of compound 4.

Substrate stock solution: Dissolve the metathesase substrate **4** (90.1 mg) in the metathesase reaction buffer in a volumetric flask (10 ml). Metathesis catalyst (abbreviated as compound **6** in Scheme 6) aliquots are prepared as follows: charge a flask with **6** (4 mg) and add dichloromethane (1 ml). Portion this stock solution into aliquots (50 μ l) inside small flasks, dispense into five test tubes and seal these with a rubber septum. Remove the solvent from the aliquots by applying a gentle vacuum through a needle. Once evaporated, flush with nitrogen to obtain aliquots of **6** (0.2 mg). Aliquots should be stored at -20°C and be used within three months. Once DMSO is added to the aliquots, they have to be used immediately.

Iminobiotin beads: The beads are sold as a suspension in 20 % ethanol. Adjust the total volume with 20 % ethanol to twice the volume of the completely settled beads. Upon homogenization by thorough shaking, the binding capacity is about 5 mg Sav ml⁻¹ suspension. The beads are stored at 4°C and maintain their Sav binding capacity for several years (> 5).

Internal standard solution: Dissolve benzyltriethylammonium bromide (272.2 mg) in MQ water in a volumetric flask (100 ml) and fill up to the mark. The solution can be stored at 4°C for several months.

A.3 BOX 1

Design of noncomplementary, site-directed mutagenesis primers, TIMING 1-2 d

1. Basic primer construct:
 - Add in the 3'-prime direction from the mutation codon, approximately 18 nucleotides from the sequence (corresponding to 6 amino acids)
 - Add in the 5'-prime direction from the mutation codon, approximately 6 nucleotides from the sequence (corresponding to 2 amino acids)
 - This affords a basic primer construct containing approximately 27 nucleotides (e.g. XXXXXYYZZZZZZZZZZZZZZZZZZ; X=5'-direction nucleotides, Y= codon to be mutated Z= 3'-direction nucleotides)
2. Substitute the codon YYY to one codon specific for the desired mutation. Mutate the wildtype codon as little as possible. If several codons are possible, select the one with the highest codon usage of *E.coli* K12.⁴⁶
3. Check the primer quality with e.g. OligoCalc: Oligonucleotide Properties Calculator. If possible, minimize the G/C-content (typically 40 - 60 %). Avoid as much as possible hairpins and 3'-primer complementary. To match the criteria listed above, the primer sequence may be optimized by addition or deletion of nucleotides from the template

sequence. Furthermore, other possible codons for the mutation position can be chosen. The resulting optimized “forward primer” should contain 25 - 35 nucleotides. Using the nearest neighbor method, estimate the primer melting temperature (hereafter T_m). It should be $55^\circ\text{C} < T_m < 70^\circ\text{C}$ (higher G/C content = higher T_m). To ensure binding of the primer at the 3'-end of the sequence, be sure to include at least one or two G/C. It is recommended to include one or two G/C nucleotides at the 5'-end as well. This ensures binding and amplification by the polymerase (the polymerase transcribes from the 5'-to 3'-end). Keep at least four nucleotides of the original sequence from the first mutated nucleotide towards the 5' end of the primer sequence. Avoid adding more than eight nucleotides, as this increases overlapping of the forward and the reverse primers.

4. To amplify the double stranded plasmid, a second primer (reverse-primer) for the reverse DNA strand is needed. This reverse-primer is designed in the same manner as described for the forward primer: as template sequence however, the complementary strand is used. Importantly, the mutated codon must be complementary to that in the forward-primer. The final complementary overlapping part of both primers should be at least 10-16 nucleotides (maximum) including the mutated codon, to prevent 3'overlapping. To ensure binding of both primers during the annealing step, the maximum difference in T_m for the forward and reverse primer should not exceed 5°C .
5. To use the same annealing temperature during one PCR (96 well plate) for 96 mutants, place the primers for specific mutations with similar T_m ($\pm 5^\circ\text{C}$) on one master plate. We strongly recommend to order and to use the pre-mixed forward and reverse-primers at the required concentration (10 μM) that companies provide for a minor fee in a 96-well plate format.

A.3 BOX 2

Preparation of chemically competent cells in a 96-deep-well plates, TIMING 1.5 d

The steps below are as described in the work of Hanahan and colleagues,^{42,43} All steps, including cell treatment, are performed under a laminar flow box to avoid contamination.

1. Prepare an overnight culture of *E.coli* TOP10 or BL21 (DE3) in LB media (5 ml). Incubate overnight (37°C at 200 rpm).
2. Inoculate LB_{SOB} (150 ml) with the overnight culture (1.5 ml). Grow the culture (37°C and 200 rpm) to an $\text{OD}_{600\text{ nm}} = 0.35$.
3. Divide the culture into aliquots in sterile falcon tubes (50 ml) and centrifuge (5 min, 4°C , 4000 g).

4. Pool and resuspend the cell pellet in RF1 buffer (30 ml). Incubate on ice (15 min). Keep cells on ice and pre-cool RF1 and RF2.
5. Centrifuge (5 min at 4 °C and 4000 g).
6. Discard the supernatant and resuspend the cell pellet in RF2 (6 ml)
7. Incubate on ice (15 min).
8. Aliquot the cell suspension (50 µl) into a 96 deep well plate for *E.coli* TOP10 or a 24 deep well plate for BL21 (DE3) on ice. Seal the plate with foil. It is recommended to use BL21 (DE3) in 24 deep well plates as this improves the transformation efficiency.
9. Freeze the plate in liquid nitrogen and store cells at -80 °C. The transformation efficiency can decrease and therefore competent cells should not be stored for more than 6 months. Competent cells which have been thawed should not be frozen again.
10. Test the transformation efficiency with e.g. pUC19 vector with a single aliquot.

A.4 PROCEDURE

Site-directed mutagenesis in 96-well format 9-10 days.

1. Design oligos for site-directed mutagenesis (See Box 1 for more information). Spin the 96-well plate (4000 g for 5 min) and either proceed immediately, or store at -20°C. For a list of oligos used in our analysis, see supplementary table 1. Primer solution can be stored at -20°C indefinitely.
2. Produce the mutagenesis template plasmid by cloning the SavK121A sequence into pET-24a (Supplementary data). We recommend synthesizing the gene sequence commercially via a gene supplier where it can be precloned in the desired expression vector. In parallel, also prepare the pET-24a Sav WT plasmid and the pET-24a empty vector control. For the Sav sequence see supplementary data.
3. Transform each plasmid into *E. coli* BL21(DE3). To do this, add 1 - 3 µl plasmid (~100 ng) to 50 µl BL21(DE3) on ice, and incubate for 30 min.
4. Heat-shock the cells in a water bath (42°C, 30 s) and then transfer the tubes back to ice for 2 min. Add LB_{Soc} (250 µl) and incubate the tubes with shaker (300 rpm for 1 h at 37°C).
5. Mix the suspension by pipetting up and down. Plate out the suspension (250 µl) on LB-Agar plates containing the resistance marker kanamycin (50 µg ml⁻¹). Incubate plates overnight at 37°C.
6. Inoculate LB media (5 ml) containing kanamycin (50 µg ml⁻¹) with a fresh single colony bearing the template plasmid and incubate overnight (37°C at 200 rpm).

7. Prepare a glycerol stock for each by mixing 0.7 ml overnight culture with sterile glycerol (0.3 ml) to obtain an end concentration of 30 % (v/v) glycerol and incubate on ice (30 min). Freeze in liquid nitrogen and store at -80°C. Then use a commercial MiniPrep plasmid isolation kit (e.g. MN NucleoBond®) and follow the instructions of the supplier for high copy plasmids. Use the remaining overnight culture for isolation. For the elution step, use sterilized MQ water (50 µl) to elute the template plasmid. For the DNA quantification, analyze the above solution (50 µl) with a NanoDrop ND-1000. The sample is pure if the absorbance ratio at 260 nm / 280 nm is ~1.8. Heat the plasmid solution (70°C, 10 min) to deactivate any DNase present. Plasmid solutions can be stored indefinitely at -20°C.
8. Prepare the QuikChange mutagenesis PCR master mix using the pET-24a SavK121A plasmid. The following is described for one 96 well plate. For QuikChange mutagenesis, a methylated circular DNA template (plasmid) is amplified using mutagenic primers (forward and reverse) and a high fidelity polymerase. After PCR, a DpnI digestion is performed which cleaves only the methylated template plasmid DNA. As the newly synthesized DNA is non-methylated, it is not digested by DpnI. This eliminates all of the background template DNA. No ligation of the resulting nicks in the newly synthesized DNA occurs during the PCR. A transformation into an efficient cloning strain, like E. coli TOP10, is thus necessary to repair the nicks present in the newly synthesized DNA.

Table A1. PCR reagents

Compound	Volume [µl]	Final in 2500 µl
MQ water	1687.5	
Q5 polymerase 5x buffer	500	1x
Template plasmid pET-24a SavK121A (25 ng µl ⁻¹)	50	0.5 ng µl ⁻¹
Dimethylsulfoxide (DMSO)	100	4 %
dNTP mix 10 mM each	50	200 µM each
Q5 polymerase (2 U µl ⁻¹)	12.5	25 U
Final volume for 100 reactions	2500	

It is possible to apply an alternative high fidelity, thermostable DNA polymerase. Mix the solution gently and spin down. Add polymerase slowly to avoid air bubbles.

9. With a multichannel pipette, aliquot the mutagenesis PCR master mix (24 µl) into each well of a 96 well plate. To avoid unnecessary loss of the master mix, use PCR tubes (0.2 ml) as reservoirs. Pipette gently to avoid air bubbles.

10. For each mutant, add the primer mix solution (1 μ l of the 10 μ M solution from step 1) to the master mix solution (24 μ l). Be sure to contact the meniscus with the tip and do not mix afterwards. Close plate tightly with an appropriate PCR lid.
11. Place the plate into a 96-well plate compatible thermocycler. Program the following temperatures, cycles and durations:

Table A2. PCR conditions

Cycle number	Denature	Anneal	Extend
1	95°C, 2 min		
2- 18	95°C, 15 s	60°C, 15 s	72°C, 5 min (~ 40 s kb ⁻¹)
19			72°C, 10 min
20	4 - 8°C		

Steps 3 to 6 should be performed without any interruption.

12. After PCR, add DpnI (0.3 μ l, 20 U μ l⁻¹) with a multichannel pipette to each well, seal the plate with a breathable membrane and incubate for two hours at 37°C. Deactivate DpnI by heating (10 min at 70°C). This step digests the methylated template DNA. Digested PCR samples can be stored at -20°C indefinitely if multiple freeze/ thaw cycles are avoided.
13. Prepare an agarose gel to check for presence of the mutated PCR product. To do this, weigh agarose (1.5 g, molecular biology grade) in 0.5x TBE buffer (150 ml, 1 % (w/v) final concentration). Heat in a microwave until agarose dissolves. Add EtBr (10 μ l), mix gently and pour it into the chamber. Add combs for 100 samples into the warm solution. Wait until the gel is solid (~30 min). Ethidium bromide (EtBr) is hazardous, toxic and maybe mutagenic for humans. Wear chemically resistant gloves for all steps and work under a ventilated hood.
14. Place the gel into the running chamber containing 0.5x TBE and remove combs. Use DpnI digested PCR product (5 μ l) and mix it with 6x loading buffer (1 μ l). This mixture (5 μ l) is then loaded into each lane. Use 1 kb DNA ladder (3 μ l) as a standard. Run the gel at 100 V/ 400 mA for 40 min. Analyze the gel under an illuminator at 302 nm and search for an amplified band at 5.7 kb. Figure 6 displays a typical gel resulting from one 96 well PCR mutagenesis plate with a strong amplified band of the vector in each lane. A band at the size of the plasmid is a good hint that the PCR was successful.

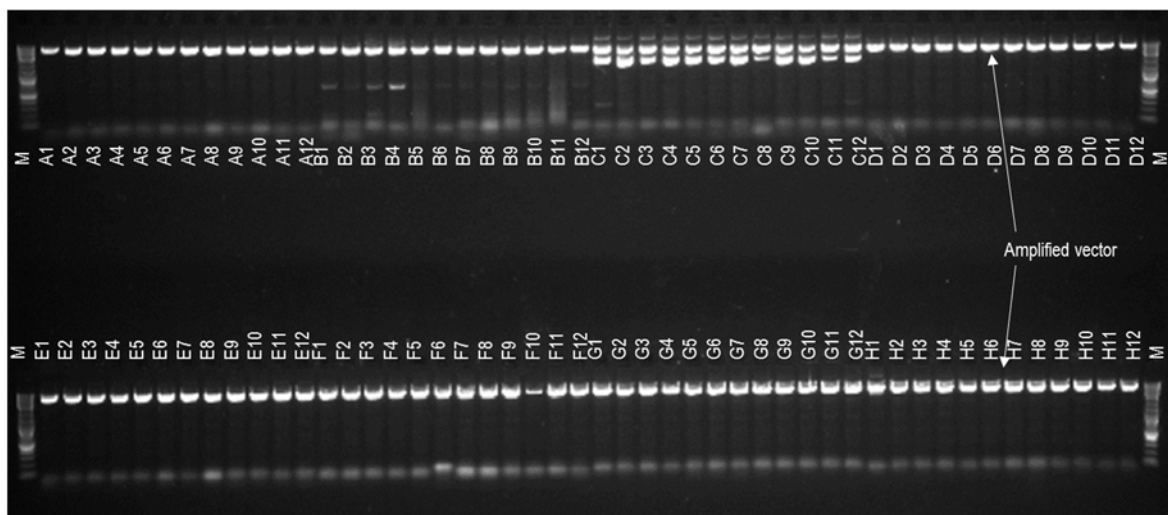


Figure A6. DNA analysis of the plasmid amplification by agarose gel electrophoresis. Analytical agarose gel (1%) with a 1-kb marker (M) using the PCR product (5 μ l) after DpnI digestion. DNA is visualized by ethidium bromide. Each lane corresponds to one mutation.

15. Perform a transformation of each successfully mutagenized plasmid into competent *E. coli* TOP10 cells. Transfer gently (do not pipette up and down) the digested PCR product (3 - 5 μ l) using a multichannel pipette into a 96 well plate containing chemically competent *E. coli* TOP10 cells (50 μ l per well). Incubate on ice for 30 min. For the preparation of chemically competent *E. coli* cells in 96 well plates, see Box 2. Use a positive control (e.g. pUC19 vector). Depending on the *E. coli* strain used (TOP10 typically yields more colony forming units (cfu) than BL21 (DE3)), one can typically expect 30 – 800 cfu's. Competent cells must be stored on ice the whole time until heat shock. Amplified plasmids are nicked: transformation into an efficient cloning strain is thus necessary.
16. Heat-shock and plate cells on 96 separate LB plates containing kanamycin (50 μ g ml⁻¹) as described in steps 4-6. Incubate overnight (37°C at 200 rpm).
17. Pick one to three colonies per mutant and grow them overnight (37°C at 200 rpm) in 96 well plates containing LB containing kanamycin (50 μ g ml⁻¹). Follow the manufacturer's protocol from the 96 well plasmid isolation kit for the preparation of overnight cultures and for the plasmid isolation procedure. Elute twice with the elution buffer (2x30 μ l). Alternatively, in a 24 deep well plate, LB can be used (6 ml per well) for overnight cultures to increase the final DNA content. Typical isolated plasmid yields are around 50 to 100 ng· μ l⁻¹.
18. Sequence plasmids with the standard T7 promoter primer. Forward sequencing is sufficient to cover the whole Sav gene (< 500 bp). To minimize costs, it is recommend

to use 96 well plate format sequencing to confirm the introduction of the desired mutations.

19. Perform transformation into competent *E. coli* BL21(DE3) cells. Add the mutated Sav plasmids (1 - 3 μ l, \sim 100 ng) to chemically competent *E. coli* BL21 (DE3) (50 μ l) in 24 deep well plates on ice. Incubate for 30 min. Repeat steps 4-5. The remaining plasmid solution can be kept at -20°C for several years.
20. Prepare overnight cultures in LB-media (5 ml) containing kanamycin (50 $\mu\text{g}\cdot\text{ml}^{-1}$) from a single colony of each *E. coli* BL21 (DE3) Sav mutant (same as step 6).
21. Create glycerol stocks as described in Step 7. Glycerol stocks can usually be stored for several years at -80°C .
22. To validate the glycerol stocks, repeat steps 6 and 7 (glycerol stock preparation not necessary). Use the 96 well plasmid isolation kit (Step 17). Prepare overnight cultures directly from the stock. Avoid thawing of the glycerol stocks by keeping them on dry ice. The remaining plasmid solution can be kept at -20°C for several years.

Sav library expression using ZYP-5052 medium TIMING 3-4 days

23. Prepare a sterile 24 deep well plate and fill the wells with LB (2 ml) containing kanamycin (50 $\mu\text{g ml}^{-1}$). Use one 24 deep well plate for each amino acid position. Inoculate 12 wells with the twelve different mutants to be introduced at this position, three with pET-24a-empty vector controls, three with pET-24a SavK121A and three with pET-24a Sav WT. The remaining three are sterile controls. Seal the plate with a permeable membrane. Incubate overnight (210 rpm, 37°C).
24. Transfer the overnight culture (10 μ l) into a new sterile 24 deep well plate containing the modified ZYP-5052 medium (6 ml) (for the 24 h expression) and kanamycin (50 $\mu\text{g ml}^{-1}$). Seal with a permeable membrane and shake (210 rpm, 30°C). To increase the harvested Sav amount, it is recommended to set up two identical plates simultaneously. Both plates can be pooled for screening purposes. For the 24 hour expression protocol, add a sterile pipette tip (0.1-10 μ l) into each well and use the modified ZYP-5052 media. For the 48 hour expression protocol, addition of a pipette tip has no effect and the normal ZYP-5052 medium should be used.
25. Determine the $\text{OD}_{600\text{nm}}$ of each well culture after 24 h, this should typically have an OD of 6 – 7. Centrifuge (4500 g, 10 min, 4°C) and discard the supernatant. Set the plate on ice for 2 min. Invert the plate on a tissue to remove remaining liquid and wait 5 min. Freeze the pellet at -20°C . The cell pellet containing Sav can be stored at -20°C for several weeks.

26. Thaw the cell pellets and resuspend in 0.2 ml (ATHase, see step 28(A)) or 0.4 ml (metathesase, see step 28(B)) lysis buffer. Do not use EDTA as this inhibits artificial metalloenzymes. Incubate for 30 min at 37°C and 200 rpm. Freeze for 1 to 2 h at -20°C. Thaw the cell lysate at RT. The lysate should be a homogeneous suspension. If not, add more DNaseI (1 $\mu\text{g ml}^{-1}$ to the initial concentration) and shake (30 min, RT).
27. To prepare the CFE, clear the cell suspension by centrifugation of the plates (4500 g, 4°C, 1 – 2 h). As an alternative, transfer the cell lysate into tubes (1.5 ml) and use a table centrifuge (21100 g, 20 min, 4°C). CFE containing Sav can be stored at 4°C for several weeks or at -20°C for up to 6 months.

ATHase or metathesase screening

28. At this point in the procedure, you can proceed with ATHase (option A) or metathesase (option B) screening.

(A)ATHase screening TIMING 3 days + 10 hours of measurement time

- (i) *Determine Sav FBS using the B4F absorption-fluorescence assay:* One 96-well plate allows for determination of the Sav FBS concentration of one 24-well plate containing the twelve mutants at one amino acid position of Sav. Perform all measurements, including the calibration curve, in triplicate. Use rows A-H columns 1-3 of a 96 well plate for the calibration curve with commercial full length streptavidin. Use the remaining wells to determine the Sav FBS of the twelve mutants for one amino acid position as well as all controls (WT Sav, K121A Sav and empty vector, each in triplicate). First, prepare the B4F working solution by combining 5.6 ml of FBS assay buffer and 0.8 ml of 0.4 mM B4F solution. As B4F is light-sensitive, protect the solutions with aluminum foil. Typically a subsequent assay dilution of the samples by five to ten is sufficient to remain in the range of the calibration curve under these conditions. By changing the amount of FBS assay buffer, other dilutions can be achieved.
- (ii) Use transparent 96 well plates (e.g., Brand, 350 μl per well, flat bottom). Measure each sample (final volume 100 μl) in triplicate. Follow the pipetting scheme for the calibration curve (rows A-H) displayed in the table below. Pipette the following into columns 1-3.

Table A3. Pipetting scheme for FBS determination

Component	Amount (μl)							
	Row A	Row B	Row C	Row D	Row E	Row F	Row G	Row H
Final FBS Sav concentration (μM)	[0]	[5]	[10]	[15]	[20]	[25]	[30]	[40]
B4F working solution	10	10	10	10	10	10	10	10
Sav stock [100 μM]	0	5	10	15	20	25	30	40
FBS assay buffer	90	85	80	75	70	65	60	50
Total	100	100	100	100	100	100	100	100

Follow the table in order during pipetting to avoid air bubbles. Hold the pipette vertically, contact the meniscus and the vessel wall with the tip when releasing the liquid.

- (iii) For measurements with the samples, pipette the B4F working solution (80 μl in each well) into the remaining 72 wells. Gently add 20 μl of the CFE into each well. Perform for each sample a triplicate determination. Shake the plate in the reader at 306 rpm for 2 min. Incubate for 15 min. Determine the absorbance (493 nm) and the fluorescence (Excitation: 485 nm/ Emission 520 nm) at 25°C. Check plate for air bubbles. They strongly influence the resulting absorbance. The presence of air bubbles does not significantly influence the fluorescence determination.
- (iv) Typical standard curves are displayed in Figure 7. Data points yielding Sav FBS < 10 μM or Sav FBS > 35 μM should be repeated at higher or lower concentrations respectively. Subtract the empty vector value and multiply by the assay dilution factor (5 when using of 20 μl CFE, see Step 26).

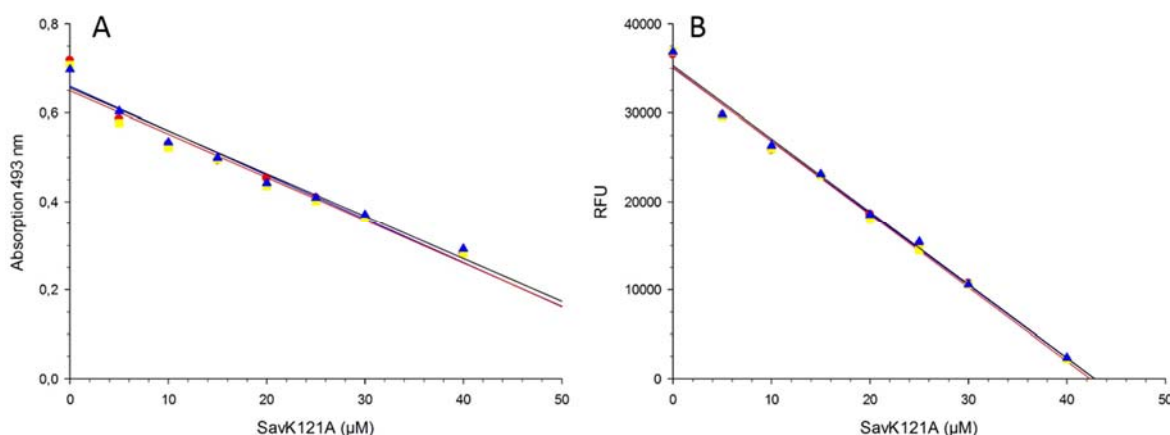


Figure A7. Typical calibration curve for Sav K121A using the B4F- assay. Absorption and relative fluorescence is displayed at increasing streptavidin concentrations. Measured data points are displayed as triangles. (a,b) The solid line corresponds to the linear regression: absorbance ($\lambda_{\text{max}} = 493 \text{ nm}$, each symbol (circle, square, and triangle) corresponds to one independent determination) (a), and relative fluorescence ($\lambda_{\text{excit}} = 485 \text{ nm}$ and $\lambda_{\text{emis}} = 520 \text{ nm}$, each symbol (circle, square, and triangle) corresponds to one independent determination) (b). RFU, relative fluorescence units.

- (v) *Diamide treatment:* Based on the Sav FBS determination, add the appropriate amount of cell lysate or CFE to an HPLC vial with a magnetic stir bar. Each vial should contain a final Sav FBS = 100 µM. Add the diamide stock solution (5 µl) and pre-incubate the solution by stirring (> 2 h). After dilution to 200 µl, the final diamide concentration should be 5 mM.
- (vi) *Catalysis set-up:* Add 2x concentrated reaction buffer (100 µl) into the preincubated cell lysates or the CFEs.
- (vii) Dilute the samples with MQ water, so the final volume after addition of the iridium and the substrate stock solutions reaches 200 µl.
- (viii) Add the iridium stock solution (5 µl) and incubate the solutions by stirring (5 min.). Following dilutions, the final iridium concentration [$\text{Cp}^*\text{Ir}(\text{Biot-}p\text{-L})\text{Cl}$] (compound **3**) should be 50 µM.
- (ix) Initiate the reaction by adding the substrate stock solution (5 µl) and seal the HPLC vials. The final substrate concentration should be 10 mM.
- (x) Stir the reaction at RT for 48 h. (e.g. in a standard plastic box for cryotubes)
- (xi) *Workup of catalysis reactions and analysis:* Dilute the reactions by addition of MQ water (500 µl). All chemicals must be handled with care and proper personal protective equipment, e.g. laboratory coat, gloves and eye protection.
- (xii) Transfer the reaction mixtures to a 2-ml polypropylene (PP) tube.
- (xiii) Add NaOH (50 µl of 20 % (w/w) solution).

- (xiv) Extract the reaction mixture twice with dichloromethane (2 x 1 ml). If a gel-like layer forms during extraction, especially when using cell lysates, spin (2000 g, 1 min) the 1.5-ml PP tubes before separating the organic layer.
- (xv) Combine the organic phases, transfer them into a new 2-ml PP tube and dry them by adding a spatula tip of anhydrous Na₂SO₄.
- (xvi) Spin down the tubes (2000 g, 5 min).
- (xvii) Transfer the supernatant into a HPLC vial using a Pasteur pipette.
- (xviii) Prepare the isocratic HPLC elution mixture containing 99.44 % hexane, 0.5 % isopropanol and 0.06 % diethylamine.
- (xix) Analyze the samples by HPLC using a Chiralpak IC column. Use a flow rate of 1 ml min⁻¹ at 25 °C, and determine the absorbance at 265 nm.
- (xx) For comparison purposes, the retention times are: (*S*)-1-phenyl-1,2,3,4-tetrahydroisoquinoline (*S*)-**2c** (7.6 min), (*R*)-1-phenyl-1,2,3,4-tetrahydroisoquinoline (*R*)-**2c** (10.5 min), and 1-phenyl-3,4-dihydroisoquinoline **1** (16 min).
- (xxi) Determine the enantiomeric excess for each sample. The yield can be estimated using a response factor (substrate **1c**)/(product **2c**) = 13.613. Determine the response factor experimentally by measuring at least three different substrate to product ratios.

(B) Metathesase screening TIMING 1 day + 10 hours measurement time for an entire 96-well plate

- (i) *Small scale imino-biotin immobilization:* Transfer the CFEs (400 µl in PBS buffer) from the 24 deep-well plates into a 96 deep-well plate. Add iminobiotin binding buffer (1 ml) to each well to adjust to pH ~ 9. Add the iminobiotin-sepharose beads (100 µl, shake the suspension thoroughly prior to pipetting (thanks to the dilution, pipetting and mixing is straightforward). Incubate the 96 deep-well plate with rapid shaking (800 rpm, RT, 1 h).
- (ii) Centrifuge the plate (5300 g, 15 min.) and discard the supernatant. Resuspend the beads in iminobiotin binding buffer (1 ml), centrifuge (5300 g, 15 min.) and discard the supernatant. Repeat this washing step three times to avoid deactivation of the catalyst. Use the thoroughly washed beads for catalysis.
- (iii) *Catalysis set-up:* To each well containing iminobiotin beads, add the metathesase reaction buffer (97 µl).

- (iv) Add a solution of the catalyst (**6**) in DMSO (3 μ l of the 3.33 mmol stock solution) to each well (to obtain the 3.33 mmol solution, take a 0.2 mg aliquot and add 69 μ l of DMSO) to obtain a final concentration of 50 μ M.
- (v) Add the solution of substrate (100 μ l of the 20 mM stock solution) to each well to get a final substrate concentration of 10 mM and place the 96 deep-well plate into a shaking incubator (37°C, 200 rpm, 12 h).
- (vi) *Workup of catalysis reactions and analysis:* Remove the plate from the incubator and add the internal standard solution (100 μ l) to each well and methanol (700 μ l). Then, centrifuge the plate (5346 g, 25 min). From each supernatant, transfer an aliquot (250 μ l) into a new 96 deep-well plate and dilute with MQ water (750 μ l).
- (vii) Schedule 10 h for an entire 96 well plate. Analyze the wells on an Aquity UPLC H-Class Bio from Waters (or a similar instrument, retention times may vary) using a BEH C18 column (1.7 μ m, 2.1 x 50 mm). Use MQ water + 0.1 % TFA as A solvent and acetonitrile + 0.1 % TFA as B solvent. Apply a gradient method as follows: 0 min 80 % A 20 % B; 1 min 80 % A 20 % B; 3 min 10 % A 90 % B; 3.5min 80 % A 20 % B and 4.5min 80 % A 20 % B. Plan 5 minutes for each sample.
- (viii) For quantification purposes, integrate the peaks of the absorbance at 210 nm. The retention times are as follows: starting material **4**, 2.15 min; internal standard, 0.47 min; product **5**, 0.67 min.
- (ix) Determine the concentration of the product with a calibration curve. For this, record samples of different concentrations of the purified product: 500 μ M, 300 μ M, 200 μ M, 100 μ M, 80 μ M, 50 μ M, 30 μ M and 10 μ M as well as constant concentrations of internal standard (250 μ M). A linear regression is obtained by plotting $\text{area}(\text{product})/\text{area}(\text{standard})$ against the calculated product concentration.
- (x) The total turnover number is obtained by dividing the calculated concentration in the sample by the catalyst concentration (50 μ M) and multiplying it with the dilution factor from the workup (20).

A.5 TIMING

Steps 1-22: site-directed mutagenesis in 96-well format: 9-10 days

Step 1 – 16: 3–4 days

Step 17 – 18 (depending on shipping duration): 4 days

Step 19 – 22: 2 days

Steps 23-27: Sav library expression using ZYP-5052 medium: 3-4 days

Step 23: 1 day

Step 24 – 25: 1 – 2 days

Step 26 – 27: 6 hours

Step 28A, ATHase screening: Total time 2.5 days + 10 hours measurement time

Step 28A (i–iv): 1 – 3 hours

Step 28A (v): 3 hours

Step 28A (vi–x): 2 days

Step 28A (xi – xxi): 12 hours for 18 samples

Step 28B, metathesase screening: 1 day + 10 hours measurement time for an entire 96-well plate

Step 28B (i, ii): 3.5 hours

Step 28B (iii–v): 19 hours

Step 28B (vi–x): 12 hours for an entire 96-well plate analysis

Box 1, primer design for noncomplementary, overlapping site-directed mutagenesis primer pair in 96-well plate format: 1-2 days

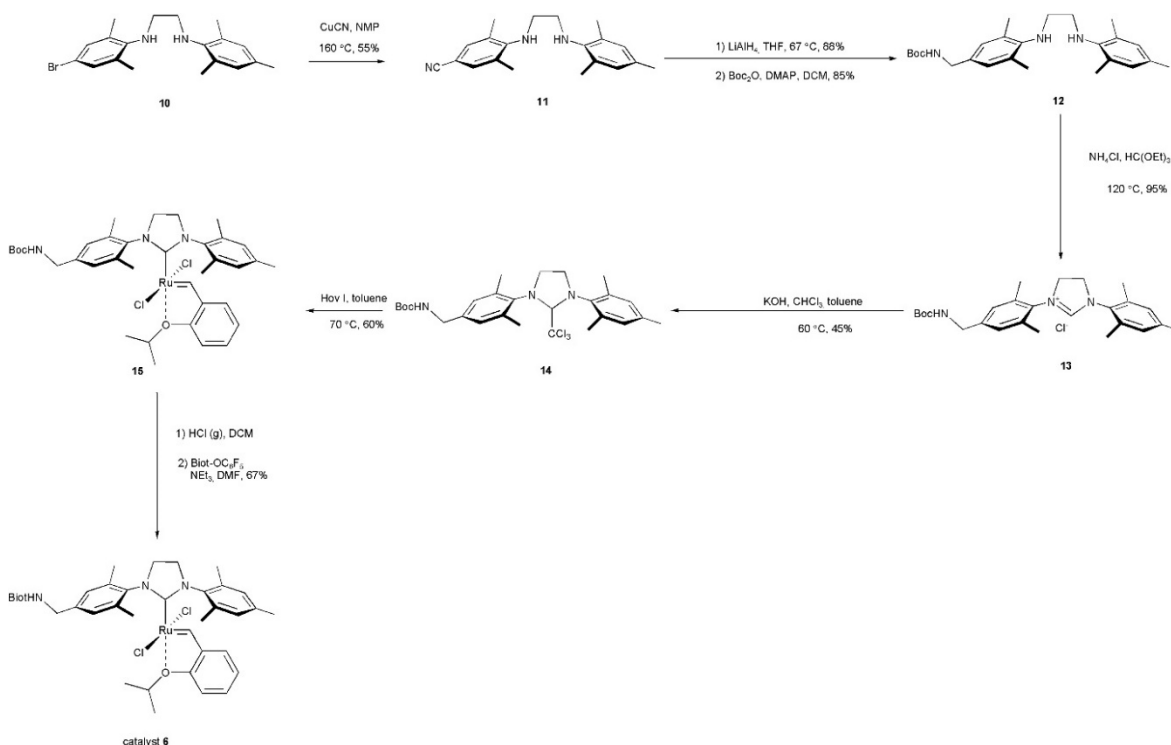
Box 2, preparation of chemically competent cells in 96-deep-well plates: 1.5 days

A. 6 SUPPLEMENTARY METHOD

A.6.1. SYNTHESIS OF BIOTINYLATED METATHESIS AND ATHASE CATALYST

A.6.1.1. Synthesis of metathesis catalyst 6

The synthesis is performed according to Scheme A2.



Scheme A2: Synthesis of metathesis catalyst 6.

4-((2-(mesitylamino)ethyl)amino)-3,5-dimethylbenzonitrile **11**:

Stir a mixture of N1-(4-bromo-2,6-dimethylphenyl)-N2-mesitylethane-1,2-diamine (**10**, 1.50 g, 4.14 mmol, 1.00 eq.) and copper (I) cyanide (749 mg, 8.28 mmol, 1.00 eq.) in NMP (7 mL) at 160°C overnight. Then, let the reaction mixture cool to room temperature and add water (10 mL) and ammonium hydroxide (10 mL). Extract the product with ethyl acetate (2×50 mL) and dry with Na_2SO_4 . Purify the product by flash chromatography (CH_2Cl_2) to obtain **11** as a white solid (700 mg, 86%). ^1H NMR (400 MHz, CDCl_3): $\delta = 7.25$ (s, 2H), 6.85 (s, 2H), 3.40 (t, $^3J_{\text{HH}} = 8$ Hz, 2H), 3.13 (t, $^3J_{\text{HH}} = 8$ Hz, 2H), 2.30 (s, 6H), 2.26 (s, 6H), 2.24 (s, 3H). ^{13}C NMR (100 MHz, CDCl_3): $\delta = 150.7$, 142.7, 133.0, 132.5, 130.5, 129.7, 127.4, 120.1, 102.7, 48.8, 48.3, 20.7, 19.2, 18.3. ESI-MS for $\text{C}_{20}\text{H}_{25}\text{N}_3$: 308.2 $[\text{M}+\text{H}]^+$.

tert-butyl (4-((2-(mesitylamino)ethyl)amino)-3,5-dimethylbenzyl) carbamate **12**:

Add a solution of **11** (2.27 g, 7.41 mmol, 1.00 eq.) in THF (10 mL) dropwise to a suspension of LiAlH₄ (0.702 g, 18.5 mmol, 2.50 eq.) in THF (30 mL). Stir the reaction mixture for 3 hours at 70 °C and let it cool to room temperature. Quench the reaction mixture with 1.0N NaOH aqueous solution. Filter off the precipitate and evaporate the solvent in vacuo to provide the crude amine product, which can be used without purification. ¹H NMR (400 MHz, CDCl₃): δ = 6.95 (s, 2H), 6.84 (s, 2H), 3.74 (s, 2H), 3.16-3.20 (m, 4H), 2.32 (s, 6H), 2.28 (s, 6H), 2.24 (s, 3H). ¹³C NMR (400 MHz, CDCl₃): δ = 144.8, 143.3, 137.0, 131.6, 129.9, 129.8, 129.6, 127.8, 49.2, 49.1, 46.1, 20.6, 18.7, 18.4. ESI-MS for C₂₀H₂₉N₃: 295.3 [M-NH₂]⁺. Purge a round-bottom flask, equipped with a magnetic stir-bar, with nitrogen and charge it with the above crude product and add Boc₂O (1.4 g, 6.4 mmol, 1.0 eq.), and degassed CH₂Cl₂ (3 mL). cool the flask to 0 °C with an ice/water bath prior to the addition of DMAP (79 mg, 0.64 mmol, 0.10 eq.). Stir at 0 °C for an additional 30 minutes prior to warming to room temperature and stir for 2 additional hours. Extract the reaction mixture with water and brine. Dry over Na₂SO₄, and evaporate the CH₂Cl₂. Chromatography on silica-gel 60 (15% EtOAc in hexanes) yields 2.0 g (85%) carbamate **12** as a white powder. ¹H NMR (400 MHz, CDCl₃): δ = 6.91 (s, 2H), 6.83 (s, 2H), 4.73 (brs, 1H), 4.18 (d, ³J_{HH} = 4 Hz, 2H), 3.31 (brs, 1H), 3.12-3.20 (m, 4H), 2.29 (s, 6H), 2.27 (s, 6H), 2.23 (s, 3H), 1.46 (s, 9H). ¹³C NMR (100 MHz, CDCl₃): δ = 155.9, 145.4, 143.3, 131.7, 130.0, 129.7, 129.6, 128.3, 110.1, 49.2, 49.1, 28.5, 27.0, 20.6, 20.0, 18.7, 18.5. ESI-MS for C₂₅H₃₇N₃O₂: 412.3 [M+H]⁺.

3-(4-(((tert-butoxycarbonyl)amino)methyl)-2,6-dimethylphenyl)-1-mesityl-4,5-dihydro-1H-imidazol-3-ium chloride **13**:

Charge an oven-dried round-bottom flask, equipped with a magnetic stir-bar, with carbamate **12** (2.00 g, 5.05 mmol), NH₄Cl (270 mg, 5.05 mmol, 1.00 eq.), HC(OEt)₃ (16.6 mL, 101 mmol, 20.0 eq.). and equip it with a condenser and purge with N₂ prior to stirring under an N₂ atmosphere at 120 °C for 16 hours. After cooling to RT, precipitate the product by addition of ether. Isolate the solid by vacuum-filtration and rinse with ether to yield 2.20 g (95 %) of product **13** as a grey powder. ¹H NMR (400 MHz, CDCl₃): δ = 9.54 (s, 1H), 7.00 (s, 2H), 6.91 (s, 2H), 5.35 (brs, 1H), 4.51 (s, 4H), 4.15 (d, ³J_{HH} = 4 Hz, 2H), 2.36 (s, 6H), 2.34 (s, 6H), 2.25 (s, 3H), 1.41 (s, 9H). ¹³C NMR (400 MHz, CDCl₃): δ = 163.9, 160.1, 155.9, 141.4, 140.0, 135.3, 134.7, 131.5, 130.1, 129.7, 127.8, 79.2, 57.3, 51.5, 43.5, 28.1, 20.8, 17.7. ESI-MS for C₂₆H₃₆ClN₃O₂: 422.3 [M-Cl]⁺.

Chloroform adduct **14**:

Add dry, degassed toluene (15 mL) to an oven-dried, 50 mL Schlenk flask equipped with stir bar and a reflux condenser. Add a large excess of powdered potassium hydroxide (5.37 g, 95.6 mmol, 127 eq.) to the flask, and stir the resulting suspension. Add chloroform (0.405 mL, 5.00 mmol, 6.67 eq.) to the suspension. After 10 min at RT, add **13** (0.344 g, 0.750 mmol, 1.00 eq.) and heat the reaction mixture at 60 °C for 75 min. Allow the mixture to cool to room temperature and filter it. Concentrate the filtrate under vacuum to obtain a light brown solid. Purify this crude product by column chromatography (20% ethyl acetate/hexane, R_f = 0.2) to yield 0.185 g (45 %) of the desired chloroform adduct **14** as a light yellow solid. ¹H NMR (400 MHz, CDCl₃): δ = 6.95 (s, 1H), 6.92 (s, 1H), 6.87 (s, 1H), 6.83 (s, 1H), 5.58 (s, 1H), 4.76 (brs, 1H), 4.22 (d, ³J_{HH} = 4 Hz, 2H), 3.89-3.92 (m, 2H), 3.25-3.35 (m, 2H), 2.49 (s, 3 H), 2.47 (s, 6H), 2.45 (s, 3H), 2.25 (s, 3H), 1.47 (s, 9H).

Precatalyst **15**:

Charge an oven-dried, 10 mL Schlenk tube with **Hov I** (36 mg, 60 μmol, 1.0 eq.), the chloroform adduct **14** (65 mg, 0.12 mmol, 2.0 eq.), and dry, degassed toluene (2 mL). Stir the reaction mixture at 70 °C for 90 min under a nitrogen atmosphere. After cooling to room temperature, remove the solvent under vacuum. Filter the dark-brown solid through a short silica gel column using ethyl acetate/cyclohexane (1:1) as eluent. Collect the green band and concentrate it to yield a green solid (**15**, 27 mg, 60%). ¹H NMR (400 MHz, CDCl₃): δ = 16.52 (s, 1H), 7.48 (t, ³J_{HH} = 8 Hz, 1H), 7.16 (s, 2H), 7.07 (s, 2H), 6.92-6.96 (m, 1H), 6.83-6.87 (m, 1H), 6.79 (d, ³J_{HH} = 8 Hz, 1H), 4.84-4.94 (m, 1H), 4.36 (d, ³J_{HH} = 4 Hz, 2H), 4.18 (s, 4H), 2.51 (s, 6H), 2.46 (s, 6H), 2.41 (s, 3H), 1.50 (s, 9H), 1.26 (d, ³J_{HH} = 4 Hz, 6H). ESI-MS for C₃₆H₄₈Cl₂N₃O₃Ru : 706.3 [M-Cl]⁺.

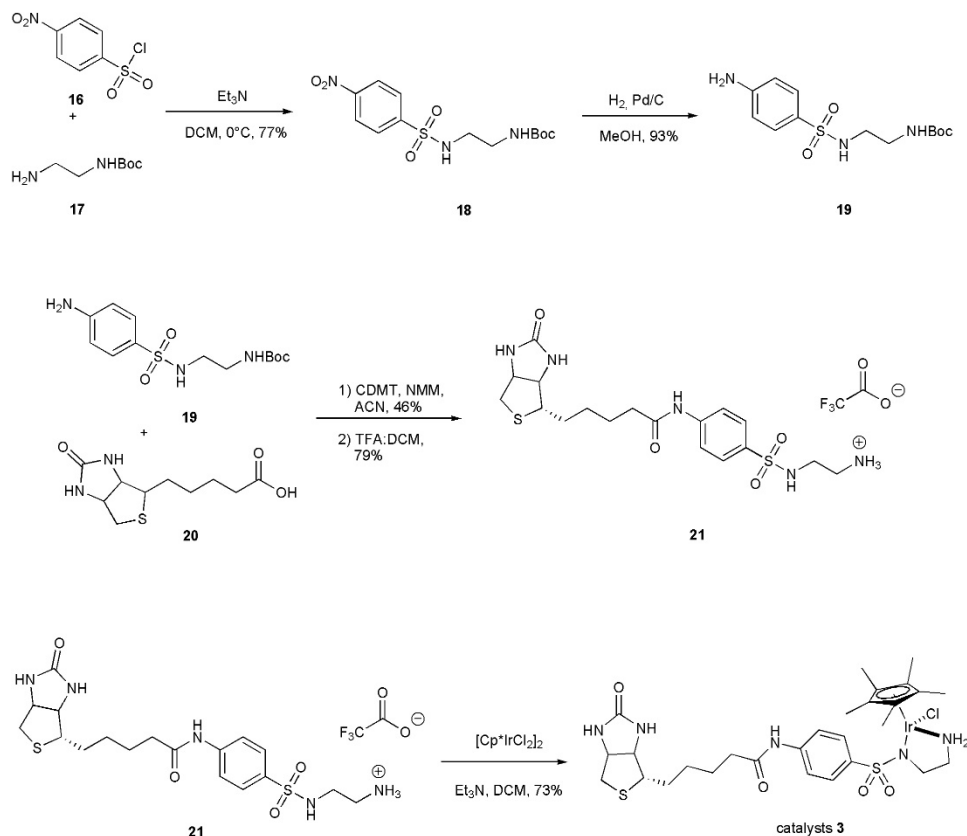
Metathesis catalyst **6**

Dissolve the boc-protected complex **15** (30 mg, 0.041 mmol, 1.0 eq.) (30 mg, 0.041 mmol, 1.0 eq.) in CH₂Cl₂ (2 mL) and purge HCl gas through the solution for 1 h at room temperature. Generate the gaseous HCl by dropwise addition of concentrated H₂SO₄ to solid NH₄Cl. Stir the solution for an additional 2 h at room temperature. Upon completion of the reaction as revealed by TLC (hexane/AcOEt 2:1), evaporate under reduced pressure. Dissolve the green solid in DMF (2 mL) and add biotin pentafluorophenol (13 mg, 0.032 mmol, 0.80 eq) and Et₃N (0.12 mL, 0.82 mmol) to the solution and stir at RT for 16 h. Remove the solvent under reduced pressure and purify the crude product by flash chromatography on silica gel using 10% MeOH/CH₂Cl₂ to yield metathesis catalyst **6** as a green solid (25 mg, 67%). ¹H NMR (400 MHz, CD₂Cl₂): δ = 16.17 (s, 1H), 7.97 (s, 1H), 7.55-7.60 (m, 1H), 7.09

(s, 2H), 6.95-7.00 (m, 3H), 5.14-5.20 (m, 2H), 4.84-4.96 (m, 2H), 4.53-4.57 (m, 1H), 4.35-4.38 (m, 1H), 4.07-4.11 (brs, 1H), 3.87-3.96 (m, 4H), 3.22 (m, 2H), 2.95 (s, 6H), 2.86 (s, 4H), 2.69-2.77 (m, 2H), 2.52 (m, 2H), 2.46 (s, 3H), 2.18 (s, 6H), 1.90 (m, 1H), 1.74 (d, $^3J_{\text{HH}} = 4$ Hz, 6H). HRMS [ESI(+)]calculated for $\text{C}_{37}\text{H}_{51}\text{ClN}_5\text{O}_3\text{RuS}$: 782.2445 $[\text{M}-\text{Cl}]^+$; found 782.2414.

A.6.1.2 Synthesis of transfer hydrogenation catalyst **3**

The synthesis is performed as summarized in Scheme A3.



Scheme A3: Synthesis of hydrogenation catalyst **3**.

N-Boc-*N'*-(4-nitrophenylsulfonyl)-ethylenediamine **18**:

To a solution of *N*-Boc-ethylenediamine **17** (1.74 g, 10.8 mmol, 1.0 eq.) and Et_3N (3 mL, 21.5 mmol, 2.0 eq.) in DCM (300 mL) add dropwise a solution of 4-nitrophenylsulfonyl chloride **16** (2.51 g, 11.3 mmol, 1.05 eq.) in DCM (100 mL) at 5°C and stir overnight. Then, concentrate the solution to 100 mL, wash with water (3 x 20 mL), dry it with MgSO_4 and evaporate the solvent under reduced pressure. Purify the crude product by flash chromatography (silicagel, EtOAc : hexane (2 : 3)) to obtain the pure product **18** as a white powder (2.87 g, 8.32 mmol, 77% yield). ^1H NMR (200 MHz, CDCl_3 - CD_3OD , 22°C): δ 1.40 (s, 9H; tBu), 3.03 (m, 2H; $\text{CH}_2\text{-CH}_2\text{-NH-S}$), 3.12 (m, 2H; $\text{CH}_2\text{-CH}_2\text{-NH-S}$), 4.47 (br, 2H; NH), 8.04 (d, $J = 8.7$ Hz, 2H; ArH), 8.37 (d, $J = 8.7$ Hz, 2H; ArH).

N-Boc-*N'*-(4-aminophenylsulfonyl)-ethylenediamine **19**:

Charge an autoclave containing a suspension of Pd/C (5%, 330 mg) in methanol (20 mL) with *N*-Boc-*N'*-(4-nitrophenylsulfonyl)-ethylenediamine **18** (2.10 g, 6.08 mmol). Purge the autoclave three times with nitrogen and fill with hydrogen (3 bars). Stir the reaction vigorously for 3 hours at RT. Then, carefully release the hydrogen pressure and remove the resulting suspension by filtration through a celite plug. Evaporate the solvent under reduced pressure to obtain **19** as a white powder (1.78 g, 5.65 mmol, 93%). ¹H NMR (400 MHz, CDCl₃-CD₃OD, 22 °C): δ 1.40 (s, 9H; ^tBu), 2.88 (m, 2H; CH₂-CH₂-NH-S), 3.12 (m, 2H; CH₂-CH₂-NH-S), 3.57 (br, 3H; NH; NH₂), 4.50 (br, 1H; NH), 6.62 (m, 2H; ArH), 7.47 (m, 2H; ArH).

N-Boc-*N'*-(4-biotinamidophenylsulfonyl)-ethylenediamine **21**:

Mix a suspension of (+)-biotin **20** (1.4 g, 5.74 mmol, 1.02 eq.), *N*-Boc-*N'*-(4-aminophenylsulfonyl)-ethylenediamine **19** (1.77 g, 5.63 mmol, 1.0 eq.) and 2-chloro-4,6-dimethoxy-1,3,5-triazine (CDMT) as a coupling agent (1.08 g, 5.96 mmol, 1.06 eq.) in acetonitrile (110 mL). Add *N*-methylmorpholine (NMM) (0.93 mL, 8 mmol, 1.5 eq.) and stir at RT for 24 hours. Heat the reaction mixture to reflux and for 6 hours. After cooling the reaction mixture cool to room temperature, add water (30 mL). Evaporate the solvent under reduced pressure until the product starts to precipitate. Collect the crude product by filtration, wash with DCM and purify by flash chromatography (silicagel using EtOAc : MeOH (4 : 1)) to obtain the product a white powder (1.4 g, 2.30 mmol, 46% yield).

¹H NMR (200 MHz, DMSO-*d*₆, 22 °C): δ 1.20-1.78 (m, 15H; CH₂; ^tBu), 2.30 (m, 2H; CH₂), 2.60-2.88 (m, 4H; CH₂-S; CH₂-CH₂-NH-S), 2.95-3.15 (m, 3H; CH-S; CH₂-CH₂-NH-S), 4.18 (br, 1H; CH-N), 4.38 (br, 1H; CH-N), 6.28 (br, 3H; NH), 7.65 (d, *J* = 8.3 Hz, 2H; ArH), 7.72 (d, *J* = 8.3 Hz, 2H; ArH).

Add trifluoroacetic acid (2.3 mL, 30 mmol, 10 eq.) dropwise to a suspension of *N*-Boc-*N'*-(biotin-4-amidophenylsulfonyl)-ethylenediamine (1.60 g, 2.95 mmol) in dry DCM (150 mL) at 0 °C and stir for 6 hours. Evaporate the solvent under reduced pressure, dissolve the crude product in MeOH and add diethyl ether until a white precipitate forms. Collect the precipitated product by filtration and dry under reduced pressure to obtain **21** as white powder (1.29 g, 2.33 mmol, 79%).

¹H NMR (400 MHz, DMSO-*d*₆, 22 °C): δ 1.23-1.63 (m, 6H; CH₂), 2.35 (m, 2H; CH₂), 2.58 (d, *J* = 12.4 Hz, 1H; CH₂-S), 2.69 (br s, 2H; CH₂-CH₂-NH-S), 2.82 (dd, *J* = 12.4, 4.9 Hz, 1H; CH₂-S), 2.89 (m, 2H; CH₂-CH₂-NH-S), 3.12 (m, 1H; CH-S), 3.48 (br, 2H; NH₂), 4.15 (br, 1H; CH-N), 4.31 (br, 1H; CH-N), 5.33 (br, 1H; NH), 6.44 (br, 1H; NH), 6.58 (br, 1H; NH),

7.68 (d, $J = 8.5$ Hz, 2H; ArH), 7.79 (d, $J = 8.5$ Hz, 2H; ArH), 10.6 (br, 1H; NH); ^{13}C NMR (100.6 MHz, DMSO- d_6 , 22 °C): δ 25.8 (CH₂), 28.9 (CH₂), 29.0 (CH₂), 37.0 (CH₂), 40.7(CH₂-S), 41.3 (CH₂-CH₂-NH-S), 46.5 (CH₂-CH₂-NH-S), 56.2 (CH-S), 60.1 (CH-N), 61.9 (CH-N), 119.5 (2C; Ar-H), 128.4 (2C; Ar-H), 134.8 (Ar-S), 143.6 (ArN), 163.7 (N-CO-N), 172.8 (CO-N); ESI-MS for C₁₈H₂₇N₅O₄S₂: 464.2 (15) [M+Na]⁺, 442.3 (100) [M+H]⁺.

Synthesis of [Cp*Ir(Biot-*p*-L)Cl] **3**:

Dissolve the [Cp*IrCl₂]₂ dimer (136.4 mg, 0.171 mmol, 0.475 eq.), the biotinylated ligand **21** (200 mg, 0.36 mmol, 1 eq.) and Et₃N (12.5 μL , 90 μmol , 2.25 eq.) in dry DCM (30 mL) under inert atmosphere. After stirring for 24 hours at room temperature, collect the precipitate, wash with DCM (3x5 mL) and cold water (3x4 mL) and dry under reduced pressure to obtain the pure catalyst **3** as a bright yellow powder (212.3 mg, 0.26 mmol, 73%). ^1H NMR (400 MHz, DMSO- d_6) δ 10.06 (s, 1H, NH), 7.80 – 7.51 (m, 4H, Ar-H), 6.44 (s, 1H, NH), 6.36 (s, 1H, NH), 5.26 (s, 2H, NH), 4.31 (dd, $J = 7.8, 5.0$ Hz, 1H, CH), 4.18 – 4.10 (ddd, $J = 7.7, 4.5, 1.8$ Hz, 1H, CH), 3.18 – 3.07 (m, 1H, CH), 2.83 (dd, $J = 12.4, 5.1$ Hz, 1H, CH), 2.58 (d, $J = 12.4$ Hz, 1H, CH), 2.47 – 2.26 (m, 6H, CH₂-CH₂-CH₂), 1.68 (s, 15H, Cp*-CH₃), 1.66 – 1.20 (m, 6H, CH₂-CH₂, CH₂). ESI-MS for IrC₂₈H₄₁N₅O₄S₂Cl: [Cp*Ir(Biot-*p*-L)Cl] : 442.1 (10) [LH+H]⁺, 768 (100) [M-Cl+H]⁺.

A7. SEQUENCES

A.7.1 SAVK121A CODON OPTIMIZED SEQUENCE USED IN THIS PROTOCOL (CONSTRUCT CLONED INTO PET-24A)

```
5' ATGGCAAGCATGACCGGTGGCCAGCAGATGGGTCGTGATCAGGCAGGTATT
ACCGGCACCTGGTATAATCAGCTGGGTAGCACCTTTATTGTTACCGCAGGCGC
AGATGGTGC ACTGACCGGTACGTATGAAAGCGCAGTTGGTAATGCAGAAAGCC
GTTATGTTCTGACAGGTCGTTATGATAGCGCACCGGCAACCGATGGTAGCGGC
ACCGCACTGGGTTGGACCGTTGCATGGAAAAATAACTATCGTAATGCACATAG
CGCAACCACCTGGTCAGGTCAGTATGTTGGTGGTGCAGAAGCACGCATTAATA
CCCAGTGGCTGCTGACCAGCGGCACCACCGAAGCAAATGCCTGGGCAAGCAC
CCTGGTTGGTCATGATACCTTTACCAAAGTTAAACCGAGCGCAGCAAGCATTG
ATGCAGCAAAAAAAGCCGGTGTGAATAATGGTAATCCGCTGGATGCAGTTCAG
CAG 3'
```

A.7.2. PRIMER SEQUENCES USED FOR MUTAGENESIS IN THIS PROTOCOL

Table A4. Primer sequences used for the mutagenesis protocol. For clarity after three nucleotides a “space” is introduced. This does not corresponds to the specific triplet code for the amino acids.

Primer Name	Sequence (5'-3')	Primer Name	Sequence (5'-3')
48A_FW	GCA GTT GCT AAT GCA GAA AGC CGT TAT G	48A_RV	CTG CAT TAG CAA CTG CGC TTT CAT ACG
48V_FW	GCA GTT GTT AAT GCA GAA AGC CGT TAT G	48V_RV	CTG CAT TAA CAA CTG CGC TTT CAT ACG
48L_FW	GCA GTT CTT AAT GCA GAA AGC CGT TAT G	48L_RV	CTG CAT TAA GAA CTG CGC TTT CAT ACG
48D_FW	GCA GTT GAT AAT GCA GAA AGC CGT TAT G	48D_RV	CTG CAT TAT CAA CTG CGC TTT CAT ACG
48E_FW	GCA GTT GAA AAT GCA GAA AGC CGT TAT G	48E_RV	CTG CAT TTT CAA CTG CGC TTT CAT ACG
48Q_FW	GCA GTT CAA AAT GCA GAA AGC CGT TAT G	48Q_RV	CTG CAT TTT GAA CTG CGC TTT CAT ACG
48K_FW	GCA GTT AAG AAT GCA GAA AGC CGT TAT G	48K_RV	CTG CAT TGT TAA CTG CGC TTT CAT ACG
48H_FW	GCA GTT CAT AAT GCA GAA AGC CGT TAT G	48H_RV	CTG CAT TAT GAA CTG CGC TTT CAT ACG
48M_FW	GCA GTT ATG AAT GCA GAA AGC CGT TAT G	48M_RV	CTG CAT TCA TAA CTG CGC TTT CAT ACG
48Y_FW	GCA GTT TAT AAT GCA GAA AGC CGT TAT G	48Y_RV	CTG CAT TAT AAA CTG CGC TTT CAT ACG
48S_FW	GCA GTT AGT AAT GCA GAA AGC CGT TAT G	48S_RV	CTG CAT TAC TAA CTG CGC TTT CAT ACG
48P_FW	GCA GTT CCT AAT GCA GAA AGC CGT TAT G	48P_RV	CTG CAT TAG GAA CTG CGC TTT CAT ACG
69A_FW	GAT GGT GCC GGC ACC GCA CTG GGT TG	69A_RV	GTG CCG GCA CCA TCG GTT GCC GGT G
69L_FW	GAT GGT CTC GGC ACC GCA CTG GGT TG	69L_RV	GTG CCG AGA CCA TCG GTT GCC GGT G
69D_FW	GAT GGT GAC GGC ACC GCA CTG GGT TG	69D_RV	GTG CCG TCA CCA TCG GTT GCC GGT G
69E_FW	GAT GGT GAA GGC ACC GCA CTG GGT TG	69E_RV	GTG CCT TCA CCA TCG GTT GCC GGT G
69Q_FW	GAT GGT CAA GGC ACC GCA CTG GGT TG	69Q_RV	GTG CCT TGA CCA TCG GTT GCC GGT G
69K_FW	GAT GGT AAG GGC ACC GCA CTG GGT TG	69K_RV	GTG CCC TTA CCA TCG GTT GCC GGT G
69H_FW	GAT GGT CAT GGC ACC GCA CTG GGT TG	69H_RV	GTG CCA TGA CCA TCG GTT GCC GGT G
69M_FW	GAT GGT ATG GGC ACC GCA CTG GGT TG	69M_RV	GTG CCC ATA CCA TCG GTT GCC GGT G
69Y_FW	GAT GGT TAC GGC ACC GCA CTG GGT TG	69Y_RV	GTG CCG TAA CCA TCG GTT GCC GGT G
69V_FW	GAT GGT GTC GGC ACC GCA CTG GGT TG	69V_RV	GTG CCG ACA CCA TCG GTT GCC GGT G
69P_FW	GAT GGT CCA GGC ACC GCA CTG GGT TG	69P_RV	GTG CCT GGA CCA TCG GTT GCC GGT G
69N_FW	GAT GGT AAC GGC ACC GCA CTG GGT TG	69N_RV	GTG CCG TTA CCA TCG GTT GCC GGT G
84A_FW	CTA TGC TAA TGC ACA TAG CGC AAC CAC C	84A_RV	CAT TAG CAT AGT TAT TTT TCC ATG CAA CGG
84V_FW	CTA TGT TAA TGC ACA TAG CGC AAC CAC C	84V_RV	CAT TAA CAT AGT TAT TTT TCC ATG CAA CGG
84L_FW	CTA TCT TAA TGC ACA TAG CGC AAC CAC C	84L_RV	CAT TAA GAT AGT TAT TTT TCC ATG CAA CGG
84D_FW	CTA TGA TAA TGC ACA TAG CGC AAC CAC C	84D_RV	CAT TAT CAT AGT TAT TTT TCC ATG CAA CGG
84E_FW	CTA TGA GAA TGC ACA TAG CGC AAC CAC C	84E_RV	CAT TCT CAT AGT TAT TTT TCC ATG CAA CGG
84Q_FW	CTA TCA GAA TGC ACA TAG CGC AAC CAC C	84Q_RV	CAT TCT GAT AGT TAT TTT TCC ATG CAA CGG
84K_FW	CTA TAA GAA TGC ACA TAG CGC AAC CAC C	84K_RV	CAT TCT TAT AGT TAT TTT TCC ATG CAA CGG
84H_FW	CTA TCA TAA TGC ACA TAG CGC AAC CAC C	84H_RV	CAT TAT GAT AGT TAT TTT TCC ATG CAA CGG
84M_FW	CTA TAT GAA TGC ACA TAG CGC AAC CAC C	84M_RV	CAT TCA TAT AGT TAT TTT TCC ATG CAA CGG
84Y_FW	CTA TTA TAA TGC ACA TAG CGC AAC CAC C	84Y_RV	CAT TAT AAT AGT TAT TTT TCC ATG CAA CGG
84S_FW	CTA TAG TAA TGC ACA TAG CGC AAC CAC C	84S_RV	CAT TAC TAT AGT TAT TTT TCC ATG CAA CGG
84P_FW	CTA TCC TAA TGC ACA TAG CGC AAC CAC C	84P_RV	CAT TAG GAT AGT TAT TTT TCC ATG CAA CGG
85A_FW	CTA TCG TGC TGC ACA TAG CGC AAC C	85A_RV	CTA TGT GCA GCA CGA TAG TTA TTT TTC CAT GC
85V_FW	CTA TCG TGT TGC ACA TAG CGC AAC C	85V_RV	CTA TGT GCA ACA CGA TAG TTA TTT TTC CAT GC
85L_FW	CTA TCG TCT TGC ACA TAG CGC AAC C	85L_RV	CTA TGT GCA AGA CGA TAG TTA TTT TTC CAT GC
85D_FW	CTA TCG TGA TGC ACA TAG CGC AAC C	85D_RV	CTA TGT GCA TCA CGA TAG TTA TTT TTC CAT GC
85E_FW	CTA TCG TGA AGC ACA TAG CGC AAC C	85E_RV	CTA TGT GCT TCA CGA TAG TTA TTT TTC CAT GC
85Q_FW	CTA TCG TCA AGC ACA TAG CGC AAC C	85Q_RV	CTA TGT GCT TGA CGA TAG TTA TTT TTC CAT GC
85K_FW	CTA TCG TAA AGC ACA TAG CGC AAC C	85K_RV	CTA TGT GCT TTA CGA TAG TTA TTT TTC CAT GC
85H_FW	CTA TCG TCA TGC ACA TAG CGC AAC C	85H_RV	CTA TGT GCA TGA CGA TAG TTA TTT TTC CAT GC
85M_FW	CTA TCG TAT GGC ACA TAG CGC AAC C	85M_RV	CTA TGT GCC ATA CGA TAG TTA TTT TTC CAT GC
85Y_FW	CTA TCG TTA TGC ACA TAG CGC AAC C	85Y_RV	CTA TGT GCA TAA CGA TAG TTA TTT TTC CAT GC
85S_FW	CTA TCG TAG TGC ACA TAG CGC AAC C	85S_RV	CTA TGT GCA CTA CGA TAG TTA TTT TTC CAT GC
85P_FW	CTA TCG TCC TGC ACA TAG CGC AAC C	85P_RV	CTA TGT GCA GGA CGA TAG TTA TTT TTC CAT GC
87A_FW	GTA ATG CAG CTA GCG CAA CCA CCT GGT C	87A_RV	GCG CTA GCT GCA TTA CGA TAG TTA TTT TTC C
87V_FW	GTA ATG CAG TTA GCG CAA CCA CCT GGT C	87V_RV	GCG CTA ACT GCA TTA CGA TAG TTA TTT TTC C

87L_FW	GTA ATG CAC TTA GCG CAA CCA CCT GGT C	87L_RV	GCG CTA AGT GCA TTA CGA TAG TTA TTT TTC C
87D_FW	GTA ATG CAG ATA GCG CAA CCA CCT GGT C	87D_RV	GCG CTA TCT GCA TTA CGA TAG TTA TTT TTC C
87E_FW	GTA ATG CAG AAA GCG CAA CCA CCT GGT C	87E_RV	GCG CTT TCT GCA TTA CGA TAG TTA TTT TTC C
87Q_FW	GTA ATG CAC AGA GCG CAA CCA CCT GGT C	87Q_RV	GCG CTC TGT GCA TTA CGA TAG TTA TTT TTC C
87K_FW	GTA ATG CAA AGA GCG CAA CCA CCT GGT C	87K_RV	GCG CTC TTT GCA TTA CGA TAG TTA TTT TTC C
87M_FW	GTA ATG CAA TGA GCG CAA CCA CCT GGT C	87M_RV	GCG CTC ATT GCA TTA CGA TAG TTA TTT TTC C
87Y_FW	GTA ATG CAT ATA GCG CAA CCA CCT GGT C	87Y_RV	GCG CTA TAT GCA TTA CGA TAG TTA TTT TTC C
87S_FW	GTA ATG CAT CAA GCG CAA CCA CCT GGT C	87S_RV	GCG CTT GAT GCA TTA CGA TAG TTA TTT TTC C
87P_FW	GTA ATG CAC CTA GCG CAA CCA CCT GGT C	87P_RV	GCG CTA GGT GCA TTA CGA TAG TTA TTT TTC C
87N_FW	GTA ATG CAA ATA GCG CAA CCA CCT GGT C	87N_RV	GCG CTA TTT GCA TTA CGA TAG TTA TTT TTC C
98A_FW	GTA TGT TGC TGG TGC AGA AGC ACG CAT TAA TAC C	98A_RV	CTG CAC CAG CAA CAT ACT GAC CTG ACC AG
98V_FW	GTA TGT TGT TGG TGC AGA AGC ACG CAT TAA TAC C	98V_RV	CTG CAC CAA CAA CAT ACT GAC CTG ACC AG
98L_FW	GTA TGT TCT TGG TGC AGA AGC ACG CAT TAA TAC C	98L_RV	CTG CAC CAA GAA CAT ACT GAC CTG ACC AG
98D_FW	GTA TGT TGA TGG TGC AGA AGC ACG CAT TAA TAC C	98D_RV	CTG CAC CAT CAA CAT ACT GAC CTG ACC AG
98E_FW	GTA TGT TGA AGG TGC AGA AGC ACG CAT TAA TAC C	98E_RV	CTG CAC CTT CAA CAT ACT GAC CTG ACC AG
98Q_FW	GTA TGT TCA AGG TGC AGA AGC ACG CAT TAA TAC C	98Q_RV	CTG CAC CTT GAA CAT ACT GAC CTG ACC AG
98K_FW	GTA TGT TAA GGG TGC AGA AGC ACG CAT TAA TAC C	98K_RV	CTG CAC CGT TAA CAT ACT GAC CTG ACC AG
98H_FW	GTA TGT TCA TGG TGC AGA AGC ACG CAT TAA TAC C	98H_RV	CTG CAC CAT GAA CAT ACT GAC CTG ACC AG
98M_FW	GTA TGT TAT GGG TGC AGA AGC ACG CAT TAA TAC C	98M_RV	CTG CAC CCA TAA CAT ACT GAC CTG ACC AG
98Y_FW	GTA TGT TTA TGG TGC AGA AGC ACG CAT TAA TAC C	98Y_RV	CTG CAC CAT AAA CAT ACT GAC CTG ACC AG
98S_FW	GTA TGT TAG TGG TGC AGA AGC ACG CAT TAA TAC C	98S_RV	CTG CAC CAC TAA CAT ACT GAC CTG ACC AG
98P_FW	GTA TGT TCCTGG TGC AGA AGC ACG CAT TAA TAC C	98P_RV	CTG CAC CAG GAA CAT ACT GAC CTG ACC AG
119V_FW	GCA AAT GTC TGG GCA AGC ACC CTG G	119V_RV	GCC CAG ACA TTT GCT TCG GTG GTG C
119L_FW	GCA AAT CTC TGG GCA AGC ACC CTG G	119L_RV	GCC CAG AGA TTT GCT TCG GTG GTG C
119D_FW	GCA AAT GAC TGG GCA AGC ACC CTG G	119D_RV	GCC CAG TCA TTT GCT TCG GTG GTG C
119E_FW	GCA AAT GAA TGG GCA AGC ACC CTG G	119E_RV	GCC CAT TCA TTT GCT TCG GTG GTG C
119Q_FW	GCA AAT CAG TGG GCA AGC ACC CTG G	119Q_RV	GCC CAC TGA TTT GCT TCG GTG GTG C
119K_FW	GCA AAT AAA TGG GCA AGC ACC CTG G	119K_RV	GCC CAT TTA TTT GCT TCG GTG GTG C
119H_FW	GCA AAT CAC TGG GCA AGC ACC CTG G	119H_RV	GCC CAG TGA TTT GCT TCG GTG GTG C
119M_FW	GCA AAT ATG TGG GCA AGC ACC CTG G	119M_RV	GCC CAC ATA TTT GCT TCG GTG GTG C
119Y_FW	GCA AAT TAC TGG GCA AGC ACC CTG G	119Y_RV	GCC CAG TAA TTT GCT TCG GTG GTG C
119S_FW	GCA AAT TCC TGG GCA AGC ACC CTG G	119S_RV	GCC CAG GAA TTT GCT TCG GTG GTG C
119P_FW	GCA AAT CCC TGG GCA AGC ACC CTG G	119P_RV	GCC CAG GGA TTT GCT TCG GTG GTG C
119N_FW	GCA AAT AAC TGG GCA AGC ACC CTG G	119N_RV	GCC CAG TTA TTT GCT TCG GTG GTG C
150A_FW	GTG AAT GCT GGT AAT CCG CTG GAT GC	150A_RV	GAT TAC CAG CAT TCA CAC CGG CTT TTT TTG C
150V_FW	GTG AAT GTT GGT AAT CCG CTG GAT GC	150V_RV	GAT TAC CAA CAT TCA CAC CGG CTT TTT TTG C
150L_FW	GTG AAT CTT GGT AAT CCG CTG GAT GC	150L_RV	GAT TAC CAA GAT TCA CAC CGG CTT TTT TTG C
150D_FW	GTG AAT GAT GGT AAT CCG CTG GAT GC	150D_RV	GAT TAC CAT CAT TCA CAC CGG CTT TTT TTG C
150E_FW	GTG AAT GAA GGT AAT CCG CTG GAT GC	150E_RV	GAT TAC CTT CAT TCA CAC CGG CTT TTT TTG C
150Q_FW	GTG AAT CAA GGT AAT CCG CTG GAT GC	150Q_RV	GAT TAC CTT GAT TCA CAC CGG CTT TTT TTG C
150K_FW	GTG AAT AAA GGT AAT CCG CTG GAT GC	150K_RV	GAT TAC CTT TAT TCA CAC CGG CTT TTT TTG C
150H_FW	GTG AAT CAT GGT AAT CCG CTG GAT GC	150H_RV	GAT TAC CAT GAT TCA CAC CGG CTT TTT TTG C
150M_FW	GTG AAT ATG GGT AAT CCG CTG GAT GC	150M_RV	GAT TAC CCA TAT TCA CAC CGG CTT TTT TTG C
150Y_FW	GTG AAT TAT GGT AAT CCG CTG GAT GC	150Y_RV	GAT TAC CAT AAT TCA CAC CGG CTT TTT TTG C
150S_FW	GTG AAT AGT GGT AAT CCG CTG GAT GC	150S_RV	GAT TAC CAC TAT TCA CAC CGG CTT TTT TTG C
150P_FW	GTG AAT CCT GGT AAT CCG CTG GAT GC	150P_RV	GAT TAC CAG GAT TCA CAC CGG CTT TTT TTG C
64A_FW	GAT AGC GCA GCG GCA ACC GAT GGT AGC	64A_RV	GGT TGC CGC TGC GCT ATC ATA ACG ACC TGT C
64V_FW	GAT AGC GCA GTG GCA ACC GAT GGT AGC	64V_RV	GGT TGC CAC TGC GCT ATC ATA ACG ACC TGT C
64L_FW	GAT AGC GCA CTG GCA ACC GAT GGT AGC	64L_RV	GGT TGC CAG TGC GCT ATC ATA ACG ACC TGT C
64D_FW	GAT AGC GCA GAT GCA ACC GAT GGT AGC	64D_RV	GGT TGC ATC TGC GCT ATC ATA ACG ACC TGT C
64E_FW	GAT AGC GCA GAG GCA ACC GAT GGT AGC	64E_RV	GGT TGC CTC TGC GCT ATC ATA ACG ACC TGT C
64Q_FW	GAT AGC GCA CAG GCA ACC GAT GGT AGC	64Q_RV	GGT TGC CTG TGC GCT ATC ATA ACG ACC TGT C
64K_FW	GAT AGC GCA AAG GCA ACC GAT GGT AGC	64K_RV	GGT TGC CTT TGC GCT ATC ATA ACG ACC TGT C

64H_FW	GAT AGC GCA CAT GCA ACC GAT GGT AGC	64H_RV	GGT TGC ATG TGC GCT ATC ATA ACG ACC TGT C
64M_FW	GAT AGC GCA ATG GCA ACC GAT GGT AGC	64M_RV	GGT TGC CAT TGC GCT ATC ATA ACG ACC TGT C
64Y_FW	GAT AGC GCA TAT GCA ACC GAT GGT AGC	64Y_RV	GGT TGC ATA TGC GCT ATC ATA ACG ACC TGT C
64S_FW	GAT AGC GCA TCG GCA ACC GAT GGT AGC	64S_RV	GGT TGC CGA TGC GCT ATC ATA ACG ACC TGT C
64N_FW	GAT AGC GCA AAT GCA ACC GAT GGT AGC	64N_RV	GGT TGC ATT TGC GCT ATC ATA ACG ACC TGT C
65V_FW	CAC CGG TAA CCG ATG GTA GCG GCA CC	65V_RV	CAT CGG TTA CCG GTG CGC TAT CAT AAC G
65L_FW	CAC CGC TAA CCG ATG GTA GCG GCA CC	65L_RV	CAT CGG TTA GCG GTG CGC TAT CAT AAC G
65D_FW	CAC CGG ACA CCG ATG GTA GCG GCA CC	65D_RV	CAT CGG TGT CCG GTG CGC TAT CAT AAC G
65E_FW	CAC CGG AAA CCG ATG GTA GCG GCA CC	65E_RV	CAT CGG TTT CCG GTG CGC TAT CAT AAC G
65Q_FW	CAC CGC AAA CCG ATG GTA GCG GCA CC	65Q_RV	CAT CGG TTT GCG GTG CGC TAT CAT AAC G
65K_FW	CAC CGA AAA CCG ATG GTA GCG GCA CC	65K_RV	CAT CGG TTT TCG GTG CGC TAT CAT AAC G
65H_FW	CAC CGC ATA CCG ATG GTA GCG GCA CC	65H_RV	CAT CGG TAT GCG GTG CGC TAT CAT AAC G
65M_FW	CAC CGA TGA CCG ATG GTA GCG GCA CC	65M_RV	CAT CGG TCA TCG GTG CGC TAT CAT AAC G
65Y_FW	CAC CGT ACA CCG ATG GTA GCG GCA CC	65Y_RV	CAT CGG TGT ACG GTG CGC TAT CAT AAC G
65S_FW	CAC CGT CAA CCG ATG GTA GCG GCA CC	65S_RV	CAT CGG TTG ACG GTG CGC TAT CAT AAC G
65P_FW	CAC CGC CAA CCG ATG GTA GCG GCA CC	65P_RV	CAT CGG TTG GCG GTG CGC TAT CAT AAC G
65N_FW	CAC CGA ACA CCG ATG GTA GCG GCA CC	65N_RV	CAT CGG TGT TCG GTG CGC TAT CAT AAC G
113A_FW	CCA GCG CCA CCA CCG AAG CAA ATG CC	113A_RV	GGT GGT GGC GCT GGT CAG CAG CCA C
113V_FW	CCA GCG TCA CCA CCG AAG CAA ATG CC	113V_RV	GGT GGT GAC GCT GGT CAG CAG CCA C
113L_FW	CCA GCC TCA CCA CCG AAG CAA ATG CC	113L_RV	GGT GGT GAG GCT GGT CAG CAG CCA C
113D_FW	CCA GCG ACA CCA CCG AAG CAA ATG CC	113D_RV	GGT GGT GTC GCT GGT CAG CAG CCA C
113E_FW	CCA GCG AAA CCA CCG AAG CAA ATG CC	113E_RV	GGT GGT TTC GCT GGT CAG CAG CCA C
113Q_FW	CCA GCC AGA CCA CCG AAG CAA ATG CC	113Q_RV	GGT GGT CTG GCT GGT CAG CAG CCA C
113K_FW	CCA GCA AAA CCA CCG AAG CAA ATG CC	113K_RV	GGT GGT TTT GCT GGT CAG CAG CCA C
113H_FW	CCA GCC ACA CCA CCG AAG CAA ATG CC	113H_RV	GGT GGT GTG GCT GGT CAG CAG CCA C
113M_FW	CCA GCA TGA CCA CCG AAG CAA ATG CC	113M_RV	GGT GGT CAT GCT GGT CAG CAG CCA C
113Y_FW	CCA GCT ACA CCA CCG AAG CAA ATG CC	113Y_RV	GGT GGT GTA GCT GGT CAG CAG CCA C
113S_FW	CCA GCA GCA CCA CCG AAG CAA ATG CC	113S_RV	GGT GGT GCT GCT GGT CAG CAG CCA C
113P_FW	CCA GCC CCA CCA CCG AAG CAA ATG CC	113P_RV	GGT GGT GGG GCT GGT CAG CAG CCA C
117V_FW	CCG AAG TAA ATG CCT GGG CAA GCA CC	117V_RV	GCA TTT ACT TCG GTG GTG CCG CTG G
117L_FW	CCG AAC TAA ATG CCT GGG CAA GCA CC	117L_RV	GCA TTT AGT TCG GTG GTG CCG CTG G
117D_FW	CCG AAG ACA ATG CCT GGG CAA GCA CC	117D_RV	GCA TTG TCT TCG GTG GTG CCG CTG G
117E_FW	CCG AAG AAA ATG CCT GGG CAA GCA CC	117E_RV	GCA TTT TCT TCG GTG GTG CCG CTG G
117Q_FW	CCG AAC AAA ATG CCT GGG CAA GCA CC	117Q_RV	GCA TTT TGT TCG GTG GTG CCG CTG G
117K_FW	CCG AAA AAA ATG CCT GGG CAA GCA CC	117K_RV	GCA TTT TTT TCG GTG GTG CCG CTG G
117H_FW	CCG AAC ATA ATG CCT GGG CAA GCA CC	117H_RV	GCA TTA TGT TCG GTG GTG CCG CTG G
117M_FW	CCG AAA TGA ATG CCT GGG CAA GCA CC	117M_RV	GCA TTC ATT TCG GTG GTG CCG CTG G
117Y_FW	CCG AAT ACA ATG CCT GGG CAA GCA CC	117Y_RV	GCA TTG TAT TCG GTG GTG CCG CTG G
117S_FW	CCG AAT CAA ATG CCT GGG CAA GCA CC	117S_RV	GCA TTT GAT TCG GTG GTG CCG CTG G
117P_FW	CCG AAC CAA ATG CCT GGG CAA GCA CC	117P_RV	GCA TTT GGT TCG GTG GTG CCG CTG G
117N_FW	CCG AAA ACA ATG CCT GGG CAA GCA CC	117N_RV	GCA TTG TTT TCG GTG GTG CCG CTG G
122A_FW	CTG GGC AGC CAC CCT GGT TGG TCA TGA TAC C	122A_RV	CAG GGT GGC TGC CCA GGC ATT TGC TTC G
122V_FW	CTG GGC AGT CAC CCT GGT TGG TCA TGA TAC C	122V_RV	CAG GGT GAC TGC CCA GGC ATT TGC TTC G
122L_FW	CTG GGC ACT CAC CCT GGT TGG TCA TGA TAC C	122L_RV	CAG GGT GAG TGC CCA GGC ATT TGC TTC G
122D_FW	CTG GGC AGA CAC CCT GGT TGG TCA TGA TAC C	122D_RV	CAG GGT GTC TGC CCA GGC ATT TGC TTC G
122E_FW	CTG GGC AGA AAC CCT GGT TGG TCA TGA TAC C	122E_RV	CAG GGT TTC TGC CCA GGC ATT TGC TTC G
122Q_FW	CTG GGC ACA GAC CCT GGT TGG TCA TGA TAC C	122Q_RV	CAG GGT CTG TGC CCA GGC ATT TGC TTC G
122K_FW	CTG GGC AAA AAC CCT GGT TGG TCA TGA TAC C	122K_RV	CAG GGT TTT TGC CCA GGC ATT TGC TTC G
122H_FW	CTG GGC ACA CAC CCT GGT TGG TCA TGA TAC C	122H_RV	CAG GGT GTG TGC CCA GGC ATT TGC TTC G
122M_FW	CTG GGC AAT GAC CCT GGT TGG TCA TGA TAC C	122M_RV	CAG GGT CAT TGC CCA GGC ATT TGC TTC G
122Y_FW	CTG GGC ATA CAC CCT GGT TGG TCA TGA TAC C	122Y_RV	CAG GGT GTA TGC CCA GGC ATT TGC TTC G
122P_FW	G GGC ACC CAC CCT GGT TGG TCA TGA TAC C	122P_RV	G GGT GGG TGC CCA GGC ATT TGC TTC G
122N_FW	CTG GGC AAACAC CCT GGT TGG TCA TGA TAC C	122N_RV	CAG GGT GTT TGC CCA GGC ATT TGC TTC G
123A_FW	GGC AAG CGC CCT GGT TGG TCA TGA TAC C	123A_RV	CAA CCA GGG CGC TTG CCC AGG CAT TTG C
123V_FW	GGC AAG CGT CCT GGT TGG TCA TGA TAC C	123V_RV	CAA CCA GGA CGC TTG CCC AGG CAT TTG C
123L_FW	GGC AAG CCT CCT GGT TGG TCA TGA TAC C	123L_RV	CAA CCA GGA GGC TTG CCC AGG CAT TTG C

123D_FW	GGC AAG CGA CCT GGT TGG TCA TGA TAC C	123D_RV	CAA CCA GGT CGC TTG CCC AGG CAT TTG C
123E_FW	GGC AAG CGA ACT GGT TGG TCA TGA TAC C	123E_RV	CAA CCA GTT CGC TTG CCC AGG CAT TTG C
123Q_FW	GGC AAG CCA ACT GGT TGG TCA TGA TAC C	123Q_RV	CCA GTT GGC TTG CCC AGG CAT TTG C
123K_FW	GGC AAG CAA ACT GGT TGG TCA TGA TAC C	123K_RV	CAA CCA GTT TGC TTG CCC AGG CAT TTG C
123H_FW	GGC AAG CCA CCT GGT TGG TCA TGA TAC C	123H_RV	CAA CCA GGT GGC TTG CCC AGG CAT TTG C
123M_FW	GGC AAG CAT GCT GGT TGG TCA TGA TAC C	123M_RV	CAA CCA GCA TGC TTG CCC AGG CAT TTG C
123Y_FW	GGC AAG CTA CCT GGT TGG TCA TGA TAC C	123Y_RV	CAA CCA GGT AGC TTG CCC AGG CAT TTG C
123S_FW	GGC AAG CTC CCT GGT TGG TCA TGA TAC C	123S_RV	CAA CCA GGG AGC TTG CCC AGG CAT TTG C
123P_FW	GGC AAG CCC CCT GGT TGG TCA TGA TAC C	123P_RV	CAA CCA GGG GGC TTG CCC AGG CAT TTG C
124A_FW	CAA GCA CCG CGG TTG GTC ATG ATA CCT TTA CC	124A_RV	CCA ACC GCG GTG CTT GCC CAG GCA TTTGC
124V_FW	CAA GCA CCG TGG TTG GTC ATG ATA CCT TTA CC	124V_RV	CCA ACC ACG GTG CTT GCC CAG GCA TTTGC
124D_FW	CAA GCA CCG ATG TTG GTC ATG ATA CCT TTA CC	124D_RV	CCA ACA TCG GTG CTT GCC CAG GCA TTTGC
124E_FW	CAA GCA CCG AGG TTG GTC ATG ATA CCT TTA CC	124E_RV	CCA ACC TCG GTG CTT GCC CAG GCA TTTGC
124Q_FW	CAA GCA CCC AGG TTG GTC ATG ATA CCT TTA CC	124Q_RV	CCA ACC TGG GTG CTT GCC CAG GCA TTTGC
124K_FW	CAA GCA CCA AGG TTG GTC ATG ATA CCT TTA CC	124K_RV	CA ACC TTG GTG CTT GCC CAG GCA TTTGC
124H_FW	CAA GCA CCC ACG TTG GTC ATG ATA CCT TTA CC	124H_RV	CCA ACG TGG GTG CTT GCC CAG GCA TTTGC
124M_FW	CAA GCA CCA TGG TTG GTC ATG ATA CCT TTA CC	124M_RV	CCA ACC ATG GTG CTT GCC CAG GCA TTTGC
124Y_FW	CAA GCA CCT ACG TTG GTC ATG ATA CCT TTA CC	124Y_RV	CCA ACG TAG GTG CTT GCC CAG GCA TTTGC
124S_FW	CAA GCA CCT CGG TTG GTC ATG ATA CCT TTA CC	124S_RV	CCA ACC GAG GTG CTT GCC CAG GCA TTTGC
124P_FW	CAA GCA CCC CGG TTG GTC ATG ATA CCT TTA CC	124P_RV	CCA ACC GGG GTG CTT GCC CAG GCA TTTGC
124N_FW	CAA GCA CCA ACG TTG GTC ATG ATA CCT TTA CC	124N_RV	CCA ACG TTG GTG CTT GCC CAG GCA TTTGC
144A_FW	GCA GCA GCA AAA GCC GGT GTG AAT AAT GG	144A_RV	GGC TTTTGCTGCTGCATCAATGCTTGC
144V_FW	GCA GCA GTA AAA GCC GGT GTG AAT AAT GG	144V_RV	GGC TTTTACTGCTGCATCAATGCTTGC
144L_FW	GCA GCA CTA AAA GCC GGT GTG AAT AAT GG	144L_RV	GGC TTTTAGTCTGCATCAATGCTTGC
144D_FW	GCA GCA GAT AAA GCC GGT GTG AAT AAT GG	144D_RV	GGC TTT ATC TGC TGC ATC AAT GCT TGC
144E_FW	GCA GCA GAA AAA GCC GGT GTG AAT AAT GG	144E_RV	GGC TTT TTC TGC TGC ATC AAT GCT TGC
144Q_FW	GCA GCA CAA AAA GCC GGT GTG AAT AAT GG	144Q_RV	GGC TTT TTG TGC TGC ATC AAT GCT TGC
144H_FW	GCA GCA CAT AAA GCC GGT GTG AAT AAT GG	144H_RV	GGC TTT ATG TGC TGC ATC AAT GCT TGC
144M_FW	GCA GCA ATG AAA GCC GGT GTG AAT AAT GG	144M_RV	GGC TTT CAT TGC TGC ATC AAT GCT TGC
144Y_FW	GCA GCA TAC AAA GCC GGT GTG AAT AAT GG	144Y_RV	GGC TTT GTA TGC TGC ATC AAT GCT TGC
144S_FW	GCA GCA AGC AAA GCC GGT GTG AAT AAT GG	144S_RV	GGC TTT GCT TGC TGC ATC AAT GCT TGC
144P_FW	GCA GCA CCA AAA GCC GGT GTG AAT AAT GG	144P_RV	GGC TTT TGG TGC TGC ATC AAT GCT TGC
144N_FW	GCA GCA AAC AAA GCC GGT GTG AAT AAT GG	144N_RV	GGC TTT GTT TGC TGC ATC AAT GCT TGC
67A_FW	CAA CCG CTG GTA GCG GCA CCG CAC TG	67A_RV	GCT ACC AGC GGT TGC CGG TGC GCT ATC
67V_FW	CAA CCG TTG GTA GCG GCA CCG CAC TG	67V_RV	GCT ACC AAC GGT TGC CGG TGC GCT ATC
67L_FW	CAA CCC TTG GTA GCG GCA CCG CAC TG	67L_RV	GCT ACC AAG GGT TGC CGG TGC GCT ATC
67E_FW	CAA CCG AAG GTA GCG GCA CCG CAC TG	67E_RV	GCT ACC TTC GGT TGC CGG TGC GCT ATC
67Q_FW	CAA CCC AAG GTA GCG GCA CCG CAC TG	67Q_RV	GCT ACC TTG GGT TGC CGG TGC GCT ATC
67K_FW	CAA CCA AAG GTA GCG GCA CCG CAC TG	67K_RV	GCT ACC TTT GGT TGC CGG TGC GCT ATC
67H_FW	CAA CCC ATG GTA GCG GCA CCG CAC TG	67H_RV	GCT ACC ATG GGT TGC CGG TGC GCT ATC
67M_FW	CAA CCA TGG GTA GCG GCA CCG CAC TG	67M_RV	GCT ACC CAT GGT TGC CGG TGC GCT ATC
67Y_FW	CAA CCT ATG GTA GCG GCA CCG CAC TG	67Y_RV	GCT ACC ATA GGT TGC CGG TGC GCT ATC
67S_FW	CAA CCT CTG GTA GCG GCA CCG CAC TG	67S_RV	GCT ACC AGA GGT TGC CGG TGC GCT ATC
67P_FW	CAA CCC CTG GTA GCG GCA CCG CAC TG	67P_RV	GCT ACC AGG GGT TGC CGG TGC GCT ATC
67N_FW	CAA CCA ATG GTA GCG GCA CCG CAC TG	67N_RV	GCT ACC TTA GGT TGC CGG TGC GCT ATC
86A_FW	CCG ATGCTA GCG GCA CCG CAC TGG GTT GG	86A_RV	GTG CCG CTA GCA TCG GTT GCC GGT GCG
86V_FW	CCG ATGTTA GCG GCA CCG CAC TGG GTT GG	86V_RV	GTG CCG CTA ACA TCG GTT GCC GGT GCG
86L_FW	CCG ATCTTA GCG GCA CCG CAC TGG GTT GG	86L_RV	GTG CCG CTA AGA TCG GTT GCC GGT GCG
86D_FW	CCG ATGATA GCG GCA CCG CAC TGG GTT GG	86D_RV	GTG CCG CTA TCA TCG GTT GCC GGT GCG
86E_FW	CCG ATGAAA GCG GCA CCG CAC TGG GTT GG	86E_RV	GTG CCG CTT TCA TCG GTT GCC GGT GCG
86Q_FW	CCG ATCAAA GCG GCA CCG CAC TGG GTT GG	86Q_RV	GTG CCG CTT TGA TCG GTT GCC GGT GCG
86K_FW	CCG ATAAAA GCG GCA CCG CAC TGG GTT GG	86K_RV	GTG CCG CTT TTA TCG GTT GCC GGT GCG
86H_FW	CCG ATCATA GCG GCA CCG CAC TGG GTT GG	86H_RV	GTG CCG CTA TGA TCG GTT GCC GGT GCG
86M_FW	CCG ATATGA GCG GCA CCG CAC TGG GTT GG	86M_RV	GTG CCG CTC ATA TCG GTT GCC GGT GCG
86Y_FW	CCG ATTATA GCG GCA CCG CAC TGG GTT GG	86Y_RV	GTG CCG CTA TAA TCG GTT GCC GGT GCG
86S_FW	CCG ATAGTA GCG GCA CCG CAC TGG GTT GG	86S_RV	GTG CCG CTA CTA TCG GTT GCC GGT GCG
86P_FW	CCG ATCCTA GCG GCA CCG CAC TGG GTT GG	86P_RV	GTG CCG CTA GGA TCG GTT GCC GGT GCG
110A_FW	GCT GGC GAC CAG CGG CAC CAC CGA AG	110A_RV	GCT GGT CGC CAG CCA CTG GGT ATT AAT GCG
110V_FW	GCT GGT GAC CAG CGG CAC CAC CGA AG	110V_RV	GCT GGT CAC CAG CCA CTG GGT ATT AAT GCG
110D_FW	GCT GGA TAC CAG CGG CAC CAC CGA AG	110D_RV	GCT GGT ATC CAG CCA CTG GGT ATT AAT GCG

110E_FW	GCT GGA GAC CAG CGG CAC CAC CGA AG	110E_RV	GCT GGT CTC CAG CCA CTG GGT ATT AAT GCG
110Q_FW	GCT GCA GAC CAG CGG CAC CAC CGA AG	110Q_RV	GCT GGT CTG CAG CCA CTG GGT ATT AAT GCG
110K_FW	GCT GAA GAC CAG CGG CAC CAC CGA AG	110K_RV	GCT GGT CTT CAG CCA CTG GGT ATT AAT GCG
110H_FW	GCT GCA CAC CAG CGG CAC CAC CGA AG	110H_RV	GCT GGT GTG CAG CCA CTG GGT ATT AAT GCG
110M_FW	GCT GAT GAC CAG CGG CAC CAC CGA AG	110M_RV	GCT GGT CAT CAG CCA CTG GGT ATT AAT GCG
110Y_FW	GCT GTA CAC CAG CGG CAC CAC CGA AG	110Y_RV	GCT GGT GTA CAG CCA CTG GGT ATT AAT GCG
110S_FW	GCT GTC GAC CAG CGG CAC CAC CGA AG	110S_RV	GCT GGT CGA CAG CCA CTG GGT ATT AAT GCG
110P_FW	GCT GCC GAC CAG CGG CAC CAC CGA AG	110P_RV	GCT GGT CGG CAG CCA CTG GGT ATT AAT GCG
110N_FW	GCT GAA CAC CAG CGG CAC CAC CGA AG	110N_RV	GCT GGT GTT CAG CCA CTG GGT ATT AAT GCG
111A_FW	CTG CTG GCC AGC GGC ACC ACC GAA GC	111A_RV	CCG CTG GCC AGC AGC CAC TGG GTA TTA ATG C
111V_FW	CTG CTG GTC AGC GGC ACC ACC GAA GC	111V_RV	CCG CTG ACC AGC AGC CAC TGG GTA TTA ATG C
111L_FW	CTG CTG CTC AGC GGC ACC ACC GAA GC	111L_RV	CCG CTG AGC AGC AGC CAC TGG GTA TTA ATG C
111D_FW	CTG CTG GAC AGC GGC ACC ACC GAA GC	111D_RV	CCG CTG TCC AGC AGC CAC TGG GTA TTA ATG C
111E_FW	CTG CTG GAA AGC GGC ACC ACC GAA GC	111E_RV	CCG CTT TCC AGC AGC CAC TGG GTA TTA ATG C
111Q_FW	CTG CTG CAA AGC GGC ACC ACC GAA GC	111Q_RV	CCG CTT TGC AGC AGC CAC TGG GTA TTA ATG C
111K_FW	CTG CTG AAA AGC GGC ACC ACC GAA GC	111K_RV	CCG CTT TTC AGC AGC CAC TGG GTA TTA ATG C
111H_FW	CTG CTG CAC AGC GGC ACC ACC GAA GC	111H_RV	CCG CTG TGC AGC AGC CAC TGG GTA TTA ATG C
111M_FW	CTG CTG ATG AGC GGC ACC ACC GAA GC	111M_RV	CCG CTC ATC AGC AGC CAC TGG GTA TTA ATG C
111Y_FW	CTG CTG TAC AGC GGC ACC ACC GAA GC	111Y_RV	CCG CTG TAC AGC AGC CAC TGG GTA TTA ATG C
111S_FW	CTG CTG TCC AGC GGC ACC ACC GAA GC	111S_RV	CCG CTG GAC AGC AGC CAC TGG GTA TTA ATG C
111P_FW	CTG CTG CCC AGC GGC ACC ACC GAA GC	111P_RV	CCG CTG GGC AGC AGC CAC TGG GTA TTA ATG C
114A_FW	GCG GCG CCA CCG AAG CAA ATG CCT GG	114A_RV	CTT CGG TGG CGC CGC TGG TCA GCA GCC
114V_FW	GCG GCG TCA CCG AAG CAA ATG CCT GG	114V_RV	CTT CGG TGA CGC CGC TGG TCA GCA GCC
114L_FW	GCG GCC TCA CCG AAG CAA ATG CCT GG	114L_RV	CTT CGG TGA GGC CGC TGG TCA GCA GCC
114D_FW	GCG GCG ACA CCG AAG CAA ATG CCT GG	114D_RV	CTT CGG TGT CGC CGC TGG TCA GCA GCC
114E_FW	GCG GCG AAA CCG AAG CAA ATG CCT GG	114E_RV	CTT CGG TTT CGC CGC TGG TCA GCA GCC
114Q_FW	GCG GCC AAA CCG AAG CAA ATG CCT GG	114Q_RV	CTT CGG TTT GGC CGC TGG TCA GCA GCC
114K_FW	GCG GCA AAA CCG AAG CAA ATG CCT GG	114K_RV	CTT CGG TTT TGC CGC TGG TCA GCA GCC
114H_FW	GCG GCC ACA CCG AAG CAA ATG CCT GG	114H_RV	CTT CGG TGT GGC CGC TGG TCA GCA GCC
114M_FW	GCG GCA TGA CCG AAG CAA ATG CCT GG	114M_RV	CTT CGG TCA TGC CGC TGG TCA GCA GCC
114Y_FW	GCG GCT ACA CCG AAG CAA ATG CCT GG	114Y_RV	CTT CGG TGT AGC CGC TGG TCA GCA GCC
114S_FW	GCG GCT CCA CCG AAG CAA ATG CCT GG	114S_RV	CTT CGG TGG AGC CGC TGG TCA GCA GCC
114P_FW	GCG GCC CCA CCG AAG CAA ATG CCT GG	114P_RV	CTT CGG TGG GGC CGC TGG TCA GCA GCC
115A_FW	GCA CCG CCG AAG CAA ATG CCT GGG CAA GC	115A_RV	GCT TCG GCG GTG CCG CTG GTC AGC AG
115V_FW	GCA CCG TCG AAG CAA ATG CCT GGG CAA GC	115V_RV	GCT TCG ACG GTG CCG CTG GTC AGC AG
115L_FW	GCA CCC TCG AAG CAA ATG CCT GGG CAA GC	115L_RV	GCT TCG AGG GTG CCG CTG GTC AGC AG
115D_FW	GCA CCG ACG AAG CAA ATG CCT GGG CAA GC	115D_RV	GCT TCG TCG GTG CCG CTG GTC AGC AG
115E_FW	GCA CCG AAG AAG CAA ATG CCT GGG CAA GC	115E_RV	GCT TCT TCG GTG CCG CTG GTC AGC AG
115Q_FW	GCA CCC AAG AAG CAA ATG CCT GGG CAA GC	115Q_RV	GCT TCT TGG GTG CCG CTG GTC AGC AG
115K_FW	GCA CCA AAG AAG CAA ATG CCT GGG CAA GC	115K_RV	GCT TCT TTG GTG CCG CTG GTC AGC AG
115H_FW	GCA CCC ACG AAG CAA ATG CCT GGG CAA GC	115H_RV	GCT TCG TGG GTG CCG CTG GTC AGC AG
115M_FW	GCA CCA TGG AAG CAA ATG CCT GGG CAA GC	115M_RV	GCT TCC ATG GTG CCG CTG GTC AGC AG
115Y_FW	GCA CCT ACG AAG CAA ATG CCT GGG CAA GC	115Y_RV	GCT TCG TAG GTG CCG CTG GTC AGC AG
115S_FW	GCA CCT CCG AAG CAA ATG CCT GGG CAA GC	115S_RV	GCT TCG GAG GTG CCG CTG GTC AGC AG
115P_FW	GCA CCC CCG AAG CA A ATG CCT GGG CAA GC	115P_RV	GCT TCG GGG GTG CCG CTG GTC AGC AG
116A_FW	CAC CAC CGC AGC AAA TGC CTG GGC AAG C	116A_RV	CAT TTG CTG CGG TGG TGC CGC TGG TCA G
116V_FW	CAC CAC CGT AGC AAA TGC CTG GGC AAG C	116V_RV	CAT TTG CTA CGG TGG TGC CGC TGG TCA G
116L_FW	CAC CAC CTT AGC AAA TGC CTG GGC AAG C	116L_RV	CAT TTG CTA AGG TGG TGC CGC TGG TCA G
116D_FW	CAC CAC CGA TGC AAA TGC CTG GGC AAG C	116D_RV	CAT TTG CAT CGG TGG TGC CGC TGG TCA G
116Q_FW	CAC CAC CCA AGC AAA TGC CTG GGC AAG C	116Q_RV	CAT TTG CTT GGG TGG TGC CGC TGG TCA G
116K_FW	CAC CAC CAA AGC AAA TGC CTG GGC AAG C	116K_RV	CAT TTG CTT TGG TGG TGC CGC TGG TCA G
116H_FW	CAC CAC CCA CGC AAA TGC CTG GGC AAG C	116H_RV	CAT TTG CGT GGG TGG TGC CGC TGG TCA G
116M_FW	CAC CAC CAT GGC AAA TGC CTG GGC AAG C	116M_RV	CAT TTG CCA TGG TGG TGC CGC TGG TCA G
116Y_FW	CAC CAC CTA TGC AAA TGC CTG GGC AAG C	116Y_RV	CAT TTG CAT AGG TGG TGC CGC TGG TCA G
116S_FW	CAC CAC CTC AGC AAA TGC CTG GGC AAG C	116S_RV	CAT TTG CTG AGG TGG TGC CGC TGG TCA G
116P_FW	CAC CAC CCC AGC AAA TGC CTG GGC AAG C	116P_RV	CAT TTG CTG GGG TGG TGC CGC TGG TCA G
116N_FW	CAC CAC CAA TGC AAA TGC CTG GGC AAG C	116N_RV	CAT TTG CAT TGG TGG TGC CGC TGG TCA G
118A_FW	GAA GCA GCT GCC TGG GCA AGC ACC CTG	118A_RV	CAG GCA GCT GCT TCG GTG GTG CCG C
118V_FW	GAA GCA GTT GCC TGG GCA AGC ACC CTG	118V_RV	CAG GCA ACT GCT TCG GTG GTG CCG C
118L_FW	GAA GCA CTT GCC TGG GCA AGC ACC CTG	118L_RV	CAG GCA AGT GCT TCG GTG GTG CCG C

118D_FW	GAA GCA GAT GCC TGG GCA AGC ACC CTG	118D_RV	CAG GCA TCT GCT TCG GTG GTG CCG C
118E_FW	GAA GCA GAA GCC TGG GCA AGC ACC CTG	118E_RV	CAG GCT TCT GCT TCG GTG GTG CCG C
118Q_FW	GAA GCA CAA GCC TGG GCA AGC ACC CTG	118Q_RV	CAG GCT TGT GCT TCG GTG GTG CCG C
118K_FW	GAA GCA AAA GCC TGG GCA AGC ACC CTG	118K_RV	CAG GCT TTT GCT TCG GTG GTG CCG C
118H_FW	GAA GCA CAT GCC TGG GCA AGC ACC CTG	118H_RV	CAG GCA TGT GCT TCG GTG GTG CCG C
118M_FW	GAA GCA ATG GCC TGG GCA AGC ACC CTG	118M_RV	CAG GCC ATT GCT TCG GTG GTG CCG C
118Y_FW	GAA GCA TAT GCC TGG GCA AGC ACC CTG	118Y_RV	CAG GCA TAT GCT TCG GTG GTG CCG C
118S_FW	GAA GCA AGT GCC TGG GCA AGC ACC CTG	118S_RV	CAG GCA CTT GCT TCG GTG GTG CCG C
118P_FW	GAA GCA CCT GCC TGG GCA AGC ACC CTG	118P_RV	CAG GCA GGT GCT TCG GTG GTG CCG C
50V_FW	GGT AAT GTA GAA AGC CGT TAT GTT CTG	50V_RV	CTT TCT ACA TTA CCA ACT GCG CTT TC
50L_FW	GGT AAT CTA GAA AGC CGT TAT GTT CTG	50L_RV	CTT TCT AGA TTA CCA ACT GCG CTT TC
50D_FW	GGT AAT GAC GAA AGC CGT TAT GTT CTG	50D_RV	CTT TCG TCA TTA CCA ACT GCG CTT TC
50E_FW	GGT AAT GAA GAA AGC CGT TAT GTT CTG	50E_RV	CTT TCT TCA TTA CCA ACT GCG CTT TC
50Q_FW	GGT AAT CAA GAA AGC CGT TAT GTT CTG	50Q_RV	CTT TCT TGA TTA CCA ACT GCG CTT TC
50K_FW	GGT AAT AAA GAA AGC CGT TAT GTT CTG	50K_RV	CTT TCT TTA TTA CCA ACT GCG CTT TC
50H_FW	GGT AAT CAT GAA AGC CGT TAT GTT CTG	50H_RV	CTT TCA TGA TTA CCA ACT GCG CTT TC
50M_FW	GGT AAT ATG GAA AGC CGT TAT GTT CTG	50M_RV	CTT TCC ATA TTA CCA ACT GCG CTT TC
50Y_FW	GGT AAT TAC GAA AGC CGT TAT GTT CTG	50Y_RV	CTT TCG TAA TTA CCA ACT GCG CTT TC
50S_FW	GGT AAT TCA GAA AGC CGT TAT GTT CTG	50S_RV	CTT TCT GAA TTA CCA ACT GCG CTT TC
50P_FW	GGT AAT CCA GAA AGC CGT TAT GTT CTG	50P_RV	CTT TCT GGA TTA CCA ACT GCG CTT TC
50N_FW	GGT AAT AAC GAA AGC CGT TAT GTT CTG	50N_RV	CTT TCG TTA TTA CCA ACT GCG CTT TC
53A_FW	GAA AGC GCC TAT GTT CTG ACA GGT CG	53A_RV	GAA CAT AGG CGC TTT CTG CAT TAC CAA C
53V_FW	GAA AGC GTT TAT GTT CTG ACA GGT CG	53V_RV	GAA CAT AAA CGC TTT CTG CAT TAC CAA C
53L_FW	GAA AGC CTT TAT GTT CTG ACA GGT CG	53L_RV	GAA CAT AAA GGC TTT CTG CAT TAC CAA C
53D_FW	GAA AGC GAT TAT GTT CTG ACA GGT CG	53D_RV	GAA CAT AAT CGC TTT CTG CAT TAC CAA C
53E_FW	GAA AGC GAG TAT GTT CTG ACA GGT CG	53E_RV	GAA CAT ACT CGC TTT CTG CAT TAC CAA C
53Q_FW	GAA AGC CAG TAT GTT CTG ACA GGT CG	53Q_RV	GAA CAT ACT GGC TTT CTG CAT TAC CAA C
53K_FW	GAA AGC AAG TAT GTT CTG ACA GGT CG	53K_RV	GAA CAT ACT TGC TTT CTG CAT TAC CAA C
53H_FW	GAA AGC CAT TAT GTT CTG ACA GGT CG	53H_RV	GAA CAT AAT GGC TTT CTG CAT TAC CAA C
53M_FW	GAA AGC ATG TAT GTT CTG ACA GGT CG	53M_RV	GAA CAT ACA TGC TTT CTG CAT TAC CAA C
53Y_FW	GAA AGC TAT TAT GTT CTG ACA GGT CG	53Y_RV	GAA CAT AAT AGC TTT CTG CAT TAC CAA C
53S_FW	GAA AGC AGT TAT GTT CTG ACA GGT CG	53S_RV	GAA CAT AAC TGC TTT CTG CAT TAC CAA C
53P_FW	GAA AGC CCT TAT GTT CTG ACA GGT CG	53P_RV	GAA CAT AAG GGC TTT CTG CAT TAC CAA C
86V_FW	GTA ATG TAC ATA GCG CAA CCA CCT GG	86V_RV	GCG CTA TGT ACA TTA CGA TAG TTA TTT TTC C
86L_FW	GTA ATC TAC ATA GCG CAA CCA CCT GG	86L_RV	GCG CTA TGT AGA TTA CGA TAG TTA TTT TTC C
86D_FW	GTA ATG ACC ATA GCG CAA CCA CCT GG	86D_RV	GCG CTA TGG TCA TTA CGA TAG TTA TTT TTC C
86E_FW	GTA ATG AAC ATA GCG CAA CCA CCT GG	86E_RV	GCG CTA TGT TCA TTA CGA TAG TTA TTT TTC C
86Q_FW	GTA ATC AAC ATA GCG CAA CCA CCT GG	86Q_RV	GCG CTA TGT TGA TTA CGA TAG TTA TTT TTC C
86K_FW	GTA ATA AAC ATA GCG CAA CCA CCT GG	86K_RV	GCG CTA TGT TTA TTA CGA TAG TTA TTT TTC C
86H_FW	GTA ATC ATC ATA GCG CAA CCA CCT GG	86H_RV	GCG CTA TGA TGA TTA CGA TAG TTA TTT TTC C
86M_FW	GTA ATA TGC ATA GCG CAA CCA CCT GG	86M_RV	GCG CTA TGC ATA TTA CGA TAG TTA TTT TTC C
86Y_FW	GTA ATT ACC ATA GCG CAA CCA CCT GG	86Y_RV	GCG CTA TGG TAA TTA CGA TAG TTA TTT TTC C
86S_FW	GTA ATT CAC ATA GCG CAA CCA CCT GG	86S_RV	GCG CTA TGT GAA TTA CGA TAG TTA TTT TTC C
86P_FW	GTA ATC CAC ATA GCG CAA CCA CCT GG	86P_RV	GCG CTA TGT GGA TTA CGA TAG TTA TTT TTC C
86N_FW	GTA ATA ACC ATA GCG CAA CCA CCT GG	86N_RV	GCG CTA TGG TTA TTA CGA TAG TTA TTT TTC C
K121A_FW ^a	CTG GGC GTC CAC GCT GGT CGG	K121A_RV ^a	GGA CGC CCA GGC GTT GGC CTC
POSITIVE__		POSITIVE__	
CONTROL_	CAT ATG GCA AGC ATG ACC GGT G	CONTROL_	GGA TCC CTA TTA CTG CTG AAC TGC
FW		RV	

^a This primer pair was used for the design of the S112XK121A mutants. Here available Sav112X mutants derived from the natural Sav sequence where mutated to K121A to obtain S112XK121A. This constructs are derived from pET-11b vector and therefore ampicillin (100 µg ml⁻¹ culture media) has to be used as antibiotic.

APPENDIX B

Supporting information for *Angew. Chem. Int. Ed.* **2018**, *130*, 1881–1886

B.1 GENERAL INFORMATION

All commercially available chemicals were purchased from commercial suppliers (Sigma-Aldrich, Acros Organics, Alfa Aesar, AppliChem, NEB, AnaSpec, Fluka or Merck) and used without further purification. Solvents for HPLC measurements were purchased from Baker and Biosolve. *E. coli* bacterial strains (BL21 and TOP10) were purchased from NEB or Invitrogen, respectively. Empty vector plasmid pET-24a empty vector was purchased from Novagen.

Milli-Q water (resistivity $\geq 18 \text{ M}\Omega \text{ cm}^{-1}$) was produced with a Millipore Synergy purification system. Sav mutants were produced, purified and characterized as previously described.^[B1]

Protein mass spectral analysis was performed on a Bruker Daltonics, ESI/microTOF MS. Protein purification was performed by means of affinity column chromatography on an Äktaprime Plus chromatography system, using a 2-iminobiotin sepharose column. PCR reactions were performed with an Eppendorf Mastercycler Gradient. ^1H and ^{13}C spectra were recorded on a Bruker 400 MHz. The chemical shifts (δ) are reported in parts per million (ppm) relative to TMS or a residual solvent peak. Analyses of the catalytic runs were performed on an Agilent 1100 normal phase HPLC with an analytical Chiralpak IC column (250 · 4.6 mm, 5 μm), or by GC using Agilent CAM column (30 m x 0.25 μm) and CP-Chirasil-DEX CB (25m x 0.25 μm) using He as carrier gas. The absorbance spectra were measured on a microplate reader Tecan, model Infinite M200.

E. coli strains used:

- TOP10 (Invitrogen, cat. no. C4040): $F^- mcrA \Delta(mrr\text{-}hsdRMS\text{-}mcrBC) \Phi80lacZ\Delta M15 \Delta lac\times 74 recA1 araD139 \Delta(araleu)7697 galU galK rpsL (\text{Str}^R) endA1 nupG$
- BL21 (DE3; NEB, cat. no. C2527): *E. coli* B $F^- dcm ompT hsdS(\text{r}_B^- \text{m}_B^-) gal \lambda(\text{DE3})$

B.2 STOCK SOLUTIONS AND BUFFERS

Lysogeny broth (LB) medium: Bactotryptone (10 g / l), yeast extract (5 g / l) and sodium chloride (10 g / l) were dissolved in Milli-Q water and the resulting solution was autoclaved (121°C for 20 min). Before use, kanamycin (KAN) was added to a final concentration of 50 $\mu\text{g}\cdot\text{ml}^{-1}$.

LB-agar plates: Bactotryptone (10 g / l), yeast extract (5 g / l), sodium chloride (10 g / l) and agar (15 g / l) were dissolved in Milli-Q water. The resulting mixture was boiled for 1 minute to dissolve the agar. After cooling to approx. 50°C, KAN was added to a final concentration of 50 $\mu\text{g}\cdot\text{ml}^{-1}$.

20 x ZYP-salts: KH_2PO_4 (54.4 g, final conc. 1 M), $(\text{NH}_4)_2\text{SO}_4$ (26.4 g, final conc. 0.5 M) and Na_2HPO_4 (56.8 g, final conc. 1 M) were dissolved in Milli-Q water (final volume 400 ml). The resulting solution was autoclaved (121°C for 20 min). For details, see reference ^[B1].

20 x ZYP-sugars: Anhydrous glycerol (40 ml, final conc. 10 % v/v), Lactose (16 g, final conc. 4% w/v) and glucose monohydrate (4.4 g, final conc. 55.5 mM) were dissolved in (final volume 400 ml). The resulting solution was sterile filtered (filter pore size 0.22 μm).

200 x MgSO_4 : MgSO_4 (4.92 g, final conc. 400 mM) was dissolved in Milli-Q water (final volume 50 ml) and sterile filtered (filter pore size 0.22 μm).

Modified ZYP-5052 medium: Bactotryptone (8 g, final conc. 10 g / l), yeast extract (4 g, final conc. 5 / l) were dissolved in Milli-Q water (664 ml) and autoclaved (121°C for 20 min). 20xZYP-salts (40 ml), 20xZYP sugars (80 ml), MgSO_4 (16 ml) stock solutions were added to the media. KAN (final conc. 50 $\mu\text{g}\cdot\text{ml}^{-1}$) was added before use.

100 mM MOPS buffer: MOPS (2.092 g) was dissolved in Milli-Q water and the pH of the resulting solution was adjusted to 7.5 using NaOH pellets.

Lysis buffer: Lysozyme (1 mg / ml) and DNaseI (4 μg / ml) were dissolved in a MOPS buffer (100 μM , pH 7.5).

MOPS/formate buffer: 3-(*N*-morpholino)propanesulfonic acid and sodium formate were dissolved in Milli-Q water to the concentrations of 6M (formate) and 1.2 M (MOPS). The pH was adjusted to 6 or 7 by addition of NaOH or HCl respectively.

Diamide stock solution (DiAm): 1,1'-Azobis(*N,N*-dimethylformamide) (72.5 mg, final conc. 200 mM) was dissolved in degassed DMSO (2 ml).

*Cp*Ir-complex 3*: 1.6 mg of [Cp*Ir(biot-*p*-L)Cl] was dissolved in degassed DMF to a final concentration of 2 mM. For a detailed synthesis procedure, see reference.^[B2]

Substrates: 1-phenyl-3,4-dihydroisoquinoline **1c** (synthesis procedure see reference^[B3]) or 5-phenyl-3,4-dihydro-2H-pyrrole **1d**^[B4] were dissolved in degassed DMSO (2 ml) to a final concentration of 400 mM. 6,7-dimethoxy-1-methyl-3,4-dihydroisoquinoline **1a** was dissolved in Milli-Q water (2 ml) to a final concentration of 400 mM.

B.3. EXPERIMENTAL PROCEDURES

B.3.1 PRIMER DESIGN

Precise and unique primers were designed for each mutation. Mature Sav^[5] with K121A mutation on a codon-optimized plasmid pET-24a SavK121A with reduced G/C content (52%) was used. The positions for mutagenesis were selected by identifying residues that lie within a 10 Å radius around the averaged position of the biotinylated metal moiety bound to Sav. After the identification of a successful “hit”, the position was fixed and new primers were designed to create another generation of Sav isoforms.

B.3.2 SITE-DIRECTED MUTAGENESIS

In PCR tubes, the following components were mixed (total volume 50 µl):

Table B1- PCR conditions

Component	Volume used (µl)	Final concentration:
Template	1	0.1-0.5 ng / µl
Primer (+)	2.5	0.3 µM
Primer (-)	2.5	0.3 µM
dNTPs	1	4 x 0.1 mM
DMSO	4	5 %
H ₂ O	29	-
Q5 polymerase	0.5	0.06 U / µl
5x Q5 polymerase reaction buffer	10	5 x

The samples were prepared in triplicates and placed in an Eppendorf Mastercycler Gradient and the following temperature program was applied:

1. 95 °C for 2 min.
2. PCR-cycle (25x): 95 °C for 1 min.; 60 - 68 °C gradient for 1 min.; 72 °C for 4 min.
3. 72 °C for 10 min.
4. Hold at 8 °C

Afterwards, an agarose gel (0.7 % agarose, TBE-buffer, Red nucleic acid stain 10'000x as marker) was carried out to determine the success of the PCR (Figure B1). Samples with amplified templates were incubated with 1 µl of DpnI (20 U) at 42°C for 3 h.

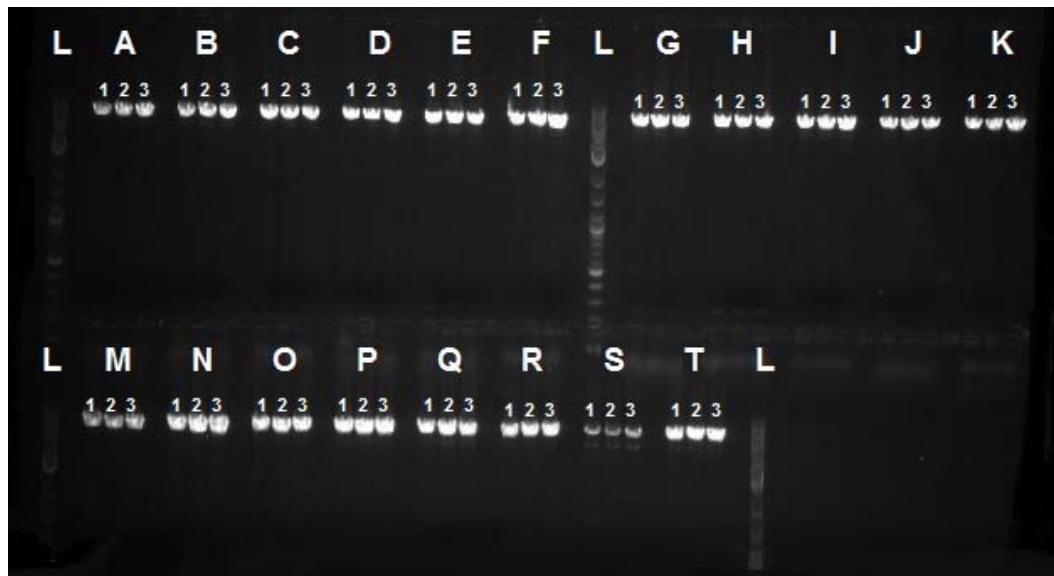


Figure B1- Analytical agarose gel (1%) with a 1-kb marker (L) using the PCR products (5 µl) before DpnI digestion. DNA is visualized by Red nucleic acid stain 10'000x. Each lane triad (A-T) corresponds to one mutation; the numbers (1-3) correspond to different temperature (50-65°C) during the PCR.

B.3.3 TRANSFORMATION OF PLASMIDS INTO CLONING OR EXPRESSION STRAIN

Chemically competent *E. coli* cells (100 µl, TOP10 strain) were transformed with 5 µl of the PRC product by applying a heat shock (30 sec, 42°C). The cells were grown in LB medium w/o antibiotic (0.5 ml, 37°C, 200 rpm) and plated on LB-agar plates containing KAN. The plates were incubated (overnight, 37°C).

LB medium (5 ml, KAN) were inoculated with a single colony from the LB-agar plate and incubated (overnight, 37°C, 200 rpm). Mini-prep was performed for each sample, following the Macherey-Nagel NucleoSpin® Plasmid kit (low-copy number protocol).^[B1] The purified plasmids were sent to Microsynth AG (Balgach, Switzerland) for sequencing.

The mutagenized plasmids were transformed into competent *E. coli* cells (100 µl, (BL21(DE3) strain) using 1 µl of the corresponding purified plasmid and the same protocol as described above.

B.3.4 LARGE SCALE EXPRESSION IN 3L CONICAL FLASKS

Precultures were grown in sterile Erlenmeyer flasks (250 ml) in LB medium (100 ml, 50 µg·ml⁻¹ KAN). After incubation (overnight, 37°C, 200 rpm), the preculture (10 ml) was transferred into a 3l conical shaking flask containing the modified ZYP-5052 medium (1 l,

50 $\mu\text{g}\cdot\text{ml}^{-1}$ KAN) and incubated (24 h, 30°C, 200 rpm). For expression in 24-deep well plates see reference.^[B1]

B.3.5 CELL HARVEST AND LYSIS

After Sav overexpression, the OD_{600nm} of each well culture was measured. Typical values after 24 h were between OD of 5-7. The cells were harvested by centrifugation (4400 rpm, 10 min, 4°C) and the supernatant was discarded. The cell pellet was frozen at -20°C. Afterwards, the pellet was thawed and resuspended in freshly prepared lysis buffer. The cell lysates were incubated (37°C, 200 rpm, 1h), frozen and thawed again at RT.

Cell free extracts were prepared by further centrifugation of the cell lysates in tubes (1.5 ml, 4400 rpm, 10 min, 4°C).

B.3.6 PROTEIN PURIFICATION

Cell lysates were transferred to dialysis bags (Spectra/Por, 6-8.000 MWCO) and dialyzed in guanidinium hydrochloride (6 M, pH 1.5, RT, overnight). The dialysis bags were then placed into a Tris/HCl buffer (20 mM, pH 7.4, 10 °C, 8 - 12h), followed by an iminobiotin binding buffer (500 mM NaCl, 50 mM NaHCO₃, pH 9.8, overnight). The cell lysates were clarified by centrifugation (45 min. at 9'000 g, 4 °C) and the supernatant was filtered (filter pore size 0.22 μm).

The resulting solution was purified by affinity chromatography (ÄKTA prime Plus chromatography system, 2-iminobiotin sepharose column). The column was first pre-washed with the iminobiotin binding buffer, followed by sample loading. After elution of the material not binding to the column, the immobilized Sav was washed using 1 % acetic acid and collected in falcon tubes and neutralized using Tris/HCl buffer (1 M, pH 8). The joined Sav-containing fractions were transferred into dialysis bags (Spectra/Por, 6-8'000 MWCO) and dialyzed in Milli-Q-water (3 x, 24 h). Finally, the samples were flash-frozen and lyophilized.

The identity of each purified Sav isoform was confirmed by mass spectrometry (Figure B2, Table B2).

Table B2 – Theoretical mass values for the Sav monomeric units and measured data.

Entry	Sav isoform	Theoretical mass of the monomer (Da)	Measured mass (Da)
1	S112T-K121A	16381.80	16381.17
2	S112R-K121A	16436.90	16436.15
3	N118P-K121A	16350.80	16350.63
4	S112A-N118P-K121A	16334.80	16334.70
5	S112T-N118K-K121A	16395.92	16395.94
6	S112T-N118K-K121A-S122K	16437.02	16437.18
7	S112A-N118P-K121A-S122M	16378.95	16377.59
8	S112R-N118P-K121A-S122M	16464.06	16463.00
9	S112R-N118P-K121A-S122M-L124Y	16514.08	16513.96

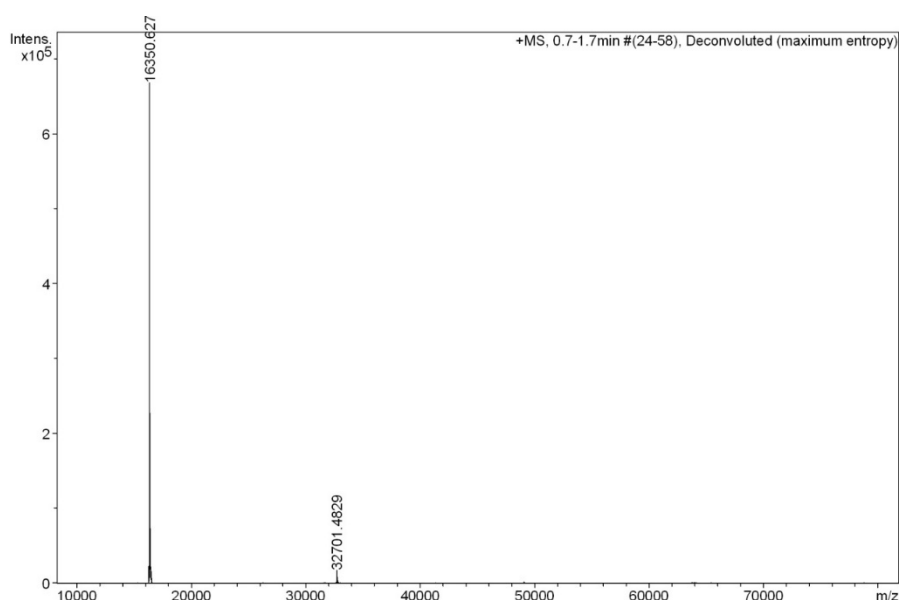


Figure B2- ESI-TOF mass spectrum after deconvolution of K121A-N118P isoform (displayed as an example). The measured value of $16350.63 \text{ g}\cdot\text{mol}^{-1}$ for the monomeric protein unit corresponds to the theoretical value of $16350.8 \text{ g}\cdot\text{mol}^{-1}$.

B.3.7 DETERMINATION OF STREPTAVIDIN BIOTIN BINDING CAPACITY ON PURIFIED PROTEINS SAMPLES

The determination of biotin binding capacity in the purified protein samples was performed using a B4F assay described elsewhere.^[B6] The fluorescence assay was performed in a black 96-well plate. Each Sav isoform was dissolved in BSA / phosphate buffer (0.1 mg / ml BSA, 0.1 M phosphate, pH 7). Sav in BSA buffer (100 μ l) were mixed with increasing amounts of B6

B4F volumes. The volume was adjusted to 130 μl using BSA in phosphate buffer, the plates was shaken (2 min) and the fluorescence was measured ($\lambda_{\text{excit}} = 485 \text{ nm}$ and $\lambda_{\text{emis}} = 520 \text{ nm}$). The measured fluorescence was plotted as a function of B4F equivalents added and the concentration of biotin binding sites was calculated from the concentration at the equivalence point.

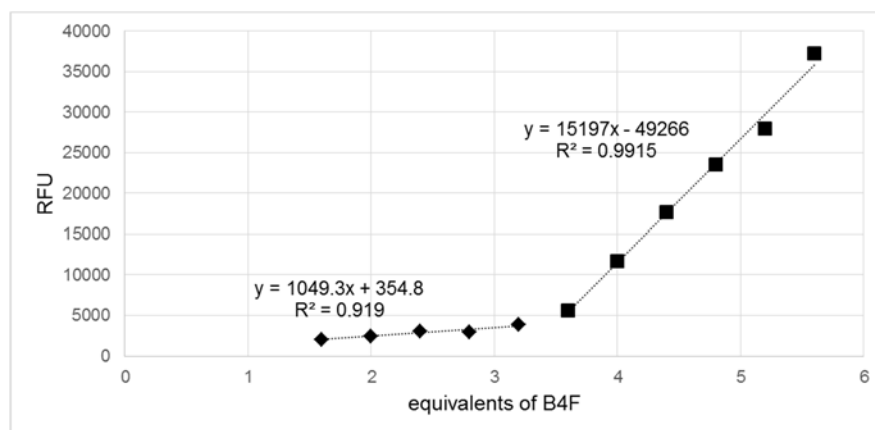
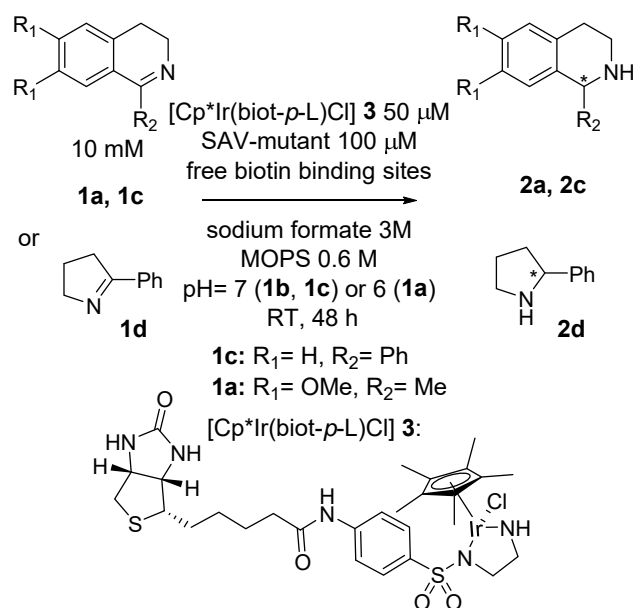


Figure B3 B4F analysis of the Sav mutant K121A-S112T-N118K-S122K. After occupation of all biotin binding sites by B4F, a strong increase in fluorescence occurs proportional to the free B4F. In this example, the biotin-binding capacity is 3.4 ± 0.09 per tetramer.

For determination of Sav Free Binding Sites in CFE, see reference.^[B1]

B.3.8 TYPICAL CATALYSIS PROCEDURE IN BUFFER

Lyophilized Sav isoforms were dissolved in MOPS / formate buffer (final conc. 200 μM of free biotin binding sites). This solution (100 μl) was transferred to a HPLC vial equipped with a magnetic stirrer followed by the addition of Milli-Q water and the Cp*Ir-complex stock solution (5 μl). After 5 min., the reaction was initiated by the addition of the substrate stock solution. The HPLC vials were sealed and the reaction mixtures were stirred for 48 h at RT. Final V = 200 μl ; [Sav free binding sites] = 100 μM ; [Cp*Ir complex] = 50 μM ; [MOPS] = 0.6 M; [formate] = 3 M; [S] = 10 mM.



Scheme B1 - ATHase of cyclic imines using purified Sav mutants.

B.3.9 TYPICAL CATALYSIS PROCEDURE IN CELL FREE EXTRACTS

To HPLC vials equipped with a stirring bar, the reaction buffer (100 μl) was added, followed by the Sav- containing cell free extracts volume corresponding to a conc. of 100 μM free binding sites) and Milli-Q water. The resulting mixture was preincubated with the DiAm stock solution (5 μl , final conc. 5 mM) for 2 h and the reaction was initiated by the addition of a substrate stock solution (5 μl). The resulting reaction mixtures were stirred for 48 hours at RT. Final V = 200 μl ; [Sav free binding sites] = 100 μM ; [Cp*Ir complex] = 50 μM ; [MOPS] = 0.6 M; [formate] = 3 M; [DiAm] = 5 mM; [S] = 10 mM. The results are summarized in Figure B4.

B.3.10 TYPICAL CATALYSIS PROCEDURE IN A BIPHASIC SYSTEM

Lyophilized Sav isoforms were dissolved in MOPS / formate buffer (final conc. 200 μM of free biotin binding sites). This solution (450 μl) was transferred to a HPLC vial followed by the addition the Cp*Ir-complex stock solution in DMSO (45 μl , final conc. 100 μM). After 5 min., the reaction was initiated by the addition of the substrate stock solution in EtOAc (500 μl , 100 mM). The HPLC vials were sealed and the reaction mixtures were vigorously shaken for the corresponding reaction time (2'000 rpm, 25°C). The procedure was adapted from reference.^[B7] Final V = 1000 μl ; [Sav free binding sites] = 200 μM ; [Cp*Ir complex] = 100 μM ; [MOPS] = 0.6 M; [formate] = 3 M; [S] = 100 mM.

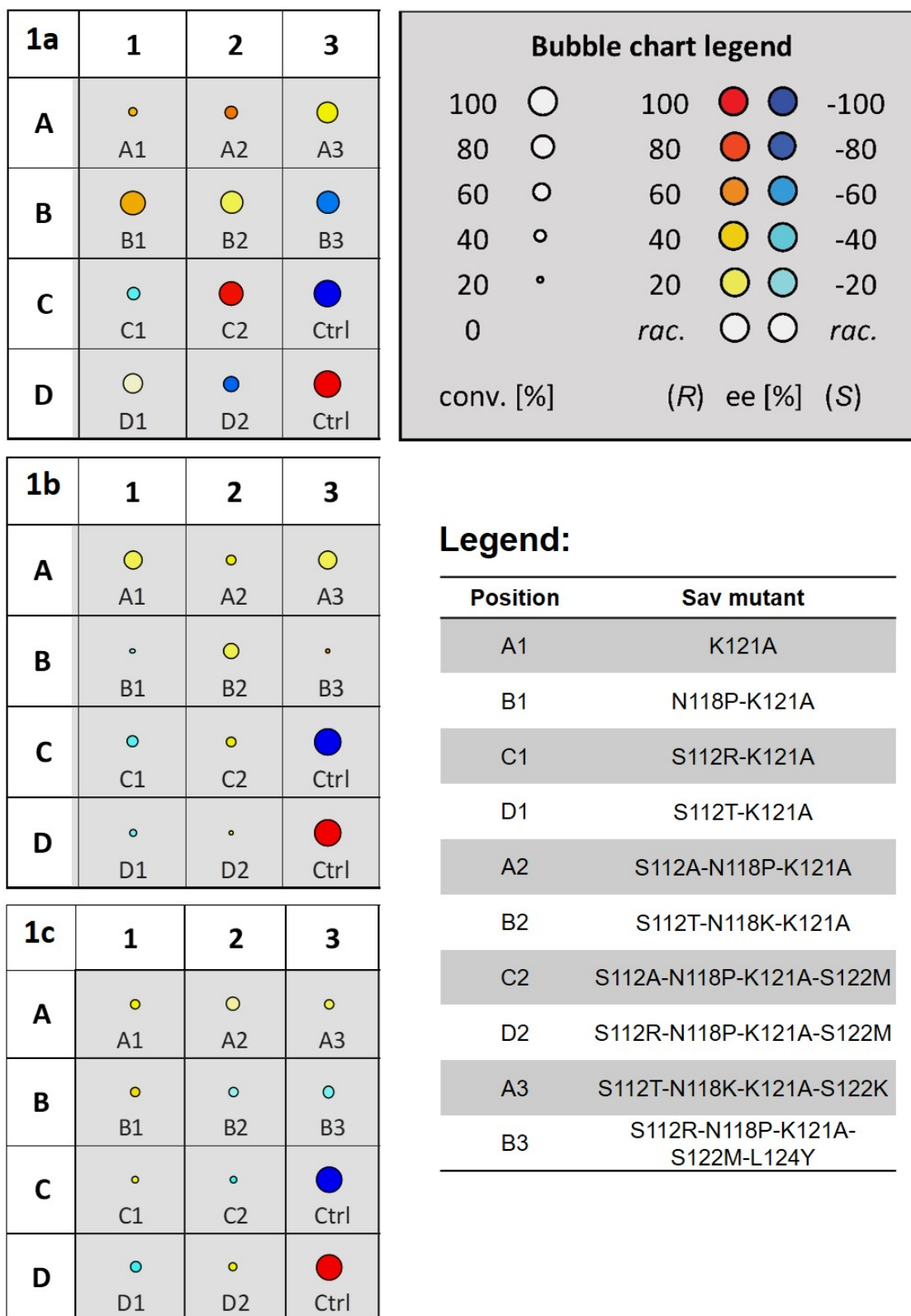


Figure B4 –Artificial Imine Reductase activity displayed as bubble chart representation for the conversion (size of the bubble) and the enantioselectivity (color of the bubble) substrate 1a, 1c or 1d. The mutant Sav variants were used in the form of cfe in the presence of DiAm as a GSH neutralizing agent

B.3.11 WORK UP AND ANALYSIS

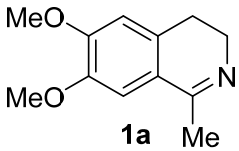
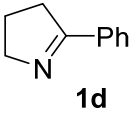
Each reaction was diluted with Milli-Q water (400 μ l) and basified using NaOH solution (20 %, 50 μ l). The resulting mixture was extracted with dichloromethane (2 x, 1 ml), the combined organic fractions were collected in a PP tube containing anhydrous sodium sulfate, and centrifuged (18800 x g, 5 min). The supernatant was analyzed by HPLC or GC.

Catalysis results for substrate **1a** were analyzed using a Chiralpak IC column (5 μ m, 4.6 mm \cdot 25 mm) and dichloromethane containing diethylamine (0.06 %) and isopropanol (0.5 %) as an eluent (1 ml / min flow; λ =280 nm, 25 $^{\circ}$ C). T_R 8.5 min ((*S*)- 6,7-dimethoxy-1-methyl-1,2,3,4-tetrahydroisoquinoline), 9.8 min (6,7-dimethoxy-1-methyl-3,4-dihydroisoquinoline), 14.6 min ((*R*)- 6,7-dimethoxy-1-methyl-1,2,3,4-tetrahydroisoquinoline). Yields were calculated using a response factor of 1.95, as determined elsewhere.^[B7]

Screening with substrate **1c** was analyzed using a Chiralpak IC column (5 μ m, 4.6 mm \cdot 25 mm) and dichloromethane containing diethylamine (0.06 %) and isopropanol (3 %) as an eluent (1 ml / min flow; λ =265 nm, 25 $^{\circ}$ C). T_R 7.6 min ((*S*)-1-phenyl-1,2,3,4-tetrahydroisoquinoline, 10.5 min ((*R*)-1-phenyl-1,2,3,4-tetrahydroisoquinoline), and 16 min (1-phenyl-3,4-dihydroisoquinoline). Yields were calculated using a response factor of 13.613 as determined elsewhere.^[B1]

Screening with substrate **1d** was analyzed by GC. Conversion was determined using an Agilent CAM column (30 m x 0.25 μ m) and He as carrier gas (1.7 ml / min) at 240 $^{\circ}$ C (injector temp. 250 $^{\circ}$ C, split 30). T_R 8.82 min (5-phenyl-3,4-dihydro-2H-pyrrole), 6.14 (2-phenylpyrrolidine). For the determination of enantioselectivity, the samples were derivatized by the addition of trifluoroacetic anhydride (TFAA, 200 μ l) followed by evaporation using a gentle stream of N₂. The measurement was performed using a chiral stationary phase column CP-Chirasil-DEX CB (25m x 0.25 μ m) and He as carrier gas (1.7 ml / min) at 140 $^{\circ}$ C (injector temp. 250 $^{\circ}$ C, split 50). 9.76 min ((*S*)-2-phenylpyrrolidine), 10.29 ((*R*)-phenylpyrrolidine); assignment of the absolute configuration was based on ref.^[B9]

Table B3- Selected results obtained from the reduction of cyclic imines **1a** or **1d** using purified proteins. The reactions were performed with 10 mM substrate concentration at RT for 48 h.

Nr.	Substrate	Sav source	ee ^[a,b] (%)	Conv. (%) ^[a]
1		[Cp*Ir(biot- <i>p</i> -L)Cl 3	0	11
2		K121A	30	72
3		N118P-K121A	-16	81
4	 1a	S112R-K121A	-34	38
5		S112T-K121A	-13	58
6		S112A-N118P-K121A	22	68
7		S112T-N118K-K121A	-36	85
8		S112T-N118K-K121A-S122K	-50	75
9		S112A-N118P-K121A-S122M	5	56
10		S112R-N118P-K121A-S122M	29	77
11	S112R-N118P-K121A-S122M-L124Y	4	91	
12		[Cp*Ir(biot- <i>p</i> -L)Cl 3	0	1
13		K121A	32	68
14		N118P-K121A	-17	79
15		S112R-K121A	-40	14
16	 1d	S112T-K121A	28	30
17		S112A-N118P-K121A	33	85
18		S112T-N118K-K121A	30	92
19		S112T-N118K-K121A-S122K	36	35
20		S112A-N118P-K121A-S122M	20	25
21		S112R-N118P-K121A-S122M	-46	48
22		S112R-N118P-K121A-S122M-L124Y	-55	86

Reactions were performed with purified proteins in 200 μ l of reaction mixture with 10 mM substrate concentration for 48 hours on substrate **1a** or **1d**. ^[a] Enantiomeric excess and conversion were determined by means of HPLC or GC analysis. ^[b] Positive ee values correspond to (*R*)-product and negative ee values correspond to (*S*)-product.

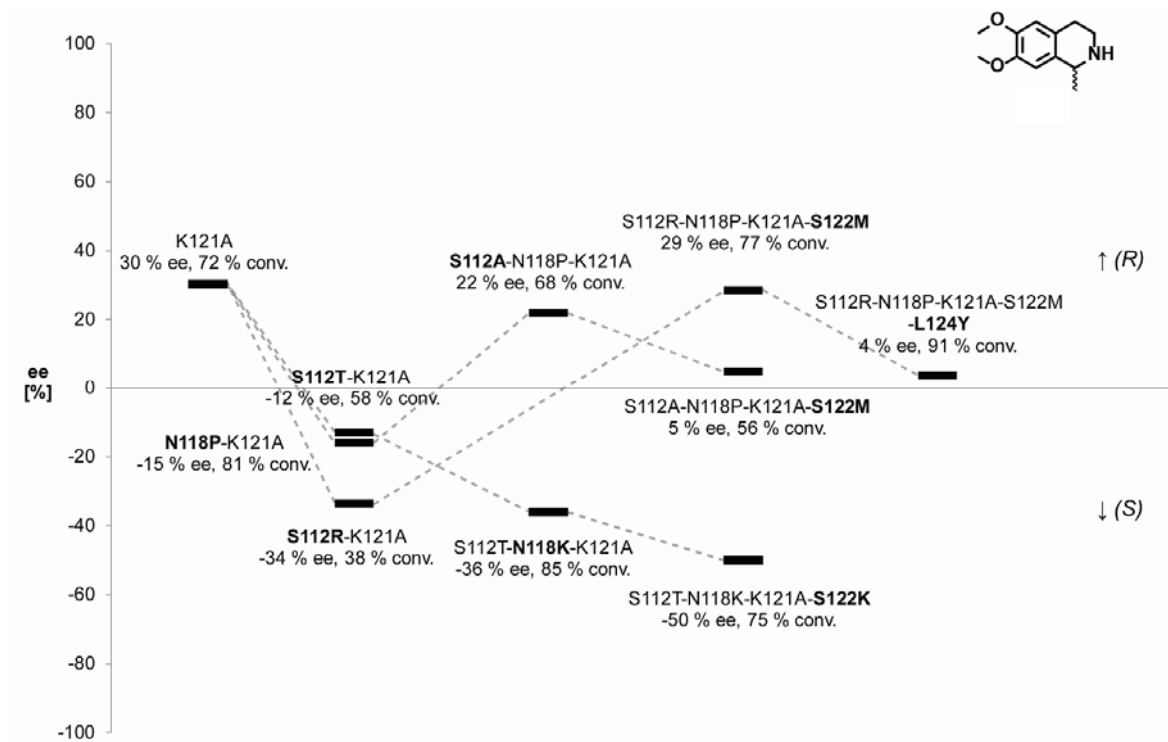


Figure B5 – Evolution tree of ATHase using substrate 1a.

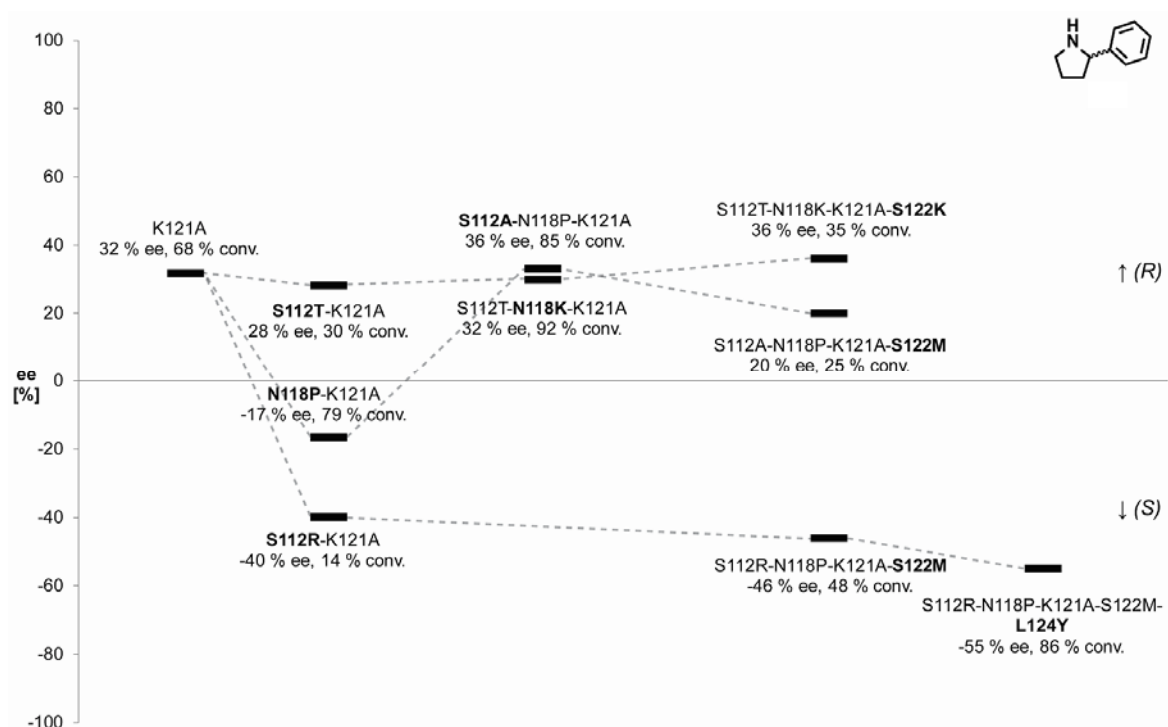


Figure B6 – Evolution tree of ATHase using substrate 1d.

B.3.12 KINETIC MEASUREMENTS

In order to determine the saturation kinetics profiles, catalytic reactions were carried out with constant concentrations streptavidin (100 μM), the iridium cofactor (50 μM), MOPS (0.6M) and sodium formate (3 M). Each Sav mutant was dissolved in Milli-Q water to a concentration of 400 mM. Next, 75 μl of this solution was added to 150 μl of the 2x concentrated MOPS and formate buffer (1.2 M MOPS, 6 M sodium formate, pH 7). 10 μl of the Cp*Ir stock solution (2 mM in DMSO) was added and the resulting solution was incubated at 25°C for 15 minutes. Corresponding amounts of Milli-Q water were added before the addition of the substrate stock solution (2.307 M, **1a** or **1c**). The final concentration of the substrate was varied (5 – 50 mM for **1c**, 500 – 25 mM for **1a**). After 10, 15, 20, 30 and 45 minutes, aliquots (50 μl) were collected and added to a freshly prepared GSH solution (40 μl , 0.25 M) to quench the catalysis. Milli-Q water (300 μl) was added to aliquots, and 200 μl of the resulting solution was further diluted in Milli-Q water (500 200 μl) to prepare the HPLC sample.

Experiments using **1c** were analyzed by normal phase HPLC using a Chiralpak IC column (5 μm , 4.6 mm \cdot 25 mm) and hexane containing diethylamine (0.06 %) and isopropanol (3 %) as an eluent (1 ml / min flow; λ = 265 nm, 25 °C). T_R 7.6 min ((*S*)-1-phenyl-1,2,3,4-tetrahydroisoquinoline, 10.5 min ((*R*)-1-phenyl-1,2,3,4-tetrahydroisoquinoline), and 16 min (1-phenyl-3,4-dihydroisoquinoline). Yields were calculated using a response factor of 13.613 at 265 nm, as determined elsewhere.^[B1] The data are collected in Table B4.

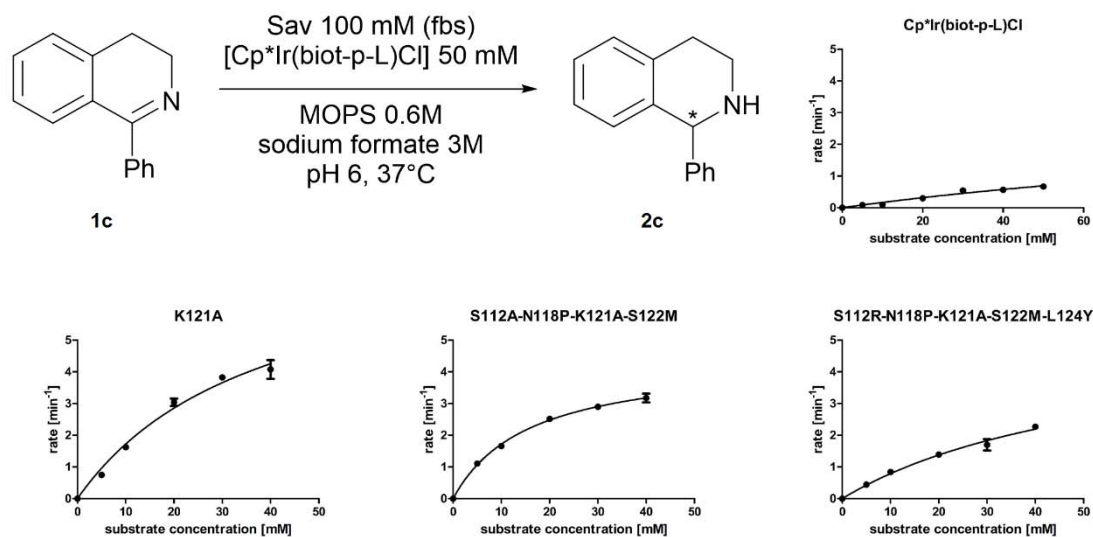
Experiments using **1a** were analyzed by reverse phase HPLC using an Eclipse XDB-C18 column (5 μm , 4.6 x 150 mm) and H₂O/MeOH/TFA 85:14.9:0.1 as an eluent (25°C, 1 ml \cdot min⁻¹, 280 nm). The retention times were 11.9 min for 6,7-dimethoxy-1-methyl-1,2,3,4-tetrahydroisoquinoline **2a** and 16.3 min for 1-methyl-6,7-dimethoxy-3,4-dihydroisoquinoline **1a**. Conversions were determined by integration of the corresponding HPLC signals, using the calibration curve to correct for the difference in extinction coefficient between substrate **1a** and product **2a**. The response factor used for the conversion determination is 1.26 at 280 nm. The data are collected in Table B4.

The resulting conversion values were plotted against the corresponding reaction times. Initial rates for measured substrate concentration were obtained by linear regression of the data (the initial rate is equal to the slope of the regression line). These were divided by the Ir-catalyst concentration and plotted against the initial substrate concentrations. A non-linear regression was applied, using GraphPad Prism 7.03[®] (least square method) with

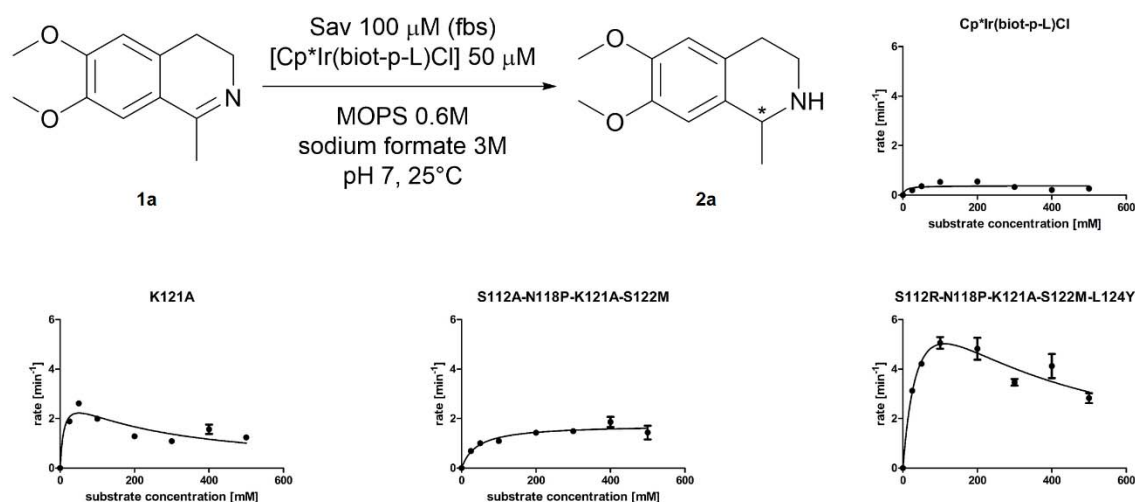
the Michaelis-Menten equation ^[B10] for the reduction of **1c**, or with Haldane equation ^[B11] for substrate inhibition for the reduction of **1a** using Sav WT and mutants K121A and K121A-N118P-S112R-S122M-L124Y.

Table B4- Kinetic parameters of the reduction of imines **1a** or **1c**, using ATHases based on streptavidin isoforms

Nr	Mutation	Sub.	k_{cat} (min^{-1})	\pm	K_M (mM)	\pm	K_i (mM)	\pm	k_{cat}/K_M (min^{-1} mM^{-1})	ee (%)
1	no protein	1c	3.2	2.2	182.5	152.9	-	-	0.02	rac.
2		1a	0.4	0.04	7.4	9	-	-	0.05	rac.
3	K121A	1c	8.3	0.9	38.5	7	234.5	72.4	0.22	30
4		1a	3.1	0.5	11	6.9	-	-	0.28	54
5	S112A-N118P- K121A-S122M	1c	4.4	0.1	15.8	0.9	-	-	0.28	5
6		1a	1.7	0.08	42.2	8.9	-	-	0.04	92
7	S112A-N118P- K121A-	1c	5.4	0.8	58.3	13	249.3	78.8	0.09	4
8	S122M-L124Y	1a	9.5	1.7	50.5	17	-	-	0.19	-78



Scheme B2 – Saturation kinetic experiments of the ATHase isoforms with substrate **1c**.



Scheme B3 - Saturation kinetic experiments of the ATHase isoforms with substrate **1b**.

B.3.13 PREPARATIVE SCALE CATALYSIS

The lyophilized Sav isoform was dissolved in a 100 ml round bottom flask in MOPS / formate buffer (30 ml, final conc. 200 μM of free biotin binding sites) and thoroughly degassed. The resulting mixture was preincubated with the Cp*Ir-complex stock solution in freshly degassed DMSO (1.5 ml, final concentration 100 μM) for 15 minutes followed by the addition of degassed Milli-Q water (27 ml). The reaction was initiated by the addition of the substrate stock solution in freshly degassed DMSO (1.5 ml). The reaction mixtures were stirred for 48 h at 37°C. Final V = 60 ml; [Sav free binding sites] = 100 μM ; [Cp*Ir complex] = 50 μM ; [MOPS] = 0.6 M; [formate] = 3 M; [S] = 10 mM (corresponds to 124 mg of substrate). The reaction mixture was basified using NaOH solution (20 %, 15 ml). The resulting mixture was extracted with dichloromethane (3 x, 100 ml), the combined organic fractions were dried over anhydrous sodium sulfate, filtered and analysed by HPLC for ee determination using the above mentioned conditions.

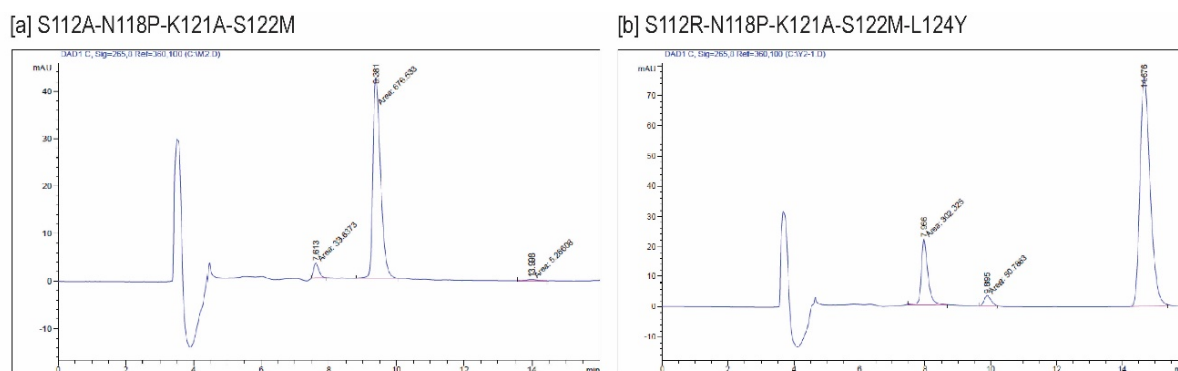


Figure B7 - HPLC chromatograms of **2c** produced in preparative scale experiments (>120 mg of substrate) using [a] [Cp*Ir(biot-*p*-L)Cl] · S112A-N118P-K121A-S122M or [b] [Cp*Ir(biot-*p*-L)Cl] · S112R-N118P-K121A-S122M-L124Y.

After concentrating the sample under reduced pressure, the crude reaction mixture was purified by flash column chromatography with hexane / EtOAc to give 86.9 mg of **2c** in 70 % yield (S112A-N118P-K121A-S122M) and 68 mg in 55 % yield (S112R-N118P-K121A-S122M-L124Y).

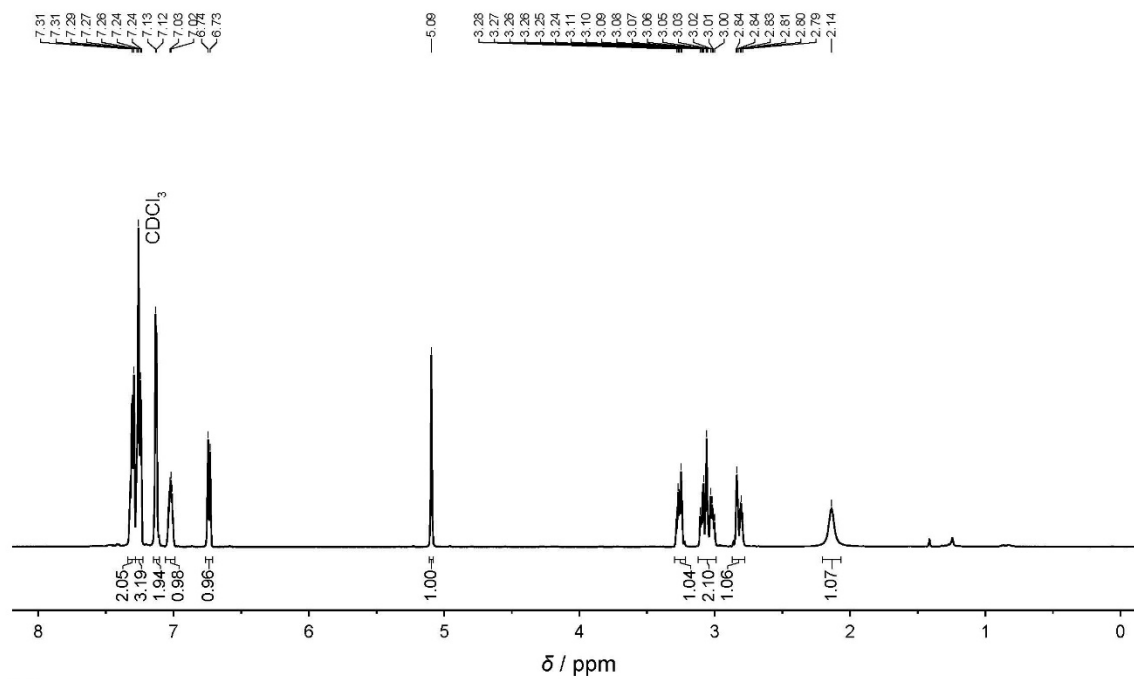
^1H NMR (500 MHz, CDCl_3) δ 7.31 (dd, $J = 8.4, 6.3$ Hz, 2H), 7.28 – 7.21 (m, 3H), 7.13 (d, $J = 4.2$ Hz, 2H), 7.02 (dt, $J = 8.2, 4.4$ Hz, 1H), 6.74 (d, $J = 7.8$ Hz, 1H), 5.09 (s, 1H), 3.31 – 3.20 (m, 1H), 3.12 – 2.98 (m, 2H), 2.82 (dt, $J = 16.0, 3.9$ Hz, 1H), 2.14 (br s, 1H).

^{13}C NMR (126 MHz, CDCl_3) δ 144.88, 138.30, 135.54, 129.1, 129.2, 128.56, 128.24, 127.54, 126.41, 125.78, 62.20, 42.37, 29.87.

[a]

^1H NMR / 500 MHz / CDCl_3

gr_wardR-.204.1.fid — S112M



[b]

^{13}C NMR / 125 MHz / CDCl_3

gr_wardR-.204.2.fid — S122M13C

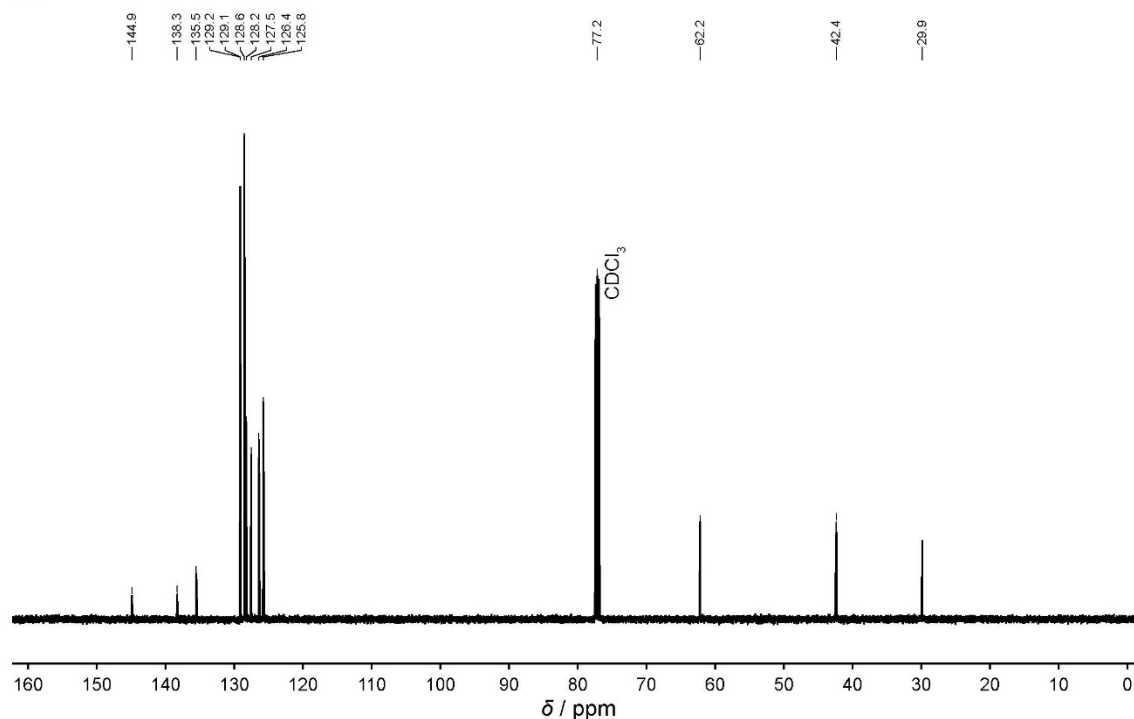


Figure B8 - a) ^1H -NMR and b) ^{13}C -NMR spectra of **2c** obtained in the preparative scale reaction.

B.4. X-RAY ANALYSIS

B.4.1 CRYSTALLIZATION OF APO-SAV MUTANTS S112A-N118P-K121A-S122M AND S112R-N118P-K121A-L124Y

Apo-Sav protein crystals were obtained at 20°C within two days using the hanging-drop vapor diffusion technique mixing 1.5 µl crystallization buffer (2.0 M ammonium sulfate, 0.1 M sodium acetate, pH 4.0) and 3.5 µL protein solution (26 mg/ml lyophilized protein in water). The droplet was equilibrated against a reservoir solution of 100 µl crystallization buffer.

B.4.2 SOAKING APO-SAV CRYSTALS WITH COMPLEX [(Cp*)Ir(BIOT-*p*-L)Cl]:

Single crystals of Sav were soaked for 1 day at 20 °C in a soaking buffer, which was prepared by mixing 0.5 µl of a 10 mM stock solution of complex [(Cp*)Ir(biot-*p*-L)Cl] (50 % DMSO), 4.5 µl crystallization buffer (2.6 M ammonium sulfate, 0.1 M sodium acetate, pH 4.0), and 0.25 µl of the original protein solution. After soaking overnight, crystals were transferred for 10 seconds into a cryo-protectant solution (30 % (v/v) glycerol in crystallization buffer). Next, crystals were shock-frozen in liquid nitrogen.

B.4.3 DATA PROCESSING:

X-ray diffraction data were collected at the Swiss Light Source (SLS) at a wavelength of 1 Å and processed with software XDS^[B12] and scaled with AIMLESS (CCP4 Suite).^[B13] The structure was solved by molecular replacement using program PHASER (CCP4 Suite)^[B13] and the structure 2QCB from the PDB as input model with ligand and water molecules removed. For structure refinement REFMAC5 (CCP4 Suite)^[B14] and PHENIX.REFINE^[B15] were used. 3D coordinates of ligand 4IR were imported from structure PDB 3PK2 to model the iridium cofactor. For water picking, electron density, and structure visualization, the software COOT^[B16] was used. Figures were generated with PyMOL (the PyMOL Molecular Graphics System, Version 1.5.0.5, Schrödinger, LLC). Crystallographic details, processing and refinement statistics are collected in Supplementary Table S5.

B.4.4 STRUCTURE REFINEMENT:

Overall Structures:

Apo-crystals of Sav mutants soaked with [(Cp*)Ir(biot-*p*-L)Cl] constituted space group I4₁22 with unit cell parameters reported in Table S5. A single Sav monomer was obtained per asymmetric unit after molecular replacement. Protein residues 2-11 and 135-159 (141-159 in case of Sav mutant S112R-N118P-K121A-S122M-L124Y) of the N- and C-terminus,

respectively, were not resolved in the electron density, presumably due to disorder. Starting from the Sav monomer, the biological homotetramer is generated by application of crystallographic C2-symmetry axes along the x-, y- and z-axes of the unit cell. The overall protein structures are virtually identical to structure biotin·WT Sav (PDB 1STP, Table S5).

Structure Refinement of complex [(Cp*)Ir(biot-*p*-L)]⁺ · Sav S112A-N118P-K121A-S122M

Residual electron density in the Fo-Fc map was observed in the biotin binding pocket and in the biotin vestibule. Anomalous dispersion density was observed in the biotin vestibule. Modeling of cofactor [(Cp*)Ir(biot-*p*-L)Cl] into the electron density projected the iridium in the position of the anomalous density peak (Figure 12a). For details of the final active site model of this crystal structure, please refer to the main text. Additional anomalous density was found in close proximity to H87 and H127 (Table B5). This suggests either partial dissociation of iridium from [(Cp*)Ir(Biot-*p*-L)Cl] or partial cofactor binding to these Lewis-basic residues.

Structure Refinement of complex [(biot-*p*-L)] · Sav S112R-N118P-K121A-S122M-L124Y

Residual electron density in the Fo-Fc map was observed in the biotin binding pocket and in the biotin vestibule. No anomalous dispersion density was observed in the biotin vestibule. Cofactor [(Cp*)Ir(biot-*p*-L)Cl] was modeled lacking the {Cp*IrCl}⁺ moiety (Figure 12b). For details of the final active site model of this crystal structure, refer to the main text. Anomalous density however was found in close proximity to H87, H127 and M122 (Table B5). This suggests either partial dissociation of iridium from [(Cp*)Ir(biot-*p*-L)Cl] or partial cofactor binding to these Lewis basic residues.

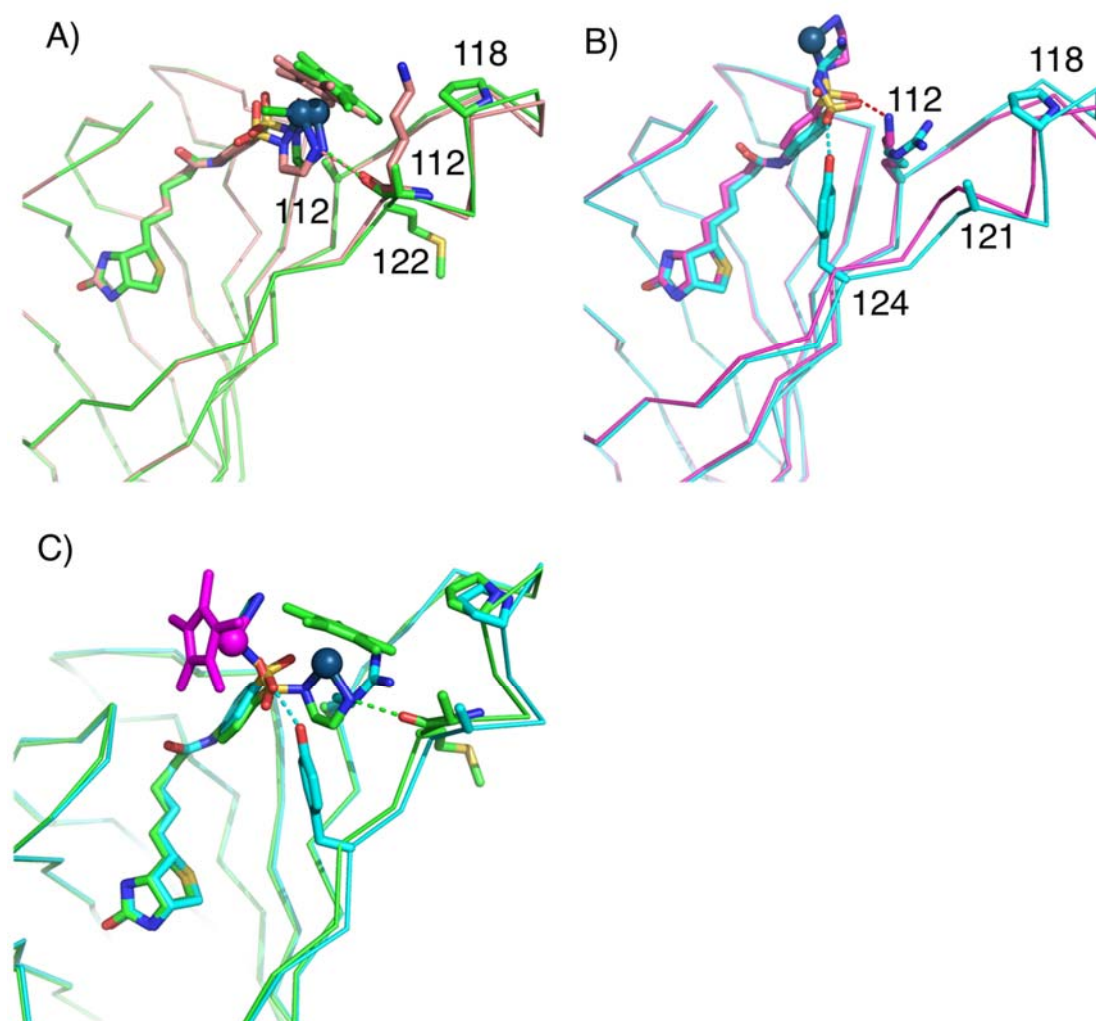


Figure B9- Superposition of crystal structures of ATHase isoforms. A) Complexes $[(\text{Cp}^*)\text{Ir}(\text{biot-}p\text{-L})]^+ \cdot \text{Sav S112A-N118P-K121A-S122M}$ (green, PDB 6ESS) and $[(\text{Cp}^*)\text{Ir}(\text{biot-}p\text{-L})\text{Cl}] \cdot \text{Sav S112A}$ (salmon, PDB 3PK2); B) Complexes $[(\text{biot-}p\text{-L})] \cdot \text{Sav S112R-N118P-K121A-S122M-L124Y}$ (cyan, PDB 6ESU) and $[\text{Ir}(\text{biot-}p\text{-L})]^{2+} \cdot \text{Sav S112K}$ (magenta, PDB 4OKA); C) Complexes $[(\text{Cp}^*)\text{Ir}(\text{biot-}p\text{-L})]^+ \cdot \text{Sav S112A-N118P-K121A-S122M}$ (green, PDB 6ESS) and $[(\text{biot-}p\text{-L})] \cdot \text{S112R-N118P-K121A-S122M-L124Y}$ (cyan, PDB 6ESU). H-bonds between protein and cofactor are highlighted with dashed lines.

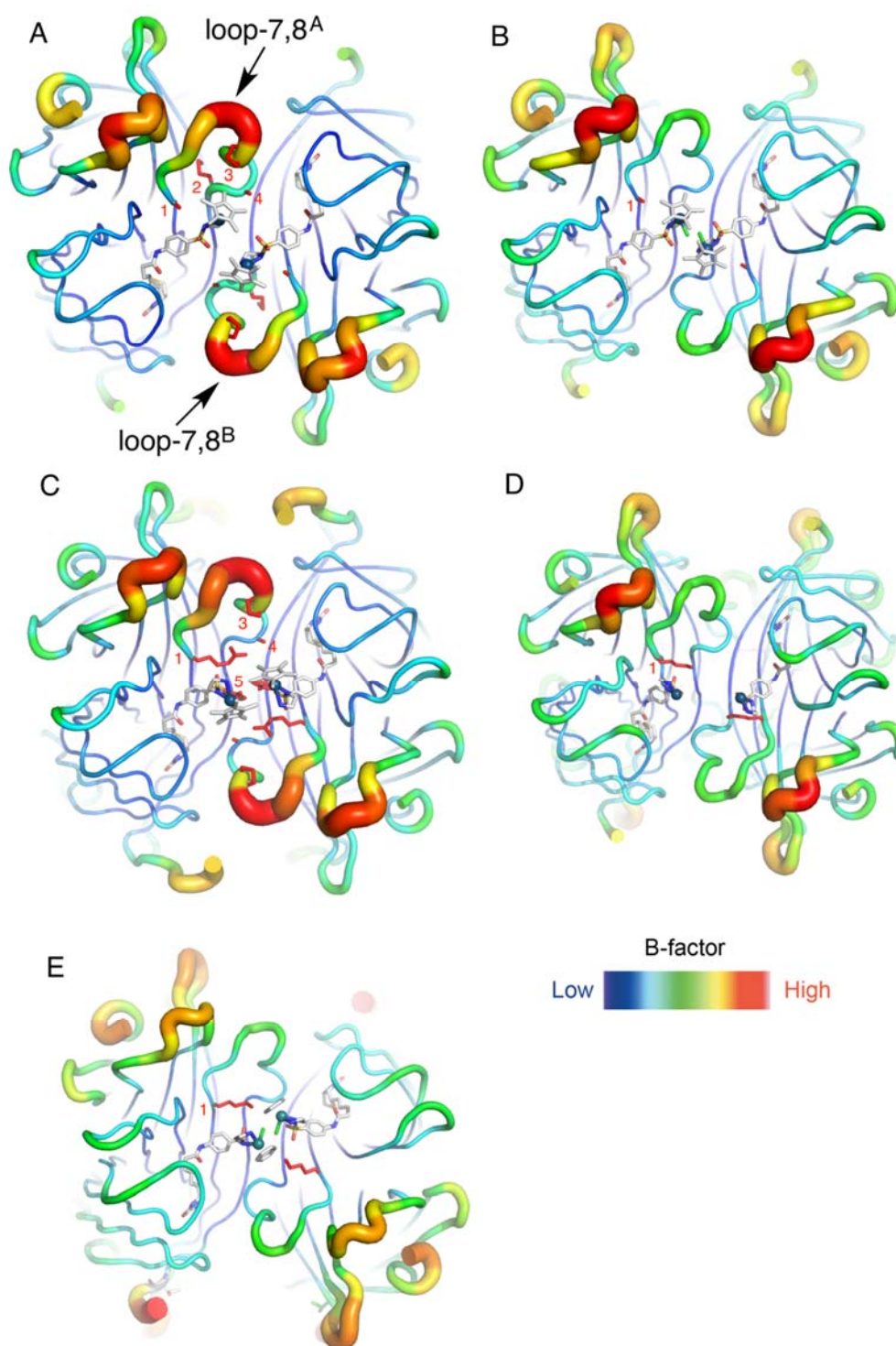


Figure B10- B-factor trace of crystal structures of ATHase isoforms: A) $[(\text{Cp}^*)\text{Ir}(\text{biot-}p\text{-L})]^+$ · Sav S112A-N118P-K121A-S122M (PDB 6ESS); B) $[(\text{Cp}^*)\text{Ir}(\text{biot-}p\text{-L})\text{Cl}]$ · Sav S112A (PDB 3PK2); C) $[(\text{biot-}p\text{-L})]$ · Sav S112R-N118P-K121A-S122M-L124Y (PDB 6ESU); D) $[\text{Ir}(\text{biot-}p\text{-L})]^{2+}$ · Sav S112K (PDB 4OKA); E) $[(\text{benzene})\text{Ru}(\text{biot-}p\text{-L})\text{Cl}]$ · Sav S112K (PDB 2QCB). Mutations are highlighted as red sticks model: 1 = 112, 2 = 122, 3 = 118, 4 = 121, 5 = 124. Cofactors are displayed in grey as a stick model.

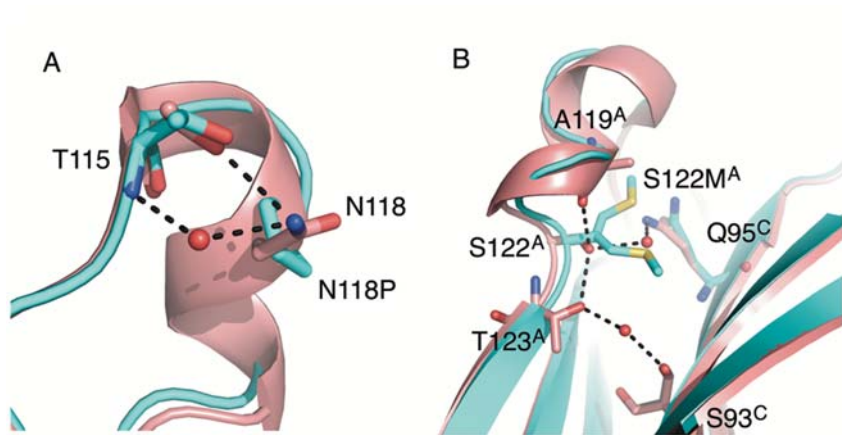


Figure B11. Deletion of H-bonds within loop 7,8 positions 118 (A) and 122 (B). Crystal structures 3PK2 (salmon) and 6ESU (cyan) are superimposed. H-bonds are displayed as black dashed lines, water molecules as red spheres. Sav monomers are labelled as superscripts.

Table B5. Crystal structure refinement statistics.

Sav Mutant	S112A-N118P-K121A-S122M	S112R-N118P-K121A-S122M-L124Y
PDB code	6ESS	6ESU
Data Processing		
Unit Cell	a, b, c = 58.1 Å, 58.1 Å, 185.1 Å; $\alpha, \beta, \gamma = 90^\circ$	a, b, c = 57.8 Å, 57.8 Å, 178.3 Å; $\alpha, \beta, \gamma = 90^\circ$
Space group	I4 ₁ 22	I4 ₁ 22
Resolution (Å)	46.3 – 1.91	55.0-1.78
Highest resolution shell (Å)	1.96 - 1.91	1.81-1.78
R _{merge} (%)	19.1 (109.8)	8.2 (244.2)
No. of unique reflections	12759 (816)	15084 (824)
Multiplicity	11.2 (7.1)	25.4 (25.1)
I/sig(I)	99.6 (97.6)	99.9 (98.0)
CC1/2	10.2 (1.5)	18.7 (1.6)
Structure Refinement		
R _{work}	0.276	0.1944
R _{free}	0.3270	0.2113
Rmsd bond length (Å)	0.019	0.022
Rmsd bond angle (°)	2.628	2.073
No ligands		
Cofactor	1	1
Water	19	29
Sulfate	-	1
Acetate	-	1
B-factor (Å ²)		
Overall protein	33	52
Ir complex	56	47
{Cp*Ir} ⁺	104	-
H ₂ O	31	52
Anomalous dispersion density peaks (σ)		
Ir complex	7	-
Ir1 (His87)	7	11
Ir2 (H127)	5	18
Ir3 (H127)	4	26
Ir4 (M122)	-	14
Distance Ir---Ir (Å)	6.4	-
Rmsd to Biotin·Sav (PDB 1STP) (Å)	0.693	0.846

B.5 COMPUTATIONAL DETAILS:

B.5.1 MODEL SYSTEMS.

A conformation of the cofactor bound to the S112A Sav from a previous study (unpublished) was used to build models of streptavidin variant S112A-N118P-K121A-S122M. For each point mutation, side chain conformations based on the Drunbak library of rotamers^[B17] implemented in Chimera program^[18] were selected to minimize steric contacts between the cofactor and the protein. For variant S112R-N118P-K121A-S122M-L124Y, the X-ray structure was used to build the model.

B.5.2. FORCE FIELD PARAMETERS FOR THE COFACTOR.

The GAFF parameters were used where available for bonding interactions. Missing bonding and bending parameters for the organometallic moiety were derived from the method proposed by Seminario.^[19] Accordingly, model compounds were optimized at the DFT (BP86) level using the def2-TZVPP basis set and the hessian matrix computed using the ORCA code.^[B20] The Ir-Cp* interaction was treated as follows. All ring C atoms of the cyclopentadienyl were bonded to the Ir. The bending terms involving the Cp* and the other ligands were handled using the geometric center of the Cp* ring, distributing the forces on the ring atoms via the chain rule. These bending terms were computed from a tcl script at each Molecular Dynamics step. All torsional terms involving the metal ion were set to zero. Atomic charges of the biocatalyst peptide chain were computed according to the RESP methodology^[B21] with the *N*-terminal group capped with an acetyl moiety. RESP charges were also derived for the biotin fragment, which, in this case, was capped with an *N*-Methyl residue.

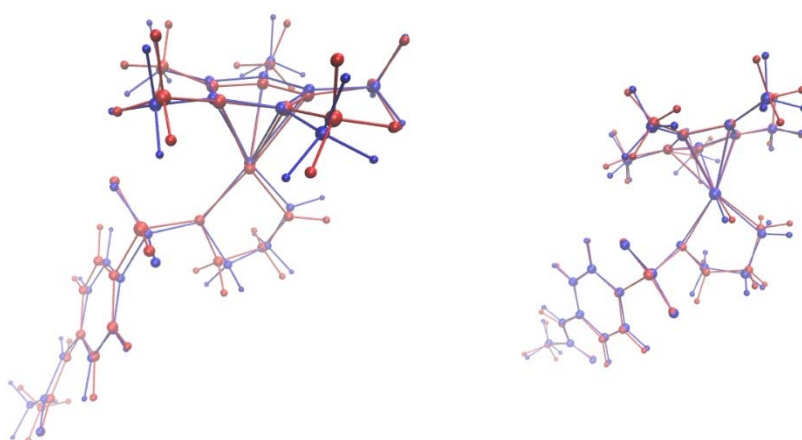


Figure B12. Comparison of the MM(red) and DFT(blue) optimized structures for the intermediate (left) and hydride (right) species. The heavy atoms RMSD is 0.20 Å for the intermediate and 0.12 Å for the hydride.

B.5.3 LIGAND-PROTEIN DOCKING.

Representative structures from selected clusters were used to dock the substrate **1c** in its protonated state. The substrate was first optimized with Gaussian09^[22] at DFT/B3LYP^[B23,B24] level with the 6-31g(d,p) basis set.^[B25,B26] Dockings were performed with the GOLD5.2 program (available through the Cambridge Crystallographic Data Center (CCDC)) and evaluated based on the ChemScore scoring function.^[B27] Aiming to discard the poses in which the asymmetric carbon of the imine would be too far from the metal centre or blocked by the Cp* fragment of the catalyst, the distance between the asymmetric carbon and the iridium were set to a range between 2 Å and 4.5 Å. Rotamers based on the GOLD rotamer library were used for all residues occupying the active pocket aiming to improve the fit of the substrate into the host active site.

MOLECULAR DYNAMICS (MD) SIMULATIONS.

Implicit solvent generalized Born molecular dynamics simulations were performed for the tetramer of streptavidin with the biotinylated Ir complex (the 16 e⁻ complex [Cp*Ir(biot-*p*-L)]⁺). Simulations were performed with the NAMD code,^[B28] which implements the Born model developed by Onufriev *et al.*^[B29] Simulations were performed at 300 K and 0 ionic strength, using a 16 Å cutoff for non-bonded interactions. The surface tension was set to 0.006 kcal/(mol·Å²).

Models initially underwent 1 ns MD simulation followed by 4 ns metadynamics simulations to enhance the exploration of the cofactor conformational space.^[B30] The dihedral angles around the C4 – S1 and S1 – N2 bonds were biased with an history-dependent potential composed of repulsive gaussian functions of 0.1 kcal/mol height and 10 degrees width added every 100 MD steps. Unfortunately, during the metadynamics simulations rotation around the N1 – C1 bond also took place, so that it was not possible to assign unique conformational basins to the metadynamics potential. We have thus used a different strategy. For each variant, 10 conformations, showing maximal cofactor RMSD, were extracted from the metadynamics trajectories and used to initialize ten independent 2 ns long GB MDs. In most of the runs, the cofactor explores more than one conformation. Because of this, the resulting trajectories were merged and used for a clustering analysis based on the cofactor RMSD (heavy, non equivalent atoms) after a best fitting of streptavidin's backbone (subunits 1 and 2). Clusters showing a population > 1% were used to estimate the cofactor binding energy based on the MM/GBSA approach (the entropic term was not included).^[31]

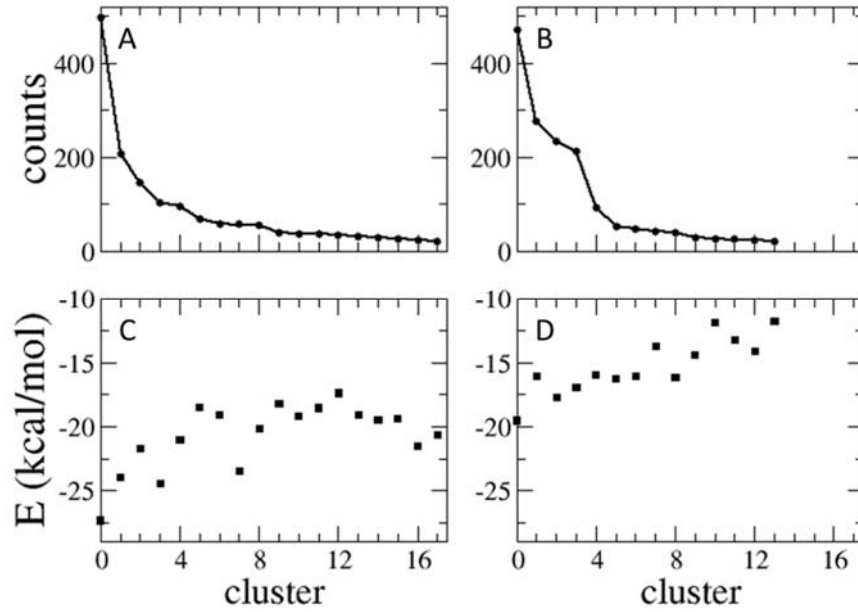


Figure B13. Cluster population (a, b) and [Ir] cofactor (excluding biotin fragment) interaction energies (c, d) for Sav variants S112A-N118P-K121A-S122M (left) and S112R-N118P-K121A-S122M-L124Y (right).

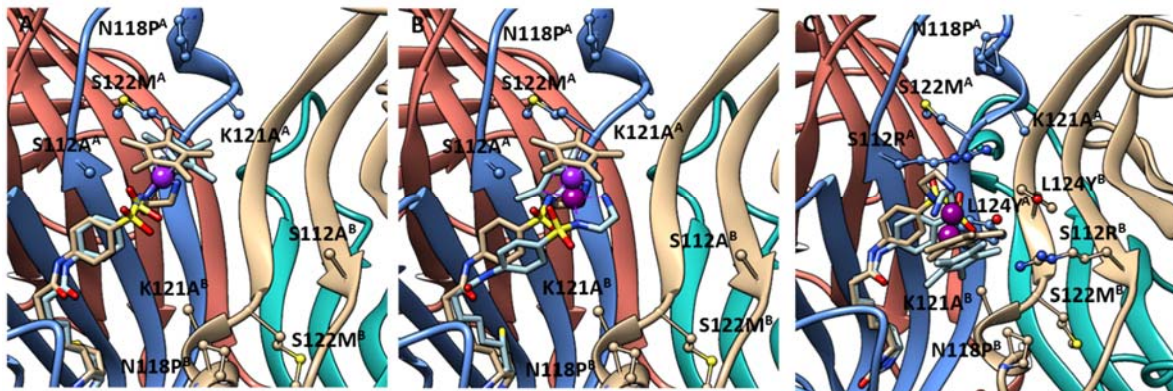


Figure B14. Comparison of the X-ray structure (turquoise and sticks) and the representative structure from the most populated cluster in the MD simulation of Sav variant a) S112A-N118P-K121A-S122M and c) S112R-N118P-K121A-S122M-L124Y, and c) the second most populated cluster for Sav variant S112A-N118P-K121A-S122M

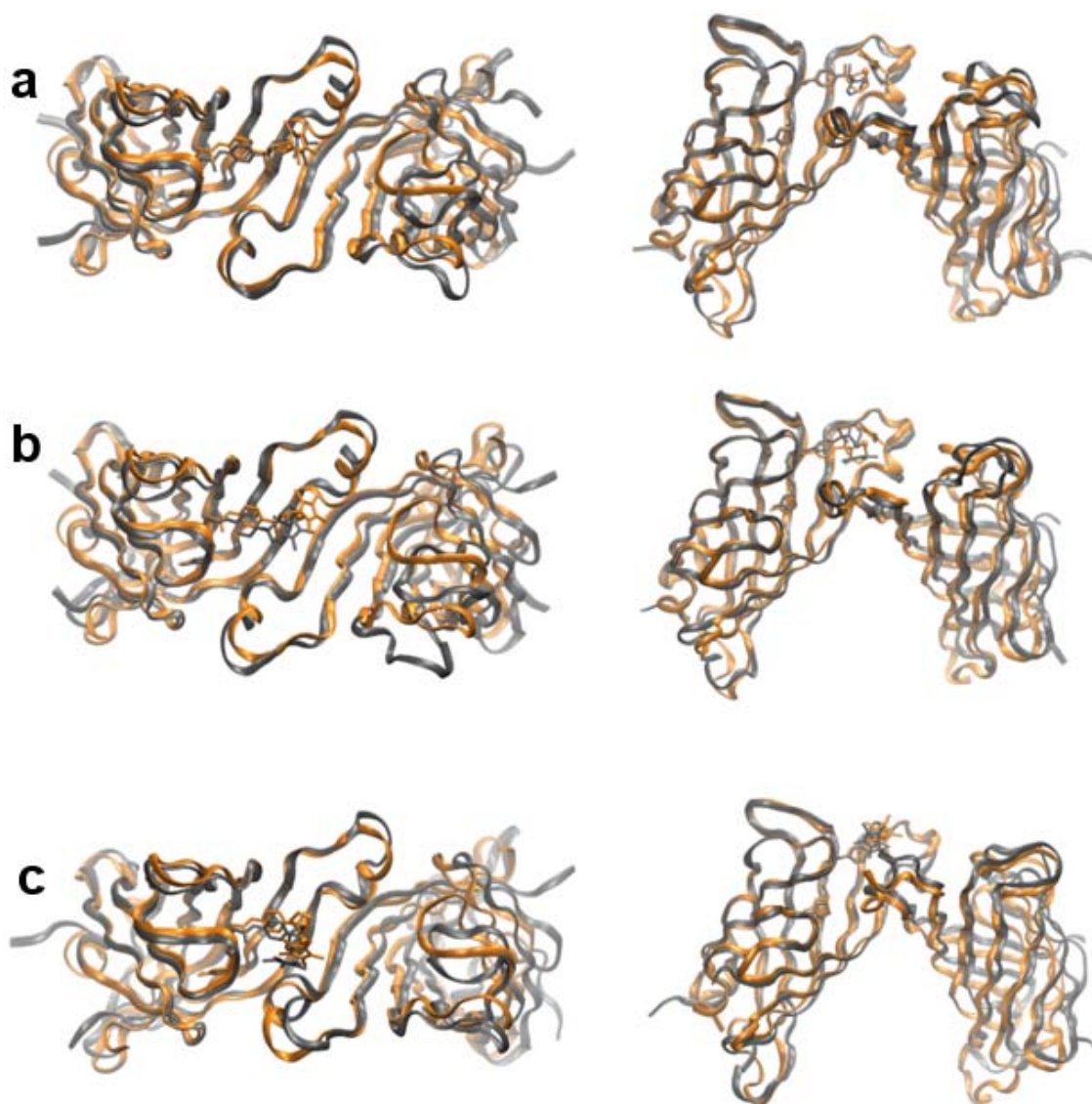


Figure B15. Comparison of the X-ray structure (orange) and the representative structures from the most populated cluster in the MD simulations (grey) of Sav variant S112A-N118P-K121A-S122M (a) and S112R-N118P-K121A-S122M-L124Y (c). In b, the representative structure from the second most populated cluster for Sav variant S112A-N118P-K121A-S122M is shown.

B.6 REFERENCES

- [B1] H. Mallin, M. Hesticová, R. Reuter, T. R. Ward, *Nat. Protoc.*, 2016, **11**, 835–852.
- [B2] C. Letondor, A. Pordea, N. Humbert, A. Ivanova, S. Mazurek, M. Novic, T. R. Ward, *J. Am. Chem. Soc.*, 2006, **128**, 8320–8328.
- [B3] I. Lantos, D. Bhattacharjee, D. S. Eggleston, *J. Org. Chem.* **1986**, *51*, 4147–4150.
- [B4] C. J. Dunsmore, R. Carr, T. Fleming, N. J Turner, *J. Am. Chem. Soc.* **2006**, *128*, 2224–2225.
- [B5] T. Sano, C. R. Cantor, *Proc. Natl. Acad. Sci. USA* **1990**, *87*, 142–146.
- [B6] G. Kada, K. Kaiser, H. Falk, H. J. Gruber, *Biochim. Biophys. Acta* **1999**, *1427*, 44–48.

- [B7] U. E. Rusbandi, Ch. Lo, M. Skander, A. Ivanova, M. Creus, N. Humbert, T. R. Ward *Adv. Synth. Catal.* **2007**, *349*, 1923–1930.
- [B8] M. Dürrenberger, T. Heinisch, Y. M. Wilson, T. Rossel, E. Nogueira, L. Knörr, A. Mutschler, K. Kersten, M. J. Zimbron, J. Pierron, T. Schirmer, T. R. Ward, *Angew. Chem. Int. Ed.*, **2011**, *50*, 3026–3029.
- [B9] a) V. Köhler, Y. M. Wilson, M. Dürrenberger, D. Ghislieri, E. Churakova, T. Quinto, L. Knörr, D. Häussinger, F. Hollmann, N. J. Turner, T. R. Ward, *Nat. Chem.* **2013**, *5*, 93–99.
b) Y. Zhang, D. Kong, R. Wang, G. Hou, *Org. Biomol. Chem.* **2017**, *15*, 3006–3012
- [B10] L. Michaelis, M. L. Menten, *Biochem. Z.* **1913**, *49*, 333–369
- [B11] J. B. S. Haldane, *Enzymes*, **1930**, 84.
- [B12] W. Kabsch, *Acta Crystallogr. Sect. D Biol. Crystallogr.* **2010**, *66*, 133–144.
- [B13] P. R. Evans, *Acta Crystallogr. Sect. D Biol. Crystallogr.* **2011**, *67*, 282–292.
- [B14] G. N. Murshudov, A. A. Vagin, E. J. Dodson, *Acta Crystallogr. Sect. D Biol. Crystallogr.* **1997**, *53*, 240–255.
- [B15] P. D. Adams, P. V. Afonine, G. Bunkóczi, V. B. Chen, I. W. Davis, N. Echols, J. J. Headd, L. W. Hung, G. J. Kapral, R. W. Grosse-Kunstleve, et al., *Acta Crystallogr. Sect. D Biol. Crystallogr.* **2010**, *66*, 213–221.
- [B16] Emsley, P. & Cowtan, K. Coot: model-building tools for molecular graphics. *Acta Crystallogr. D. Biol. Crystallogr.* **60**, 2126–2132 (2004)
- [B17] R. L. Dunbrack, *Curr. Opin. Struct. Biol.* **2002**, *12*, 431–440.
- [B18] E. F. Pettersen, T. D. Goddard, C. C. Huang, G. S. Couch, D. M. Greenblatt, E. C. Meng, T. E. Ferrin, *J. Comput. Chem.* **2004**, *25*, 1605–1612.
- [B19] J. M. Seminario, *Int. J. Quantum Chem.* **1996**, *30*, 1271–1277.
- [B20] F. Neese, *Wiley Interdiscip. Rev. Comput. Mol. Sci.* **2012**, *2*, 73–78.
- [B21] C. I. Bayly, P. Cieplak, W. Cornell, P. A. Kollman, *J. Phys. Chem.* **1993**, *97*, 10269–10280.
- [B22] Gaussian 09, Revision D.01, M. J. Frisch, G. W. Trucks, H. B. Schlegel, G. E. Scuseria, M. A. Robb, J. R. Cheeseman, G. Scalmani, V. Barone, B. Mennucci, G. A. Petersson, H. Nakatsuji, M. Caricato, X. Li, H. P. Hratchian, A. F. Izmaylov, J. Bloino, G. Zheng, J. L. Sonnenberg, M. Hada, M. Ehara, K. Toyota, R. Fukuda, J. Hasegawa, M. Ishida, T. Nakajima, Y. Honda, O. Kitao, H. Nakai, T. Vreven, J. A. Montgomery, Jr., J. E. Peralta, F. Ogliaro, M. Bearpark, J. J. Heyd, E. Brothers, K. N. Kudin, V. N. Staroverov, T. Keith, R. Kobayashi, J. Normand, K. Raghavachari, A. Rendell, J. C. Burant, S. S. Iyengar, J. Tomasi, M. Cossi, N. Rega, J. M. Millam, M. Klene, J. E. Knox, J. B. Cross, V. Bakken, C. Adamo, J. Jaramillo, R. Gomperts, R. E. Stratmann, O. Yazyev, A. J. Austin, R. Cammi, C. Pomelli, J. W. Ochterski, R. L. Martin, K. Morokuma, V. G. Zakrzewski, G. A. Voth, P. Salvador, J. J. Dannenberg, S. Dapprich, A. D. Daniels, O. Farkas, J. B. Foresman, J. V. Ortiz, J. Cioslowski, and D. J. Fox, Gaussian, Inc., Wallingford CT, **2013**.

- [B23] A. D. Becke, *J. Chem. Phys.* **1993**, *98*, 5648–5652.
- [B24] P. J. Stephens, F. J. Devlin, C. F. Chabalowski, M. J. Frisch, *J. Phys. Chem.* **1994**, *98*, 11623–11627.
- [B25] G. A. Petersson, A. Bennett, T. G. Tensfeldt, M. A. Al-Laham, W. A. Shirley, J. Mantzaris, *J. Chem. Phys.* **1988**, *89*, 2193–2218.
- [B26] G. A. Petersson, M. A. Al-Laham, *J. Chem. Phys.* **1991**, *94*, 6081–6090.
- [B27] M. D. Eldridge, C. W. Murray, T. R. Auton, G. V Paolini, R. P. Mee, *J. Comput. Aided. Mol. Des.* **1997**, *11*, 425–445.
- [B28] J. C. Phillips, R. Braun, W. Wang, J. Gumbart, E. Tajkhorshid, E. Villa, C. Chipot, R. D. Skeel, L. Kalé, K. Schulten, *J. Comput. Chem.* **2005**, *26*, 1781–1802.
- [B29] A. Onufriev, D. Bashford, D. A. Case, *Proteins Struct. Funct. Genet.* **2004**, *55*, 383–394.
- [B30] A. Laio, M. Parrinello, *Proc. Natl. Acad. Sci. U. S. A.* **2002**, *99*, 12562–12566.
- [B31] P. A. Kollman, I. Massova, C. Reyes, B. Kuhn, S. Huo, L. Chong, M. Lee, T. Lee, Y. Duan, W. Wang, et al., *Acc. Chem. Res.* **2000**, *33*, 889–897.

APPENDIX C

Supporting information for *Chem. Commun.* **2016**, *52*, 9462–9465

C.1 GENERAL INFORMATION

Tetraethyl orthosilicate (TEOS, $\geq 99\%$), (3-aminopropyl)-triethoxysilane (APTES, $\geq 98\%$), ammonium hydroxide (ACS reagent, 28–30%), ethanol (anhydrous), glutaraldehyde (Grade I, 25% in water), 6,7-dimethoxy-1-methyl-3,4-dihydroisoquinoline, 2-(N-morpholino)ethanesulfonic acid, 3-(N-morpholino)propanesulfonic acid, sodium formate, sodium hydroxide, DCM, isopropanol, diethylamine, DMF, DMSO, *N*-Boc-ethylenediamine, 4-nitrophenylsulfonyl chloride, diethyl ether, *N*-methylmorpholine, 2-chloro-4,6-dimethoxy-1,3,5-triazine, Et₃N, acetonitrile, [Cp*IrCl₂]₂ dimer and NAD⁺ were purchased from commercial suppliers and used without further purification.

Mili-Q water (resistivity $\geq 18\text{ M}\Omega\text{ cm}^{-1}$) was produced with a Millipore Synergy purification system. Streptavidin Sav mutants were produced, purified and characterized as previously described. ^[C1]

¹H and ¹³C spectra were recorded on a Bruker 400 MHz. The chemical shifts (δ) are reported in parts per million (ppm) relative to tetramethylsilane or a residual solvent peak, and the *J* values are given in Hz. Signals are quoted as s (singlet), d (doublet), t (triplet) and m (multiplet). Analyses of the catalytic runs were performed on an Agilent 1100 normal phase HPLC with an analytical Chiralpack IC column (250 · 4.6 mm, 5 μm). ESI-MS measurements were performed on a Bruker AmaZonTM X. The absorbance spectra were measured on a microplate reader Tecan, model Infinite M200.

Nanoparticles were imaged using a Zeiss SUPRA 40VP field emission scanning electron microscope, their size was measured using the acquired micrographs with the Olympus Analysis® software package.

ICP-MS analysis was performed on a 7500cx ICP-MS system (Agilent, Basel, Switzerland). ¹⁹¹Ir was used for quantification, ¹⁹³Ir for verification of the results.

C.2 STOCK SOLUTIONS AND BUFFERS

MOPS/formate buffer: 3-(N-morpholino)propanesulfonic acid and sodium formate were dissolved in Milli-Q water to the concentrations of 6M (formate) and 1.2 M (MOPS). The pH was adjusted to 7 by addition of NaOH.

MES buffer: 2-(N-morpholino)ethanesulfonic acid was dissolved in Mili-Q water to a final concentration of 10 mM. The pH was adjusted to 6.2 by the addition of NaOH.

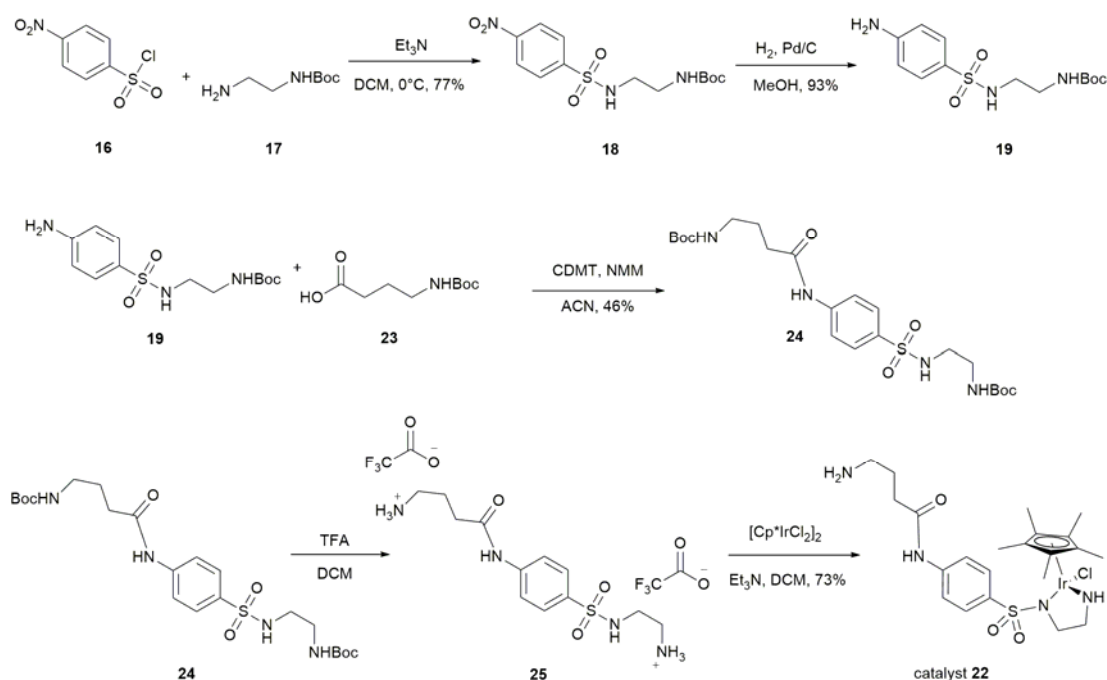
Activity assay buffer: Sodium formate and K_2HPO_4 were dissolved in Mili-Q water to a final concentration of 200 mM (formate) and 50 mM (phosphate). The pH was adjusted to 7.5 by addition of NaOH.

*Cp*Ir-complexes:* $[Cp^*Ir(biot-p-L)Cl]$ was dissolved in DMF to a final concentration of 500 mM. For a detailed synthesis procedure, see reference.^[C2] $[Cp^*Ir(4C-L)Cl]$ was dissolved in DMF to a final concentration of 400 mM.

Substrate: 6,7-dimethoxy-1-methyl-3,4-dihydroisoquinoline **1a** was dissolved in Mili-Q water (2 ml) to a final concentration of 1 M.

C.3 SYNTHESIS OF THE NON-BIOTINYLATED CATALYST **22**

The synthesis was performed as summarized in following Scheme C1.



Scheme C20- Synthesis of catalyst 22

C.3.1 N-Boc-N'-(4-NITROPHENYLSULFONYL)-ETHYLENEDIAMINE **18**

To a solution of *N*-Boc-ethylenediamine **17** (1.74 g, 10.8 mmol, 1.0 eq.) and Et₃N (3 ml, 21.5 mmol, 2.0 eq.) in DCM (300 ml), a solution of 4-nitrophenylsulfonyl chloride **16** (2.51 g, 11.3 mmol, 1.05 eq.) in DCM (100 ml) was added dropwise at 5 °C and stirred overnight. The solution was concentrated to 100 ml, washed with water (3 x 20 ml), and dried over Na₂SO₄. The solvent was evaporated under reduced pressure and the crude product was purified by flash chromatography (silicagel, EtOAc : hexane (2 : 3)) The pure product **18** was obtained as a white powder (2.87 g, 8.32 mmol, 77 % yield).

¹H NMR (200 MHz, CDCl₃-CD₃OD, 22 °C): δ 1.40 (s, 9H; *t*-Bu), 3.03 (m, 2H; CH₂-CH₂-NH-S), 3.12 (m, 2H; CH₂-CH₂-NH-S), 4.47 (br, 2H; NH), 8.04 (d, J = 8.7 Hz, 2H; ArH), 8.37 (d, J = 8.7 Hz, 2H; ArH).

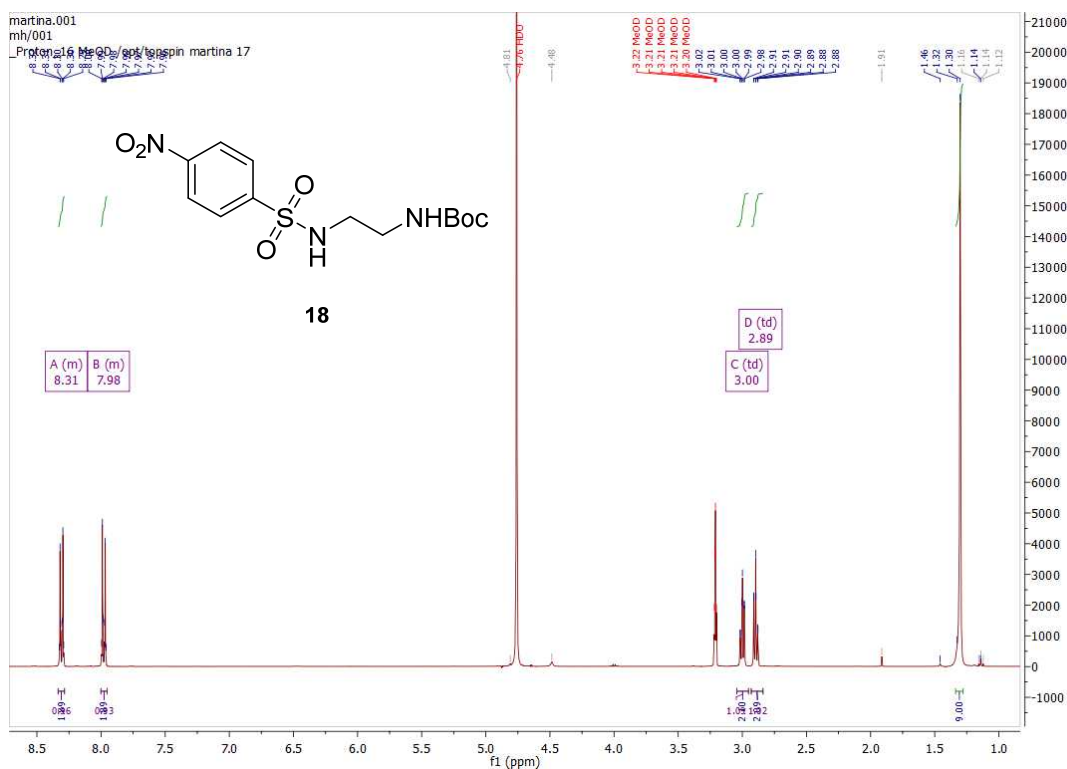


Figure C1- ¹H NMR of **18**

C.3.2 N-Boc-N'-(4-AMINOPHENYLSULFONYL)-ETHYLENEDIAMINE **19**

An autoclave containing a suspension of Pd/C (5 %, 330 mg) in methanol (20 ml) was charged with *N*-Boc-*N'*-(4-nitrophenylsulfonyl)-ethylenediamine **18** (2.10 g, 6.08 mmol). The autoclave was purged three times with nitrogen and filled with hydrogen (3 bars). The reaction was stirred vigorously for 3 hours at RT. The hydrogen pressure was carefully

released and the resulting suspension was removed by filtration through a celite plug. The solvent was evaporated under reduced pressure, which yielded product **19** as a white powder (1.78 g, 5.65 mmol, 93 %).

^1H NMR (400 MHz, $\text{CDCl}_3\text{-CD}_3\text{OD}$, 22 °C): δ 1.40 (s, 9H; *t*-Bu), 2.88 (m, 2H; $\text{CH}_2\text{-CH}_2\text{-NH-S}$), 3.12 (m, 2H; $\text{CH}_2\text{-CH}_2\text{-NH-S}$), 3.57 (br, 3H; NH; NH_2), 4.50 (br, 1H; NH), 6.62 (m, 2H; ArH), 7.47 (m, 2H; ArH).

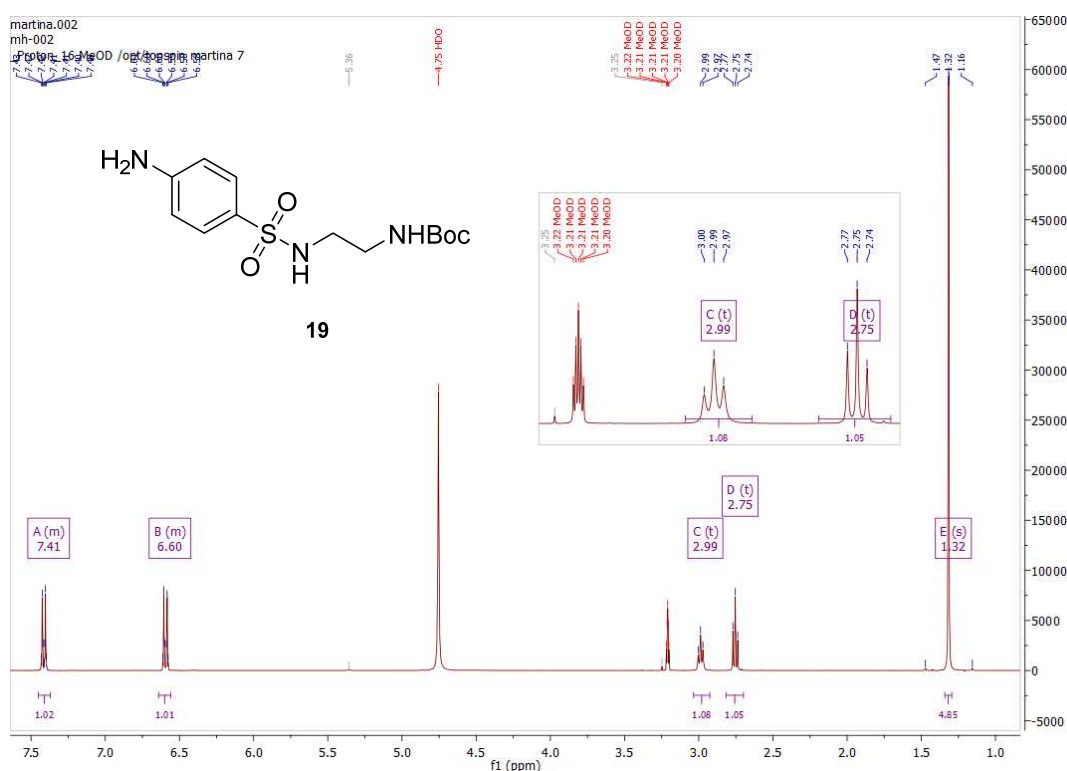


Figure C2- ^1H NMR of **19**

C.3.3 N-Boc-N'-(4-(N'-Boc-4-aminobutanamido)phenylsulfonyl)-ethylenediamine **24**

To a suspension of *N*-Boc-4-aminobutanoic acid **23** (13.2 mg, 0.065 mmol, 1.03 eq.), *N*-Boc-*N'*-(4-aminophenylsulfonyl)-ethylenediamine **19** (20 mg, 0.063 mmol, 1.0 eq.) and 2-chloro-4,6-dimethoxy-1,3,5-triazine (CDMT) as a coupling agent (11.8 mg, 0.067 mmol, 1.06 eq.) in acetonitrile (10 ml), *N*-methylmorpholine (NMM) (9.6 μl , 0.095 mmol, 1.5 eq.) was added. The resulting reaction mixture was stirred at RT for 24 hours and heated to reflux for 6 hours. After cooling the reaction mixture to room temperature, water (3 ml) was added. The solvent was evaporated under reduced pressure. The crude product was purified by flash

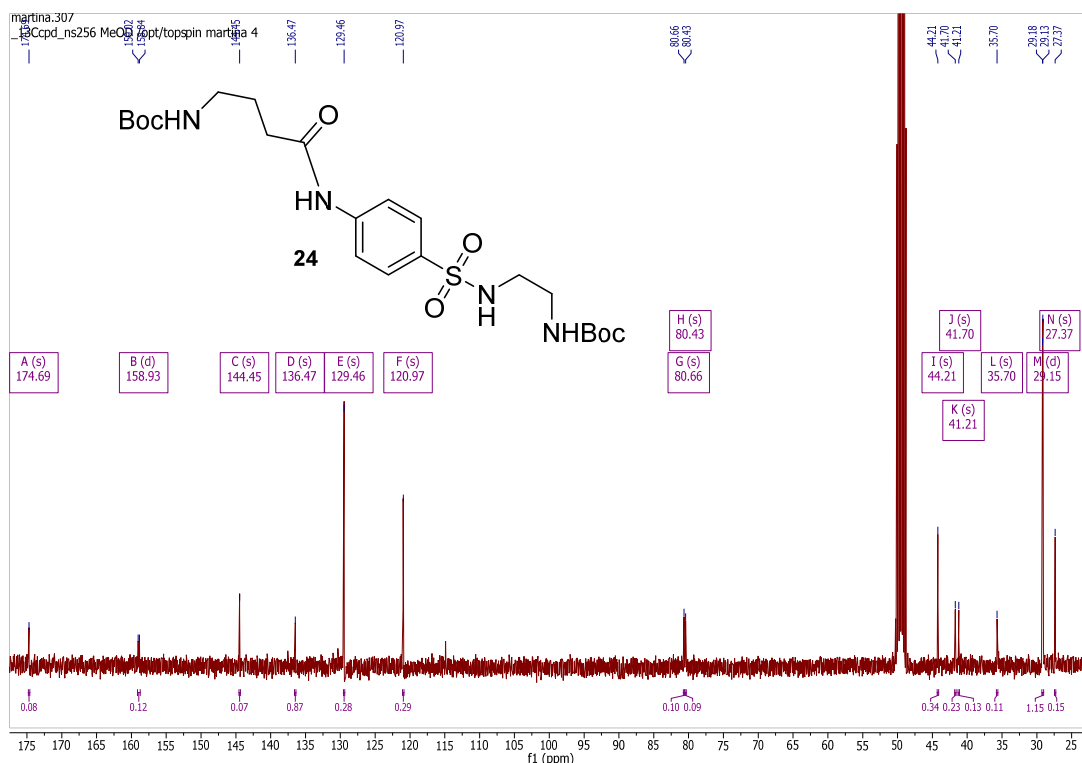


Figure C4- ^{13}C NMR of **24**

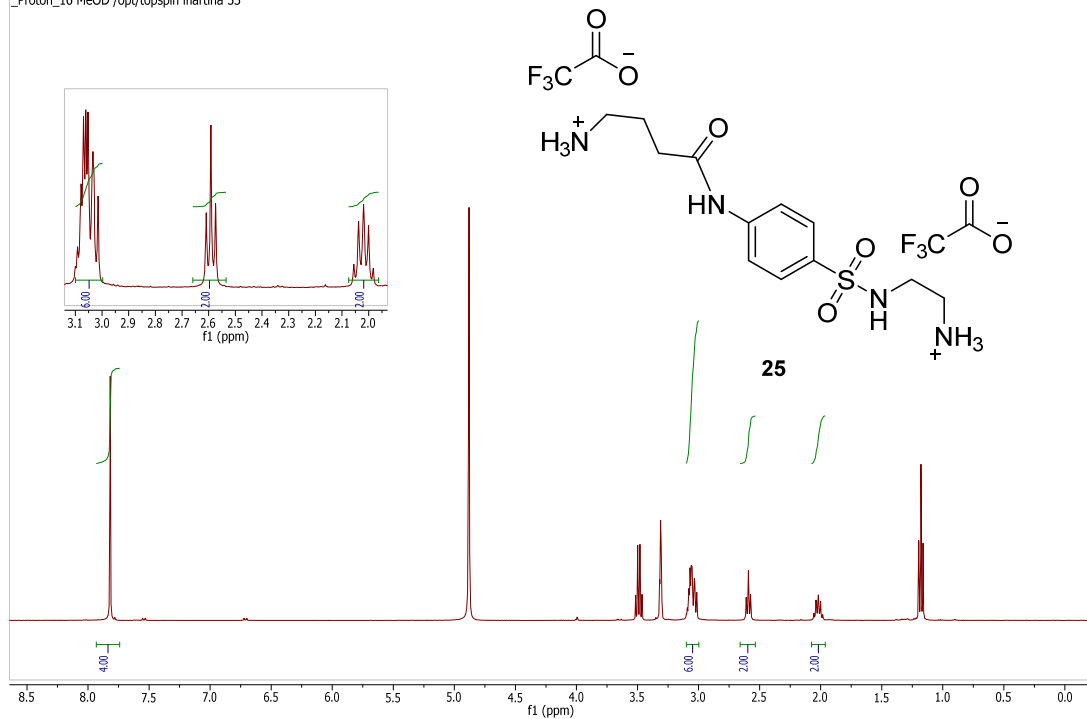
C.3.4 N-(4-(4-AMINOBTANAMIDO)PHENYLSULFONYL)-ETHYLENEDIAMINE **25**

TFA (300 μl , 3 mmol, 30 eq.) was added dropwise to a suspension of *N*-Boc-*N'*-(4-(*N'*-Boc-4-aminobutanamido)phenylsulfonyl)-ethylenediamine **24** (50 mg, 0.1 mmol) in dry DCM (5 ml) at 0 °C. The resulting solution was stirred at RT for 6 hours. The solvent was evaporated under reduced pressure. The crude product dissolved in MeOH and diethyl ether was added until a white precipitate formed. The precipitated product was collected by filtration and dried under reduced pressure. Pure product **25** was obtained as white powder (39 mg, 0.074 mmol, 75 %).

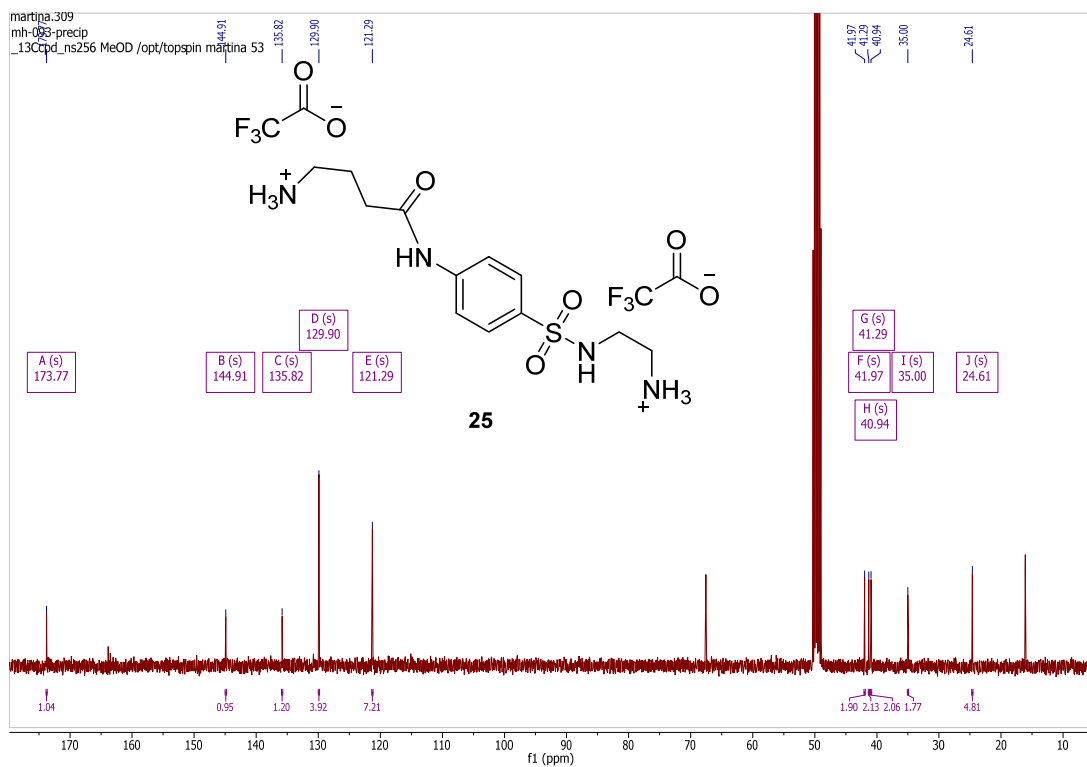
^1H NMR (400 MHz, Methanol- d_4) δ 7.82 (s, 4H, ArH), 3.11 – 3.00 (m, 6H, $\text{CH}_2\text{-CH}_2\text{-CH}_2$), 2.59 (t, $J = 7.0$ Hz, 2H, CH_2), 2.02 (p, $J = 7.1$ Hz, 2H, CH_2).

^{13}C NMR (101 MHz, Methanol- d_4) δ 173.77 (CO), 144.91 (Ar-NH), 135.82 (Ar-S), 129.90 (2C, ArH), 121.29 (2C, ArH), 41.97 ($\text{CH}_2\text{-NH}_2$), 41.29 ($\text{CH}_2\text{-NH}_2$), 40.94 ($\text{CH}_2\text{-NH}_2$), 35.00 ($\text{CH}_2\text{-NH}_2$), 24.61 ($\text{CH}_2\text{-CH}_2\text{-CH}_2$).

martina.309
mh-093-precip
_Proton_16 MeOD /opt/topspin martina 53



martina.309
mh-093-precip
_13Ccpd_ns256 MeOD /opt/topspin martina 53



C.3.5 SYNTHESIS OF CATALYST [Cp*Ir(4C-L)Cl] **22**

The [Cp*IrCl₂]₂ dimer (30 mg, 0.038 mmol, 0.475 eq.), the sulfonamide ligand **25** (40 mg, 0.076 mmol, 1 eq.) and Et₃N (26 μl, 0.19 mmol, 5 eq.) were dissolved in dry DCM (5 ml) under inert atmosphere. After stirring for 24 hours at room temperature, the solution was heated to reflux for 3 hours. The precipitate was filtrated, dissolved in MeOH (1 ml) and precipitated with diethyl ether. The pure catalyst **22** was obtained as a dark orange powder (15 mg, 0.022 mmol, 60 %).

¹H NMR (400 MHz, Methanol-d₄) δ 7.90 (d, *J* = 8.9, 2.7 Hz, 2H, ArH), 7.62 (d, *J* = 8.8, 2.0 Hz, 2H, ArH), 3.02 (t, 2H, CH₂), 2.63 – 2.51 (m, 4H, CH₂-CH₂), 2.48 – 2.42 (m, 2H, CH₂), 2.04 – 1.96 (m, 2H CH₂), 1.73 (s, 15H, Cp*-CH₃).

¹³C NMR (101 MHz, Methanol-d₄) δ 172.95 (CO), 142.07(Ar-NH), 139.41 (Ar-S), 130.09 (2C, ArH), 119.98(2C, ArH), 86.76 (5C, Cp*-C), 40.42 (2C, CH₂-NH₂), 34.50 (2C, CH₂), 24.11 (CH₂), 9.45 (5C, Cp*-CH₃). ESI-MS for C₂₂H₃₄ClIrN₄O₃S: [Cp*Ir(4C-L)Cl] : 625,2 [M-Cl].

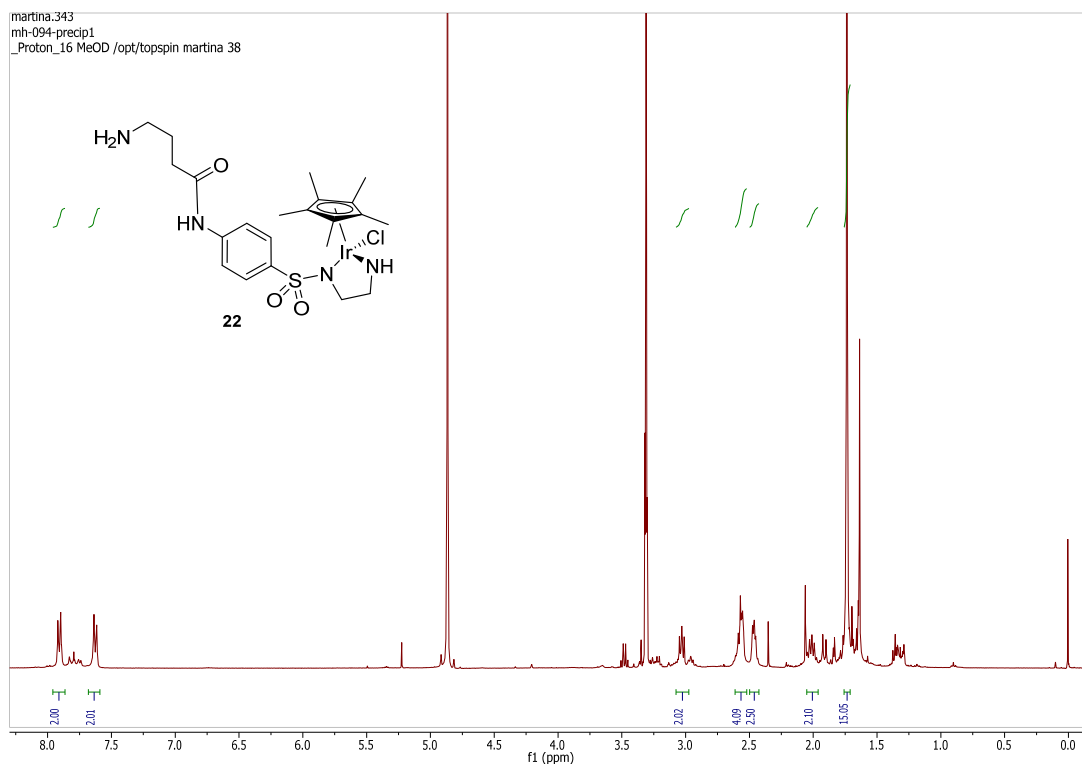


Figure C7- ¹H NMR of [Cp*Ir(4C-L)Cl] **22**.

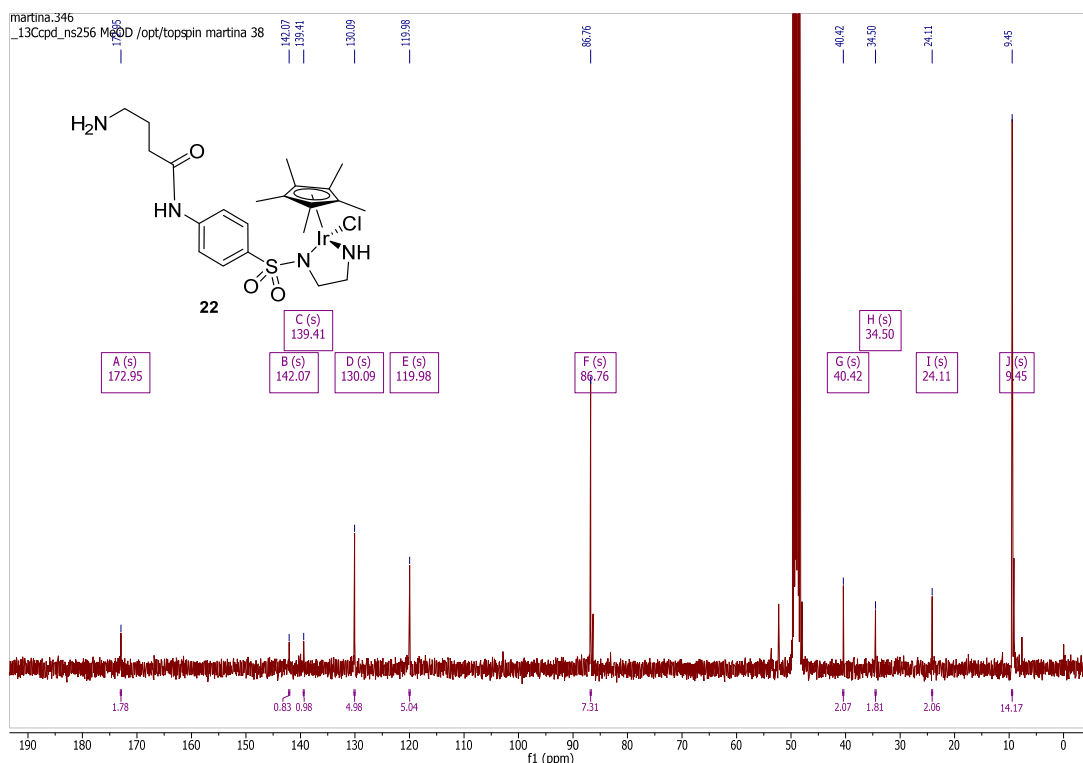


Figure C8- ^{13}C NMR of $[\text{Cp}^*\text{Ir}(4\text{C-L})\text{Cl}]$ **22**.

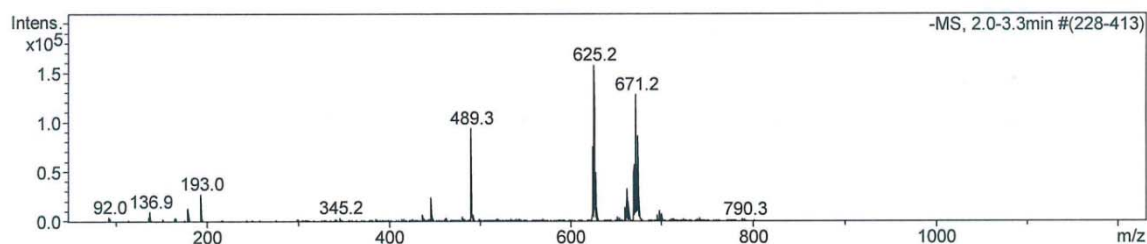


Figure C9- ESI-MS of $[\text{Cp}^*\text{Ir}(4\text{C-L})\text{Cl}]$ **22**.

C.4 SNPs PREPARATION AND CHARACTERIZATION

C.4.1 SNPs SYNTHESIS

The SNPs were prepared by adapting the procedure described elsewhere ^[C3] as follows. All chemicals and solvents were equilibrated in a water bath (20 °C, 1 h) before use. Ammonium hydroxide (40 ml, 28–30 %) and ethanol (345 ml) were mixed in a round bottom flask (1 l), under stirring (600 rpm). TEOS (15 ml) was added and the solution kept under stirring for 20 h. The resulting milky suspension was centrifuged (3'220 g, 10 min) and the white pellet resuspended in ethanol. This operation (hereafter called 'washing cycle') was repeated once with ethanol and three times with water to yield the SNPs (4 g). Into the stock solution of SNPs in water (18 ml of 3.2 mg·ml⁻¹), APTES was added (11 μl, 0.047 mmol) and incubated in a water bath (30 min, 20 °C, 400 rpm). After two washing cycles, the resulting

nanoparticles were stored at 4 °C.

All washing steps were performed by centrifugation (3'220 g, 5 min) and the pellets were resuspended by ultrasonic treatment using an ultrasonic bath (2 min).

C.4.2 SAV PREINCUBATION AND LYOPHILISATION

In a typical experiment, purified Sav mutant (25 mg , approx. $3,8 \times 10^{-7}$ mol) was dissolved in water. The average number of free binding sites per purified Sav tetramer was determined with a biotin-4-fluorescein assay, as described elsewhere.^[C4] The corresponding amount of [Cp*Ir(biot-*p*-L)Cl] ligand stock solution was added to produce protein with binding sites fully filled with the iridium cofactor (ratio of Ir : free binding sites 1 : 1) , or half filled respectively (ratio of Ir : free binding sites 1 : 2). Samples were incubated (37 °C, 2 h), frozen (-80°C) and lyophilised to dryness. A stock solution (3 mg / ml) was used for protein immobilization.

C.4.3 SNPs SYNTHESIS AND PROTECTION

The aminomodified nanoparticles (15 ml, 3 mg / ml) were incubated (30 min) with aqueous glutaraldehyde solution (60 µl of 25% (v/v)). After two washing cycles with Mili-Q water, the particles were spinned down (3'220 g for 10 min), resuspended in MES buffer (14 ml, 10 mM, pH 6.2) and incubated with the corresponding Sav mutant or iridium catalyst **22** while stirring (1 h, 400 rpm). Subsequently, TEOS was added to the reaction mixture (72 µl, 0.324 mmol) and allowed to react for 1 h. To produce the protected SNPs, the nanoparticles were incubated with APTES (18 µl, 4 , 20°C). Protected nanoparticles were centrifuged (4000 rpm, 5 min) and, after two washing cycles, resuspended in Mili-Q water. The concentration of each SNPs stock solution was determined by freeze-drying of each stock solution (100 µl) and weighted using a microbalance.

C.4.4 ACTIVITY ASSAY

In a typical experiment, SNPs (3.2 mg) were resuspended in MES buffer (250 µl, 10 mM, pH 6.2). The solution was mixed with the activity assay buffer (1 : 1 ratio, total V : 400 µl) and NAD⁺ (20 µl, 2 mM stock solution) was added.

The reaction medium was then incubated and shaken (30 °C, 1200 rpm). After the desired reaction time (1h), the suspension was centrifuged (16'100 g, 1 min) and the supernatant (70 µl) was collected for UV-Vis analysis on a TECAN plate reader (absorbance spectrum 240 – 360 nm).

C.4.5 BRADFORD ASSAY

A bovine serum albumin standard curve was prepared in buffer (see reference ^[C5]). 5X Bradford blue reagent (50 μ l) was added to a sample or albumin solution (200 μ l), mixed and incubated for 5 min at room temperature. The sample was pipetted into a 96-well plate and the absorbance was determined at 595 nm by a spectrophotometer (Synergy™ H1 Hybride reader from BioTek).

C.4.6 SCANNING ELECTRON MICROSCOPY AND PARTICLE SIZE MEASUREMENT

Each sample (2 μ l) was spread on freshly cleaved mica sheets, dried at room temperature and sputter-coated with a gold–platinum alloy (15 s, 10 mA, SC7620 Sputter coater). Micrographs were acquired using the InLens mode with an accelerating voltage of 20 kV. Particle sizes were measured using the acquired micrographs with the Olympus Analysis® software package. About 100 measurements were recorded per type of nanoparticles. The protective layer thickness was determined by comparing their diameter with the diameter of unprotected native Stöber SNPs.

Table C1 Particle size measurement analysis

	size (nm)	diameter increase (nm)	st dev \pm	st error	layer thickness
SNP native	241	-	9.12	0.91	nm
Cp*Ir(biot- <i>p</i> -L)Cl]·S112A@prot-SNP	264	23	10.08	1.00	12
Cp*Ir(biot- <i>p</i> -L)Cl]·S112K@prot-SNP	266	25	11.05	1.10	13
Cp*Ir(biot- <i>p</i> -L)Cl]·S112A-K121A@prot-SNP	264	23	9.47	0.94	13

C.4.7 ICP-MS DETERMINATION OF THE TOTAL IR CONTENT

Each type of lyophilized nanoparticles (1 mg) was incubated with NaOH solution (0.5 M, 95°C, 5 min) until complete dissolution.^[C6] Samples were neutralized using HNO₃ solution (65 %, semiconductor grade, Sigma Aldrich) and diluted using Milli-Q water (final HNO₃ concentration 3 %). Analysis was performed on a 7500cx ICP-MS system (Agilent, Basel, Switzerland) using standard operational settings as described elsewhere.^[C7] Quantification was performed via multi-element standards (Sigma-Aldrich) in matrix-matched calibration solutions containing the same amount of NaOH / HNO₃ as the samples. Rh was used as

internal standard to account for residual matrix effects. The octopole was pressurized ($4.5 \text{ mL} \cdot \text{min}^{-1}$ helium) to remove polyatomic interferences.

C5. CATALYSIS

C.5.1 TYPICAL CATALYSIS PROCEDURE IN BUFFER

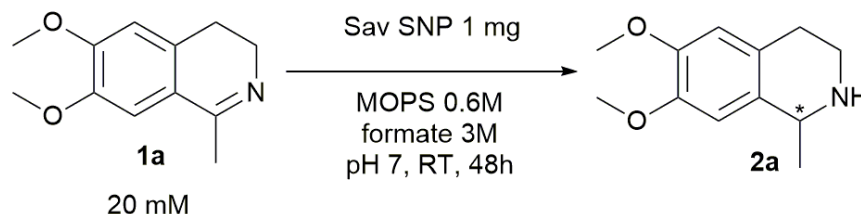


Figure C10- Typical catalysis reaction

Protected nanoparticles (1 mg) were resuspended in MOPS / formate buffer (50 μl , 1.2 M MOPS, 3 M sodium formate, pH 7) and Mili-Q water (48 μl) in an HPLC vial, equipped with a stirring bar. The reaction was initiated by addition of the substrate stock solution (2 μl , 1 M stock solution) and the resulting mixture was shaken for 48 hours or 7 days at room temperature (final volume: 100 μl).

The reaction was quenched by centrifugation of the reaction mixture (30 s, 3'220 g). The supernatant was collected and the nanoparticle pellet was washed with Mili-Q water (3 x). The joined water phases were basified by addition of NaOH solution (50 μl , 20 % stock solution), extracted with DCM (2 x 0.5 ml), dried over Na_2SO_4 and analyzed by the means of normal phase HPLC.

C.5.2 TYPICAL CATALYSIS PROCEDURE IN CELLULAR DEBRIS

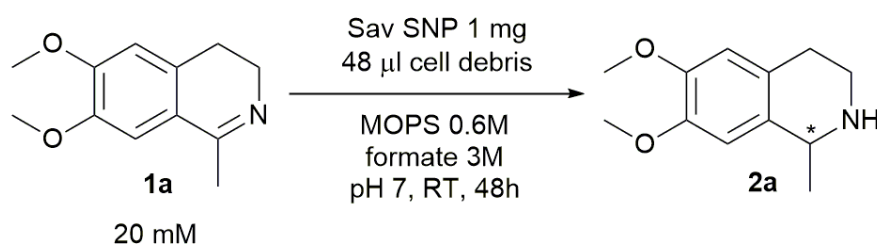


Figure C11- Catalysis in the presence of cellular debris

Protected nanoparticles (1 mg) were resuspended in MOPS / formate buffer (50 μl , 1.2 M MOPS, 3 M sodium formate, pH 7) and cellular debris containing solution (48 μl) in an HPLC vial, equipped with a stirring bar. The reaction was initiated by addition of the substrate stock solution (2.5 μl , 400 mM stock solution) and the resulting mixture was shaken for 48 hours at room temperature (final volume: 100 μl).

The reaction was quenched by centrifugation of the reaction mixture (30 s, 3'220 g). The supernatant was collected and the nanoparticle pellet was washed with Mili-Q water (5 x). The joined water phases were basified by addition of NaOH solution (50 μ l, 20 % stock solution), extracted with DCM (2 x 0.5 ml), dried over Na₂SO₄ and analyzed by the means of normal phase HPLC.

Table C2 Asymmetric imine reduction yielding salsolidine **2a** using Cp*Ir(biot-*p*-L)Cl]·Sav@prot-SNP in the presence of E. coli cell lysate.

Entry	SNP	ee (%) ^{a,b}	Conv. (%) ^b	TON
1	[Cp*Ir(biot- <i>p</i> -L)Cl]·S112A Sav@prot-SNP	25	1	78
2	[Cp*Ir(biot- <i>p</i> -L)Cl]·S112K Sav@prot-SNP	-20	1	171
3	[Cp*Ir(biot- <i>p</i> -L)Cl]·S112A-K121A Sav@prot-SNP	31	1	131
4	[Cp*Ir(biot- <i>p</i> -L)Cl]·S112A Sav free enzyme	0	0	0
5	[Cp*Ir(biot- <i>p</i> -L)Cl]·S112K Sav free enzyme	0	0	0
6	[Cp*Ir(biot- <i>p</i> -L)Cl]·S112A-K121A Sav free enzyme	0	0	0
7	[Cp*Ir(biot- <i>p</i> -L)Cl]	0	0	0

Reactions performed in a reaction buffer using 1 mg of SNPs of free enzyme with the corresponding Ir concentration in 100 μ l reaction mixture with 20 mM substrate concentration at RT for 48 h; ^[a]Enantiomeric excess and conversion was determined by HPLC analysis on a Chiracel-IC column. ^[b]Positive ee values correspond to (*R*)-**2a**; negative ee values correspond to (*S*)-**2a**.

C.5.3 HPLC MEASUREMENTS

Each reaction mixture was analyzed by HPLC using a Chiralpak IC column (5 μ m, 4.6 mm · 25 mm) using dichloromethane containing diethylamine (0.06 %) and isopropanol (0.5 %) as an eluent, flow of 1 ml/min; detection at λ =280 nm, 25 °C.

T_R 8.5 min ((*S*)-6,7-dimethoxy-1-methyl-1,2,3,4-tetrahydroisoquinoline); 9.8 min (6,7-dimethoxy-1-methyl-3,4-dihydroisoquinoline); 14.6 min ((*R*)- 6,7-dimethoxy-1-methyl-1,2,3,4-tetrahydroisoquinoline; referred to as salsolidine). Yields were calculated using a response factor of 1.95, as determined elsewhere.^[C8]

C.5.4 EVOLUTION OF ENANTIOSELECTIVITY OVER TIME

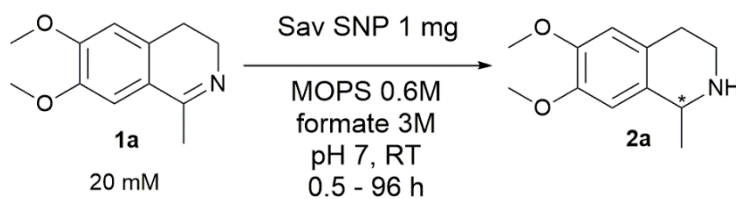


Figure C12- Reaction set up for the time-point assay

SNPs (1 mg) were resuspended in MOPS / formate buffer (50 μ l) and Mili-Q water (48 μ l) in an HPLC vial, equipped with a stirring bar. The reaction was initiated by addition of the substrate stock solution (2 μ l, 1 M stock solution) and the resulting mixture was shaken for 0.5 to 96 h at RT (final volume: 100 μ l). The reaction was quenched by centrifugation of the reaction mixture. The supernatant was collected and the nanoparticle pellet was washed with MQ water (3 x). The joined water phases were basified by addition of NaOH solution (50 μ l, 20 % stock solution), extracted with DCM (2 x 0.5 ml), dried over Na₂SO₄ and analyzed by the means of normal phase HPLC.

Table C3: Salsolidine precursor reduction using [Cp*Ir(biot-*p*-L)Cl]·S112A Sav SNPs

entry	Reaction time (h) ^a	ee (%) ^{b,c}	Conv. (%) ^c	TON
1	0,5	87	1.2	91
2	1	86	4.6	357
3	3	87	6.1	477
4	5	86	9.8	764
5	24	84	22.2	1723
6	48	83	30.7	2384
7	72	81	34.3	2662
8	96	78	41.5	3222

^[a]Reactions performed in a reaction buffer using 1 mg of SNPs in 100 μ l reaction mixture with 20 mM substrate concentration, ^[b] Enantiomeric excess and conversion was determined by HPLC analysis. ^[c] Positive ee values correspond to (*R*)-**2a**; negative ee values correspond to (*S*)-**2a**.

C.5.5 NAD⁺ REDUCTION MEASUREMENTS

SNPs (1 mg) or free enzymes were resuspended in MES buffer (120 μ l, 10 mM, pH 6.2). The solution was mixed with the activity assay buffer (1 : 1 ratio, total V : 245 μ l) and NAD⁺ (5 μ l, 10 mM) was added. The reaction medium was then incubated at 30 °C and shaken (1200 rpm). After the desired reaction time, the suspension was centrifuged (16'100 g, 1 min) and the supernatant (200 μ l) was collected for UV-Vis analysis (λ = 340 nm). The NADH quantification was calculated using $\epsilon = 6220 \text{ M}^{-1}\text{cm}^{-1}$.

Table C4 NADH regeneration catalyzed by protected [Cp*Ir(biot-*p*-L)Cl]₂·Sav@prot-SNP or [Cp*Ir(biot-*p*-L)Cl]₂·Sav as purified proteins.

t (h)	NADH Concentration (uM)						TON					
	nanoparticles			free enzymes			nanoparticles			free enzymes		
	Cp*Ir(biot- <i>p</i> -L)Cl] ₂ ·S112A@prot-SNP	Cp*Ir(biot- <i>p</i> -L)Cl] ₂ ·S112K@prot-SNP	Cp*Ir(biot- <i>p</i> -L)Cl] ₂ ·S112A-K121A@prot-SNP	Cp*Ir(biot- <i>p</i> -L)Cl] ₂ ·S112A	Cp*Ir(biot- <i>p</i> -L)Cl] ₂ ·S112K	Cp*Ir(biot- <i>p</i> -L)Cl] ₂ ·S112A-K121A	Cp*Ir(biot- <i>p</i> -L)Cl] ₂ ·S112A@prot-SNP	Cp*Ir(biot- <i>p</i> -L)Cl] ₂ ·S112K@prot-SNP	Cp*Ir(biot- <i>p</i> -L)Cl] ₂ ·S112A-K121A@prot-SNP	Cp*Ir(biot- <i>p</i> -L)Cl] ₂ ·S112A	Cp*Ir(biot- <i>p</i> -L)Cl] ₂ ·S112K	Cp*Ir(biot- <i>p</i> -L)Cl] ₂ ·S112A-K121A
0	0	0	0	0	0	0	0	0	0	0	0	0
0.1	9.3	9.3	12.7	3.6	2.8	4.1	714	1557	1687	278	459	544
0.2	14.8	9.0	13.1	4.6	5.1	10.7	1137	1498	1749	354	856	1430
0.3	15.3	12.8	17.3	5.3	6.7	11.6	1176	2127	2306	410	1120	1551
0.5	15.3	14.7	22.5	8.6	7.8	16.3	1177	2448	2994	659	1301	2170
0.8	16.0	16.1	25.4	13.9	12.4	22.7	1235	2681	3392	1068	2067	3025
1	16.8	17.8	26.4	16.7	15.9	29.7	1292	2971	3520	1288	2644	3961
2	18.6	18.5	32.4	29.0	29.1	48.7	1431	3076	4322	2231	4853	6489
3	37.4	27.8	36.5	38.4	39.0	65.0	2878	4628	4867	2951	6495	8662
4	38.9	28.1	39.1	48.4	44.9	76.9	2993	4683	5218	3723	7488	10247
5	45.4	29.3	42.8	59.8	52.2	84.4	3495	4882	5707	4601	8707	11252
6	49.9	35.8	49.3	68.1	58.2	91.2	3836	5965	6569	5235	9697	12162
7	59.0	40.6	65.0	74.4	61.1	96.9	4539	6764	8672	5725	10184	12915
8	68.0	47.2	65.5	88.2	70.0	99.3	5232	7874	8734	6783	11671	13236
9	77.0	50.2	74.3	93.4	70.6	106.0	5926	8361	9908	7182	11764	14129
10	83.5	55.3	79.3	100.8	73.8	106.7	6426	9221	10576	7752	12294	14233
11	92.0	57.7	92.3	103.4	74.6	109.0	7080	9619	12309	7958	12427	14528
12	127.6	112.5	115.3	114.2	76.2	112.2	9818	18750	15374	8787	12695	14956
24	128.8	119.2	127.3	122.1	101.1	115.7	9910	19860	16975	9390	16845	15431
36	134.8	123.3	135.1	130.3	105.7	118.0	10367	20554	18016	10023	17623	15739
48	137.6	146.2	138.8	131.0	106.1	120.8	10583	24366	18508	10073	17682	16109

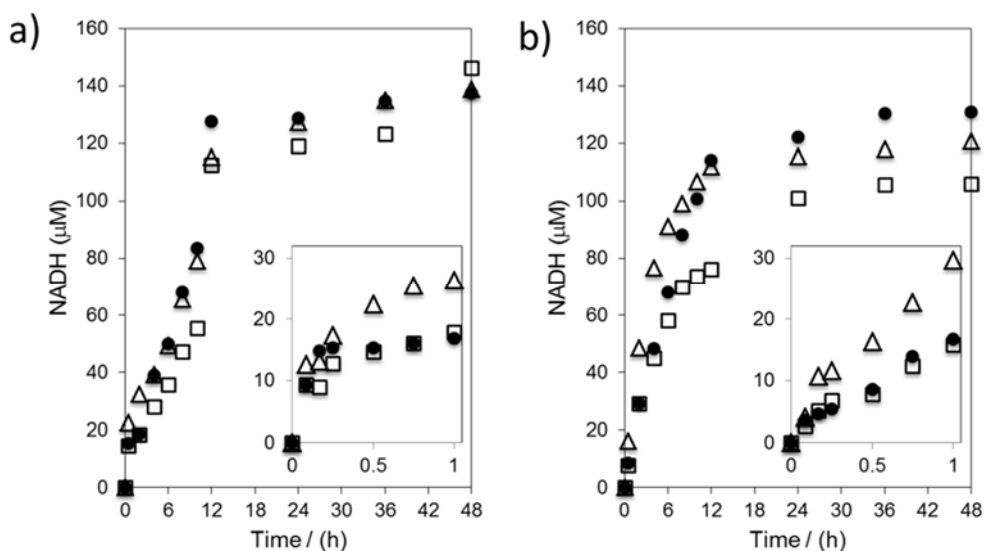


Figure C13- NADH regeneration catalyzed by a) protected $[\text{Cp}^*\text{Ir}(\text{biot-}p\text{-L})\text{Cl}]\cdot\text{Sav@prot-SNP}$ and b) $[\text{Cp}^*\text{Ir}(\text{biot-}p\text{-L})\text{Cl}]\cdot\text{Sav}$ as purified proteins over time as determined by absorption at $\lambda=340\text{ nm}$. Mutant S112A is shown as full circles, S112K as empty squares and S112A-K121A as triangles.

C.6 REFERENCES:

- [C1] V. Köhler, J. Mao, T. Heinisch, A. Pordea, A. Sardo, Y. M. Wilson, L. Knörr, M. Creus, J. C. Prost, T. Schirmer and T. R. Ward, *Angew. Chemie - Int. Ed.*, 2011, **50**, 10863–10866.
- [C2] C. Letondor, A. Pordea, N. Humbert, A. Ivanova, S. Mazurek, M. Novic and T. R. Ward, *J. Am. Chem. Soc.*, 2006, **128**, 8320–8328.
- [C3] W. Stöber, A. Fink and E. Bohn, *J. Colloid Interface Sci.*, 1968, **26**, 62–69.
- [C4] G. Kada, K. Kaiser, H. Falk and H. J. Gruber, *Biochim. Biophys. Acta - Gen. Subj.*, 1999, **1427**, 44–48.
- [C5] M. M. Bradford, *Anal. Biochem.*, 1976, **72**, 248–254.
- [C6] M. D. Angelica and Y. Fong, *October*, 2008, **141**, 520–529.
- [C7] Y. S. Zimmermann, A. Schäffer, P. F. X. Corvini and M. Lenz, *Environ. Sci. Technol.*, 2013, **47**, 13151–13159.
- [C8] M. Dürrenberger, T. Heinisch, Y. M. Wilson, T. Rossel, E. Nogueira, L. Knörr, A. Mutschler, K. Kersten, M. J. Zimbron, J. Pierron, T. Schirmer and T. R. Ward, *Angew. Chem. Int. Ed.*, 2011, **50**, 3026–3029.

APPENDIX D

Supporting information for *Dalton Trans.*, **2018**, *47*, 10837-10841.

D.1. General information

All commercially available chemicals were purchased from commercial suppliers (Acros Organics, Alfa Aesar, AnaSpec, AppliChem, Fluka, Merck, NEB, Sigma-Aldrich) and used without purification. Solvents for HPLC measurements were purchased from Baker and Biosolve. Horse spleen apoferritin (HsAf) was purchased from Sigma Aldrich and subjected to gel filtration prior to use.

Size exclusion chromatography was performed on an Äktaprime Plus chromatography system, using a HiLoad 16/60 Superex 200 pg column from GE Healthcare.

Dynamic light scattering (DLS) was performed using a Malvern Instruments Zetasizer Nano ZS Dynamic Light Scattering Instrument.

Mili-Q water (resistivity $\geq 18 \text{ M}\Omega \text{ cm}^{-1}$) was produced with a Millipore Synergy purification system. Streptavidin (Sav) mutants were produced, purified and characterized as previously described.^[D1]

Analyses of the catalytic runs were performed on an Agilent 1100 normal phase HPLC with an analytical Chiralpack IC column (250 · 4.6 mm, 5 μm). ICP-MS analysis was performed on a 7500cx ICP-MS system (Agilent, Basel, Switzerland). ^{191}Ir was used for quantification, ^{193}Ir for verification of the results.

D.2 STOCK SOLUTIONS AND BUFFERS

MOPS/formate buffer: 3-(N-morpholino)propanesulfonic acid and sodium formate were dissolved in Milli-Q water to a concentration of 6M (formate) and 1.2 M (MOPS). The pH was adjusted to 8 by addition of NaOH.

Tris-HCl buffer: Tris base and NaCl were dissolved in Milli-Q water to a concentration of 50 mM (Tris) and 100 mM (NaCl). The pH of the solution was adjusted to 8 by the addition of 37% HCl.

Catalyst 3 stock solution: $[\text{Cp}^*\text{Ir}(\text{biot-}p\text{-L})\text{Cl}]$ was dissolved in DMF to a final concentration of 500 mM. For a detailed synthesis procedure, see reference.^[D2]

Substrate stock solutions:

- 6,7-dimethoxy-1-methyl-3,4-dihydroisoquinoline **1a** was dissolved in Milli-Q water (2 ml) to a final concentration of 1 M.
- 1-phenyl-3,4-dihydroisoquinoline **1c** (synthesis procedure see reference ^[3]) was dissolved in degassed DMSO (2 ml) to a final concentration of 400 mM.

D.3 SAV PREINCUBATION AND LYOPHILISATION

In a typical experiment, purified Sav mutant (25 mg, approx. $3,8 \times 10^{-7}$ mol) was dissolved in Milli-Q water. The average number of free binding sites per purified Sav tetramer was determined with a biotin-4-fluorescein assay, as described elsewhere ^[4]. The corresponding amount of [$\text{Cp}^*\text{Ir}(\text{biot-}p\text{-L})\text{Cl}$] ligand stock solution was added to produce protein with binding sites half filled with the iridium cofactor (ratio of Ir : free binding sites 1 : 2). Samples were incubated (37 °C, 2 h), frozen (-80°C) and lyophilised to dryness.

D.4 APOFERRITIN ENCAPSULATION

The apoferritin sample purified by gel filtration was subjected to the re-assembly process. The protein solution was diluted to a concentration of 30 mg / ml and the pH of the solution was decreased below 2 using 37% HCl. The resulting solution was incubated for 20 minutes at 600 rpm at RT followed by the addition of a lyophilized ATHase. The pH of the resulting solution was increased to 8 using 10 M NaOH solution. After incubation for 2 hours at RT, iminobiotin-sepharose beads were added and the solution was incubated for further 1h at rapid shaking (800 rpm). After binding the non-encapsulated Sav to beads, the solution was centrifuged (5300 g, 15 min), the supernatant was filtered and subjected to another 2 rounds of immobilization. The resulting cargo-containing ferritin samples were further purified by size-exclusion chromatography.

D.5 SIZE-EXCLUSION CHROMATOGRAPHY

In order to confirm the guest loading, Sav S112A-K121A was incubated with biotin-4-fluorescein and encapsulated in HsAf. The purified samples were subjected to SEC monitored at $\lambda=280$ and 495 nm (Figure D1).

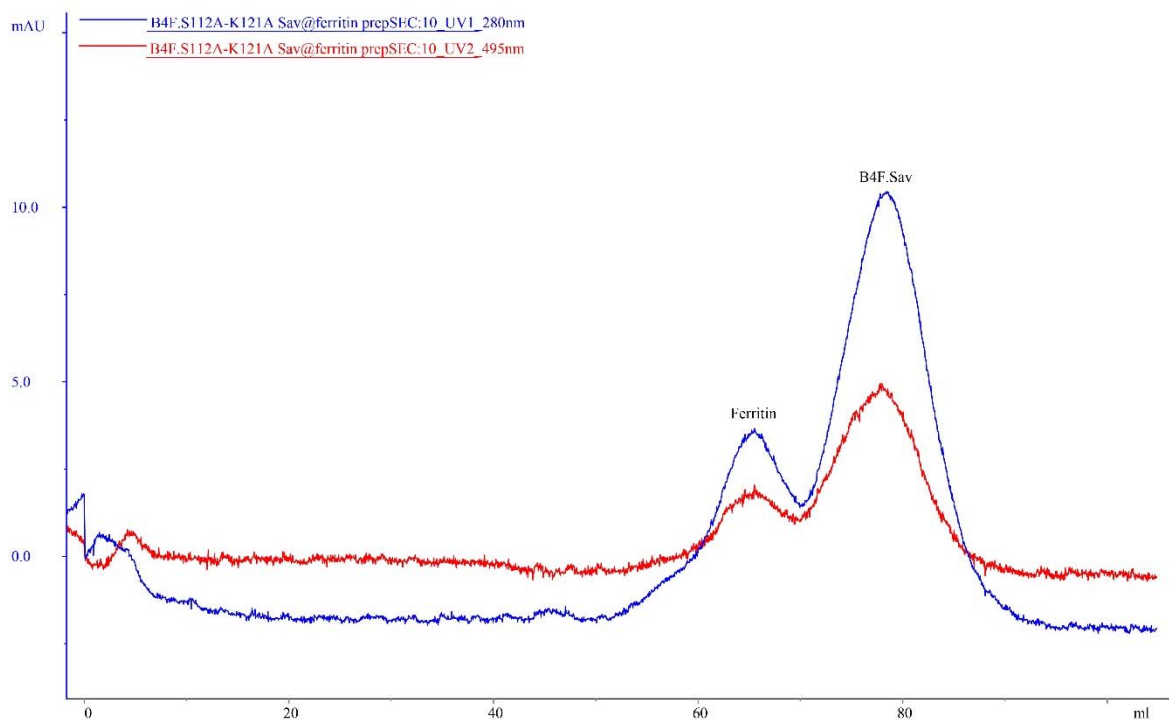


Figure D1. Size exclusion chromatogram of B4F·S112A-K121A Sav@ferritin in 50 mM Tris-HCl, 100 mM NaCl, pH8. Column: HiLoad 16/60 Superdex 200 pg.

ATHases bearing mutations S112A, S112K and S112A-K121A were encapsulated and purified following the same procedure. The fractions corresponding to the ferritin signal (elution volume around 60 mL, Figure D2) were pooled, concentrated using a Amicon Ultra-15 centrifugal filter unit with a 30 kDa cut-off (Merck Millipore) and stored at 4°C prior to analysis by ICP-MS and catalysis.

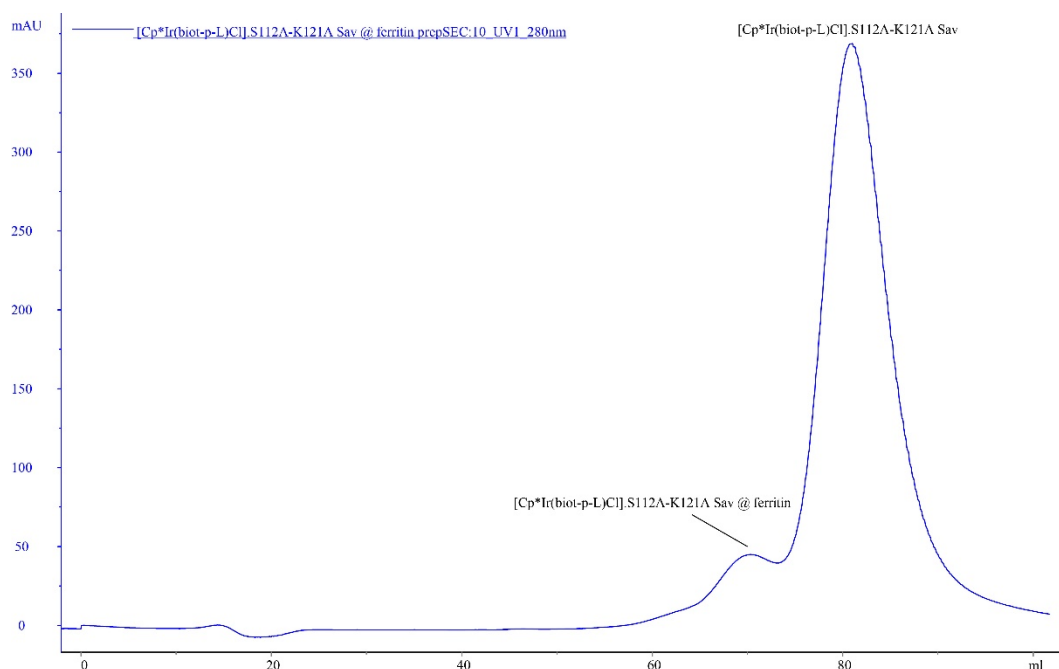


Figure D2. Size exclusion chromatogram of [CP*Ir(biot-*p*-L)Cl]·S112A-K121A Sav@ferritin in 50 mM Tris-HCl, 100 mM NaCl, pH8. Column: HiLoad 16/60 Superdex 200 pg.

D.6 DYNAMIC LIGHT SCATTERING MEASUREMENTS (DLS)

Dynamic light scattering (DLS) measurements of the combined fractions containing the assembled ferritin were performed on a Malvern Instruments Zetasizer Nano ZS Dynamic Light Scattering Instrument. Sample measurements were performed with purified ferritin samples at an approx. concentration of 0.1 mg/ml in 50 mM Tris-HCl, 100 mM NaCl, pH 8 using a low-volume quartz cuvette. All solutions were filtered through a 0.2 μ m filter to prevent further aggregation.

Table D1. Average size of apoferritin and ferritin samples containing ATHase cargo

entry	Sample	Diameter	PDI
1	Apoferritin	13.43	0.052
2	[Cp*Ir(biot- <i>p</i> -L)Cl]·S112A-K121A Sav@ferritin	15.71	0.488
3	[Cp*Ir(biot- <i>p</i> -L)Cl]·S112A Sav@ferritin	17.66	0.658
4	[Cp*Ir(biot- <i>p</i> -L)Cl]·S112K Sav@ferritin	14.44	0.783

PDI = polydispersity index

D.7 ELECTROPHORESIS

D.7.1 SDS-PAGE

The pooled samples from SEC purification were concentrated using a Amicon Ultra -15 centrifugal filter unit with a 30 kDa cut-off (Merck Millipore) and the protein concentration was determined by Nanodrop2000 (ThermoFisher) using $\epsilon_{280\text{ nm}} = 4.8 \times 10^5 \text{ M}^{-1} \text{ cm}^{-1}$). The gel analysis was performed according to a published procedure ^[D7] using hand-casted 10% acrylamide gels, followed by B4F detection under UV and staining with Coomassie Brilliant Blue. The stacking layer (6% final acrylamide concentration) was prepared at pH 6.8.

20 μl of each sample type (diluted so the final amount of loaded protein would be 2 μg per lane) was combined with a 6x loading buffer and either heated to 90°C for 10 min prior to loading or directly loaded. The gel was run at 200 V until for approx. 1.5 hours. After B4F visualization the gels were stained with Coomassie Brilliant blue R-250 dye in MeOH and acetic acid, followed by de-staining.^[D5]

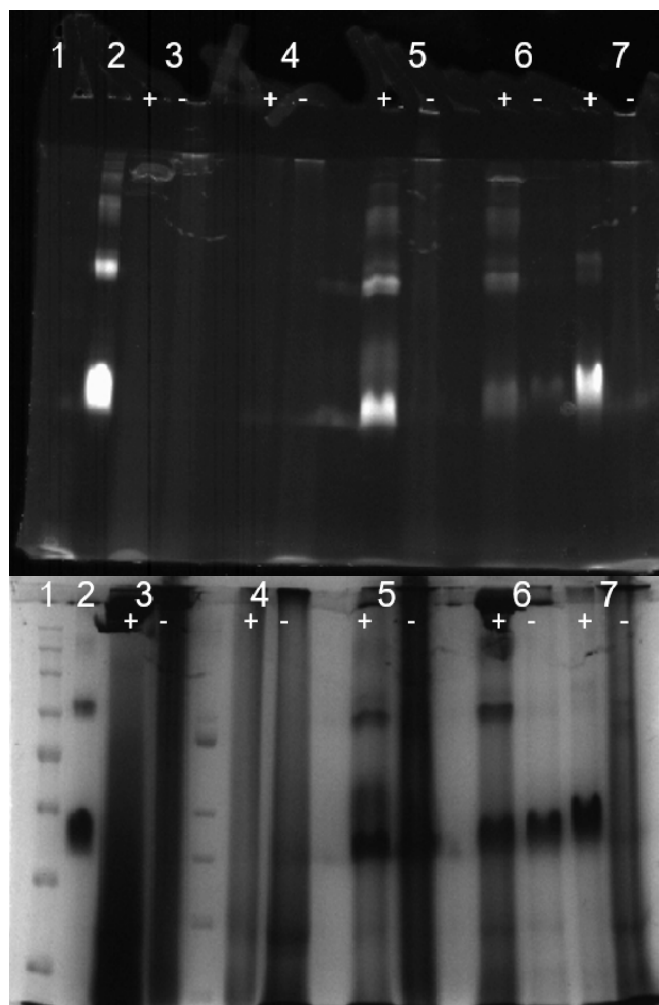


Figure D3. SDS-PAGE gel under UV (B4F visualization) and Vis (coomassie staining). + indicates heating during sample preparation, - indicates semi-native conditions (absence of heating) Lane 1: ladder; 2: Sav WT (control); 3: apoferritin; 4: reassembled apoferritin; 5: [Cp*Ir(biot-p-L)Cl]·S112A-K121A Sav@ferritin; 6: [Cp*Ir(biot-p-L)Cl]·S112A Sav@ferritin; 7: [Cp*Ir(biot-p-L)Cl]·S112K Sav@ferritin

D.7.2 NATIVE PAGE

The pooled samples from SEC purification were concentrated using a Amicon Ultra -15 centrifugal filter unit with a 30 kDa cut-off (Merck Millipore) and the protein concentration was determined by Nanodrop2000 (ThermoFisher) using $\epsilon_{280\text{ nm}} = 4.8 \times 10^5 \text{ M}^{-1}\text{cm}^{-1}$. The gel analysis was performed according to a published procedure ^[D7] using hand-casted 10% native acrylamide gels, followed by B4F detection under UV and staining with Coomassie Brilliant Blue. The stacking layer (6% final acrylamide concentration, no SDS added) was prepared at pH 6.8.

20 μ l of each sample type (diluted so the final amount of loaded protein would be 2 μ g per lane) was combined with a 6x loading buffer (without DTT or mercaptoethanol) and directly loaded. The gel was run at 200 V until for approx. 1.5 hours. After B4F visualization, the gels were stained with Coomassie Brilliant Blue R-250 dye in MeOH and acetic acid, followed by de-staining.

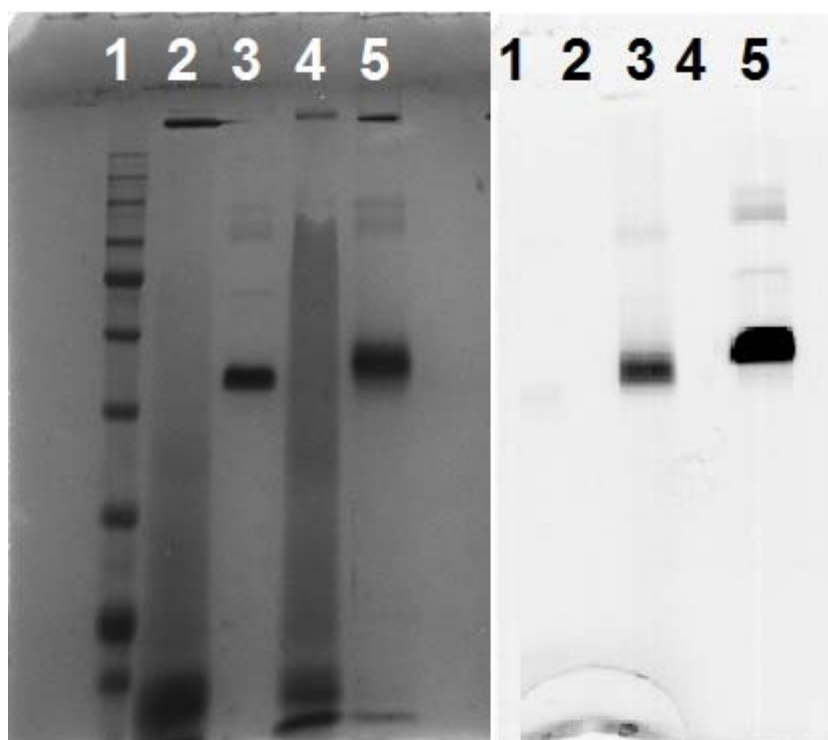


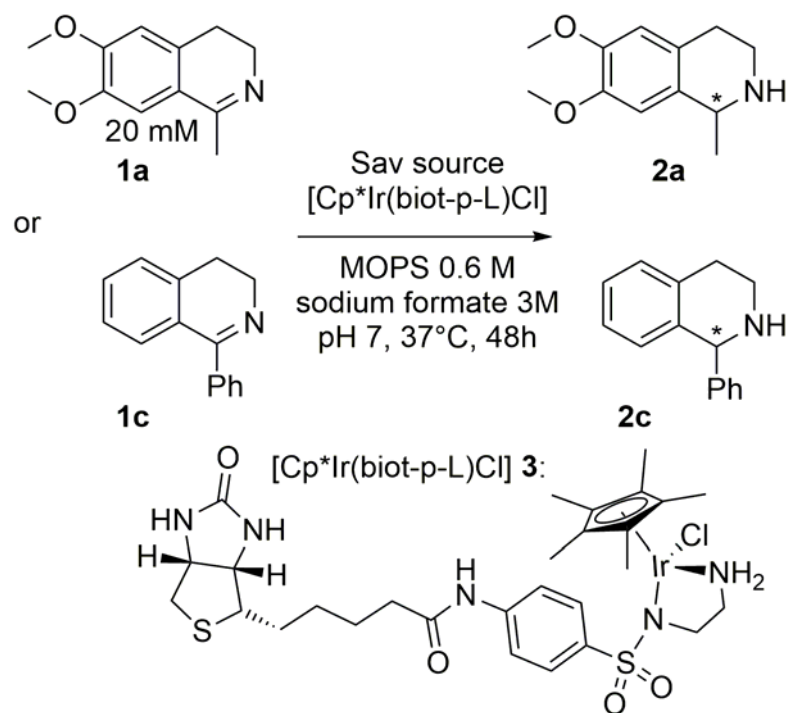
Figure D4. Native-PAGE gel under Vis (Coomassie staining) and UV (B4F visualization). Lane 1: ladder; 2: apoferritin sample; 3: Sav S112A-K121A; 4: [Cp*Ir(biot-p-L)Cl]·S112A-K121A Sav@ferritin; 5: apoferritin + Sav S112A-K121A.

D.8 ICP-MS DETERMINATION OF THE TOTAL IR CONTENT

Fractions from SEC containing the ferritin species were combined and the sample (10 μ l) was incubated with concentrated HNO₃ solution (65 %, semiconductor grade, Sigma Aldrich) at 95°C for 30 min. The resulting samples were diluted to end concentration of 3 % HNO₃ using Milli-Q water. Analysis was performed on a 7500cx ICP-MS system (Agilent, Basel, Switzerland) using standard operational settings as described elsewhere^[D6]. Quantification was performed via multi-element standards (Sigma-Aldrich) in matrix-

matched calibration solutions containing the same amount of HNO_3 as the samples. Rh was used as internal standard to account for residual matrix effects. The octopole was pressurized ($4.5 \text{ mL} \cdot \text{min}^{-1}$ helium) to remove polyatomic interferences.

D.9 CATALYSIS



Scheme D1. Catalysis set up

In a typical catalysis procedure, the cofactor, an ATHase or ATHase@ferritin solution (45 μl) were dissolved in MOPS / formate buffer (50 μl , 1.2 M MOPS, 6 M sodium formate, pH 8) in a HPLC vial. The reaction was initiated by addition of a substrate stock solution (5 μl , end concentration 20 mM). The vials were sealed and the reaction mixtures were shaken at 600 rpm in a Thermoshaker at 37°C (final volume 100 μl).

Each reaction mixture was diluted with Milli-Q water (400 μl) and basified using NaOH solution (20 %, 50 μl). The resulting mixture was extracted with dichloromethane (2 x, 1 ml), the combined organic fractions were collected in a PP tube containing anhydrous sodium sulfate, and centrifuged (18800 x g, 5 min). The supernatant was analyzed by HPLC.

D.10 HPLC MEASUREMENTS

Catalysis results for substrate **1a** were analyzed using a Chiralpak IC column (5 μ m, 4.6 mm \cdot 25 mm) and dichloromethane containing diethylamine (0.06 %) and isopropanol (0.5 %) as an eluent (1 ml / min flow; λ =280 nm, 25 $^{\circ}$ C).

T_R 8.5 min ((*S*)- 6,7-dimethoxy-1-methyl-1,2,3,4-tetrahydroisoquinoline), 9.8 min (6,7-dimethoxy-1-methyl-3,4-dihydroisoquinoline), 14.6 min ((*R*)- 6,7-dimethoxy-1-methyl-1,2,3,4-tetrahydroisoquinoline). Yields were calculated using a response factor of 1.95, as determined elsewhere.^[D8]

Screening with substrate **1c** was analyzed using a Chiralpak IC column (5 μ m, 4.6 mm \cdot 25 mm) and hexane containing diethylamine (0.06 %) and isopropanol (3 %) as an eluent (1 ml / min flow; λ =265 nm, 25 $^{\circ}$ C). T_R 7.6 min ((*S*)-1-phenyl-1,2,3,4-tetrahydroisoquinoline, 10.5 min ((*R*)-1-phenyl-1,2,3,4-tetrahydroisoquinoline), and 16 min (1-phenyl-3,4-dihydroisoquinoline). Yields were calculated using a response factor of 13.613 as determined elsewhere.^[D9]

D.11 REFERENCES

- [D1] V. Köhler, J. Mao, T. Heinisch, A. Pordea, A. Sardo, Y. M. Wilson, L. Knörr, M. Creus, J. C. Prost, T. Schirmer and T. R. Ward, *Angew. Chem. Int. Ed.*, 2011, **50**, 10863–10866.
- [D2] C. Letondor, A. Pordea, N. Humbert, A. Ivanova, S. Mazurek, M. Novic and T. R. Ward, *J. Am. Chem. Soc.*, 2006, **128**, 8320–8328.
- [D3] I. Lantos, D. Bhattacharjee, D. S. Eggleston, *J. Org. Chem.* **1986**, *51*, 4147–4150.
- [D4] G. Kada, K. Kaiser, H. Falk and H. J. Gruber, *Biochim. Biophys. Acta - Gen. Subj.*, 1999, **1427**, 44–48.
- [D5] F. W. Studier, *Prot. Expr. Purif.* **2005**, *41*, 207–234.
- [D6] Y. S. Zimmermann, A. Schäffer, P. F. X. Corvini and M. Lenz, *Environ. Sci. Technol.*, **2013**, *47*, 13151–13159.
- [D7] U. K. Laemmli, *Nature* **1970**, *227*, 680–685.
- [D8] U. E. Rusbandi, Ch. Lo, M. Skander, A. Ivanova, M. Creus, N. Humbert, T. R. Ward *Adv. Synth. Catal.* **2007**, *349*, 1923-1930.
- [D9] H. Mallin, M. Hesticová, R. Reuter, T. R. Ward, *Nat. Protoc.*, 2016, **11**, 835–852.

